ROCKET
(3)
101
750

ON THE NATURE AND ORIGIN OF SOME PALEOGENE MELILITITIC PILLOWED LAVAS, BRECCIAS, AND INTRUSIVES FROM BERMUDA

by

John Maurice Peckenham

Submitted in partial fulfilment of the
requirements for the degree of
Master of Science

at

Dalhousie University
Halifax, Nova Scotia

July, 1981

Examiners:

External: Dr. G. Pe-Piper

Reader: Dr. P.T. Robinson

Chairman: r. M. Zentilli
for Dr. P.E. Schenk

Reader: Dr. P.J.C. Ryall

Supervisor: Dr. J. [illegible]all

DALHOUSIE UNIVERSITY

Date 14 September 1981

Author John Maurice Peckenham

Title On the Nature and Origin of some Paleogene Melilititic Pillowed Lavas, Breccias, and Intrusives from Bermuda

Department or School Geology

Degree M.Sc. Convocation Fall Year 1981

Permission is herewith granted to Dalhousie University to circulate and to have copied for non-commercial purposes, at its discretion, the above title upon the request of individuals or institutions.

Signature of Author

THE AUTHOR RESERVES OTHER PUBLICATION RIGHTS, AND NEITHER THE THESIS NOR EXTENSIVE EXTRACTS FROM IT MAY BE PRINTED OR OTHERWISE REPRODUCED WITHOUT THE AUTHOR'S WRITTEN PERMISSION.

TABLE OF CONTENTS

		Page
	Abstract	iii
	List of Figures	iv
	List of Tables	vi
	Abbreviations and Symbols	vii
	Acknowledgements	ix
1.	PREVIOUS STUDIES	
	Introduction	1
	Geological	1
	Geophysical	14
	Radiometric Ages	31
	1980 Drilling Project	33
2.	PETROGRAPHY AND PHYSICAL VOLCANOLOGY	
	Introduction	37
	Extrusives	37
	Intrusives	46
	Conglomerate - Breccia	48
	Physical Volcanology	51
3.	MINERALOGY	
	Introduction	65
	Clinopyroxene	65
	Spinel	79
	Biotite	86
	Melilite	95
	Olivine	98
	Sphene	99
	Other Phases	102
4.	GEOCHEMISTRY	
	Introduction	103
	Methods	103
	Results and Interpretation	104

		Page
5.	PETROGENESIS	
	Introduction	137
	Experimental Studies	140
	Model 1	140
	Model 2	146
	Model 3	147
	Low-Pressure Studies	147
	Nature of the Parent Mantle	153
	Synthesis	154
	Nephelinite Associations	154
6.	MAGNETIC PROPERTIES	
	Introduction	157
	Techniques	157
	Results	158
	Discussion	178
7.	BERMUDA RISE	
	Introduction	194
	The Bermuda Rise - Redefined	194
	Geological Studies	198
	Geophysical Studies	213
8.	SUMMARY AND CONCLUSIONS	
	Summary	222
	Hot-Spots	225
	Oceanic Islands	228
	Conclusion	233
	The Model	234
	REFERENCES	236
	APPENDIX I - 1980 Core Log	257
	PLATE I - Deep Drill-1972 Core Log	

ABSTRACT

A recent (1980) 98-meter-deep drill hole on the island of Bermuda cored nearly 50 meters of submarine melilititic pillowed-lavas and associated clastic rocks which are cut by narrow anastomosing melilite-bearing intrusives. Foraminifera (Orbulina and Globigerinids) found in the interpillow sediments yield mid-Tertiary ages. The mineralogies of both igneous rock-types are similar and modes fall within these ranges: phenocrysts of titan-augite and Mg-Al titanomagnetite (5-15%), groundmass of titan-augite (5-50%), Mg-Al titanomagnetite (2-15%), melilite (1-60%), biotite (0-10%), altered sphene (0-5%), altered olivine (0-5%) and altered glassy or cryptocrystalline material (2-80%). The rocks contain abundant calcite which is evenly dispersed through the rocks and in veins. The degree of alteration varies from extensive chloritization of cooling-unit margins to relatively unaltered cooling unit interiors. Chemically these rocks are silica undersaturated (31-39% SiO_2), titanium rich (4.1-5.6%) and volatile rich (4.4-12.5%). A paleomagnetic study yielded few stable inclinations. The stable inclinations are not reproducible using different analytical techniques. The rocks have high Curie temperatures (~570°C) which do not correspond to the temperatures predicted from experimental studies on Al- and Mg-bearing titanomagnetites. The correlation of the rocks with Oligocene volcaniclastic turbidites found at DSDP Site 386 and the lack of other volcanogenic horizons in the sediments on the Bermuda Rise suggest that the Bermuda Volcano was formed during a single eruptive cycle. Geological and geophysical studies are cited which indicate that the Bermuda Rise did not exist until the mid-Tertiary, approximately the same time as the eruption of the newly collected lavas.

LIST OF FIGURES

Figure No.		Page
1-1	Location Map - Northwestern Atlantic	2
1-2	Drill-site Locations	5
1-3	Core Log of 1912 hole	8
1-4	Isogonic Chart of Bermuda	15
1-5	Seismic Cross-section of Bermuda	17
1-6	Theoretical Magnetic Profile of the Seamount	20
1-7	Aeromagnetic Profiles of Bermuda	22
1-8	Aeromagnetic Anomalies over Plantagenet Bank	25
1-9	Bouguer Anomaly map of Bermuda	27
1-10	Seismic Profiles of Castle Harbour	29
1-11	Sketch Lithologic Column - 1980 Core	34
2-1	Photograph of Cooling Unit	38
2-2	Photomicrograph of Cooling Unit Margin	38
2-3	Photomicrograph of Cooling Unit Interior	41
2-4	Down-hole modal variations in the extrusive rocks	44
2-5	Photograph of an intrusive sheet	47
2-6	Photograph of breccia	49
2-7	Frequency of distribution of apparent cooling unit thicknesses	52
2-8	Frequency distribution of apparent intrusive thicknesses	56
2-9	Down-hole variation in cooling unit thickness, breccia thickness, and percentage of dikes	59
2-10	Contact angles between cooling unit margins corrected for sampling bias $N_{corrected} = \frac{N_{measured}}{\cos \theta}$ where θ = contact angle.	62
3-1	Photomicrograph of Concentrically Zoned Pyroxene	67
3-2	Photomicrograph of Hourglass Zoned Pyroxene	67
3-3	Pyroxene Substitution Trends	74
3-4	Photomicrograph of Spinel	80
3-5	Spinel Composition Variations	82
3-6	Substitution Trends in Spinels	84
3-7	Step Scan of Zoned Spinel	87
3-8	Spinel Compositions Projected onto Miscibility Diagram	89
3-9	Biotite Compositional Trends	93
3-10	Photomicrograph of Melilite	96
3-11	Photomicrograph of Altered Sphene	100

Figure No.		Page
4-1	Down-hole Changes in Chemistry	112
4-2	Plot of (H_2O + CO_2) versus Percent Oxide	114
4-3	Plot of (H_2O + CO_2) versus $Fe_2O_3/(FeO+Fe_2O_3)$	117
4-4	Plot of Alkalis versus SiO_2	119
4-5	AFM Plot of Analyses	122
4-6	Nephelinite Composition Trends	124
4-7	Plot of Oxides versus SiO_2	126
4-8	Differentiation Index versus Percent Oxide	130
4-9	Plot of Analyses in Oi'-Na'-Q'	132
4-10	Plot of Color Index versus Normative Plagioclase Composition	135
5-1	Paragenetic Sequence	138
5-2	CMAS Flow Sheet	142
5-3	Flow Sheet for Na_2O-CMAS	144
5-4	Crystallization Trends in Di-Ak-Ne-$CaTiAl_2O_6$	149
5-5	Flow Sheet for Ab-Fo-La-Q	151
6-1	Alternating Field Demagnetization Curves	160
6-2	Thermal Demagnetization Curves	164
6-3	Typical Curie Temperature Determination	166
6-4	Stereonet Plots of Specimens Analyzed	169
6-5	Representative Zijderveld Plots	172
6-6	Demagnetization Spectra	179
6-7	DIRM Model	188
6-8	Stereonet Plot of DIRM Experiment Results	191
7-1	Redefined Limits of the Bermuda Rise	196
7-2	Stratigraphy of Site 386 Core	200
7-3	Stratigraphy of Site 387 Core	203
7-4	Distribution of Acoustic Horizons in the Northwestern Atlantic Ocean	206
7-4a	Seismic Profile Running West from Bermuda	208
7-5	Seismic Cross-section of Crust SE of Bermuda	211
7-6	Magnetic Anomalies in the Northwestern Atlantic Ocean	215
8-1	Correlation of Volcanism and Sedimentation of the Northwestern Coast of Africa	231

LIST OF TABLES

Table No.		Page
1-1	1912 Rocks - Modes and Chemistry	7
1-2	Average Composition of Deep Drill-1972 Rocks	13
1-3	Physical Properties of Deep Drill-1972 Rocks	32
3-1	Comparative Mineralogies - Extrusives and Intrusives	66
3-2	Clinopyroxene Analyses	70
3-3	Spinel Analyses	81
3-4	Biotite Analyses	92
3-5	Melilite Analyses	97
3-6	Altered Sphene Analyses	101
4-1	Whole Rock Chemistry - Complete	105
4-2	Whole Rock Chemistry - Calcite Free	107
4-3	Whole Rock Chemistry - Volatile Free	108
4-4	Whole Rock Chemistry - Fe-Adjusted	109
4-5	Average Composition of Kimberlite, Nephelinite and Alkali Basalt	111
6-1	Summary of Paleomagnetic Results	159
6-2	Viscous Decay Experiment Results	168

ABBREVIATIONS AND SYMBOLS

Ab - Albite

af - Alternating field

Ak - Akermanite = $Ca_2MgSi_2O_7$

An - Anorthite = $Ca_2Al_2SiO_8$

BD - Bermuda 1980 prefix for intrusives

BF - Bermuda 1980 prefix for cooling units

^oC - Degrees Centigrade

cm - Centimeter

CMAS - System $CaO-MgO-Al_2O_3-SiO_2$

Cord - Cordierite = $Al_3(Mg, Fe)_2Si_5 Al O_{18}$

D - Declination

Di - Diopside

DIRM - Drilling Induced Remanent Magnetism

DSDP - Deep Sea Drilling Project

emu - Electromagnetic unit

Fo - Forsterite = Mg_2SiO_4

fO_2 - Oxygen fugacity

g - Gram

I - Inclination

IUGS - International Union of Geological Sciences

kb - Kilobars

km - Kilometer

kms^{-1} - Kilometers per second

l - Liquid

m - Meter

M - Magnetic moment

Ma - 10^6 years

MDF - Median Destructive Field

Ne - Nepheline = $Na_3(Na, K)Al_4 Si_4 O_{16}$

NRM - Natural Remanent Magnetism

Oe - Oersted

Ol - Olivine = $(Mg, Fe)_2SiO_4$

P - Perovskite = $CaTiO_3$

PH_2O - Partial pressure of water

Pr - Proto-enstatic = $MgSi_{1-x}O_3$, x = 0-1

Q - Quartz = SiO_2

s.d. - Standard Deviation

S or Sp - Spinel

sec. - Second

SIRM - Shock Induced Remanent Magnetism

Tr - Tridymite = SiO_2

TRM - Thermoremanent Magnetism

Wo - Wollastonite = $CaSiO_3$

γ - 10^{-5} Oersted

Ω-m - Ohm-meter

ACKNOWLEDGEMENTS

Numerous people have helped me considerably in preparing this thesis but most of all I thank my wife, Mary, for the moral support, typing, drafting, errand running, proof-reading, and still loving me through it all.

My supervisor and mentor, Jim Hall, kindly supported me in my research and provided much impetus and direction.

My supervisory committee of Marcos Zentilli, Gunter Muecke and Paul Robinson kept me on the right road with well-placed criticisms and assistance on various matters.

Jim Hall, Paul Robinson, Paul Schenk and the Bermudian Government, through John Shand, provided the funding for the drilling project.

John Shand, Chief Engineer, Mark Rowe, Geologist, and Vince Robinson, customs and general logistics wizard, all of the Bermuda Department of Public Works, gave much of their time and logistical support to the project.

I thank the Bermuda Government for permission to drill in the Government Quarry at Bailey Bay. Lieutenant Commander John Duke, Chief Petty Officer Saundry and the personnel at the United States Naval Air Station Annex in Southampton willingly and patiently supported the drilling at George's Bay.

Wolfgang Sterrer, Director of the Bermuda Biological Station, Margaret Emmott and all the other people at the station helped to make the expedition both scientifically and personally rewarding and enjoyable.

Rejean Clement of Bradley Brothers Ltd. of Noranda, Quebec ran the drill rig and supervised all the real aspects of drilling.

Gordon Brown made all my high quality thin-sections.

Bob MacKay helped me on numerous occasions with the microprobe studies.

Si Parikh analyzed my whole-rock powders in his wet-chemical lab.

This thesis was funded in part by a graduate fellowship from Dalhousie University and from funds from the Department of Geology.

I have enjoyed working with my fellow students who have contributed to my research in various ways and they certainly have made the working atmosphere more pleasant.

Finally, I give special thanks to Charles (Charlie) Walls, Geophysics Technician, chief engineer of the Curie balance and general all around nice guy to work with, and Pat Ryall, who deserves to have his name mentioned in partial payment for all of his time I've helped him to waste.

CHAPTER 1

PREVIOUS STUDIES

Introduction

The islands of Bermuda lie on top of the only volcanic island in the northwestern Atlantic Ocean. The island is made up of a linear series of three smaller peaks and one main peak which run from north to south (Figure 1-1). Its location on the Bermuda Rise does not seem to bear any relationship to regional seamount trends (i.e. New England Seamounts). The islands are covered by a sequence of Pleistocene reef and reef-derived sedimentary rocks up to 150 metres thick (shallow marine to sub-aerial carbonates, paleosols, and corals): there are no outcrops of volcanic rock (Schenk, 1973; Land et al., 1967).

This thesis has two purposes. The first is to describe some newly collected submarine melilite bearing extrusives and related intrusives. The petrography and mineralogy of these rocks are described, geochemical analyses are presented, and possible genetic origins are discussed. The second purpose is to examine the geological and geophysical nature of the Bermuda Rise in order to trace the development of the rise and the possible contemporaneous evolution of the Bermuda volcanic island.

Geological

Other than the occurrence of heavy black sands on the beach at Whalebone Bay and some small volcanic-rock pebbles in the paleosols, little was known of the volcanic nature of the islands until the advent of deep drilling. Pirsson (1914) described volcanic rocks which were

Figure 1-1. The location of the Bermuda Seamount and Rise in the northwestern Atlantic. Compiled from many sources. The Bermuda Rise is outlined in a dotted line. The more pronounced magnetic anomalies, M-25, M-16, M-4 and M-0 are shown in heavy lines, dashed where correlations are uncertain. DSDP sites on, or near, the Rise are marked with diamonds.

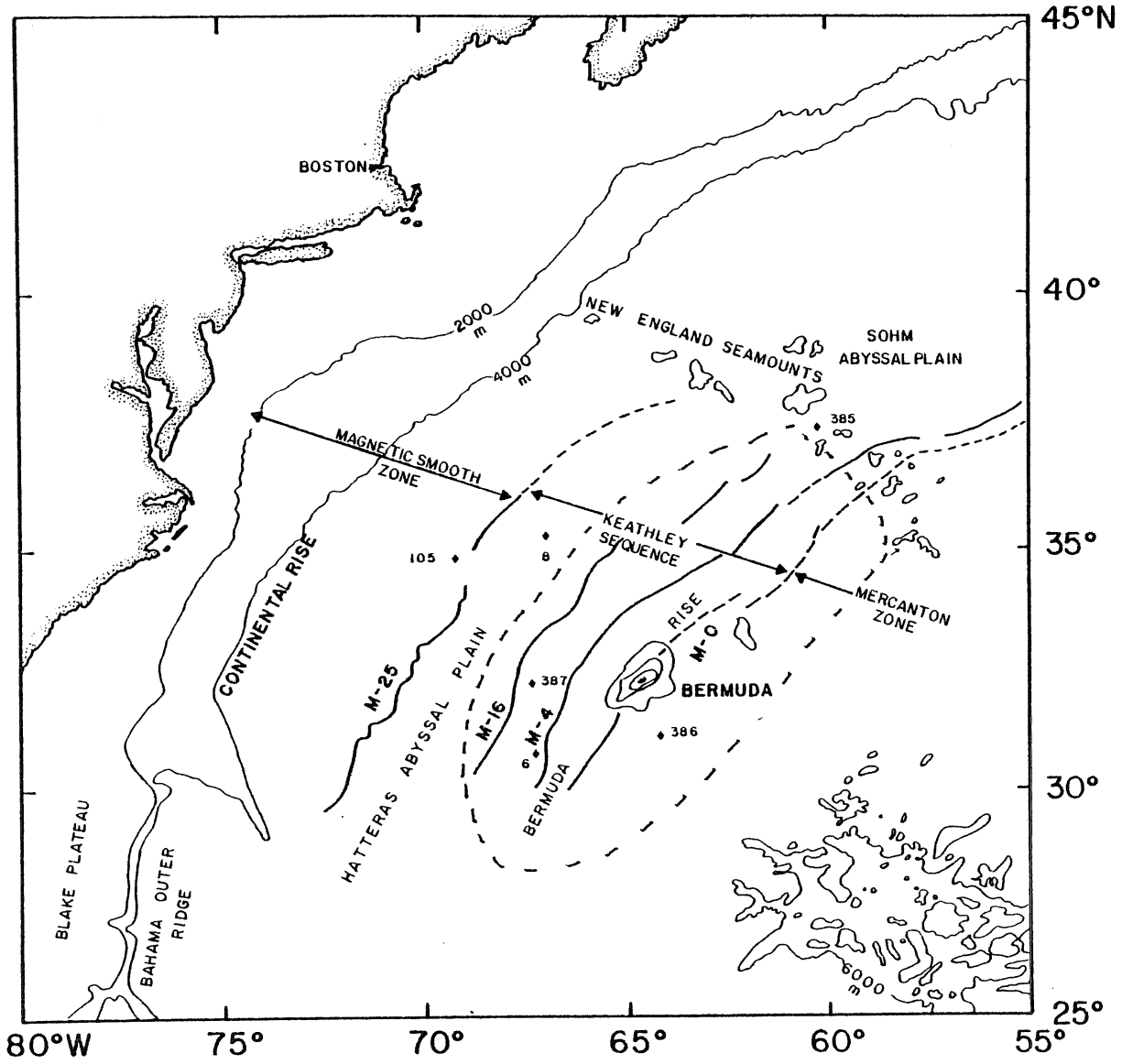
45°N
40°
35°
30°
25°
80°W
75°
70°
65°
60°
55°
BOSTON
2000 m
4000 m
NEW ENGLAND SEAMOUNTS
SOHM ABYSSAL PLAIN
385
MAGNETIC SMOOTH ZONE
KEATHLEY SEQUENCE
MERCANTON ZONE
105
8
1
CONTINENTAL RISE
M-25
M-16
M-4
M-0
HATTERAS ABYSSAL PLAIN
BERMUDA RISE
BERMUDA
387
386
6
10
BLAKE PLATEAU
BAHAMA OUTER RIDGE
6000 m

recovered from a 430-meter-deep churn-drill hole. This hole was located on the grounds of the Princess Hotel, approximately 1.6 kilometers to the east of the Gibb's Hill Lighthouse (Figure 1-2). This hole intersected volcanogenic sediments and some possible tuff at 100 meters below sea-level and unweathered volcanic rocks at 115 meters below sea-level (Figure 1-3).

Pirsson (1914) reported the presence of three distinct lithologies in the volcanic section: basalt, lamprophyre, and keratophyre. Sample modes of these units are shown in Table 1-1. The basalt (melilite-basalt) samples have mineralogies which suggest a physical mixture of altered oceanic tholeiite and a silica-undersaturated rock (melilite-bearing ultramafic volcanic rock). The lamprophyre is most akin to monchiquite and was called 'Bermudite' by Pirsson. The keratophyre was found in the upper part of the volcanic section (140-145 meters below sea-level) in the weathered basalts and consists of albite and microperthite with minor biotite and apatite. The occurrence of this unit is not unique since a similar lithology has been found in the Azores by Schmincke and Staudigel (1976). A representative chemical analysis of an aggregate sample from the unweathered volcanic rocks is shown in Table 1-1.

In 1958, a hole was drilled by the percussion method near the Ferry Reach causeway (Figure 1-2). Dark sands of obvious volcanogenic origin were found interbedded with some sedimentary units. Basalt was encountered after penetrating about 35 meters of sedimentary rocks (Gees, 1969).

Figure 1-2. The location of the drill-holes which penetrated the volcanic basement (hole-1980b is shown for reference only).

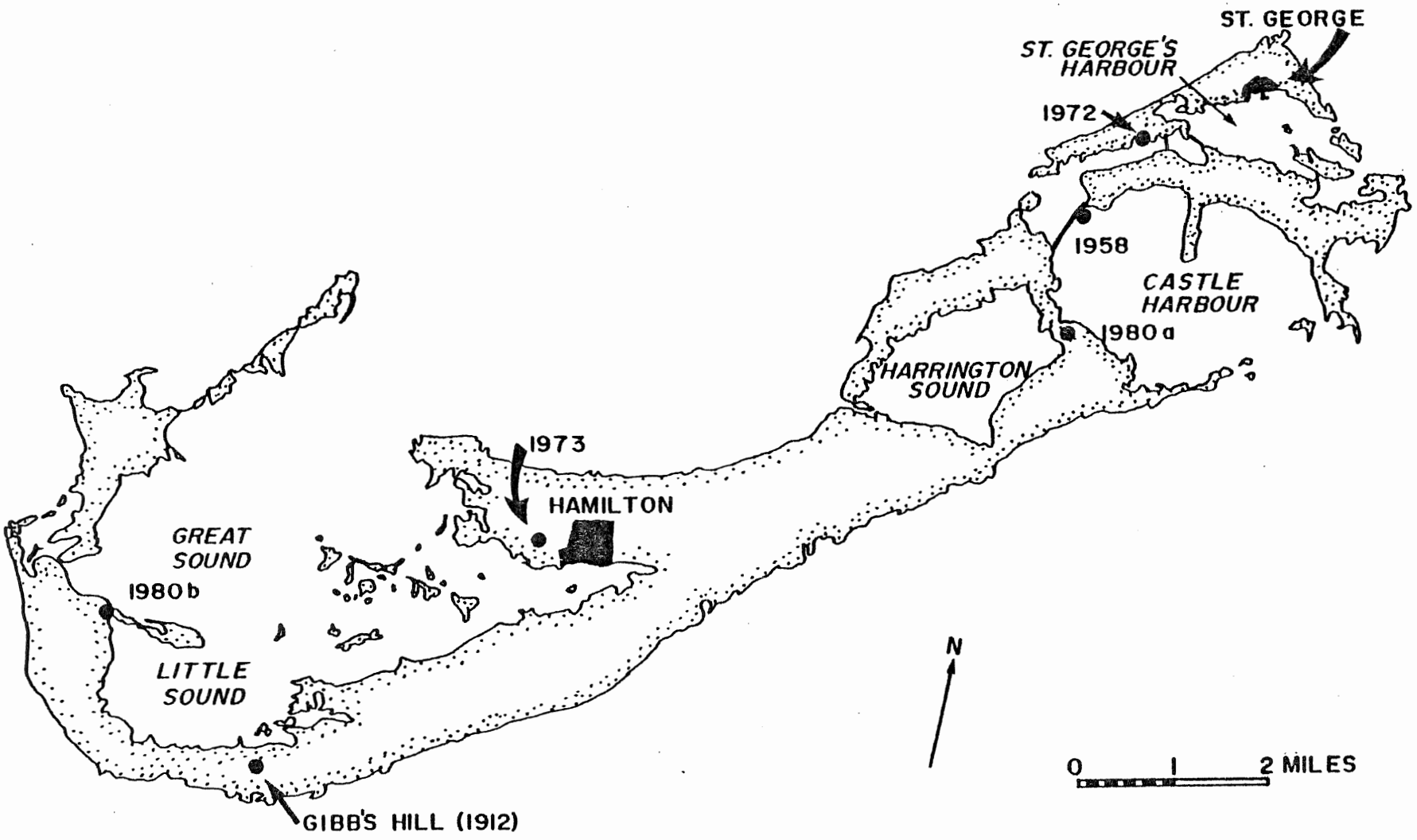
ST. GEORGE
ST. GEORGE'S HARBOUR
1972
1958
CASTLE HARBOUR
1980a
HARRINGTON SOUND
1973
HAMILTON
GREAT SOUND
1980b
LITTLE SOUND
GIBB'S HILL (1912)
N
0 1 2 MILES

Table 1-1

MODES OF THE 1912 LITHOLOGIES

Unit	Melilite Basalt	Lamprophyre	Keratophyre
Pyroxene	35	75	-
Biotite	-	-	20?
Olivine	5	-	-
Melilite	35	-	-
Analcite	15	-	-
Feldspar	-	-	60?
Apatite	2	-	20?
Iron Ore	8	-	-
Perovskite	-	tr	-
Calcite	-	tr	-
Total	100	100	100

* * * * * * *

Whole-rock chemical analysis of sample from 338.3 meters (Pirsson, 1914).

SiO_2	38.79
TiO_2	0.80
Al_2O_3	14.55
Cr_2O_3	---
Fe_2O_3	5.67
FeO	6.68
MgO	7.78
CaO	14.65
Na_2O	2.78
K_2O	2.54
CO_2	3.56
H_2O^+	1.99
H_2O^-	0.67
Total	100.46

Norms	No Calcite	With Calcite
Or	---	6,12
An	19.46	19.46
Ne	12.78	12.78
Lc	11.77	6.98
Di	16.46	24.68
Ol	13.80	9.97
Am	10.37	---
Mt	8.35	8.35
Il	---	1.52
Pf	1.36	---
H_2O	2.66	2.66
CO_2	3.56	---
Cc	---	8.08
Total	98.57	100.30

Figure 1-3. Schematic core log for the 1912 drill-hole near Gibbs Hill Lighthouse (from Pirsson, 1912).

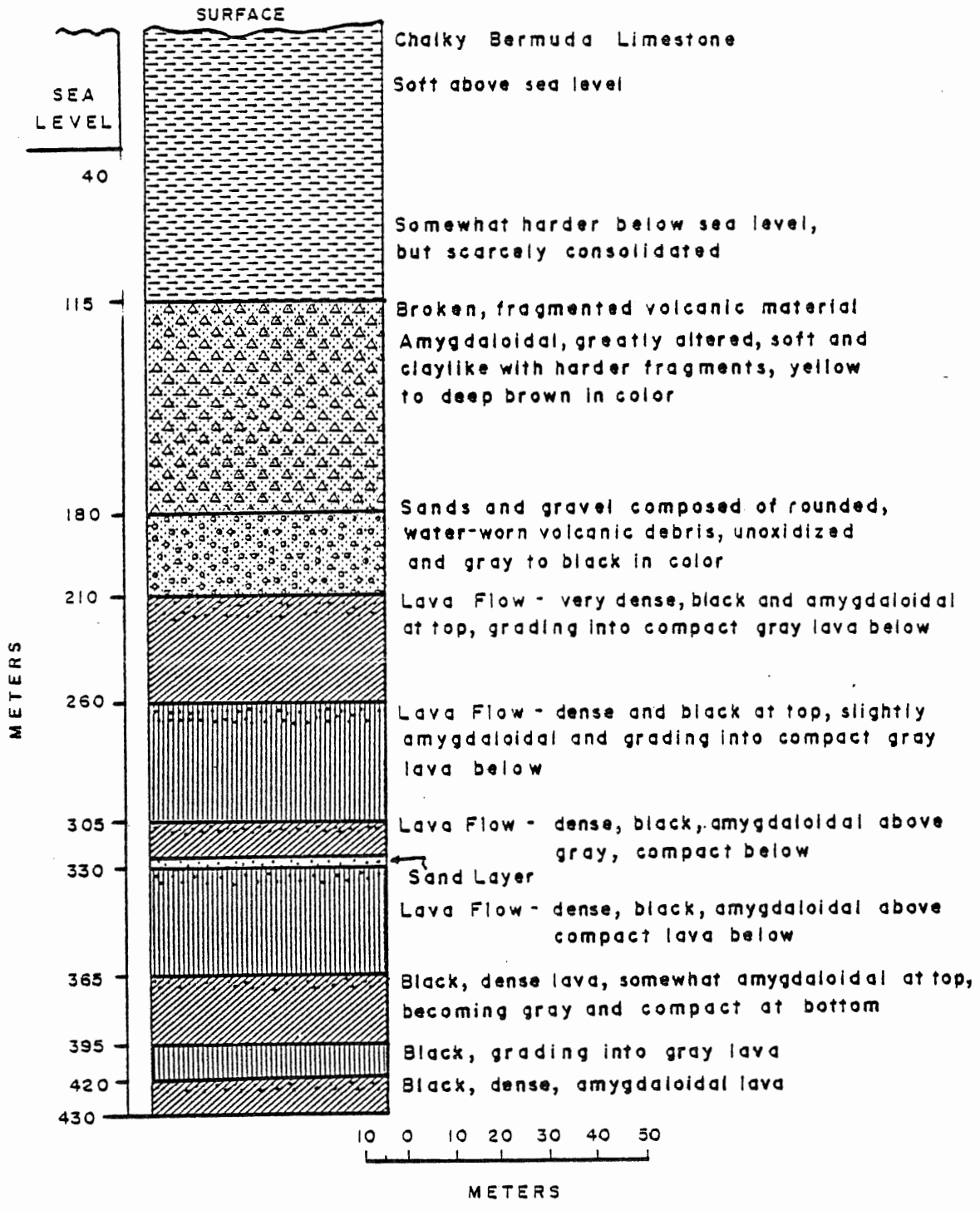
SURFACE
SEA LEVEL
40
115
180
210
260
305
330
365
395
420
430
METERS
Chalky Bermuda Limestone
Soft above sea level
Somewhat harder below sea level, but scarcely consolidated
Broken, fragmented volcanic material
Amygdaloidal, greatly altered, soft and claylike with harder fragments, yellow to deep brown in color
Sands and gravel composed of rounded, water-worn volcanic debris, unoxidized and gray to black in color
Lava Flow - very dense, black and amygdaloidal at top, grading into compact gray lava below
Lava Flow - dense and black at top, slightly amygdaloidal and grading into compact gray lava below
Lava Flow - dense, black, amygdaloidal above gray, compact below
Sand Layer
Lava Flow - dense, black, amygdaloidal above compact lava below
Black, dense lava, somewhat amygdaloidal at top, becoming gray and compact at bottom
Black, grading into gray lava
Black, dense, amygdaloidal lava
10 0 10 20 30 40 50
METERS

A recent investigation termed Deep Drill-1972 (Aumento et al., 1975), was conducted by a team from Dalhousie University and the Lamont-Doherty Geological Observatory. This project resulted in a continuously cored 802-meter-deep hole sited on the grounds of the Biological Station (Figure 1-2). The core from this hole has yielded much interesting data. Beneath 35.4 meters of sedimentary cover, there are over 900 volcanic cooling units (pillowed lavas and sheeted intrusives). The igneous rocks are strikingly bimodal in several respects and consist of a succession of very altered submarine basalts, probably tholeiites, which is intruded by sheets of lamprophyric affinities. Nearly 40 percent of the core consists of sheets which were intruded preferentially between the lavas in the pillow zones.

A detailed core log can be found in the map pocket (Plate 1). Aumento and Gunn (unpublished data) subdivided the two lithologies on the basis of their petrography. The lavas were divided into four categories: (1) non-porphyritic pillowed, (2) non-porphyritic variolitic (the most common type), (3) non-porphyritic variolitic with interstitial clinopyroxene and, (4) olivine (altered) phyric. The dikes were divided into seven categories: (1) non-porphyritic aphanitic (very altered), (2) non-porphyritic with recognizable crystals in the groundmass, (3) porphyritic with about 20 percent clinopyroxene phenocrysts (rare), (4) porphyritic with about 50 percent clinopyroxene and about 10 percent pseudomorphed olivine phenocrysts, (5) porphyritic with about 40 percent clinopyroxene or olivine phenocrysts, (6) porphyritic with olivine phenocrysts (up to 20 percent calcite pseudomorphs), and (7) diabasic with large plagioclase laths and interstitial clinopyroxenes (uncommon).

The groundmass of the lavas and sheets consists of chlorite, clay minerals, calcite, and titanomagnetite. Microlites of altered plagioclase (<0.5mm) and clinopyroxene are common. In the sheets, the groundmass consists of the same minerals mentioned above plus the common addition of biotite. The phenocrysts in the sheets are either concentrically zoned titan-augites or calcite+chlorite pseudomorphs of olivine. The pyroxenes are most interesting. They are very titanium rich, with an increase in atomic titanium from core to rim (D. Plasse, pers. comm., 1980). The only other documented occurrences of such high titanium augites (average percentage TiO_2 = 4.0-6.0%) are from lunar pyroxenes, the Allende meteorite, and the island of Tahiti (Tracey and Robinson, 1977).

Representative whole-rock chemical analyses of the lavas and sheets are shown in Table 1-2. The average composition of the lavas differs from the average ocean ridge tholeiitic basalt in several elements. The lavas have lower percentages of SiO_2, Al_2O_3, and possibly MgO and higher percentages of Na_2O, K_2O and H_2O. This enrichment in alkali elements and loss of SiO_2, Al_2O_3 and MgO is typically found in altered basalts due to chemical interaction with sea water to form spilites (Aumento et al., 1976). The sheets, however, are very unusual, being very silica-undersaturated, alkaline, and titanium-rich with lamprophyric affinities.

In 1973, Island Engineering Association, Ltd. of Hamilton, Bermuda sank a 55-meter-deep rotary drill hole. This hole was sited at the intersection of Rosemount Avenue and Serpentine Road, just outside of Hamilton (Figure 1-2). Rock chips collected from this hole indicate a volcanic basement at 46.9 to 55.5 meters subsurface.

The volcanic rocks from this hole are possibly porphyritic lamprophyres. On the basis of the few sections observed the typical mineralogy is: phenocrysts (10-20 percent) of biotite (concentrically zoned with titanium enriched rims), and a groundmass of spinel (15 percent), apatite (5 percent), clinopyroxene (1-2 percent), altered glassy material and unidentified microlites (53 percent). Calcite+analcite veins are common and biotite is often altered to chlorite. In one sample (B2-169) a clinopyroxene (5mm) poikilitically encloses biotite and spinel and is in turn rimmed by biotite.

Recent deep-sea drilling (DSDP-IPOD, Leg 43) on the Bermuda Rise suggests that the lamprophyric intrusives were the source of a major sedimentary horizon. At DSDP Site 386, to the south-east of the Bermuda Islands (Figure 1-1), a thick volcanogenic-sand turbidite was found interbedded with other upper- to middle-Oligocene sedimentary rocks (Tulcholke et al., 1979). The heavy minerals in these turbidites are: clinopyroxene (81 percent), apatite (10 percent), hornblende, epidote, and garnet (2-3 percent each), as well as small amounts of biotite and unidentified opaque minerals (Galehouse, 1979). All of these minerals have been found in the rocks on Bermuda (i.e. in the paleosols), and all but the hornblende and garnet have been identified in the known igneous rocks. These turbidites are very strong sonic reflectors and can be traced right up to the foot of the Bermuda Seamount on seismic reflection profiles (Tucholke et al., 1979).

A preliminary analysis of the alteration mineralogy of the 1972 core indicates a weakly defined vertical zonation of secondary minerals, which is correlative with color. The basalts vary in color from

Table 1-2

AVERAGE CHEMICAL COMPOSITION AND NORMS OF DEEP DRILL-1972 SAMPLES FROM AUMENTO AND GUNN (UNPUBLISHED)

	Lavas	All Sheets	Non-Porphyritic Sheets	Porphyritic Sheets	Average Oceanic Ridge Tholeiite[c]
SiO_2	48.16	38.32	39.71	38.49	49.14
TiO_2	1.31	4.63	4.95	4.54	1.17
Al_2O_3	14.16	10.94	11.50	10.21	15.64
Fe_2O_3[a]	8.61	12.78	12.93	13.02	9.14[d]
MaO	0.16	0.20	0.20	0.20	0.16
MgO	5.53	6.82	6.13	7.86	8.22
CaO	11.45	13.93	13.31	14.86	11.84
Na_2O	3.81	2.23	2.54	1.69	2.40
K_2O	0.66	2.05	2.23	2.09	0.20
P_2O_5	0.16	0.69	0.77	0.69	0.12
S	0.07	0.25	0.30	0.23	0.04
H_2O[b]	2.72	2.67	2.99	2.43	1.09
CO_2	3.21	4.48	5.14	3.72	n.d.[e]
Total	100.01	99.99	102.70	100.03	99.16
Q	0.46	0	0	0	0
OR	4.05	12.64	13.44	12.83	1.20
AB	33.45	15.41	21.86	8.32	20.66
AN	20.33	14.37	13.67	14.68	31.87
NE	0	2.31	0	3.54	0
DI	13.31	18.71	12.35	26.21	21.83
HY	14.47	0	0.48	0.78	15.50
OL	0	9.74	9.84	8.84	2.36
MT	3.23	4.84	4.77	4.91	3.90
IL	2.58	9.17	9.58	8.96	2.26
AP	0.38	1.67	1.80	1.67	0.28
CC	7.58	10.62	11.90	8.79	0
Total	99.85	99.46	99.69	99.53	99.92

Notes:

a = Total Fe as Fe_2O_3
b = Total H_2O
c = From Wedepohl (1981)
d = Total Fe as FeO
e = n.d. - not determined

reddish-gray at the top of the section, to green at the base with a gradual transition between the two colors. The major alteration assemblage is chlorite+calcite+clay (smectite) with the addition of epidote+quartz in the lower two-thirds of the core (below 260 meters). Albite+analcite is found in several veins throughout the core. The sheets are less altered than the flows, but there is pervasive chloritization of the groundmass. The sheets contain a large amount of calcite (10-15 percent by volume) in veins, amygdules and as pseudomorphs of calcite. The total absence of zeolite minerals (often found in altered volcanic rocks) and the common occurrence of calcite-clay assemblages indicate low to moderate temperature hydrothermal alteration with high CO_2 activity in the fluid (Thompson, 1971; Ivanov and Gurevich, 1975).

Geophysical

There have been several geophysical investigations of the Bermuda Islands. The first on record was performed by Cole (1908). He examined local magnetic field anomalies in the declination and the vertical components. Numerous local anomalies were defined and the compiled data are shown in Figure 1-4.

Officer et al. (1952) studied the crustal structure of the islands and surrounding Bermuda Rise using seismic refraction techniques. In the region to the west of St. George's Island the sediment (± volcanics) thickness ranges from 35 to 96 meters, with basement velocities ranging from 5.13 to 5.34 kilometers second^{-1}. An interpretive cross-section of the upper volcanic platform for the whole island is given in Figure 1-5.

Figure 1-4. Isogonic chart for the Bermuda Islands. Contours are in degrees (Cole, 1908).

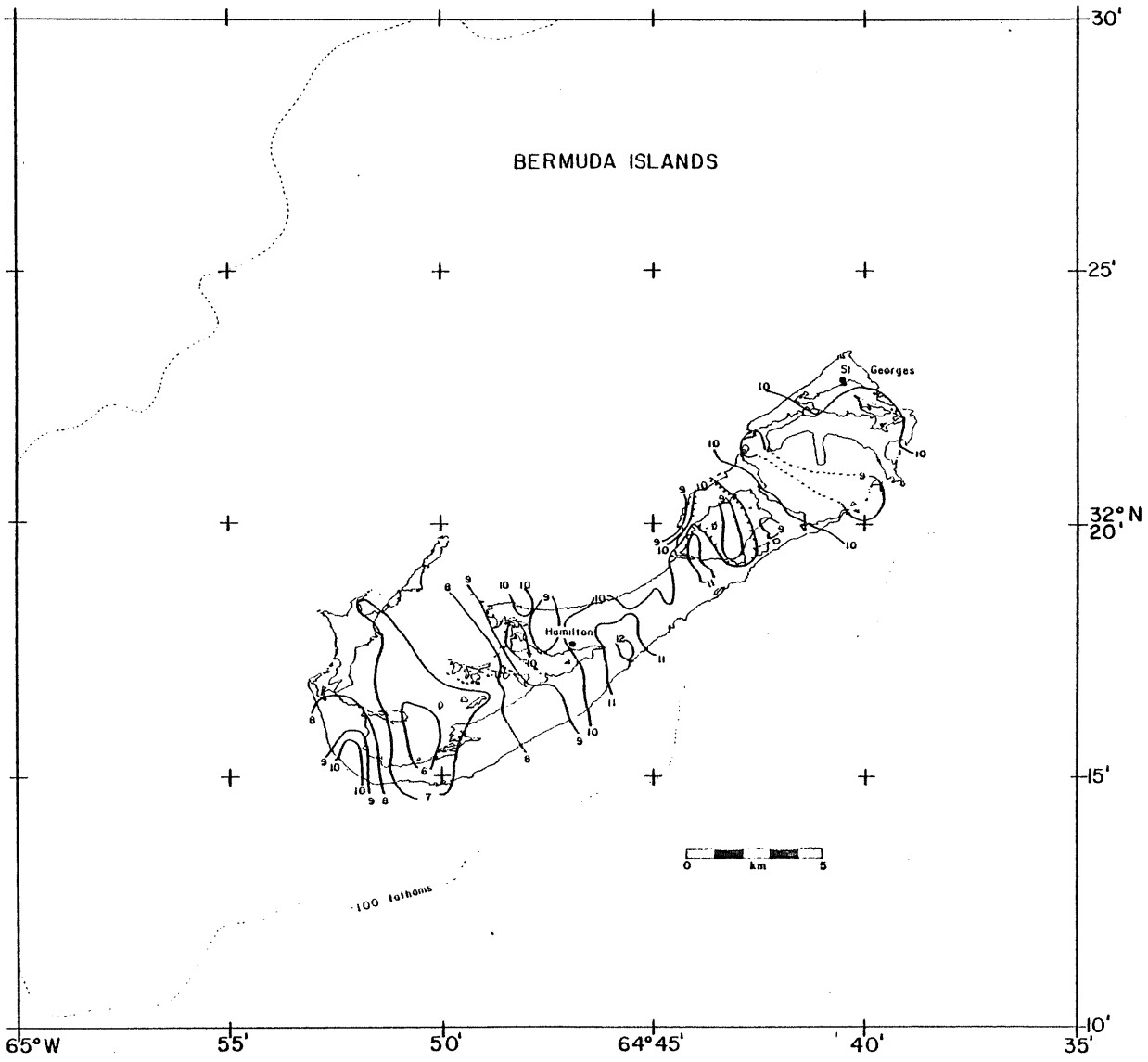
BERMUDA ISLANDS
30'
25'
32° N
20'
15'
10'
65°W
55'
50'
64°45'
40'
35'
St Georges
Hamilton
0 km 5
100 fathoms

Figure 1-5. Interpretative cross-section of the top of the seamount from seismic profiles (Officer et al., 1952).

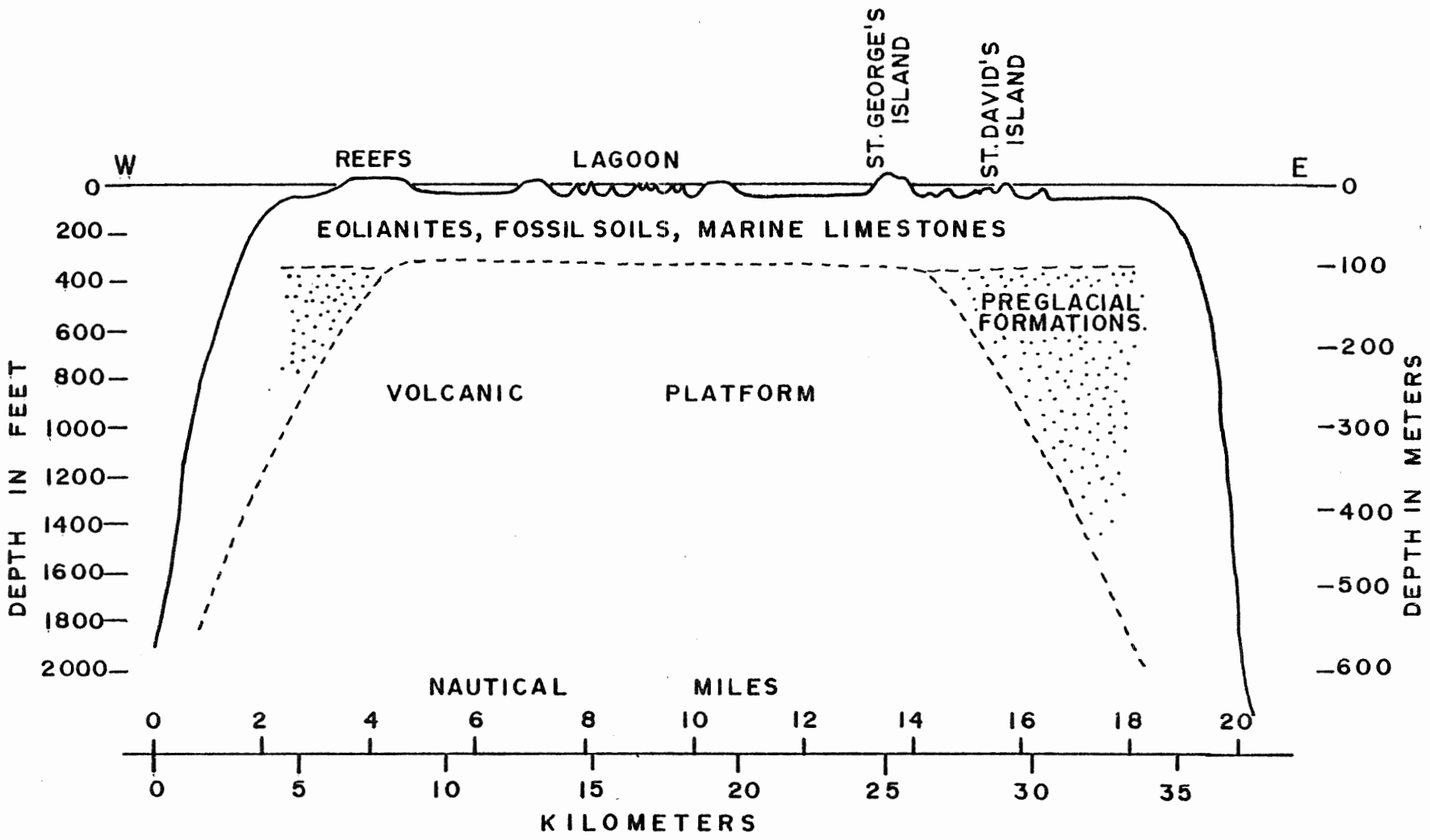
W
REEFS
LAGOON
ST. GEORGE'S ISLAND
ST. DAVID'S ISLAND
E
0
EOLIANITES, FOSSIL SOILS, MARINE LIMESTONES
PREGLACIAL FORMATIONS.
VOLCANIC
PLATFORM
DEPTH IN FEET
200
400
600
800
1000
1200
1400
1600
1800
2000
DEPTH IN METERS
-100
-200
-300
-400
-500
-600
NAUTICAL MILES
0 2 4 6 8 10 12 14 16 18 20
0 5 10 15 20 25 30 35
KILOMETERS

Press and Ewing (1952) computed a theoretical magnetic profile over the seamount based upon induction from the present field. The theoretical anomalous field is shown in Figure 1-6. The parameters used to calculate this anomaly are (for the main field): vertical intensity = 47,000γ, horizontal intensity = 23,000γ, inclination = 64°, and susceptibility = 0.01 cgs units. The average anomaly predicted is nearly 300γ with a range from -400γ on the north flank to nearly +700γ along the southern rim of the island.

Keller et al. (1954) produced six aeromagnetic profiles across the Bermuda Islands. These data are shown in Figure 1-7. The islands are characterized by strong local anomalies (mainly positive but some negative) with total field intensities up to 5000γ. The flight parallel to the theoretical profile of Press and Ewing (1952) shows poor agreement between the predicted and the real anomaly.

Woollard (1954) summarized all previous geophysical investigations of Bermuda. He also made gravity measurements from 68 terrestrial stations and produced a Bouguer anomaly map of Bermuda. A pronounced local residual anomaly of +55 milligals is centered over Great Sound. This area also shows a negative magnetic anomaly and the combination of the anomalies is interpreted as indicating the presence of a volcanic plug.

A detailed aeromagnetic survey of Plantagenet Bank at altitudes ranging from 1.8 to 6.1 kilometers, 45 kilometers southwest of Bermuda was reported by Young and Kontis (1964). The average main field orientation and intensity were found to be: total intensity = 51,280γ, inclination = 65°, declination = 13.8° west. The amplitude of the

Figure 1-6. Theoretical magnetic anomaly for the seamount (Press and Ewing, 1952).

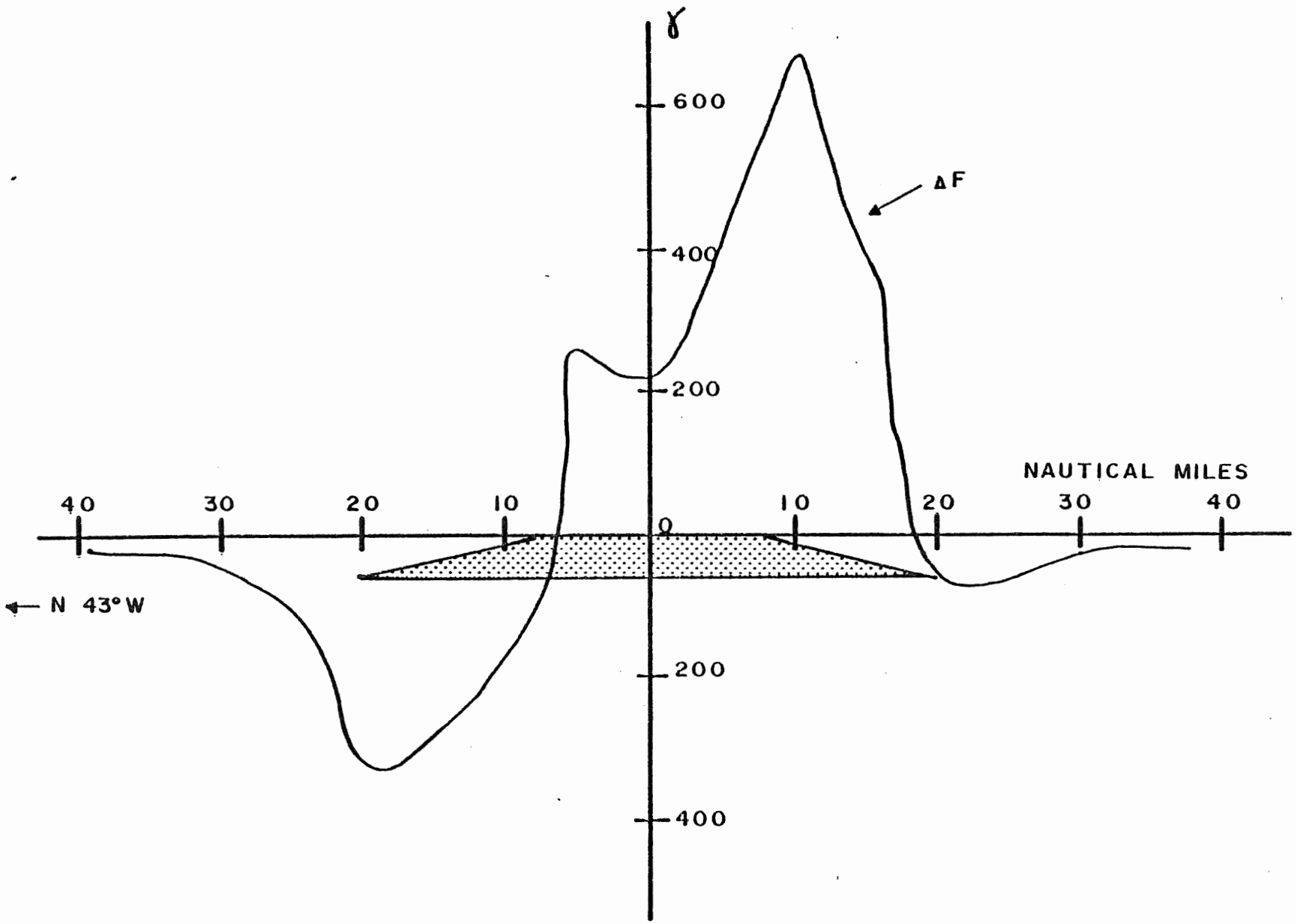
γ
600
400
200
ΔF
NAUTICAL MILES
40
30
20
10
0
10
20
30
40
N 43°W
200
400

Figure 1-7. Aeromagnetic profiles over the seamount. Notice the poor match between profile 4 and the theoretical anomaly in Figure 1-6 (Keller et al., 1954).

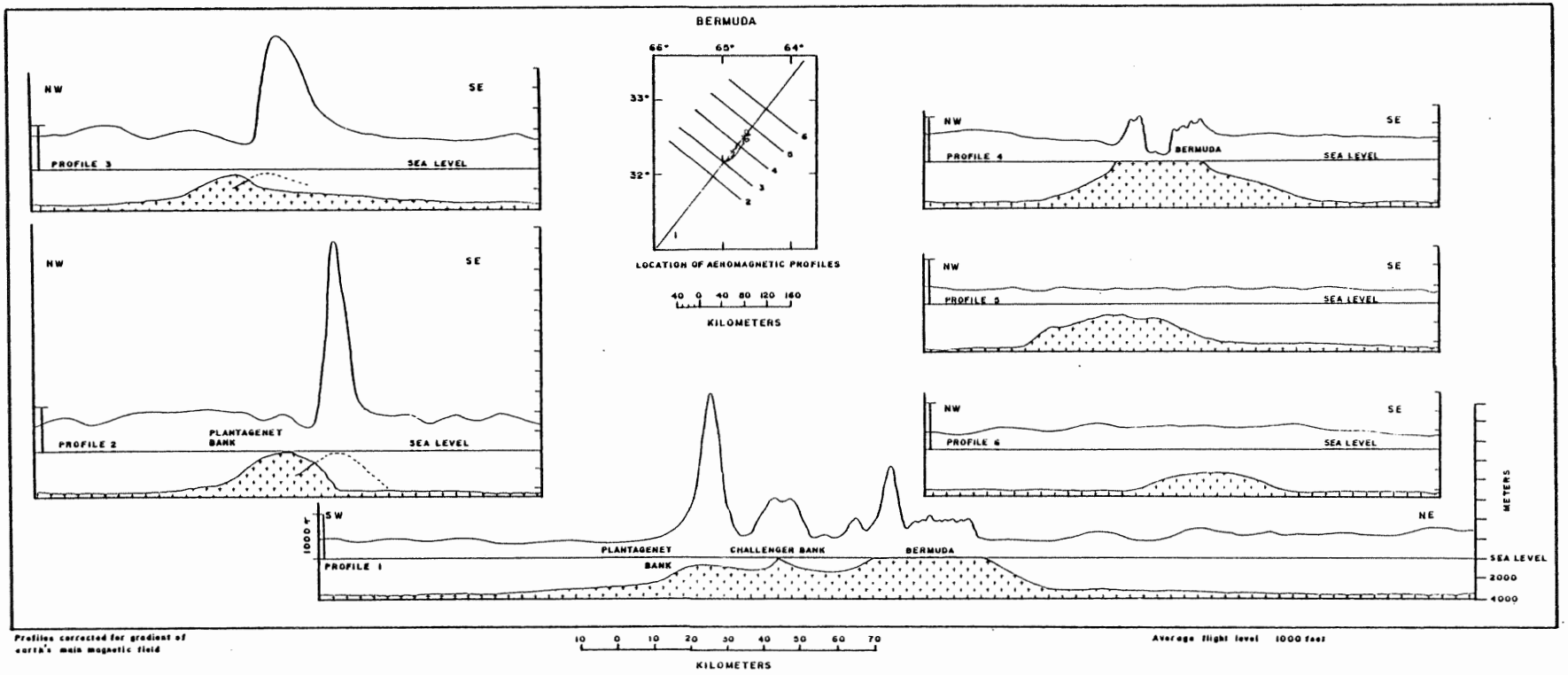
BERMUDA
NW
SE
PROFILE 3
SEA LEVEL
NW
SE
PROFILE 2
PLANTAGENET BANK
SEA LEVEL
66°
65°
64°
33°
32°
1
2
3
4
5
6
LOCATION OF AEROMAGNETIC PROFILES
40 0 40 80 120 160
KILOMETERS
NW
SE
PROFILE 4
BERMUDA
SEA LEVEL
NW
SE
PROFILE 5
SEA LEVEL
NW
SE
PROFILE 6
SEA LEVEL
SW
NE
PROFILE 1
PLANTAGENET BANK
CHALLENGER BANK
BERMUDA
1000 ft
METERS
SEA LEVEL
2000
4000
Profiles corrected for gradient of earth's main magnetic field
10 0 10 20 30 40 50 60 70
KILOMETERS
Average flight level 1000 feet

anomaly is nearly 4200γ. The best fit interpretation of the anomaly is given in Figure 1-8.

Stuart (1969) made a detailed gravity survey with 212 land and sea based stations. These data were reduced using detailed density measurements of the sedimentary rocks and an approximation of the density of the volcanic rocks. The resultant anomaly is nearly identical to that of Woollard (1954) and is shown in Figure 1-9.

Gees and Medioli (1969) carried out a detailed seismic reflection profile in Castle Harbour. The depth to volcanic basement below sea-level varies from 30 meters near Ferry Reach to 100 meters in the center of the harbour. Interpretive cross-sections are given in Figure 1-10.

The heat flow and physical properties of the Deep Drill-1972 units were studied by several investigators. Hyndman and Aumento (1973) calculated a corrected heat flux of 1.1 microcalories centimeter^{-2} second^{-1}. This value is nearly equal to old stable ocean crust and indicates a low radioactive heat production for the igneous rocks. Hall et al. (1973) measured the paleomagnetic inclinations of all the major lava units. The magnetic properties are complex and variable, but the stable inclinations can be subdivided into two groups which are not antiparallel: -42^{o} and $+21^{o}$. Barrett et al. (1973) measured the elastic wave seismic properties of the rocks. Compressional wave velocities of the basalts were found to be nearly identical to typical layer 2 values (6 km s^{-1}) at pressures up to 2.5 kilobars. The velocities of the sheets were found to be as high or higher than those of layer 3 (6.9 km s^{-1}).

Figure 1-8. Measured magnetic anomalies over Plantagenet Bank and two interpretive models (Young and Kontis, 1964).

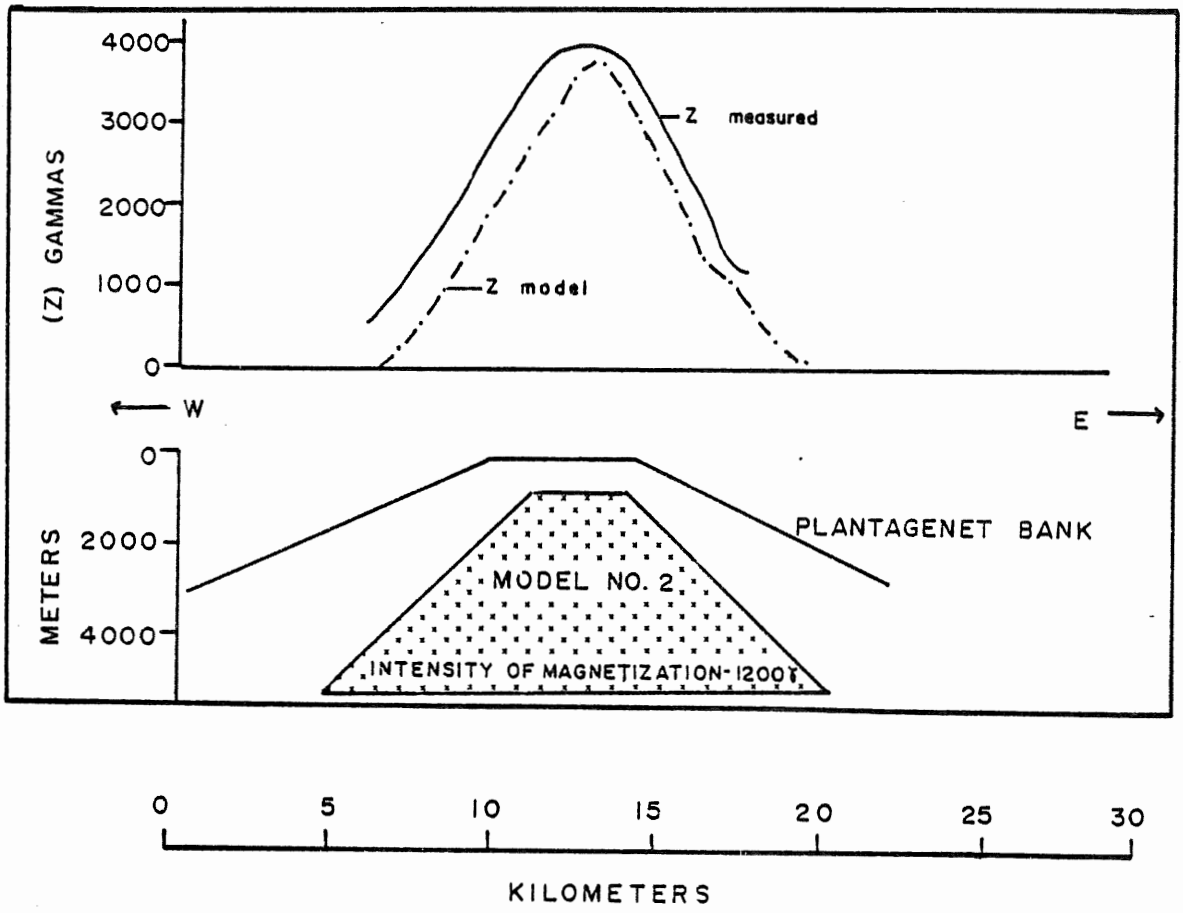
4000
3000
2000
1000
0
(Z) GAMMAS
Z measured
Z model
W
E
0
2000
4000
METERS
PLANTAGENET BANK
MODEL NO. 2
INTENSITY OF MAGNETIZATION-1200γ

0
5
10
15
20
25
30
KILOMETERS

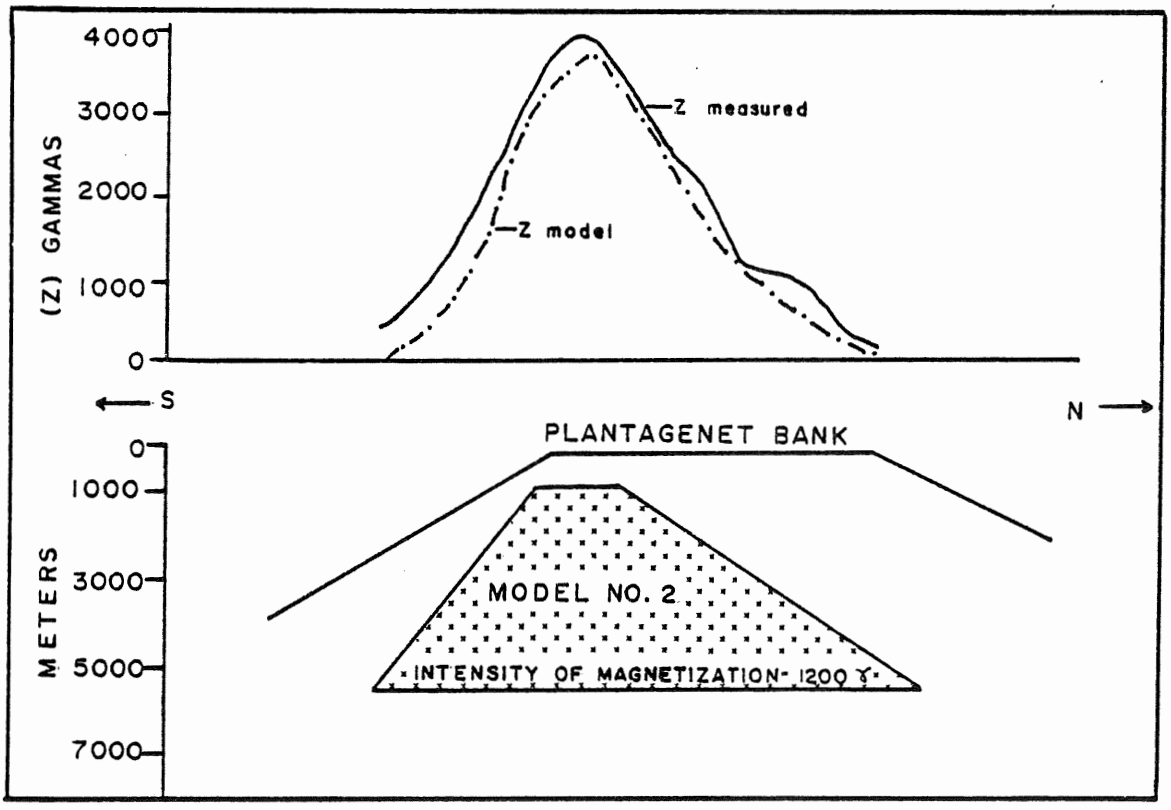
4000
3000
2000
1000
0
(Z) GAMMAS
Z measured
Z model
S
N
0
1000
3000
5000
7000
METERS
PLANTAGENET BANK
MODEL NO. 2
INTENSITY OF MAGNETIZATION-1200γ

Figure 1-9. Bouguer anomaly gravity map of the seamount based on studies by Woollard (1954) and Stuart (1969). Contours are in milligals.

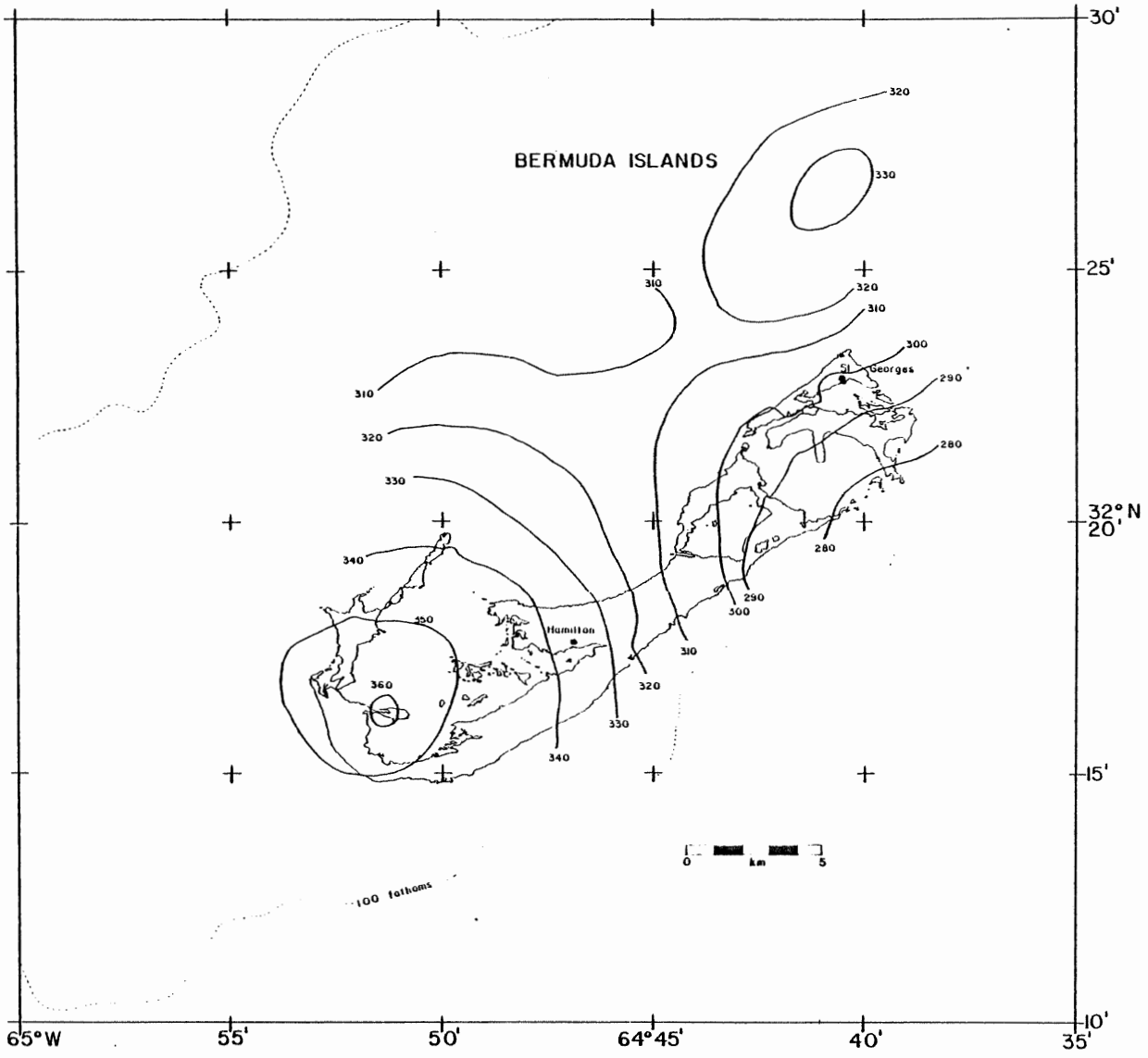
BERMUDA ISLANDS
320
330
310
320
310
310
300
St Georges
290
320
280
330
340
280
290
300
450
Hamilton
310
320
360
330
340
0
km
5
100 fathoms
30'
25'
32° N
20'
15'
10'
65° W
55'
50'
64° 45'
40'
35'

Figure 1-10. Interpretive seismic reflection profiles of Castle Harbour (Gees and Medioli, 1969).

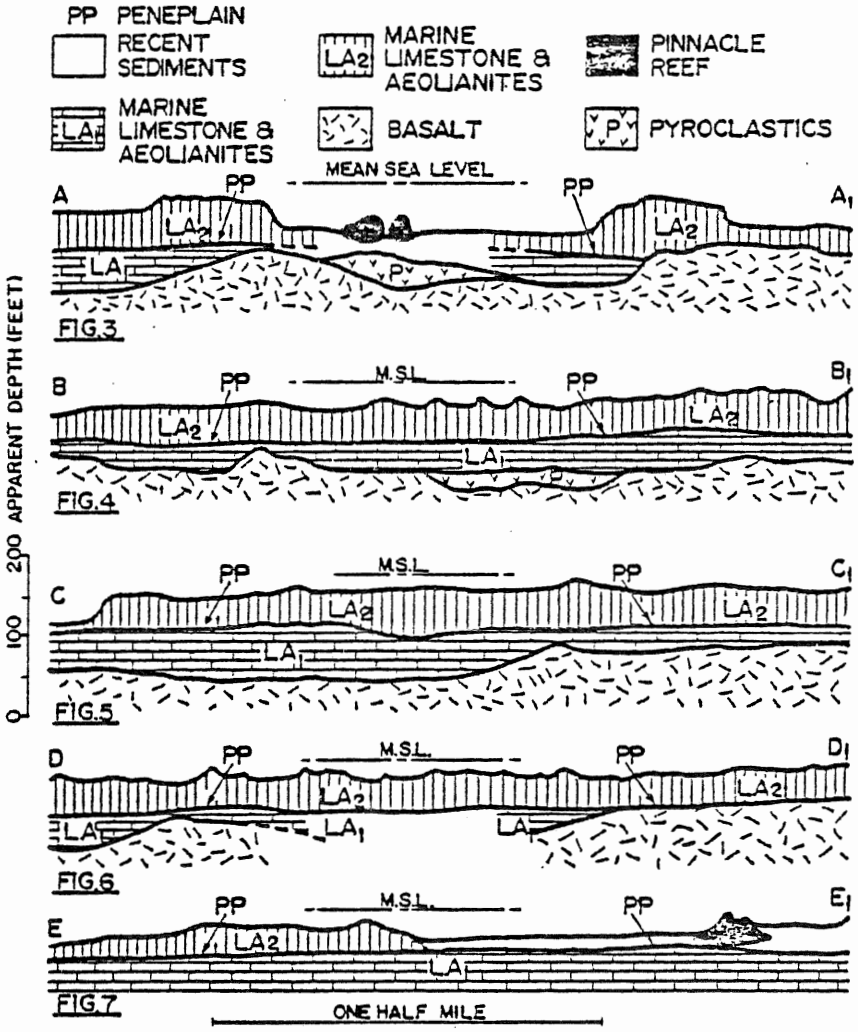

- Castle Harbour – Simplified geological cross sections based on the data of the seismic survey.

Hyndman et al. (1979) describe the physical properties of the 1972 core in much greater detail. The data are not different from the preliminary findings mentioned above and are summarized in Table 1-3. In general the sheets are denser and more electrically conductive than the lavas, although the compressional velocities are similar.

Rice (1977) and Rice et al. (1980) re-examined the magnetic properties of the 1972 core. Statistically, the lavas are progressively more intensely magnetized as the percentage of sheets in any sample zone increases. In addition, as the percentage of sheets approaches 100 percent, the stable inclination of the lavas (which averages -40^{o} where dikes are absent) approaches that of the sheets ($+21^{o}$).

Radiometric Ages

Gees (1969) obtained radiometric ages from basaltic chips from the 1912 and Ferry Reach holes using the K-Ar technique. The resulting ages respectively, are 34.4±3.0 Ma and 52.2±2.5 Ma years. A detailed investigation of the K-Ar ages for the 1972 core was reported by Reynolds and Aumento (1974). The basalts, due to their altered state yielded poorly confined ages ranging from 50 to 100 Ma. The sheets yielded a more confined age, averaging about 33 Ma. Interestingly, the volcanic-sand turbidites from the immediate area of Bermuda are of Oligocene age (30-35 Ma). The lithologic compositions and ages suggest that the sheets are part of a major Oligocene volcanic event centered on Bermuda.

Table 1-3

PHYSICAL PROPERTIES OF THE DEEP DRILL-1972 ROCKS
(HYNDMAN ET AL., 1979)

Physical Properties of Samples from Bermuda

Property	Lava Flows		Lamprophyric Sheets		All Samples	
	Number	Mean	Number	Mean	Number	Mean
Compressional velocity (0.4 kbar) km s^{-1} (Vp)	12	5.97 ± 0.03	8	5.89 ± 0.07	20	5.94 ± 0.05
Shear velocity (0.4 kbar) km s^{-1} Vs)	12	3.22 ± 0.06	8	3.07 ± 0.05	20	3.16 ± 0.04
Poisson's ratio (σ)	12	0.295 ± 0.003	8	0.314 ± 0.006	20	0.303 ± 0.004
Bulk density, g cm^{-3}	27	2.79 ± 0.01	16	2.90 ± 0.003	43	2.83 ± 0.02
Grain density, g cm^{-3}	17	2.81 ± 0.01	8	2.92 ± 0.005	25	2.85 ± 0.02
Porosity, % vol.	17	2.6 ± 0.4	8	3.4 ± .05	25	2.9 ± 0.3
Electrical resistivity ohm m	17	1320 ± 400	6	340 ± 120	23	780 ± 210
Thermal conductivity W m^{-1} K^{-1}	32	2.08 ± 0.02	21	2.19 ± 0.07	53	2.12 ± 0.03

1980 Drilling Project

There are several key problems involving the volcanic basement of Bermuda which previous studies have not resolved. Most of these problems are petrologic in nature. Basically, these are the problems: (1) why are there only two well-documented rock types - an altered submarine tholeiite and a highly evolved alkaline intrusive, with a possible third unit being Pirsson's keratophyre, (2) what is the origin of the alkaline intrusives - can they be from the same parent as the tholeiites, (3) what was the alteration state of the altered tholeiites prior to the diking and were they formed at a mid-ocean ridge, (4) to what degree and in what way has the volcanic pile been hydrothermally altered (mechanisms), (5) how has the alteration affected the physical properties of the rocks, (6) is there a magnetic stratigraphy and do the magnetic properties compare with the results from the 1972-core, (7) are the samples gathered to date representative of the upper part of the seamount, and (8) are the volcanic processes here the same as those forming other seamounts and islands in the Atlantic Ocean? In order to properly attack these problems, more samples of the volcanic rocks were desired and collected.

During the months of May and June, 1980, the author supervised a small scale drilling project on Bermuda. The drilling was performed by Bradley Brothers, Ltd., of Noranda, Quebec. The first drill site was located in the Government Quarry at Bailey Bay on the south shore of Castle Harbour (Figure 1-2) where the carbonate cap is known to be less than 50 meters thick. In this 89-meter-deep drill-hole the lowermost 60 meters recovered were igneous rocks (Figure 1-11). Core recovery for the first hole averaged about 40 percent for the sedimentary units

Figure 1-11. Sketch lithological column for the igneous portion of the 1980 drill-hole core from the Government Quarry in Bailey Bay.

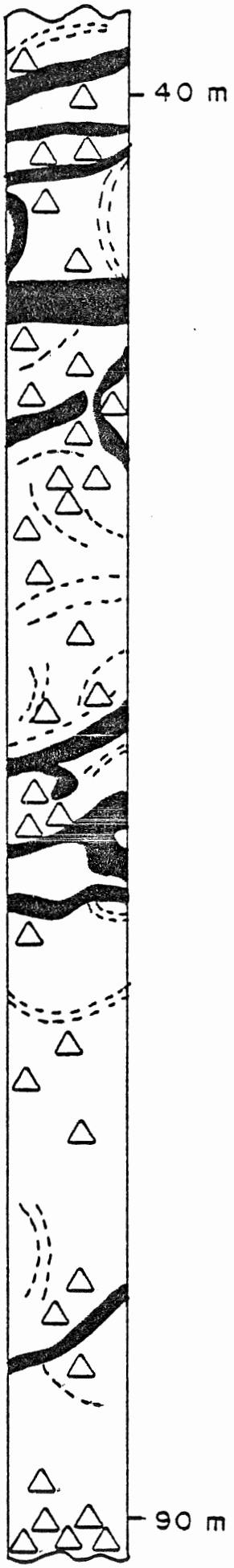

KEY

Pillowed Cooling Unit

Breccia

Intrusives

(several caves were drilled) and about 95 percent for the igneous units. The second hole was sited on the grounds of the Naval Air Station Annex at the head of George's Bay in Sandys Parish over the gravity maximum. The total depth drilled at this site was 42 meters. After drilling through some very fossiliferous sedimentary units, an unconsolidated horizon was encountered which was undrillable. The complete, detailed core logs are presented in Appendix 1.

This thesis has several related themes. The major purpose is to describe the rocks collected in 1980. A general description of the petrography, mineralogy, and petrology, paleomagnetic, and volcanological properties of these lithologies constitutes the main body of the thesis. The remainder deals with developing a framework for interpreting the evolution of this seamount.

CHAPTER 2

PETROGRAPHY AND PHYSICAL VOLCANOLOGY

Introduction

The igneous rocks recovered from the 1980 hole at Government Quarry are strikingly bimodal, consisting of pillowed lavas and intrusives. These units display four distinct textural-structural styles: intrusives with chilled margins, lavas with pillowed margins, volcanic conglomerate, and breccia. A blue-gray biomicrite is intimately associated with the pillowed lavas, especially in the upper one-third of the igneous section. In this chapter I will describe the igneous rocks, their distribution down the hole, and some of their gross structures.

Extrusives

The extrusives account for more than 50 percent of the igneous section (Figure 2-1). They are readily identified on the basis of textures. Arcuate chlorite-rich zones backed by hematite-enriched areas which grade into very dark aphyric material are interpreted as representing pillowed cooling-unit margins. The chilled margins grade into phyric to micro-porphyritic, dark-gray crystalline material. This lithology produces a very distinctive grayish-blue color in the rock powder slurry during drilling. Pillow thickness varies from about 0.25 to over 2 meters. Locally, the pillows are intensely brecciated, especially in zones of diking, with angular fragments (<6 cm^2) being supported in a carbonate matrix. Cooling-unit fragments make up the clasts of the volcanic conglomerate (or breccia).

The cooling units are quite homogeneous on the microscopic scale. With the exception of alteration in the chilled zones and along cracks,

Figure 2-1. Photograph of typical cooling unit (top).

Figure 2-2. Photomicrograph of a chilled margin (bottom).

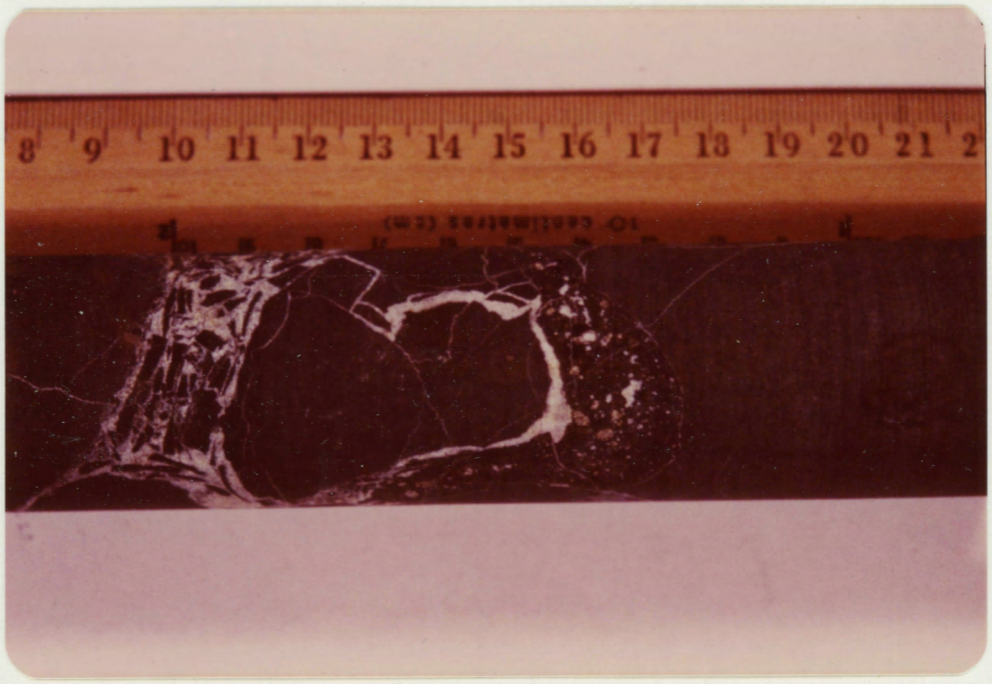
8 9 10 11 12 13 14 15 16 17 18 19 20 21

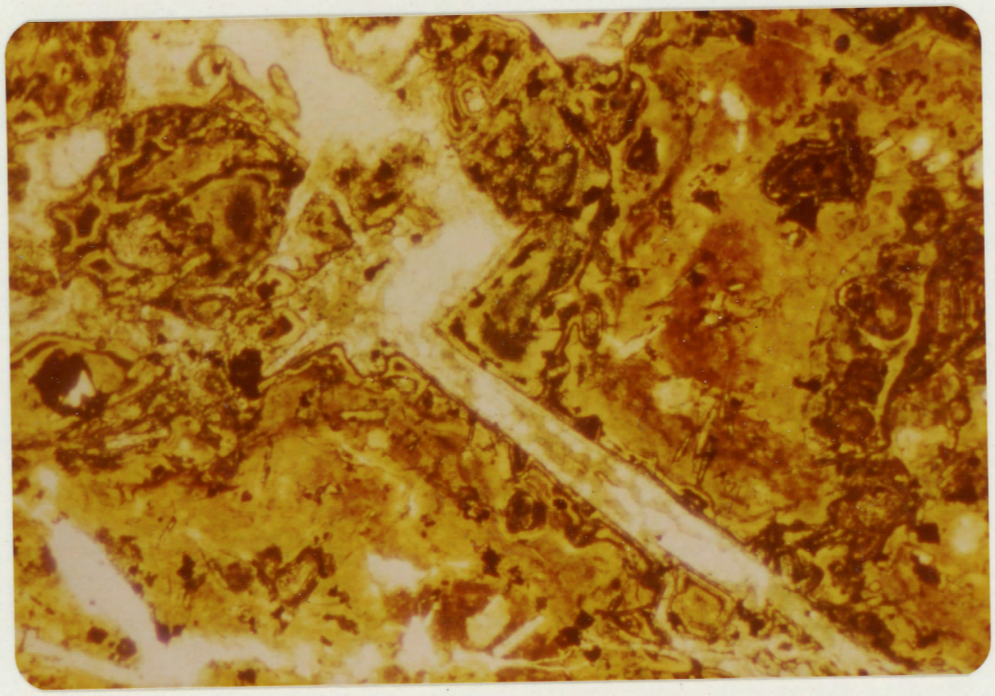

the major minerals in these rocks appear to be relatively fresh. Chlorite commonly occurs along calcite filled veinlets which sometimes have hematite rich zones (0.25 - 0.75 cm) surrounding the veins. Carbonate is ubiquitous; the whole rock effervesces in dilute hydrochloric acid.

The cooling units show the greatest amount of textural variation over a zone less than five centimeters wide at the chilled margin. The margin is spherulitic to cryptocrystalline, probably devitrified glass, with up to 25 percent microlites (Figure 2-2). The devitrified glassy material is most often light-brown, but is sometimes an apple-green color. Both varieties commonly are optically isotropic. The altered glass generally grades into a blue-green spherulitic zone which is pervasively chloritized. Occasional microphenocrysts of spinel ($\leq$ 1 mm) and zoned clinopyroxene (0.5 - 1.0 mm) occur in a groundmass of microlites and altered mesostasis. The microlites in the brown-glassy material are: spinel (~10%), chloritized clinopyroxene (5%), and a reddish-brown phase tentatively identified as altered sphene ($\leq$10%). In the bluish-green spherulitic zone the common constituents are: altered glassy material (~70%), partially chloritized clinopyroxene (<15%), spinel (5%), altered melilite (<10%) and trace amounts of altered sphene.

The cooling-unit interiors exhibit a more consistent mineralogy (Figure 2-3). The volume of microphenocrysts is variable (0 - 5%), with twinned and concentrically-zoned clinopyroxenes predominating. These clinopyroxenes can have more than six zones, generally with rounded cores, and contain numerous inclusions, especially around the

Figure 2-3. Photomicrograph of a cooling unit interior.

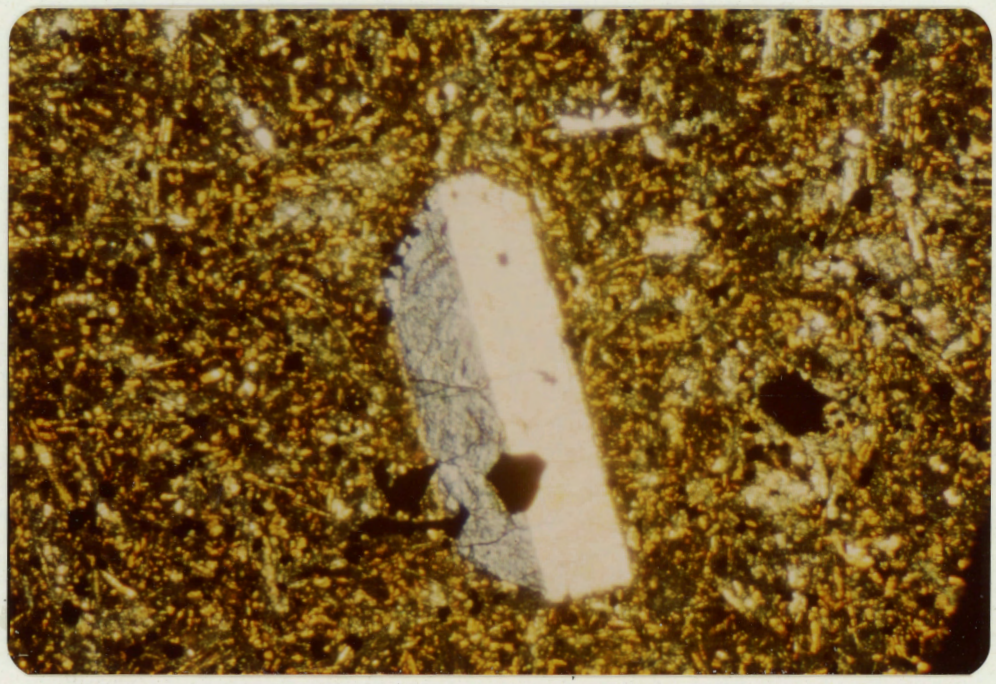

rim, of spinel or rarely, biotite. Infrequently, spinels are large enough to be considered as phenocrysts. Clinopyroxene microlites (34%: 5 - 60%) (Average:Range), some with hourglass zoning are the major groundmass minerals. Melilite, often with well developed peg-structures and pervasively altered to calcite and other unidentified minerals, makes up 19 percent (0 - 60%) of the groundmass. These rocks are also very rich in a spinel phase (12%: 4 - 15%). Strongly pleochroic (reddish-brown to light brown or tan) biotite is found as small (~0.4 mm) interstitial flakes (8%: 1 - 15%). A red colored, semi-opaque phase, which can either exist by itself or as the core or rim of a spinel (tentatively identified as altered sphene) makes up three percent (1 - 4%) of the volume. Relatively fresh, skeletal olivine (<4%) is found in two samples (BF4-2.4 and BF11.5.6). More commonly, olivine is found pseudomorphed by calcite and chlorite. A large amount of the groundmass consists of altered glassy and cryptocrystalline material (22%: 15 - 80%) which is at least partly isotropic. However, the blue-green color of the altered glassy material suggests alteration to chlorite and calcite. A schematic depiction of the down-hole modal variations for the extrusives is given in Figure 2-4.

The bluish-gray sedimentary material found between the pillow is nearly 100 percent carbonate material and well indurated. Planktonic foraminiferal fossils and fossil fragments are often preserved in this lithology; although generally they have been recrystallized. Spalled-off and altered glassy shards of the pillowed extrusives are found totally immersed in this biomicrite. It appears that the pillowed lavas flowed into a limey mud soon after eruption and formed the admixture seen in the core.

Figure 2-4. Down-hole modal variations in the extrusive rocks.

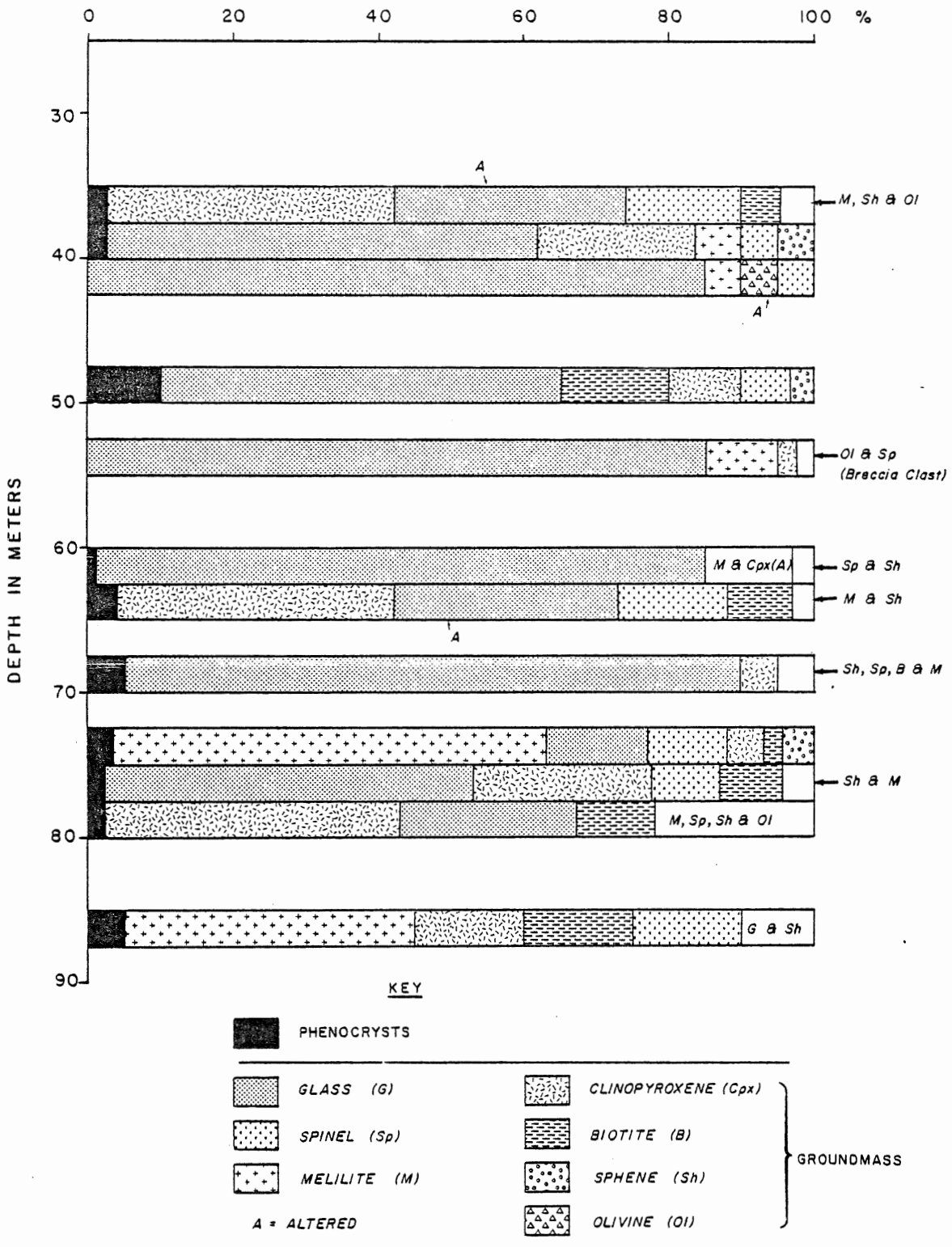
0
20
40
60
80
100 %
30
40
50
60
70
80
90
DEPTH IN METERS
A
A'
M, Sh & Ol
Ol & Sp
(Breccia Clast)
M & Cpx(A)
Sp & Sh
M & Sh
A
Sh, Sp, B & M
Sh & M
M, Sp, Sh & Ol
G & Sh
KEY
PHENOCRYSTS
GLASS (G)
SPINEL (Sp)
MELILITE (M)
A = ALTERED
CLINOPYROXENE (Cpx)
BIOTITE (B)
SPHENE (Sh)
OLIVINE (Ol)
GROUNDMASS

Intrusives

The textures of these dark-gray rocks vary from aphanitic to porphyritic to amygdaloidal. Often the intrusives can be differentiated from the extrusives only by their dark black chilled margins. They form sheets one to two meters thick or, more commonly, narrow ($\lesssim$0.15 m) dikelets which intimately intrude along flow margins or as anastomosing fingers within the brecciated sections (Figure 2-5).

Petrographically this lithology is quite variable. Phenocrysts of twinned and concentrically zoned clinopyroxene, as well as some minor amounts of spinel make up 5 to 15 percent of the total rock volume. In sample BD4-7.5 altered sphene is phenocrystic. In sample BD4-4.9, olivine, altered to a mixture of chlorite, calcite, quartz and steatite, is the major phenocryst phase. The groundmass mineralogy is nearly identical to that of the extrusives. Microlitic clinopyroxene is the major crystalline phase (5 - 60%). Altered melilite is present in variable amounts (0 - 25%). Spinel is a very consistent phase (10 - 15%), occurring both as phenocrysts and in the groundmass. Altered sphene (3%) is found in only one sample (BD4-7.5). Strongly pleochroic biotite is rather common (1 - 15%), and may even form phenocrysts. Trace amounts of altered or totally pseudomorphed olivine are found in most samples. Altered brown to apple-green colored glass, rich in carbonates, is a ubiquitous component (10 - 45%) making up a large portion of the groundmass. Generally, calcite is found in veins and amygdules as large well-formed crystals or in a microcrystalline state. The amygdules may also contain dolomite, smectites, chlorites, and apatite. In some cases the amygdules are zoned with an outer rim of chlorite and a core of calcite and clay minerals.

Figure 2-5. Photograph of an intrusive sheet.

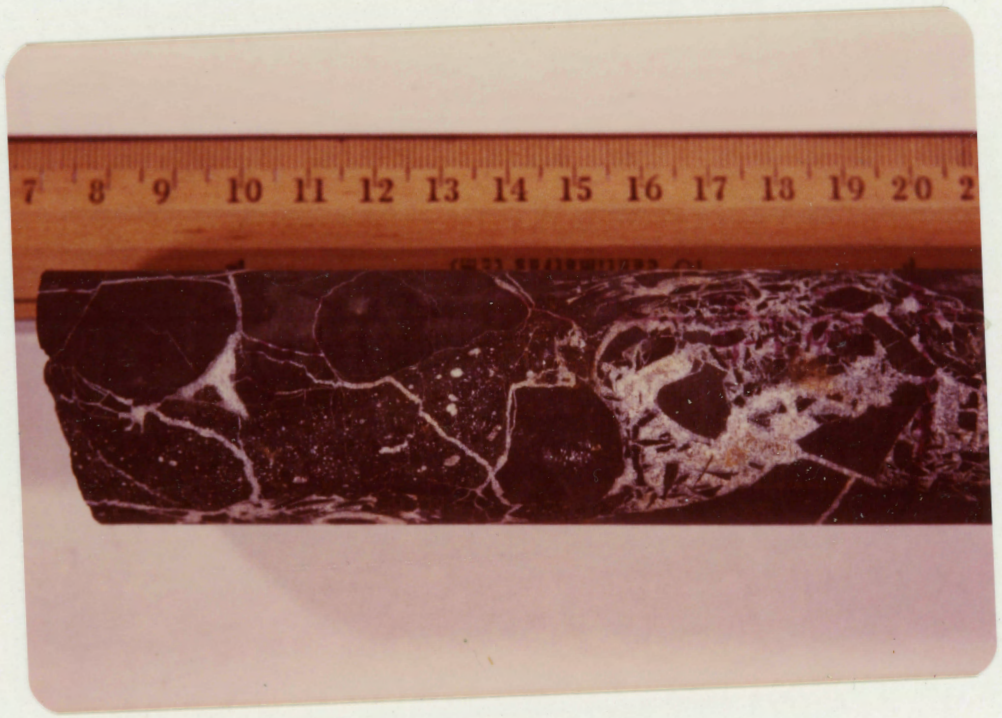

The extrusives and intrusives are cut by numerous zoned, calcite filled veins (<1 mm wide). A typical zoned sequence is, from edge to center: chlorite + opaques (mainly magnetite?), calcite + smectite, and analcite. Trace elements of fluorite, or possibly halite are also found in the center of some veins.

Conglomerate-Breccia

The conglomerates are volcanoclastic rocks with varying degrees of cementation and freshness of clasts (Figure 2-6). The dark conglomerate is composed of subrounded clasts of the flow material, often with dark chilled margins. These dark conglomerates have less than 15 percent by volume carbonate cement. The light conglomerates are similar to the dark in all respects except that they have matrix supported clasts. The altered clast conglomerate has both large (≥2 cm) subrounded clasts and small arcuate plates (0.5 - 1.0 cm) of altered volcanic rock which are completely surrounded by a bluish-white carbonate cement. The larger clasts are concentrically zoned with chloritized glassy rims, extensively hematized zones and dark gray, relatively unaltered cores. The platy fragments are nearly 100 percent chloritized shards of altered glass.

In thin section, the clasts appear to be similar to the chilled margins of the extrusives. In general, they are made up of light brown glass (isotropic) having concentric zones of chloritization which may have formed along perlitic cracks. This partially crystallized, less altered material has the following identifiable crystals (which make up <15% of the total volume): clinopyroxene (45%), opaques (probably spinel) (45%), olivine - calcite and chlorite pseudomorphs (10%). There

Figure 2-6. Photograph of volcanic conglomerate.

are also trace amounts of a cubic phase tentatively identified as nepheline. The matrix consists mainly of calcite with minor chlorite, smectite, and possibly analcite.

The two main lithologies are classified on the basis of Streckeisen's (1979) recommendations to the I.U.G.S. The extrusives contain variable amounts of altered glass (5 - 80%) and thus the modal analyses can only be used for a general grouping. However, the presence of melilite is distinctive and along with the modal preponderance of clinopyroxene, readily places the extrusives into a select grouping: melilite-bearing ultramafic volcanic rocks. Tentatively, these extrusives can be considered to range from altered glass-bearing to glass-rich melilite-bearing nephelenites to melilitites. Note that nephelinites do not necessarily have modal nepheline (or any other common feldspathoidal mineral) but are silica-poor and nepheline normative. The intrusives are much more difficult to classify because of their broad mineralogical variations. In general they can be described as melilite-bearing lamprophyres; but they may also be grouped as the intrusive equivalent of the extrusives, uncompahgrites to possibly alnoites. Unfortunately, these terms are too specific for the amount of cryptocrystalline material found in most samples.

These lithologies appear to be similar to the melilite-basalts of the 1912 hole. The rocks from the 1973 hole and possibly the monchiquite described by Pirsson (1914) are similar to the intrusives. The altered lavas from the 1972 hole are distinctively different mineralogically, as are the lamprophyres from the same hole which are feldspar-bearing and thus more silica-rich than the other known Bermudian lamprophyres.

An approximate age for these rocks is derived from foraminiferal fossils and fossil fragments found in the intrapillow sedimentary material which is similar to the bluish-gray cement of the agglomerates. These fossils are poorly preserved Orbulina and Globigerinids of no later than middle-late Tertiary age (M. Williamson, pers. comm., 1981). This is the first reported paleontological age for the volcanic and related sedimentary rocks.

Physical Volcanology

In this section some of the gross physical structures of the Bermudian volcanic rocks are described in order to ascertain the significance of the observed structures and what they tell us about the style of volcanism. This information will be used to interpret the evolution of the island. The most important questions to be answered are: 1) are the extrusives truly pillowed, submarine cooling-units, 2) are the gross structures and lithologies typical of volcanic islands, and 3) can an approximate volcanic evolution of the islands be defined?

The thicknesses of the cooling units recovered from the 1980 hole are variable (Figure 2-7). Measured values range from several centimeters to greater than one meter. These thicknesses were measured parallel to the drill hole and are only a measure of the vertical thickness in the drill core. The mean cooling-unit thickness is 21±21 centimeters (±1.s.d.). The peak in this distribution is at 10 to 12 centimeters, producing a positive skewness.

Figure 2-7. Frequency distrubition of apparent cooling unit thicknesses.

APPARENT THICKNESS OF COOLING UNITS (From Core Intersections)

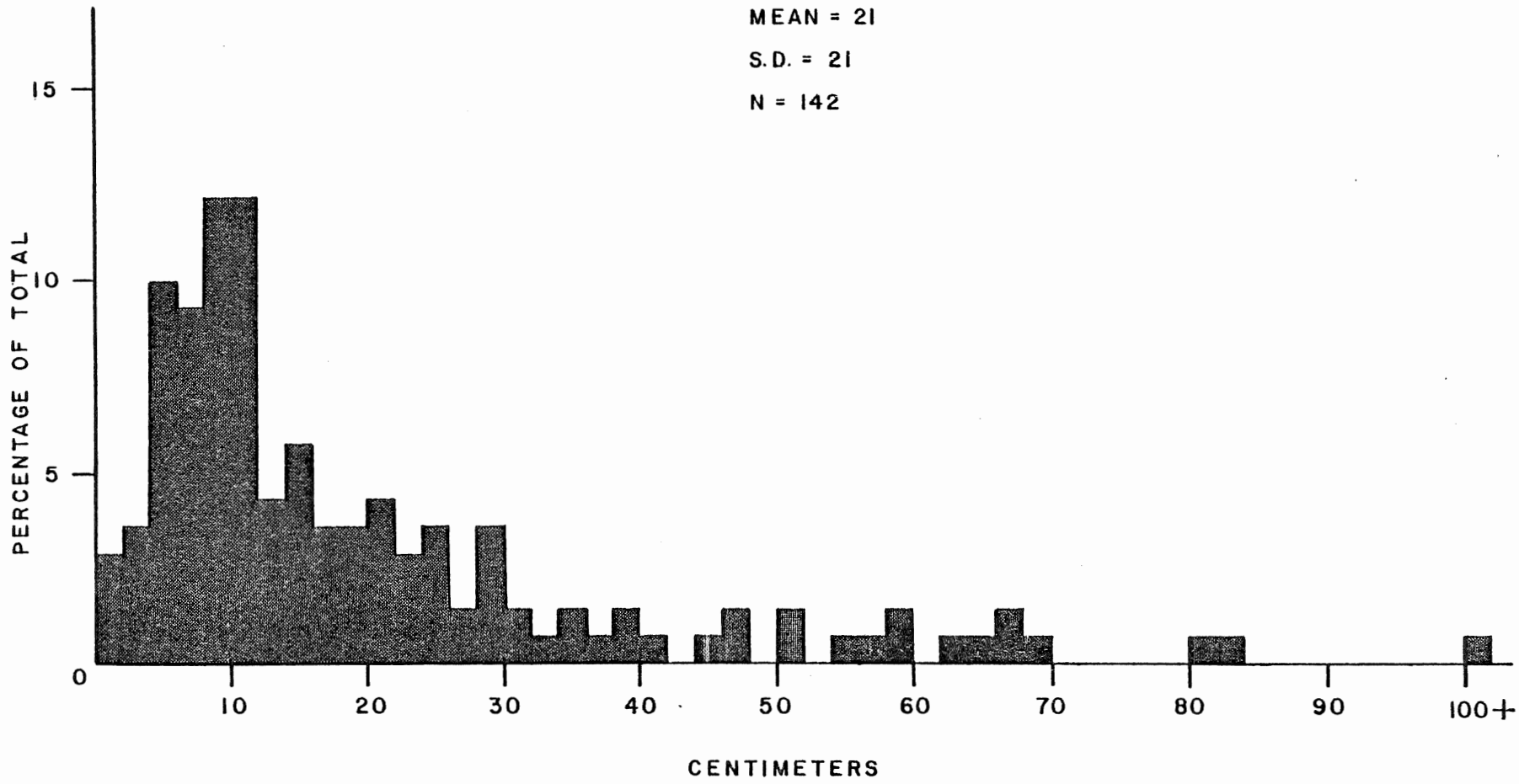

These units are considered to be pillowed flows from megascopic and petrographic evidence, but in fact they may be the distal ends of one, or a series of, relatively thin sheet flows. One independent way to check this distribution is to compare the thicknesses with those determined from terrains of well-exposed pillow lavas.

Furnes and Fridleifsson (1978) measured the axial dimensions of several hundred pillows from lavas in Iceland and the Azores. The frequency distribution of the vertical and horizontal axes are both very similar to the flow thicknesses encountered in the Bermuda lavas. Their data indicate that the pillows are only slightly elliptical, but that for pillows less than 20 centimeters thick they become nearly spherical. The axial ratios depend upon melt viscosity, angle of slope, and depth of water at the time of emplacement.

Robinson et al. (1980) measured pillow thicknesses of samples from D.S.D.P. sites 417A, 417D, and 418A and found that the mean vertical diameter is nearly 50 centimeters. This is somewhat thicker than the Icelandic values described above and may reflect the deeper water origin of the Leg 51, 52 and 53 samples. These cooling units are significantly larger than those found in Bermuda.

Pillow lavas may also be genetically related to pillow breccias and agglomerates. Rapid transitions from pillows to pillow breccias in a tuffaceous matrix are commonly found in ophiolite complexes (see Dewit and Stern, 1978). The breccias may represent lavas erupted under different internal conditions (wetter, hotter, etc.), or perhaps these lavas were erupted near sea level and then flowed subaerially before entering the sea, as has occurred on Hawaii (Moore et al., 1973).

Although these lavas are notably non-vesicular, this does not preclude eruption near sea level.

Jones (1969) examined some pillowed lavas from Iceland and found that the quantity and size of vesicles decreases with depth. Although the trends do not appear to be precise, they do indicate that a tholeiitic pillowed lava can have less than five percent vesicles of sizes smaller than one millimeter at depths of approximately 0.5 kilometers. These relationships are obviously very dependent upon the viscosity and volatile content of the parent magma. Mapstone et al., (1975) described a subaerial flow in the Azores, which, upon reaching and entering the sea, formed about 15 meters of pillow lavas with smooth, non-vesicular, glassy margins, with a blocky lava flow containing boulders occurring over the 5 meter interval near the paleo-sea level.

The occurrence of these pillow lavas and related breccias of possible shallow water origin agree with observations of seamount evolution described by Staudigal and Schmincke (1981). In their examination of the LaPalma complex in the Canary Islands, they found coexisting hyaloclastites, pillow fragment breccias and thin pillow lavas at a depth of less than 490 meters below sea-level. Also of great interest is that over this same interval the percentage of breccias is between 50 and 75 percent, thicknesses of eruptive cooling units is 5.0 centimeters or less, and the percentage of dikes is variable but generally averages about 10 percent.

The intrusives, as mentioned earlier, are quite thin. Figure 2-8 shows the distribution of thicknesses as measured parallel to the core. The mean thickness is 15 (±23) centimeters with a pronounced skew. The

Figure 2-8. Frequency distribution of apparent intrusive thicknesses.

APPARENT THICKNESS OF INTRUSIVES

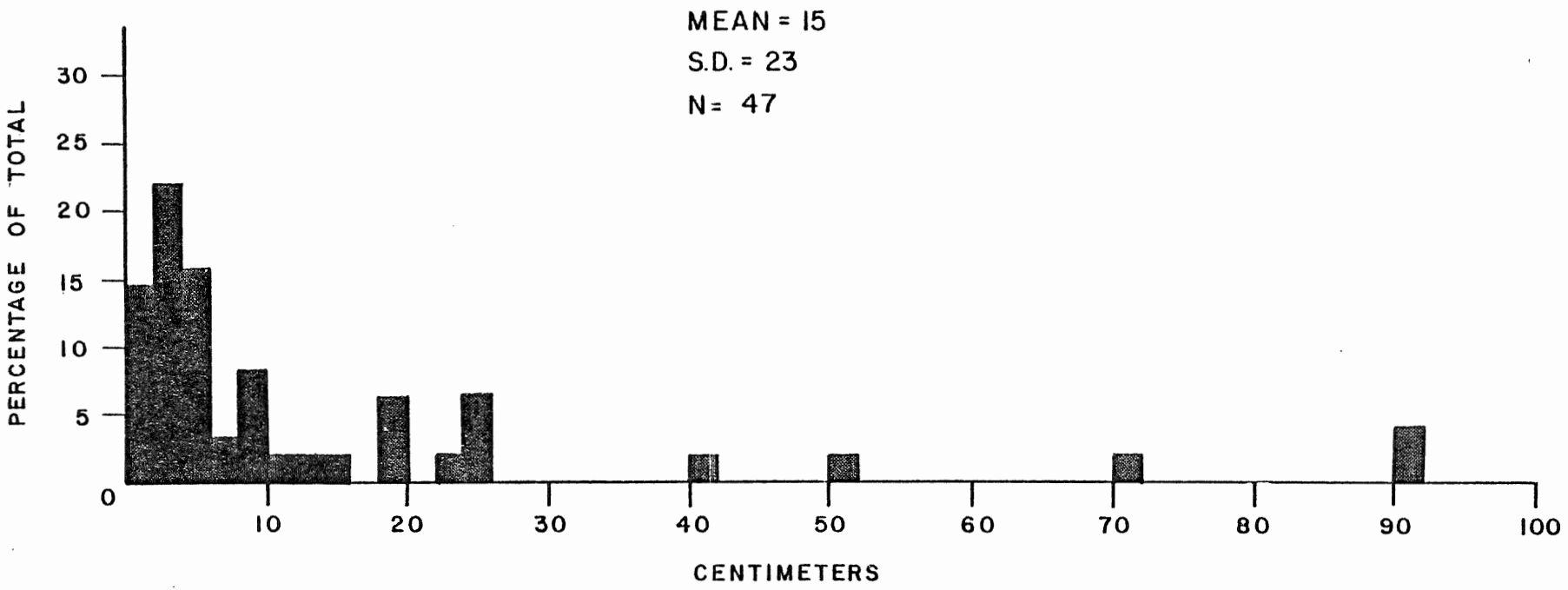

population has its greatest density around 2 to 4 centimeters.

The thickness and structural style of the eruptive rocks observed in the drill core should reflect the stratigraphic evolution of part of the island. Figure 2-9 gives the variation of measured cooling unit thickness, apparent breccia or agglomerate thickness, and percentage of intrusives all averaged over two meter intervals. There are no statistically significant trends, and the following comparisons are derived from a qualitative visual inspection of the diagram. Where cooling units are relatively thin and uniform in thickness, the percentage of intrusives (dikes) is high, especially in the depth interval from 40 to 60 meters. However, this same interval also has a very high breccia content, and the intrusives probably prefer this more easily breached zone. It is quite possible that the thin cooling units in an area of brecciation are actually pillows in a flow breccia such as those described by Dewit and Stern (1978, p. 70) (see also, Carlisle, 1963).

A sense of structure for the cooling units may be derived from the measurement of cooling unit contact orientations. Williams and McBirney (1979) indicate that pillows form on steep slopes, while more massive flows form on shallower slopes. A steep slope is also prone to be covered with brecciated pillows. The average contact angle should reflect the degree of flattening of pillows such that nearly spherical pillows have angular distributions peaking near 45^{o} and flatter pillows will yield a maximum at shallower angles.

Contact angles between cooling units greater than several centimeters thick were measured using a core dip-meter described by

Figure 2-9. Down-hole variation in cooling unit thickness, breccia thickness, and percentage of dikes.

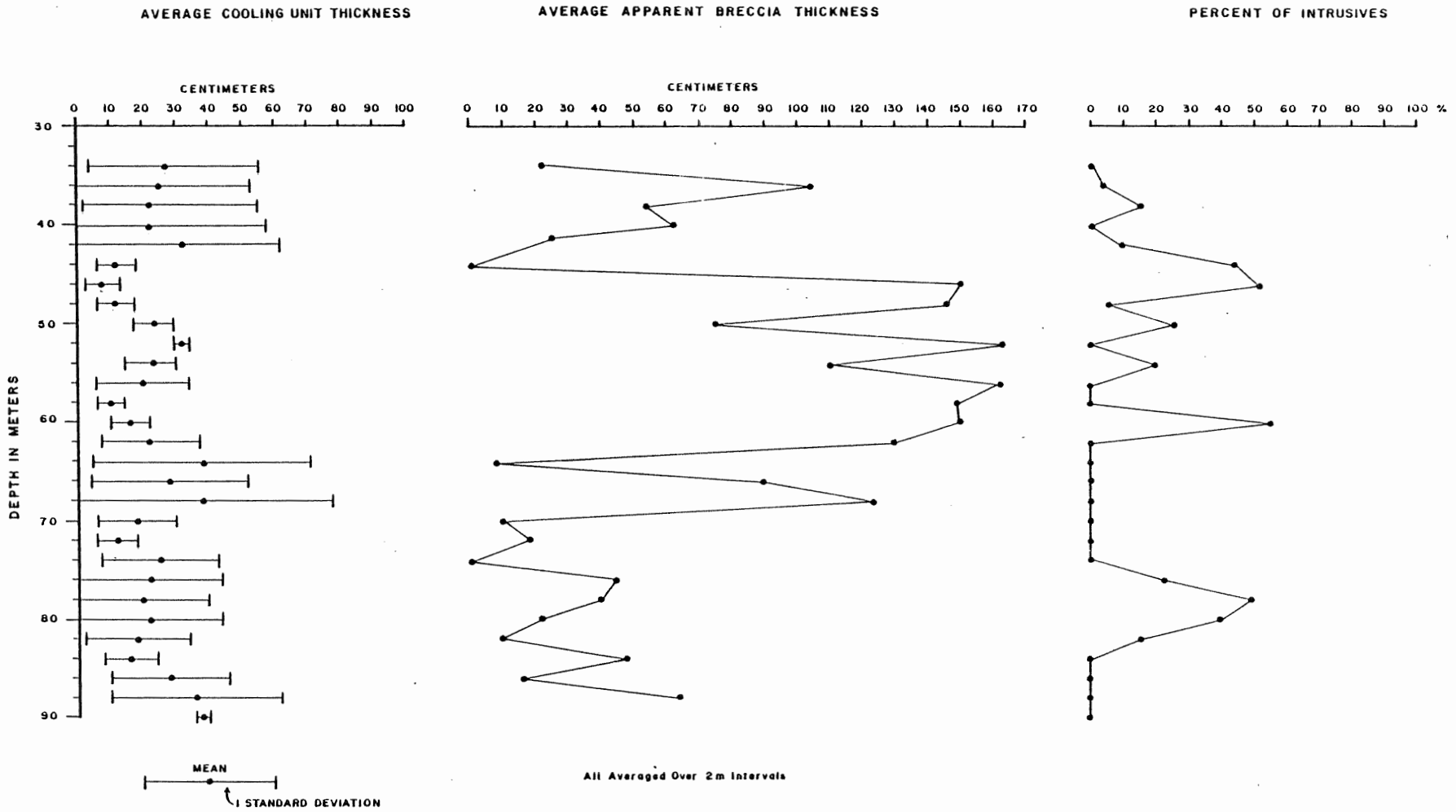
AVERAGE COOLING UNIT THICKNESS
CENTIMETERS
0 10 20 30 40 50 60 70 80 90 100
DEPTH IN METERS
30
40
50
60
70
80
90
MEAN
1 STANDARD DEVIATION
AVERAGE APPARENT BRECCIA THICKNESS
CENTIMETERS
0 10 20 30 40 50 60 70 80 90 100 110 120 130 140 150 160 170
All Averaged Over 2m Intervals
PERCENT OF INTRUSIVES
0 10 20 30 40 50 60 70 80 90 100 %

Hall et al. (1981). Measurement accuracy varies from ±1° to ±4° depending upon the dip angle and clarity of the contact. The angles were corrected to account for vertical sampling bias. Since there is no consistent azimuth control for the core other than the arbitrary azimuth of the fiducial line, only the dip angles were recorded. Cooling unit-intrusive contacts, where they obviously followed cooling unit contacts, were also measured. The measurements are summarized in Figure 2-10. The average dip for the cooling unit contacts is 42° (±18°) and for cooling unit - dike contacts, 32° (±18°). The mean for all contacts is 40° (±18°). These values suggest pillows with little relative flattening.

A final problem to be addressed is the nature of the breccias or agglomerates. Such lithologies may represent blocky lava flows, remnants of a phreatomagmatic explosion, or rapidly degraded and redeposited lavas. The lowermost breccia (83.5-89.6 m) is very altered and may represent a longer period of alteration than seen further up in the core, or a localized zone of alteration. The other breccias are not as strongly altered, although the smaller clasts (<<1 cm) are chloritized while the larger (>>1 cm) clasts are comparatively fresh. The smaller clasts are rounded and lapilli-sized while the larger clasts are angular to subrounded.

There must be a mechanism for mixing together the small and large clasts. Since the larger clasts are so fresh, and evenly distributed within the breccia, they could not have been dropped (i.e., volcanic blocks) into the lapilli-sized material after a period of weathering (subaerial, or more probably, submarine). The mixture could be produced

Figure 2-10. Contact angles between cooling unit margins corrected for sampling bias $N_{corrected} = \frac{N \text{ measured}}{\cos \theta}$ where θ = contact angle.

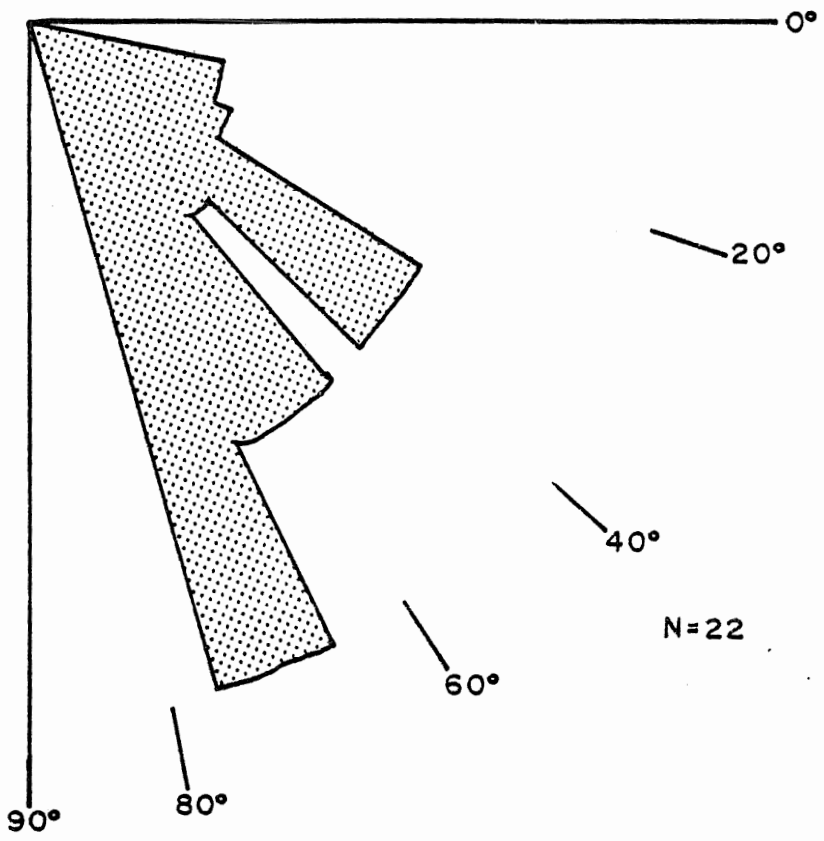
0°
20°
40°
N=22
60°
80°
90°

by a violent eruption that mixed together older and younger material. A possible method is: (1) formation of lapilli-sized clasts, (2) alteration of these clasts, (3) violent eruption (possibly phreato-magmatic if near to sea level) with the new lava forming blocks which are intermixed with the smaller clasts, (4) re-deposition of the new unit, possibly intermixed with submarine flows. An alternative hypothesis is that the smaller clasts were more susceptible to alteration, perhaps being the scaled off portions of the larger clasts, making the breccia a type of pillow or flow breccia. Judging from the submarine nature of the extrusives, the formation of a pillow or flow breccia with the spalled-off glassy rinds becoming more extensively altered than the pillow interiors seems to be the most probable mechanism.

Thus, in summary, the cooling units appear to be small pillows with perhaps small degrees of relative flattening. The pillows appear to be smaller than those found in normal ocean crust, although the apparent size distribution is similar to those pillows measured in the Azores. Associated with these pillows is a breccia which may be of contemporaneous formation.

CHAPTER 3

MINERALOGY

Introduction

The minerals found in the igneous rocks are most interesting. Nearly all of the major phases have unusual compositions, but they are not atypical for alkaline rocks. The extrusives and intrusives have similar mineralogies (Table 3-1). This chapter will describe the identifiable phases as well as outline the chemistry of the important mineral species.

A quick re-examination of Figure 2-4 (modal analyses) points out several modal properties of these rocks. The phenocrysts consist of clinopyroxene with the occasional spinel, or a rare altered olivine. The groundmass is dominated by three phases: melilite, clinopyroxene, and spinel. The melilite and clinopyroxene together make up approximately the same total volume. The other phases: altered sphene, biotite, olivine, apatite, and undifferentiated secondary minerals are of minor volumetric importance.

Clinopyroxene

Clinopyroxene occurs as phenocrysts and in the groundmass. These pyroxenes show oscillatory zoning with rounded and resorbed cores up to 0.1 mm across (Figure 3-1). In rare cases, the core is situated on a nucleus of rounded biotite or spinel. Along the boundaries of the more distinctive zones, especially near the outer rim, are numerous inclusions of euhedral to subhedral spinel. Symplectic intergrowths of pyroxene and spinel (possibly with some glass), often cut across the zoning patterns. The outermost rims are generally a complex intergrowth

Table 3-1

COMPARATIVE MINERALOGIES OF THE INTRUSIVES AND EXTRUSIVES

	Extrusives (BF prefix)	Intrusives (BD prefix)
Phenocrysts:	Clinopyroxene Spinel	Clinopyroxene Spinel Pseudomorphs of Olivine
Groundmass:	Clinopyroxene Spinel Melilite (altered) Altered Sphene Biotite	Clinopyroxene Spinel Melilite (altered) Altered Sphene Biotite
Other Major Components:	Glass (altered)	Glass (altered) Amygdules (calcite filled)

Note: The proportions of these phases in any one sample is quite variable, but generally all are present in all samples.

Figure 3-1. Photomicrograph of a typically zoned clinopyroxene phenocryst (top photo). Crossed-polars, 50X.

Figure 3-2. Photomicrograph of a groundmass clinopyroxene with hourglass zoning (bottom photo). Crossed polars, 320X.

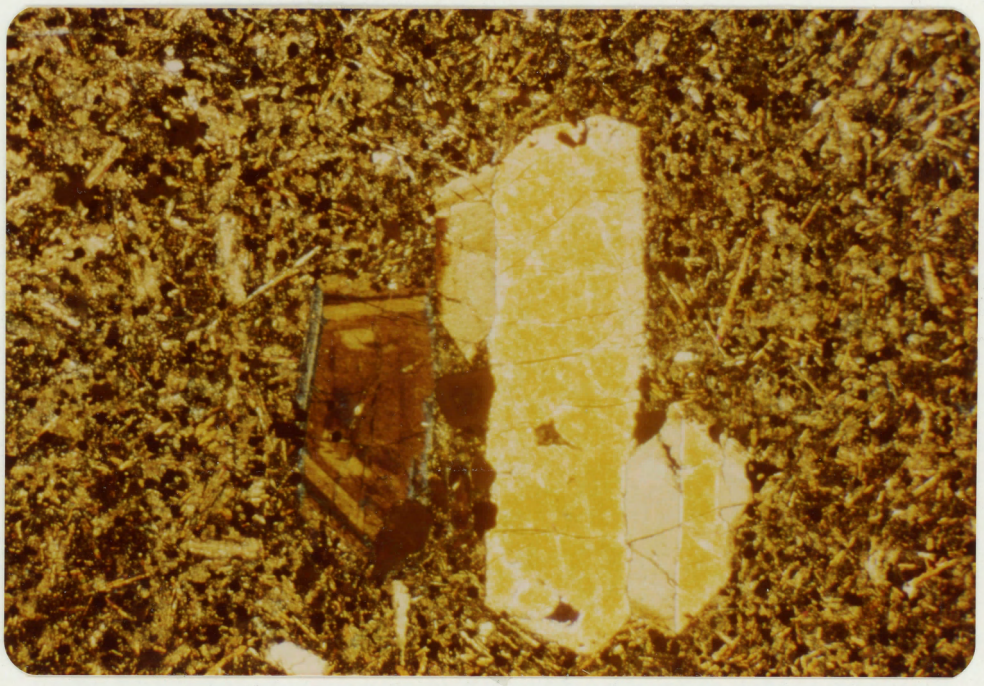

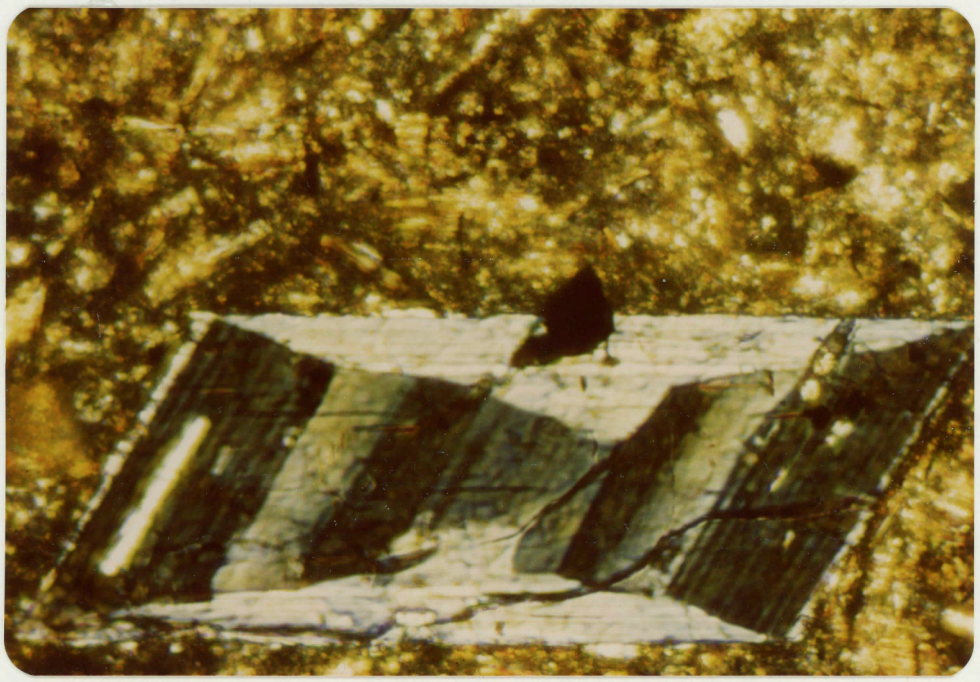

of small grains (<0.2 mm) of spinel and pyroxene. Some grains are twinned parallel to (100).

The groundmass pyroxenes are typically small blocky microlites less than 0.2 x 0.05 mm, often with one or two lamellar twins parallel to their long axes. About ten percent of the groundmass pyroxenes show hourglass zoning (Figure 3-2). The microlites are cream to very light tan colored in plane polarized light and have anomalous gray to light blue interference colors. A few crystals show anomalous pink to green interference colors suggesting titan-augite. In general, these crystals are fresh, although somewhat more altered than the phenocrysts, with a few specimens showing partial chloritization.

Chemically, these pyroxenes are quite titanium rich. Typical values of TiO_2 range from three to five weight percent with maximum values near six weight percent (Table 3-2). This high titanium content, as well as a relatively high aluminum content distorts the projection of these pyroxenes in the commonly used pyroxene quadrilateral of $MgSiO_3$-$FeSiO_3$-$CaMgSi_2O_6$-$CaFeSi_2O_6$. To avoid erroneous interpretations and also account for the non-quadrilateral components, Ti and Al, the pyroxene nomenclature proposed by Cameron and Papike (1981) is used.

Using their systematics the general name for all the pyroxenes analyzed, phenocrysts and groundmass, is Mg-augite. The percent others (non-quadrilateral components) ranges from 14 to 48 percent with an average of 31 percent. In general the analyses plot in the others projection along the join between Ca-Tschermaks molecule (CATS) or $R^{2+}R^{3+}(SiAl)O_6$, where $R^{2+} = Ca^{2+}$, Mn^{2+}, Fe^{2+} and $R^{3+} = Fe^{3+}$, Cr^{3+}, Al^{3+}, and Ti-Al pyroxene (TAL) or $R^{2+}Ti^{4+}_{0.5}\ R^{2+}_{0.5}\ (SiAl)O_6$ with some minor

Table 3-2

REPRESENTATIVE GROUNDMASS CLINOPYROXENES

Sample	BF9-7.8	BF9-7.8	BF10-11.25	BF10-11.25	BD9-2.70	BD9-2.70
SiO_2	40.06	45.03	47.54	45.59	46.35	45.08
TiO_2	6.20	3.71	3.00	3.98	2.66	2.91
Al_2O_3	10.65	7.07	4.93	7.99	6.84	7.27
Cr_2O_3	0.0	0.0	0.0	0.11	0.0	0.0
Fe_2O_3	0.0	0.0	0.0	0.0	0.0	0.0
FeO	8.13	6.19	5.75	6.37	6.38	6.33
MnO	0.17	0.0	0.09	0.05	0.0	0.0
MgO	11.26	13.40	14.88	13.23	13.60	13.08
CaO	23.57	24.04	24.48	23.47	22.84	22.76
Na_2O	0.50	0.24	0.36	0.52	0.50	0.25
K_2O	0.04	0.0	0.0	0.0	0.0	0.0
Total	100.58	99.68	101.03	101.31	99.17	97.68
			Recalculated to 6 oxygens			
Si	1.524	1.696	1.761	1.687	1.745	1.725
Al	.476	.304	.215	.313	.255	.275
Al	.001	.010	0	.035	.049	.053
Ti	.177	.105	.084	.111	.075	.084
Cr^{3+}	0	0	0	.003	0	0
Fe^{3+}	0	0	0	0	0	0
Fe^{2+}	.259	.195	.178	.197	.201	.203
Mn	.005	0	.003	.002	0	0
Mg	.638	.752	.822	.730	.763	.746
Ca	.960	.970	.972	.930	.921	.933
Na	.037	.018	.026	.037	.036	.019
K	.002	0	0	0	0	0

Table 3-2 (continued)

REPRESENTATIVE CLINOPYROXENE PHENOCRYSTS COMPOSITIONS
(BF = EXTRUSIVE, BD = INTRUSIVE)

Sample	BF4-2.4 Ac[1]	BF4-2.4 A	BF4-2.4 A	BF4-2.4 Ar	BF4-2.4 Bc	BF4-2.4 Br	BD4-4.9 Ac	BD4-4.9 Ar	BD4-4.9 Ar
SiO_2	44.78	47.36	43.00	45.62	39.46	46.02	49.97	44.10	47.61
TiO_2	3.78	3.05	3.95	3.44	6.31	3.31	1.10	4.17	2.65
Al_2O_3	7.00	4.67	7.41	5.77	10.35	5.39	4.04	8.04	4.71
Cr_2O_3	0.13	0.0	0.0	0.14	0.10	0.0	0.97	0.12	0.15
Fe_2O_3	0.00	0.0	0.0	0.0	0.0	0.0	0.0	0.0	0.0
FeO	6.17	5.71	8.01	6.45	8.15	6.48	5.71	7.80	6.86
MnO	0.12	0.12	0.05	0.16	0.0	0.10	0.06	0.05	0.13
MgO	12.61	13.67	12.78	14.07	11.03	14.00	16.84	12.75	14.70
CaO	23.88	23.86	23.62	23.84	23.36	23.96	21.02	23.61	23.34
Na_2O	0.39	0.39	0.35	0.52	0.54	0.28	0.38	0.43	0.27
K_2O	0.00	0.0	0.0	0.06	0.0	0.0	0.25	0.0	0.0
Total	98.86	98.83	99.17	100.07	99.30	99.54	100.34	101.07	100.42
				Recalculated to 6 oxygens					
Si	1.703	1.790	1.649	1.718	1.521	1.738	1.841	1.653	1.777
Al	.297	.208	.335	.256	0.470	.240	.159	0.347	.207
Al	.016	0	0	0	0	0	.016	.008	0
Ti	.108	.087	.114	.097	.183	.094	.030	.118	.074
Cr_{3+}	.004	0	0	.004	.003	0	.028	.004	.004
Fe^{2+}	0	0	0	0	0	0	0	0	0
Fe	.196	.180	.257	.203	.263	.205	.176	.244	.214
Mn	.004	.004	.002	.005	0	.003	.002	.002	.004
Mg	.715	.770	.730	.790	.634	.788	.925	.712	.818
Ca	.973	.966	.970	.962	.965	.970	.830	.948	.933
Na	0	.029	.026	.038	.040	.021	.027	.031	.020
K	.029	0	0	.003	0	0	.012	0	0

[1] core = c, rim = r

Table 3-2 (continued)

TAHITIAN CLINOPYROXENES

	Maximum TiO_2	Minimum TiO_2
SiO_2	37.31	48.21
TiO_2	8.73	2.36
Al_2O_3	13.64	6.38
Cr_2O_3	0.06	0.84
Fe_2O_3	--	--
FeO	9.40	5.94
MnO	0.22	0.09
MgO	7.58	13.79
CaO	21.56	22.74
Na_2O	1.13	0.44
K_2O	--	--
Total	99.63	100.80
	Recalculated to 6 oxygens	
Si	1.430	1.672
Al	.570	.230
Al	.045	.046
Ti	.252	.065
Cr_{3+}	.001	.024
Fe_{2+}	.098	.060
Fe	.178	.122
Mn	.007	.002
Mg	.433	.755
Ca	.886	.895
Na	.074	.031
K	--	--

content of the sodic-titan-pyroxene (NATAL) molecule or $NaTiAlO_6$.

Since these minerals are optically and chemically zoned, substitution trends can be discerned from atomic variation diagrams (Figure 3-3). Considering the general pyroxene formula, XYZ_2O_6, where X = Na, Ca, Mn, Fe^{2+}, Mg, Li (tetrathedrally coordinated), Y = Mn, Fe^{2+}, Mg, Fe^{3+}, Al, Cr, Ti (octahedrally coordinated) and Z = Si, Al (tetrahedrally coordinated) substitutions may occur in any of the three sites by the appropriate cations, but the net charge of the unit formula must be zero. This physical requirement limits the amounts of any element that may be incorporated into the crystal lattice. One manner by which these substitutions may occur is by coupled exchanges whereby two or more elements substitute for another couple thus maintaining no net change in charge for the unit formula.

Coupled substitutions tend toward the non-quadrilateral pyroxenes (CATS-TAL-NATAL) from the common pyroxenes, thus the changes can best be seen with respect to these cation groups: NaAl, AlAl, TiAlAl. These trends are shown for representative analyses of phenocrysts in Figures 3a, 3b, and 3c. In all cases a well-defined linear substitution trend towards (or from) these non-quadrilateral end-members is clearly depicted.

The rims of most pyroxenes are enriched in Ti, Al, and Na with respect to the cores. However, some phenocrysts show reversed trends and even opposing rims of the same phenocryst may show different substitution trends. These differences between opposite ends of a crystal clearly indicate localized chemical disequilibrium. The average groundmass pyroxenes have compositions and substitution ratios

Figure 3-3. Pyroxene substitution trends.

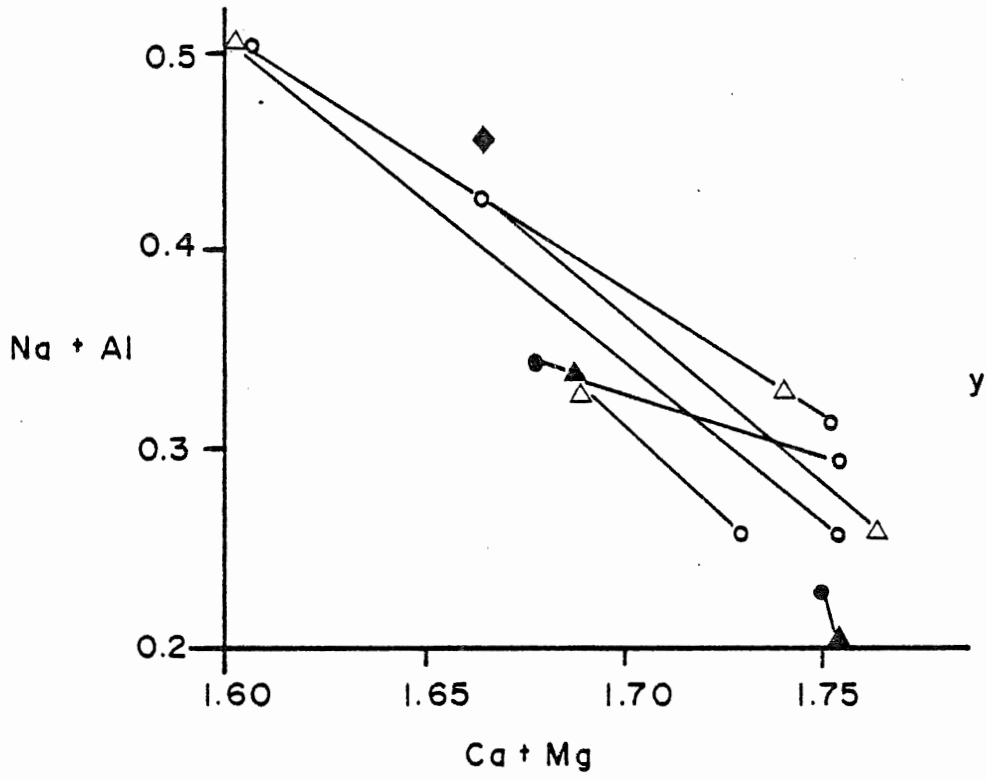

EXTRUSIVES

△ Core

o Rim

INTRUSIVES

▲ Core

● Rim

◆ Average Groundmass

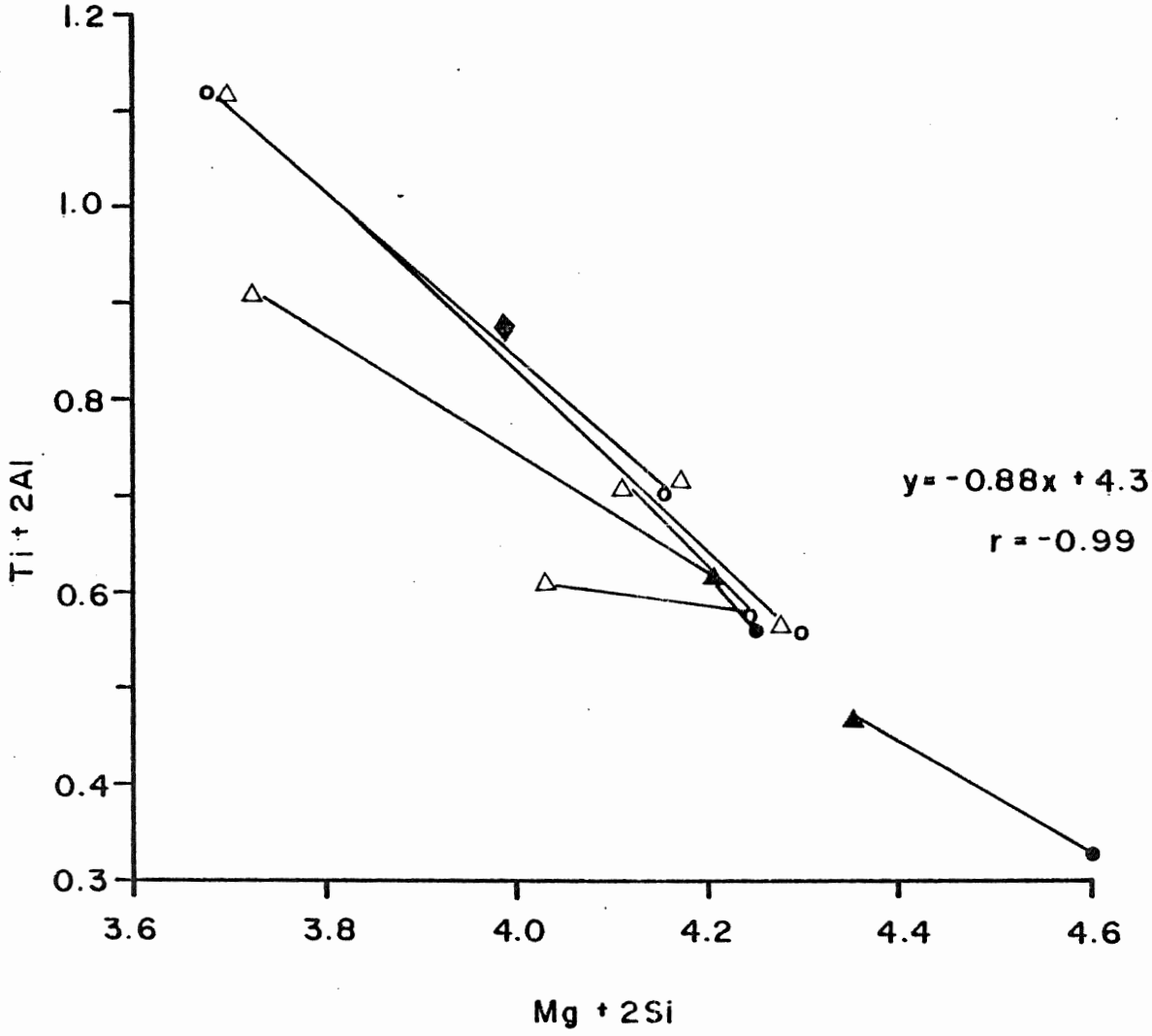
1.2
1.0
0.8
0.6
0.4
0.3
Ti + 2Al
3.6
3.8
4.0
4.2
4.4
4.6
Mg + 2Si
y = -0.88x + 4.37
r = -0.99

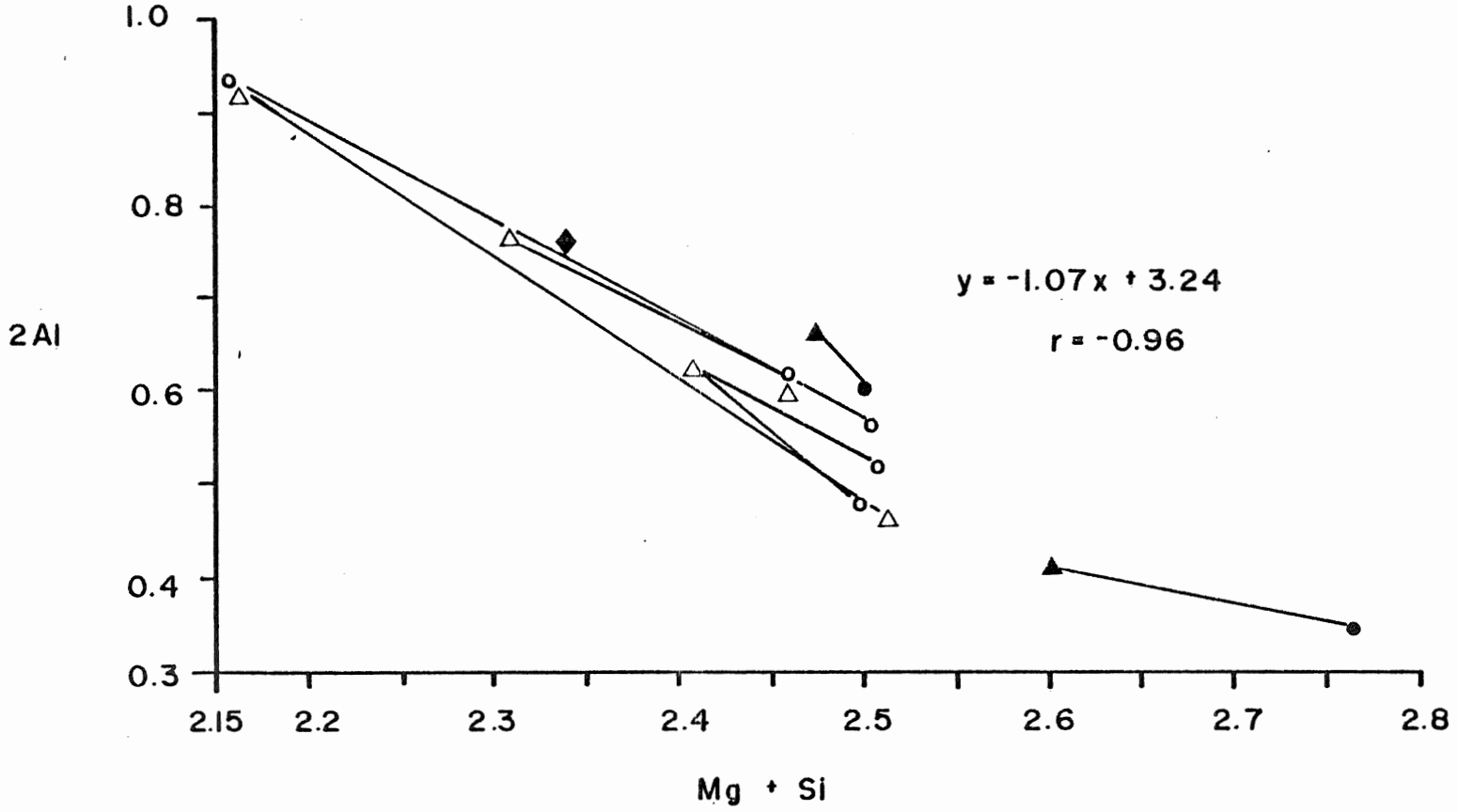
1.0
0.8
0.6
0.4
0.3
2Al
2.15
2.2
2.3
2.4
2.5
2.6
2.7
2.8
Mg + Si
y = -1.07x + 3.24
r = -0.96

intermediate between the core and rim extremes of the phenocrysts. This suggests that the groundmass pyroxenes were growing at about the same time as the outer rims of the phenocrysts.

Experimental studies in the system, $CaMgSi_2O_6$-$CaFeAlSiO_6$-$CaTiAl_2O_6$ at one atmosphere corroborate some of the observed trends. Akasaka and Onuma (1980) state that the clinopyroxenes forming from a melt at 1260°C (liquidus for this system) contains less Ti, Al and Fe^{3+} than the liquid and the later formed clinopyroxene. This indicates that the diopside-rich liquids become relatively enriched in those same elements. The pyroxene continuously reacts with the liquid and becomes progressively richer in Ti, Al and Fe^{3+} until a maximum of nine weight percent TiO_2 is reached. If equilibrium is not maintained then zoned pyroxenes may form (Akasaka and Onuma, 1980, p. 309-310).

The clinopyroxenes from Bermuda are very similar to some zoned titanian augites from Tahiti described by Tracey and Robinson (1977). These Tahitian pyroxenes occur as phenocrysts or overgrowths on spinel lherzolite xenoliths in an alkali basalt. A representative analysis is given in Table 3-2. They interpret the zoning trends in the Tahitian pyroxenes as reflecting a progressive enrichment of Ti and Fe/Mg ratio in the melt. A low oxygen fugacity prevented the co-precipitation of magnetite and ilmenite until the Ti content of the melt became extremely high. These opaque phases eventually did form and as a result the pyroxenes with the highest Fe/Mg ratios have TiO_2 contents less than the maximum values.

Spinel

Spinel occurs as relatively large phenocrysts (1-2 mm) and as small grains in the groundmass (<0.25 mm), and has a distinct bimodal size distribution. Nearly all of these crystals, phenocrysts and groundmass, are euhedral with cubic or octahedral outlines and may show skeletal growth. Occasionally they may contain a core or rim of altered sphene, or even inclusions of silicates (or glass). In reflected light, these spinels are isotropic, and light tan to bluish gray in color (Figure 3-4). Often they are zoned with patchy, tan colored cores and very clean light-bluish gray rims.

Chemically, the spinels are diverse, but they are consistently low in Cr. In the multicomponent spinel system, the spinels fall in the high $TiO_2/[TiO_2 + Al_2O_3 + Cr_2O_3 - FeO/FeO + MgO]$ region (Figure 3-5 and Table 3-3). The spinels can be quite titaniferous, with up to 18 weight percent TiO_2, although most of the samples have less than 16 weight percent TiO_2. The larger spinels tend, on the average, to be richer in MgO with a maximum of over 8.0 weight percent, compared to an average of about 6.0 weight percent for all. The Mg-rich spinels also tend to be aluminous (<7 weight percent maximum). In general, these minerals trend towards titanomagnetite (ulvöspinel) from pleonaste-rich magnesio-ferrite with progressive crystallization.

These spinels are very Cr-poor for such mafic rocks. In fact, for many samples, Cr_2O_3 is below the level of detection. An examination of Figure 3-6 shows the crystallization trends for the spinels as a whole. They probably formed from a liquid which was at least partially depleted in Cr but relatively rich in Al, and became enriched in Fe and

Figure 3-4. Photomicrograph of spinels showing the distribution between the phenocrysts and groundmass. Reflected light, 320X.

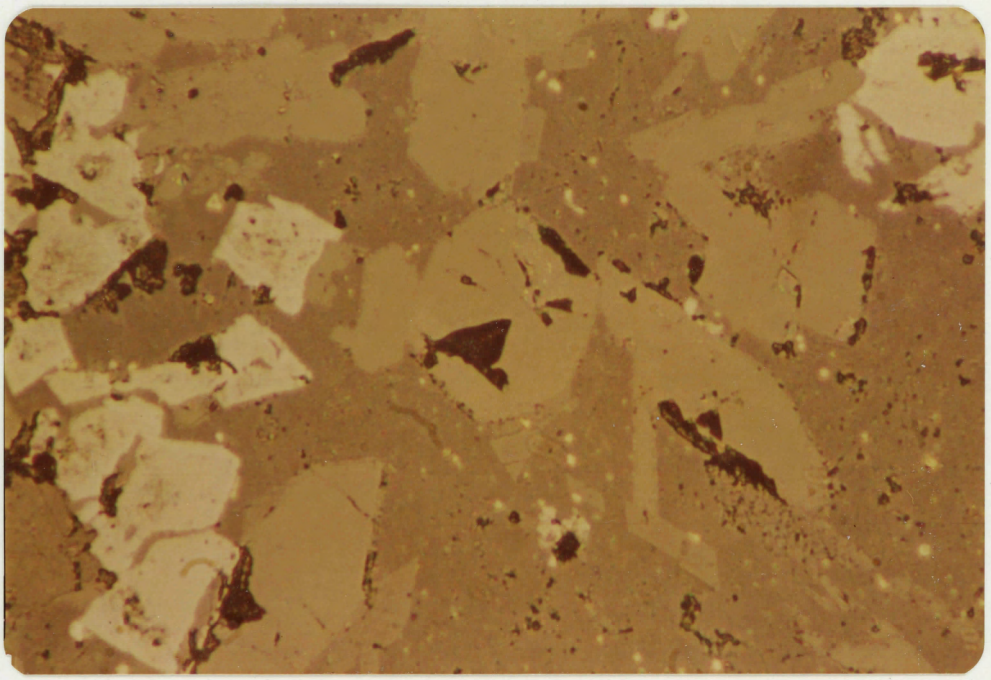

Table 3-3

REPRESENTATIVE ANALYSES OF SPINELS

	Phenocrysts					Groundmass		
Sample	BD9-2.70 Ai	BD9-2.70 A	BD9-2.70 B	BD9-2.70 B	BF4-2.4	BF4-2.4	BF10-11.25	BD4-7.5
SiO_2	1.09	0.48	0.45	0.50	0.10	1.68	0.64	2.54
TiO_2	17.23	16.81	18.14	17.85	15.40	15.76	16.62	14.68
Al_2O_3	7.07	7.92	6.23	4.75	5.52	6.03	5.43	6.26
Fe_2O_3[1]	28.44	30.41	29.35	29.24	39.74	30.91	31.12	0.0
FeO	38.76	34.66	38.18	43.18	31.04	36.17	37.01	64.42
Cr_2O_3	0.09	0.10	0.06	0.06	0.0	0.0	0.06	0.0
MnO	0.41	0.41	0.52	0.44	0.54	0.49	0.43	0.52
MgO	6.88	8.77	7.09	3.49	10.18	7.78	6.66	5.47
CaO	0.13	0.07	0.07	0.10	0.07	0.26	0.13	0.23
Total	100.10	99.63	100.09	99.51	102.59	99.08	98.09	94.12
	Recalculated to 32 oxygens							
Si	.301	.131	.125	.144	.027	.467	.182	.805
Ti	3.576	3.452	3.782	3.866	3.097	3.293	3.557	3.500
Al	2.299	2.549	2.035	1.612	1.740	1.975	1.821	2.338
Cr^{3+}	.020	.022	.013	.014	0	0	.014	0
Fe^{3+}	5.906	6.250	6.124	6.337	7.998	6.464	6.664	0
Fe^{2+}	8.945	7.916	8.853	10.400	6.943	8.406	8.808	7.079
Mn	.096	.095	.122	.107	.122	.105	.104	.140
Mg	2.830	3.570	2.930	1.498	4.058	3.222	2.821	2.585
Ca	.038	.020	.021	.031	.020	.077	.040	.078

[1] Fe^{3+}/Fe^{2+} set on basis of magnetite - ulvöspinel.

Figure 3-5. Spinel compositions in the system $MgAl_2O_4$-$MgCr_2O_4$-$FeCr_2O_4$-Mg_2TiO_4-Fe_2TiO_4.

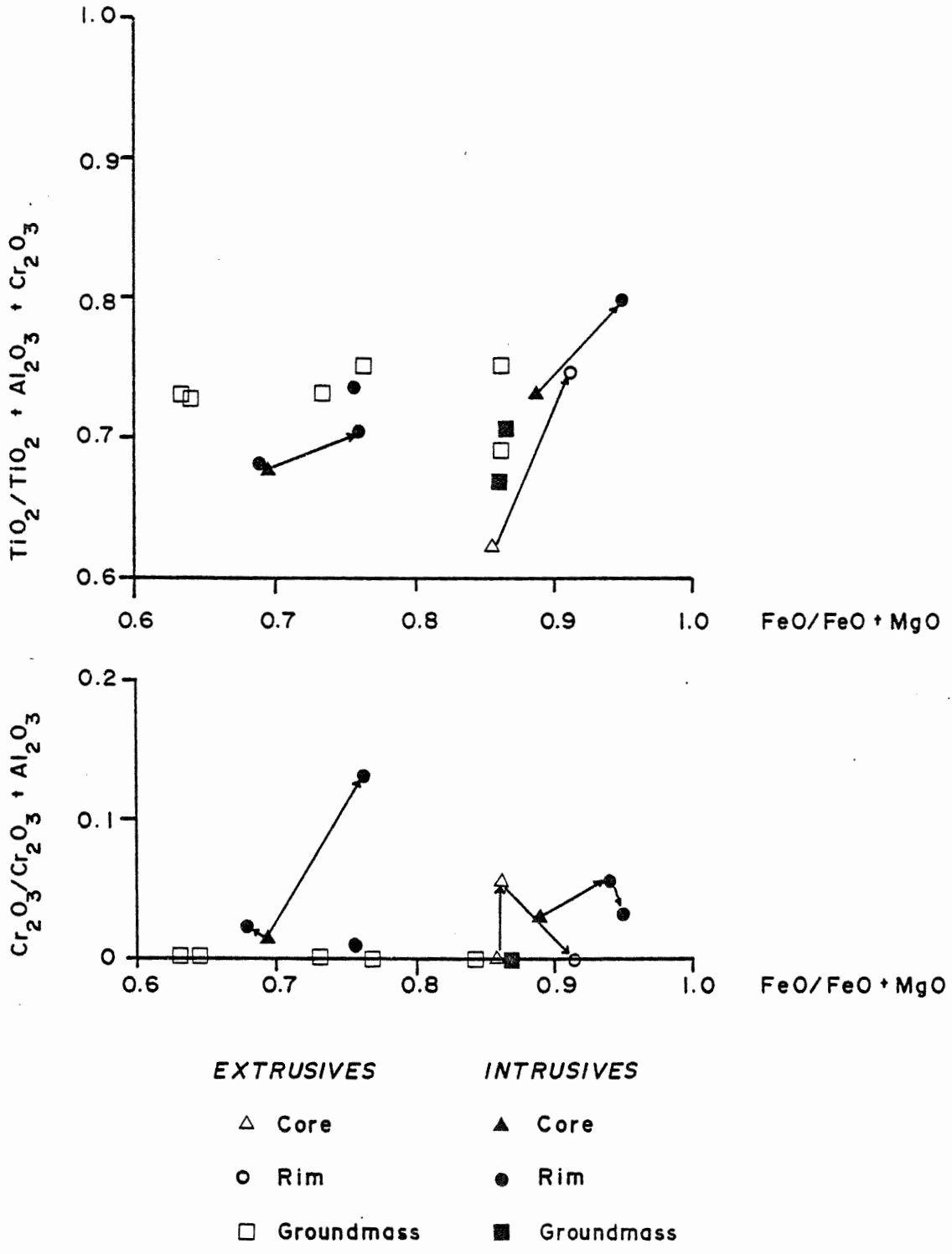
1.0
0.9
0.8
0.7
0.6
$TiO_2/TiO_2 + Al_2O_3 + Cr_2O_3$
0.6
0.7
0.8
0.9
1.0
FeO/FeO + MgO
0.2
0.1
0
$Cr_2O_3/Cr_2O_3 + Al_2O_3$
0.6
0.7
0.8
0.9
1.0
FeO/FeO + MgO
EXTRUSIVES
INTRUSIVES
Core
Rim
Groundmass
Core
Rim
Groundmass

Figure 3-6. Crystal chemical substitution trends in the spinels.

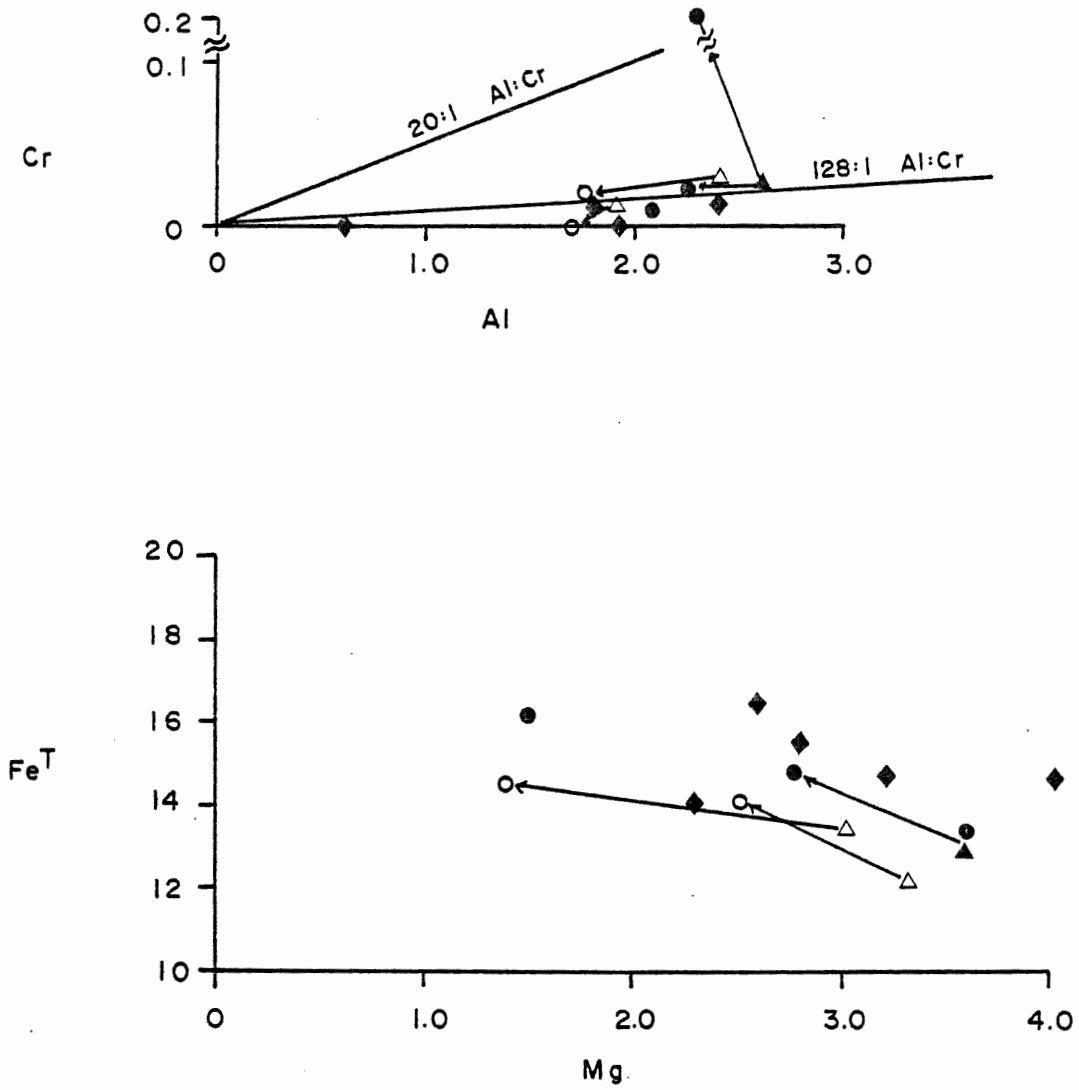
0.2
0.1
0
Cr
20:1 Al:Cr
128:1 Al:Cr
0
1.0
2.0
3.0
Al
20
18
16
14
12
10
Fe^T
0
1.0
2.0
3.0
4.0
Mg
EXTRUSIVES
△ Core
○ Rim
INTRUSIVES
▲ Core
● Rim
◆ Groundmass

Ti with progressive crystallization. A step scan of a large spinel (Figure 3-7) indicates a steep increase from core to rim of FeO and MnO, a step decrease in MgO and Al_2O_3, and no total change in TiO_2 and V_2O_5. The values of Cr_2O_3 and V_2O_5 vary erratically and probably are an artifact of their low concentrations, near the lower detection limits of the microprobe.

An estimation of crystallization temperature for these spinels can be derived from the results of Muan et al. (1972). In the system $FeO-Al_2O_3-TiO_2$ and $MgO-Al_2O_3-TiO_2$ there is a subsolidus exsolution of Ti and Al rich phases between 1000°C to 1300°C at atmospheric pressure. Since only one spinel is found (no exsolution), these minerals formed outside the miscibility gap. Projections of these spinel compositions into the system $Fe_2TiO_4-FeAl_2O_4-FeCr_2O_4$ and $Mg_2TiO_4-MgAl_2O_4-MgCr_2O_4$ are shown in Figure 3-8. Notice that for both of these projections the spinels plot up to the solvus at 1200°C, therefore, these spinels must have crystallized above this temperature and were quenched rapidly to ambient temperatures.

Biotite

Biotite is a relatively minor phase in these rocks occurring as an early phase in the core of some pyroxene phenocrysts and as an interstitial mineral in the groundmass. The biotite (phlogopite rich) found in the pyroxenes is small (25 to 75 microns) and rounded. These biotites are relatively rare and may be confused with secondary biotite which grows along fractures in the pyroxenes. The groundmass biotites are all small (<200 microns) blocky to rectangular crystals. These

Figure 3-7. Step scan across a typical zoned pyroxene phenocryst.

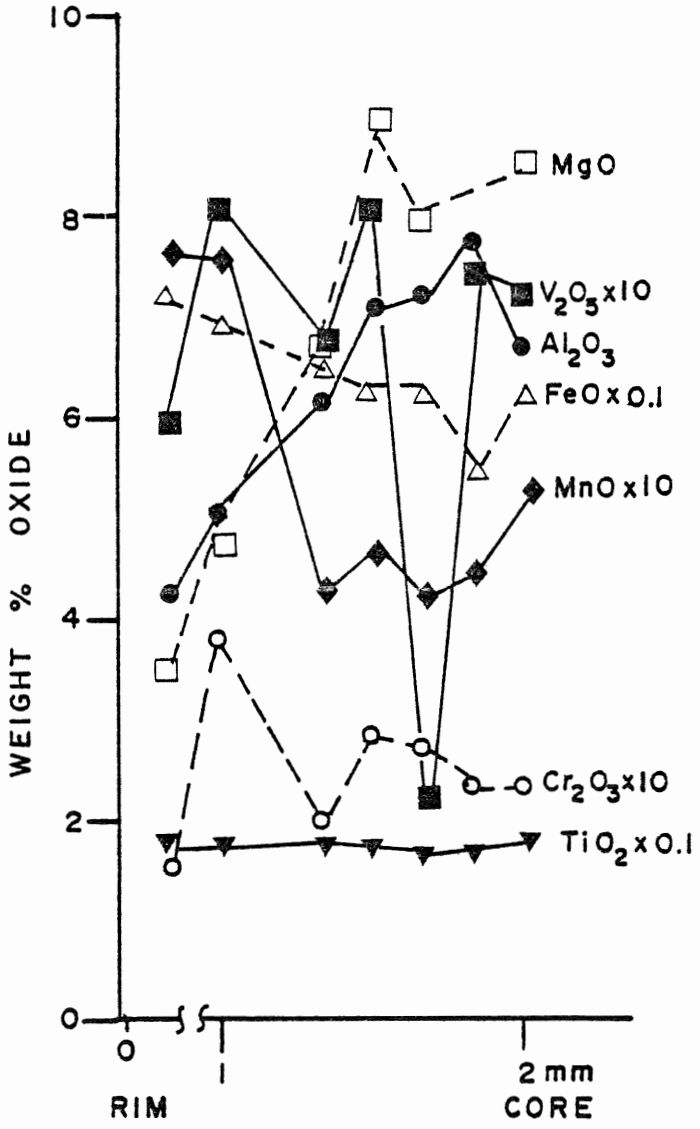
10
8
6
4
2
0
WEIGHT % OXIDE
MgO
V2O5x10
Al2O3
FeOx0.1
MnOx10
Cr2O3x10
TiO2x0.1
0
RIM
2 mm
CORE

Figure 3-8. Projections of the spinel compositions onto the miscibility diagrams of Muan et al. (1972).

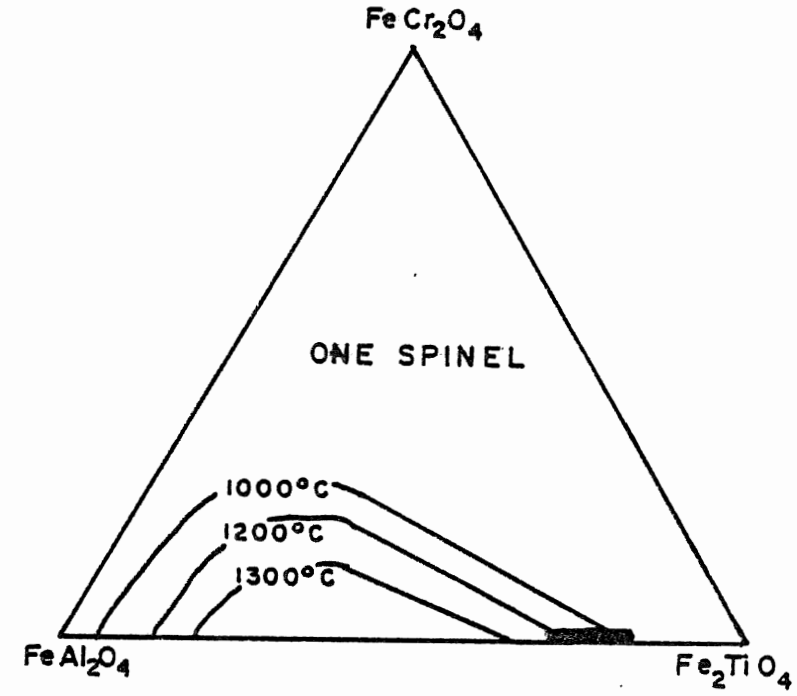
$FeCr_2O_4$
ONE SPINEL
1000°C
1200°C
1300°C
$FeAl_2O_4$
Fe_2TiO_4

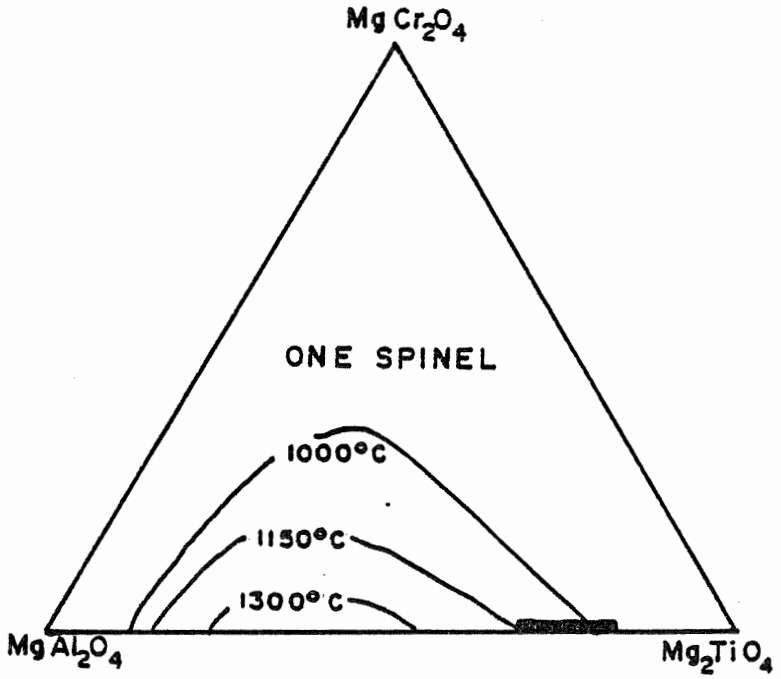
$MgCr_2O_4$
ONE SPINEL
1000°C
1150°C
1300°C
$MgAl_2O_4$
Mg_2TiO_4

crystals are strongly pleochroic, dark red to brown. Some crystals are concentrically zoned and a smaller subset appears to have weakly defined hourglass zoning. The groundmass crystals form interstitially to the groundmass pyroxene and melilite and may also form small intergrowths with the extreme outer rim of some pyroxene phenocrysts.

Many of the biotites are titanium rich with up to seven weight percent TiO_2 (Table 3-4). This probably accounts for their marked pleochroism (Deer et al., 1975). Compositionally the biotites fall along, or very near to, the phlogopite-annite boundary. The titanium rich analyses are recalculated to account for the Ti in their structures. Figure 3-9 shows the distribution of the analyses plotted with respect to phlogopite - $K_2Mg_6Al_2Si_6O_{20}(OH)_2$, annite - $K_2Fe_{4-6}Al_2Si_6O_{20}(OH)_2$, and a theoretical titanium mica - $K_2Ti_3Al_2Si_6O_{20}(OH)_2$. All of the recalculated biotites have less than 10 percent of the titanium mica component and plot in the phlogopite rich portion of the diagram.

On the basis of some experimental studies by Edgar et al. (1976) there is an interrelationship between the Ti content of phlogopite and the crystallizing liquid. The Ti content of the mica increases with crystallizing temperature and Mg number of the liquid, while the Ti content falls with decreasing pressure. Also, Ti is preferentially incorporated into Fe-rich phlogopite so that as the liquid and biotite become richer in Fe, more Ti can enter into the phlogopite structure. This relationship can be seen in Figure 3-9 where the plots fall along a line which passes through the phlogopite corner and show an increasing Fe and Ti content with Ti/Fe about 0.2.

Table 3-4

REPRESENTATIVE BIOTITE ANALYSES

Sample	BF4-2.4	BD9-2.70	BF10-11.25	BF4-2.4	BF10-11.25	BD9-2.70	BF4-2.4
SiO_2	57.10	44.10	41.36	36.09	35.49	35.47	34.51
TiO_2	0.28	0.43	5.92	6.41	6.39	6.81	7.17
Al_2O_3	19.95	13.58	13.86	14.35	14.55	15.56	14.03
Cr_2O_3	0.09	0.0	0.0	0.0	0.09	0.0	0.0
Fe_2O_3	0.0	0.0	0.0	0.0	0.0	0.0	0.0
FeO	5.87	11.78	19.39	18.60	11.05	13.17	11.75
MnO	0.12	0.12	0.47	0.38	0.23	0.13	0.25
MgO	2.74	18.76	5.58	10.95	16.76	15.77	15.91
CaO	1.99	1.34	0.49	0.31	0.08	0.11	0.64
Na_2O	0.81	0.16	1.87	0.28	0.23	0.14	0.26
K_2O	7.34	4.90	6.65	8.23	8.63	8.86	8.51
H_2O[1]	4.54	4.23	4.02	3.96	3.99	4.06	3.94
Total	100.83	99.40	99.61	99.56	97.49	100.08	96.67
			Recalculated to 24 oxygens				
Si	7.536	6.240	6.163	5.466	5.324	5.229	5.246
Al	.464	1.760	1.837	2.534	2.572	2.703	2.513
Al	2.638	.504	.597	.028	0	0	0
Ti	.028	.046	.663	.730	.721	.755	.820
Cr^{3+}	.009	0	0	0	.011	0	0
Fe^{2+}	0	0	0	0	0	0	0
Fe	.648	1.394	2.416	2.356	1.386	1.624	1.494
Mn	.013	.014	.059	.049	.029	.016	.032
Mg	.539	3.956	1.239	2.472	3.747	3.465	3.605
Ca	.281	.203	.078	.050	.013	.017	.104
Na	.207	.044	.540	.082	.067	.040	.077
K	1.236	.884	1.264	1.590	1.651	1.666	1.650
H	4	4	4	4	4	4	4

[1] H_2O added on stoichiometric basis to let H = 4.

Figure 3-9. Compositions of biotites in the system Phlogopite-Annite-Titanium mica.

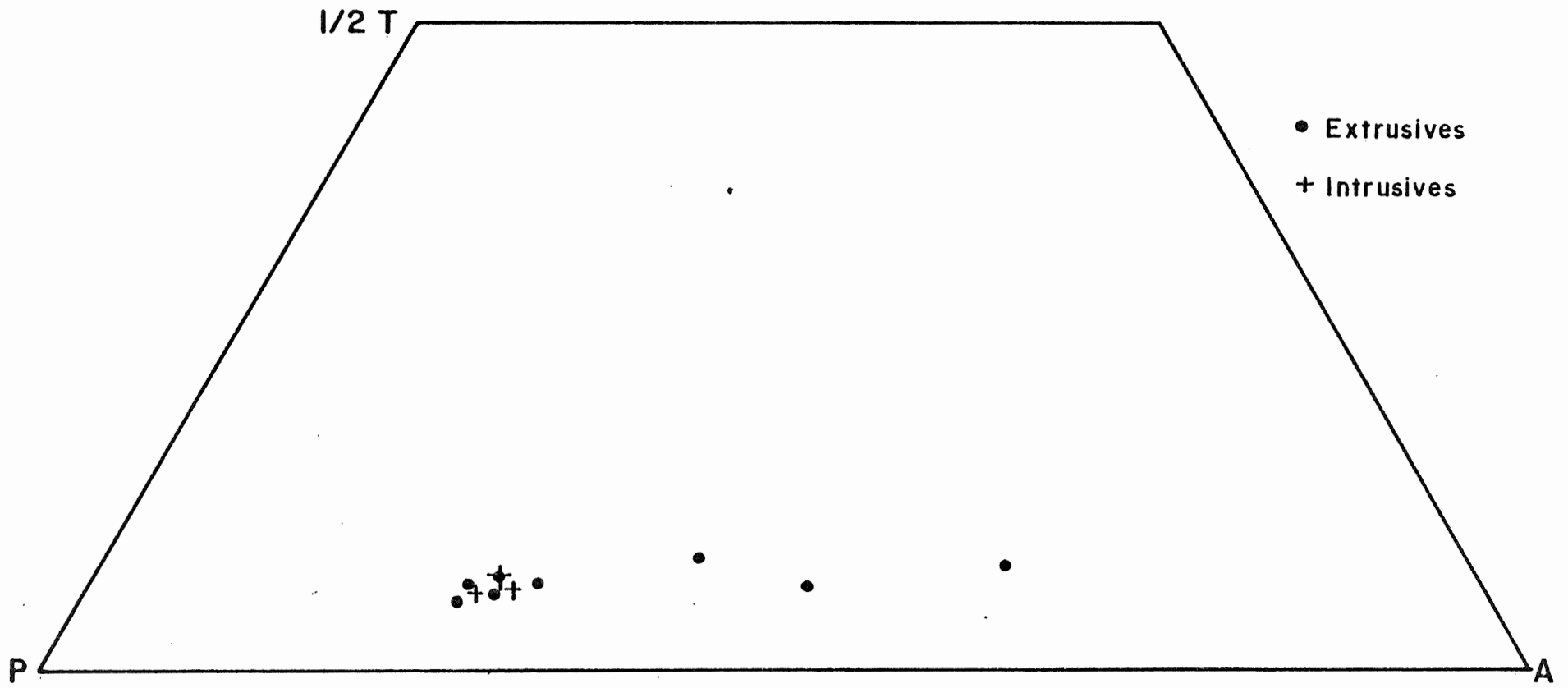
1/2 T
P
A
• Extrusives
+ Intrusives

The biotite stability is also sensitive to the oxidation state of the melt. At a constant pressure and temperature, the stability of biotite is dictated by the oxygen fugacity. For biotites with greater than 50 percent phlogopite component, the breakdown temperature increases with increase in oxygen fugacity until a maximum of about 10^{-15} bars f_{O_2} (Wones and Eugster, 1965). This value may represent a possible maximum for oxygen activity in these rocks.

Melilite

The melilite found in these rocks is very altered and is often difficult to distinguish from the altered groundmass (Figure 3-10). Where relatively fresh, these rectangular (1 mm x 0.25 mm or less) crystals are clear to honey-yellow in plane polarized light and have anomalous blue interference colors. In nearly all cases, the characteristic peg-structure is well-developed. Typically the melilites are altered to calcite and other unidentified minerals.

Melilite is a relatively rare mineral, being restricted to Al, Ca, and Na rich, silica-undersaturated rocks. It is commonly associated with the feldspathoidal minerals nepheline and leucite. Commonly, melilite alters to garnet, vesuvianite, diopside, and a fibrous brown mineral - cebollite, $Ca_5Al_2Si_3O_{14}(OH)_2$ (Deer et al., 1976).

The analyzed melilites have chemical compositions quite different from the example given by Deer et al. (1976)(Table 3-5). The analyses all have low totals, suggesting large volatile contents. Often the low-total analyses have high CaO contents which probably reflect extensive alteration to calcite. None of the analyses appear to be of a melilite,

Figure 3-10. Photomicrograph of a relatively fresh melilite with peg-structure. 320X.

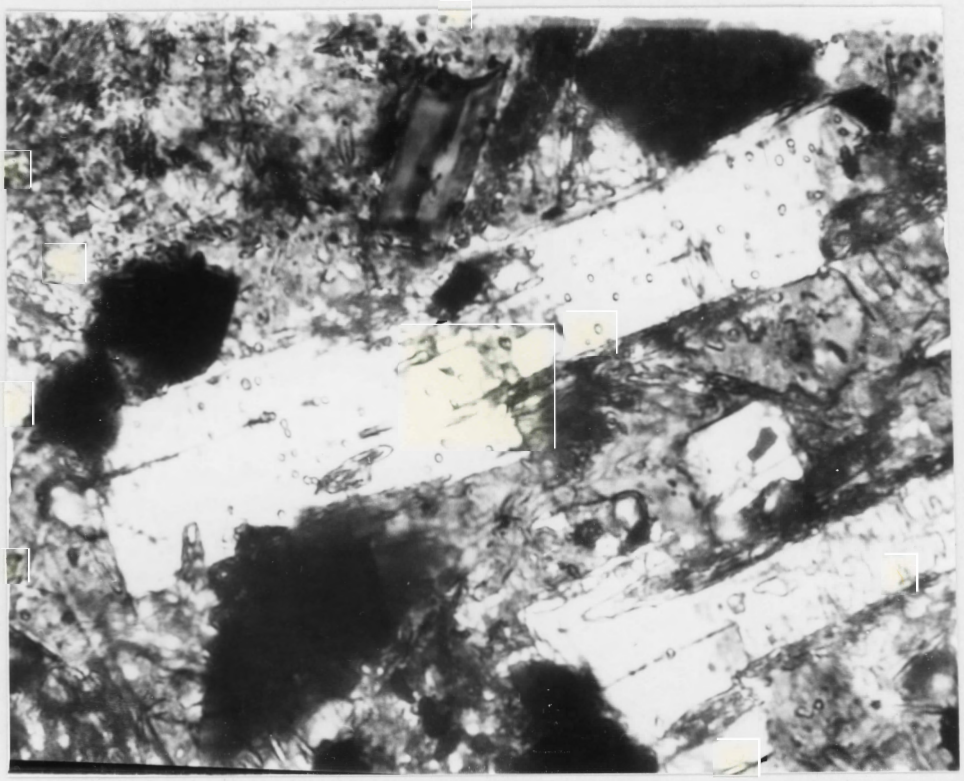

Table 3-5

MELILITE COMPOSITIONS

Sample	BF9-7.8 M1	BF9-7.8 M2	BF9-7.8 M3	BF9-7.8 M4	BF9-7.8 M5	BF9-7.8 M6
SiO_2	45.34	44.78	47.49	45.15	32.50	27.21
TiO_2	0.57	0.12	0.39	0.39	0.16	0.12
Al_2O_3	16.28	11.16	10.55	14.38	13.00	4.79
FeO*	11.33	4.99	6.45	8.85	5.80	3.54
MnO	0.15	0.14	0.10	0.21	0.45	0.26
MgO	14.74	5.68	5.31	18.34	6.73	6.97
CaO	0.59	16.49	14.94	0.34	19.34	33.13
Na_2O	0.22	3.88	3.88	0.27	0.33	1.60
K_2O	6.93	2.62	3.53	7.71	2.89	1.03
Total	96.15	89.86	92.81	95.65	82.07	78.65

	BF9-7.8 M7	BF10-11.25 MR1	BF10-11.25 MR2(Peg)	Deer et al. (1976) Melilite
SiO_2	42.97	35.12	24.00	42.81
TiO_2	0.26	0.09	0.23	0.12
Al_2O_3	16.96	10.75	7.21	6.59
FeO	4.29	6.55	7.62	4.96
MnO	0.14	0.09	0.16	0.08
MgO	6.92	8.04	11.07	7.48
CaO	8.75	17.25	23.27	33.27
Na_2O	4.99	2.50	0.40	3.75
K_2O	3.05	2.17	2.07	0.33
Total	88.33	82.63	76.03	99.79

*Total Fe as FeO.

in fact, many appear to be similar to biotite analyses. It is likely that a mixture of alteration products were analyzed. Optically, the melilite appears altered, but not sufficiently so to prevent a confident identification of the fresher grains.

This type of alteration may not be too unusual for melilites. Sahama (1976) examined the alteration of melilites from the Nyiragongo volcanics in Zaire. The alteration is characterized by the loss of Ca and Mg, the addition of K, and enrichment of Si, Al, and Fe in the pegs. The alteration is complex and a very hydrous, K-rich, phase is commonly encountered. The K-rich phase may indicate the formation of nepheline or kalsilite as well as some more siliceous minerals. Thus, it appears that melilite did form in the Bermudian rocks but high volatile concentrations, especially CO_2, altered nearly all the melilite to a mixture of calcite and a hydrous K-rich phase which resembles biotite.

Olivine

Olivine is quite altered but fresh specimens were identified in a few rocks. Even altered and pseudomorphed crystals often have very small relict inclusions of fresh olivine. Typically the olivine is altered to and pseudomorphed by calcite, talc, chlorite, quartz and magnetite. The freshest olivine is confined to the groundmass of the finer grained units. These olivines have skeletal shapes with some isotropic material as well as other unidentified groundmass phases between thin strands of olivine. This morphology is characteristic of rapid crystallization. Small (< 0.2 mm) rounded olivines with calcite or chlorite rims are found in a few rare instances.

Based on textural evidence, olivine formed early in the cooling history of these rocks, and again just prior to total crystallization. Some experimental studies indicate that olivine occurs over a very narrow temperature range in alkaline rocks and is very sensitive to oxidation and more importantly, carbonation (re: Chapter 5). Thus, the occurrence of olivine can be a reflection of the volatile flux in these rocks.

Sphene

Altered sphene is identified by its deep red color, and six-sided, bi-pyramidal outline (Figure 3-11). This mineral is always altered and is commonly found in the nucleus of a spinel. In one sample, the sphene is large enough to be considered a micro-phenocryst (>2 mm) while most are confined to the groundmass (<2 mm). This mineral may also be an altered perovskite, a phase which is commonly associated with melilite. Microprobe analyses of this phase yield high TiO_2 contents with low totals and moderate amounts of SiO_2 (Table 3-6). This substantiates the poor optical resolution and red color of these minerals which is interpreted to indicate alteration to TiO_2 and hydrous or carbonate minerals. A possible alteration scheme is:

Sphene $\rightarrow$ Rutile + Calcite + Quartz + Perovskite,

this reaction is generally initiated with increased activity of CO_2 (Deer et al., 1975).

The stability of sphene is strongly dependent upon fo_2 and the activity of silica. In the absence of physical or chemical changes, sphene becomes more stable with oxidation. A decreasing activity of SiO_2 (increased silica-undersaturation) will favor the formation of perovskite. The formation of sphene also prevents Ti from going into

Figure 3-11. Photomicrograph of an altered sphene. Reflected light, 300X.

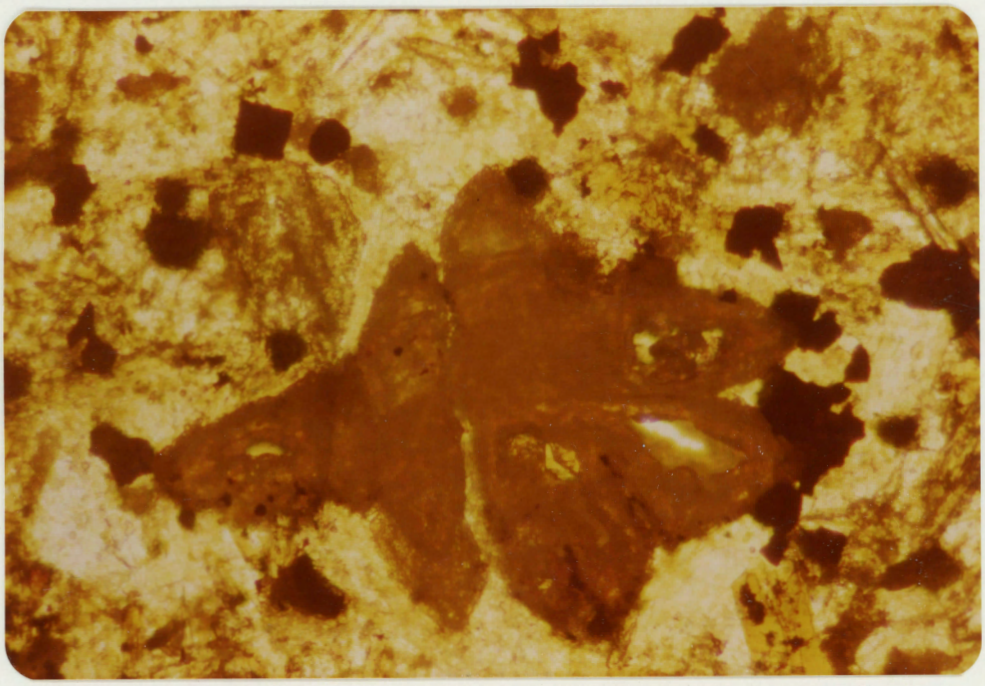

Table 3-6

MICROPROBE ANALYSIS OF THE ALTERED SPHENE

	BF4-2.4 51B	BD4-7.5 55A	BD4-7 56A	Deer et al. (1976) Sphene
SiO_2	11.21	10.09	2.41	30.35
TiO_2	75.31	72.47	82.21	35.44
Al_2O_3	3.49	2.37	0.44	2.15
$FeO = Fe^{Total}$	2.16	6.02	2.87	2.50
MnO	0.00	0.00	0.00	0.25
MgO	0.20	3.12	0.06	0.10
CaO	0.49	0.65	0.56	26.46
				REE* 1.06
Total	92.86	94.72	88.55	98.31

*REE = Rare Earth Elements.

spinel or forming ilmenite. On the basis of a compilation by Haggerty (1976, p. Hg-173) the formation and loss of sphene can be considered as either a change in oxidation state or silica activity. In the first case, sphene could form from an oxidized melt such that:

Diopside + Ulvospinel + O_2 = Magnetite + Sphene + Enstatite.

A drop in fo_2 or an increase in temperature would cause this reaction to be reversed.

Other Phases

Apatite forms small ($\lesssim$1 mm) needles often intergrown with biotite in the groundmass of these rocks. It is more common to the dikes than the flows.

Sulfide blebs of pyrite (<0.1 mm) with rounded outlines and highly convoluted margins are common in the groundmass. This morphology suggests a silicate-sulfide immiscibility for these rocks.

There are a variety of secondary minerals; the commonest being calcite. Calcite occurs as an alteration product of the mesostasis, and olivine, and is ubiquitous in small veins. Chlorite generally forms by the alteration of the mesostasis or of olivine. It may also occur along the edge of the calcite-filled veins. Unidentified clay minerals occur in amygdules and in veins. Analcite is only found in the calcite veins. Serpentine-talc minerals are found in a few olivine pseudomorphs. Hematite is found in veins and disseminated in the groundmass. Finally, dolomite is found in the amygdules of dike BD9-2. With the exception of calcite and chlorite, these secondary minerals are of little volumetric importance.

CHAPTER 4

GEOCHEMISTRY

Introduction

The whole-rock geochemistry of the extrusives and intrusives indicates that chemically all the units sampled are similar (Table 4-1). They are markedly silica-undersaturated and rich in TiO_2 and CO_2. In fact, the extrusives are one of the most silica-deficient lavas found on any island in the Atlantic Ocean (Mitchell-Thomé, 1976). This chapter will give an overview of the major element geochemistry, as well as present a brief comparison with similar rocks.

Methods

Ten minicore samples from six cooling units and four intrusives were crushed until the fines were less than 100 mesh using a tungsten-carbide swing mill. The powders were homogenized and then fused into glass beads using an electric arc. The beads were mounted on an epoxy block and polished. The individual beads were analyzed using a Cambridge-5 Microprobe and an Ortec energy dispersion analyzer (relative error <5%). Five or more replicate analyses were made on each bead until each replication showed less than five percent variance from the running average. Sample DPL (Dalhousie Pillow Lava) was used as a reference standard. The ferric-ferrous ratios, H_2O and CO_2 values were determined using standard techniques. Note: this technique yields anomalously high sulfur values; for a more detailed discussion of whole-rock analyses using the Dalhousie probe, see MacKay (1981).

Results and Interpretation

The complete major element analyses are given in Table 4-1. CIPW norms were calculated using the original compositions and several modifications of the chemistry: 1) complete (Table 4-1), 2) calcite free (Table 4-2), 3) volatile free (Table 4-3), and 4) $Fe_2O_3/FeO+Fe_2O_3$ set at 0.53 (Table 4-4). The purpose of using these various modifications is to determine the effects of the volatiles and oxidation state upon the normative mineralogy. The rationale for the adjustments to the major element analyses are as follows. The calcite-free analyses assume that all the carbonate is introduced from an external source and that all the CO_2 plus an equivalent amount of CaO forms calcite. No account for Mg in the calcite has been made. This calcite may have been added from rock-seawater interaction (e.g. Aumento et al., 1976). The volatile-free corrections assume that the high volatile content of the rocks is of a secondary origin, but that no other components were added to the parent rock. This implies that much of the variation can be attributed to hydration and carbonation of the rocks. The ferric-ferrous ratio is sensitive to oxidation during emplacement and post-cooling, low-grade alteration. The commonly used algorithm of $Fe_2O_3 = TiO_2+1.5\%$ or $Fe_2O_3 = 1.5\%$ (Irvine and Baragar, 1971) cannot be used in these lavas because they are so silica-deficient and titanium rich. The method used here was derived from the inspection of the ferric-ferrous ratios reported in analyses of alkaline rocks from Atlantic Ocean islands (Mitchell-Thomé, 1976; Carmichael et al., 1975). Apparently, the alkaline rocks are more oxidized than the commoner igneous rocks with an average $Fe_2O_3/FeO+Fe_2O_3 = 0.53$.

Table 4-1

CORRELATION OF SAMPLE LABELS AND REFERENCE NUMBERS USED IN FIGURES

Figure Number	Sample Label
1	BF4-4
2	BF5-4
3	BF8-12
4	BF9-9
5	BF11-7
6	BF12-12
7	BD4-4
8	BD5-4
9	BD9-2
10	BD10-4

Note: Analyses are systematically high in S. This is an artifact of the microprobe technique.

$H_2O = H_2O_{total}$

Table 4-1

WHOLE-ROCK GEOCHEMISTRY AND NORMS - COMPLETE

Sample	BF4-4*	BF5-4	BF8-12	BF9-9	BF11-7	BF12-12	BD4-4	BD5-4	BD9-2	BD10-4
SiO_2	37.72	37.44	36.57	38.05	38.06	35.69	35.84	35.86	30.43	30.98
TiO_2	5.40	5.30	5.11	5.45	5.60	5.10	4.12	5.21	5.00	4.88
Al_2O_3	11.49	11.30	11.13	11.66	11.97	11.07	9.92	9.79	8.65	8.88
Cr_2O_3	0.00	.03	0.00	.07	0.00	0.00	0.00	0.00	0.00	0.00
Fe_2O_3	7.15	8.17	7.66	7.26	6.84	6.80	5.29	8.14	7.05	9.39
FeO	5.75	5.12	5.94	5.65	6.40	5.64	5.91	6.04	5.25	4.63
MnO	.19	.18	.10	.20	.15	.19	.24	.15	.12	.18
NiO	0.00	0.00	0.00	0.00	0.00	0.00	0.00	0.00	0.00	0.00
MgO	7.10	8.42	5.18	6.94	6.66	6.52	6.71	12.24	8.74	9.06
CaO	11.15	9.90	9.17	13.18	9.96	12.13	16.31	9.72	16.18	16.28
Na_2O	2.27	2.45	1.97	1.89	4.11	2.92	1.99	1.81	1.38	1.38
K_2O	2.79	2.40	3.18	2.97	1.59	2.25	1.78	1.18	1.55	1.45
P_2O_5	1.21	1.17	1.11	1.21	1.27	1.12	.60	1.30	.70	.65
CO_2	2.74	2.58	5.91	2.87	3.13	4.45	7.49	2.57	9.25	9.25
H_2O	4.70	4.79	4.67	3.62	5.25	5.37	3.30	5.86	4.72	4.72
S	.93	.88	1.16	1.38	1.10	1.47	.60	1.03	1.09	.94
Total	100.59	100.13	98.86	102.40	102.09	100.72	100.10	100.90	100.11	102.67
Q	0.00	0.00	5.14	0.00	0.00	0.00	0.00	0.00	0.00	0.00
Or	17.22	14.90	19.99	17.80	9.72	13.97	10.88	7.35	9.62	8.76
Ab	14.12	17.63	17.71	7.79	25.04	16.98	17.40	16.12	12.25	11.93
An	13.48	13.37	.92	14.75	9.83	10.97	13.31	15.90	13.46	14.05
Ne	3.21	2.24	0.00	4.56	5.90	4.85	0.00	0.00	0.00	0.00
Lc	0.00	0.00	0.00	0.00	0.00	0.00	0.00	0.00	0.00	0.00
Di	13.94	10.13	0.00	19.54	9.49	11.66	13.49	6.85	3.58	3.41
Hy	0.00	0.00	13.71	0.00	0.00	0.00	5.02	8.65	10.49	11.33
Ol	8.40	12.13	0.00	5.92	8.93	8.16	4.20	14.20	7.49	7.10
Cr	0.00	.05	0.00	.10	0.00	0.00	0.00	0.00	0.00	0.00
Mt	.15	0.00	.50	0.00	.94	0.00	5.91	1.20	0.00	0.00
Hm	7.36	8.57	7.79	7.36	6.42	7.14	1.39	7.75	7.40	9.59
Il	10.70	9.54	10.31	9.14	10.99	9.28	8.09	10.42	9.20	8.11
Ru	0.00	.54	0.00	.71	0.00	.47	0.00	0.00	.40	.71
Ap	2.93	2.85	2.74	2.84	3.04	2.73	1.44	3.18	1.70	1.54
C	0.00	0.00	4.38	0.00	0.00	0.00	0.00	0.00	0.00	0.00
CC	6.50	6.16	14.28	6.61	7.36	10.62	17.60	6.15	22.07	21.49
Total	98.00	98.10	97.47	97.12	97.66	96.83	98.72	97.77	97.65	98.03

*BF = Extrusives, BD = Intrusives

Table 4-2

CALCITE-FREE ANALYSES AND NORMS

Sample	BF4-4	BF5-4	BF8-12	BF9-9	BF11-7	BF12-12	BD4-4	BD5-4	BD9-2	BD10-4
SiO_2	39.66	39.42	42.13	39.39	39.72	38.87	42.06	37.45	37.29	36.81
TiO_2	5.68	5.58	4.86	5.64	5.84	5.55	4.83	5.44	6.13	5.80
Al_2O_3	12.08	11.90	12.76	12.07	12.49	12.06	11.64	10.22	10.60	10.55
Cr_2O_3	0.00	.03	0.00	.07	0.00	0.00	0.00	0.00	0.00	0.00
Fe_2O_3	7.52	8.60	8.78	7.52	7.14	7.40	6.21	8.50	8.64	11.16
FeO	6.05	5.39	6.81	5.85	6.68	6.10	6.93	6.31	6.43	5.50
MnO	.16	.19	.11	.21	.16	.20	.28	.16	.15	.21
NiO	0.00	0.00	0.00	0.00	0.00	0.00	0.00	0.00	0.00	0.00
MgO	7.46	8.87	5.94	7.18	6.95	7.10	7.87	12.78	10.71	10.76
CaO	8.84	7.71	3.74	10.67	7.13	8.36	10.35	7.47	8.49	8.35
Na_2O	2.39	2.58	2.26	1.96	4.29	3.18	2.33	1.89	1.69	1.64
K_2O	2.93	2.53	3.65	3.07	1.66	2.45	2.09	1.23	1.90	1.72
P_2O_5	1.27	1.23	1.27	1.25	1.32	1.22	.70	1.36	.86	.77
CO_2	0.00	0.00	0.00	0.00	0.00	0.00	0.00	0.00	0.00	0.00
H_2O	4.94	5.04	5.35	3.75	5.48	5.85	3.99	6.12	5.78	5.61
S	.98	.93	1.33	1.43	1.15	1.60	.70	1.07	1.33	1.11
Total	99.96	100.00	99.99	100.06	100.01	99.94	99.98	100.00	100.00	99.99
Q	0.00	0.00	1.82	0.00	0.00	0.00	0.00	0.00	0.00	0.00
Or	18.25	15.77	22.83	18.87	10.39	15.42	12.88	7.76	11.94	10.79
Ab	12.09	15.83	20.22	5.33	23.41	13.81	15.66	17.05	12.13	12.66
An	14.29	14.13	10.83	15.65	10.50	12.12	15.76	16.81	16.70	17.33
Ne	4.99	3.89	0.00	6.45	8.14	8.03	2.65	0.00	1.66	1.11
Lc	0.00	0.00	0.00	0.00	0.00	0.00	0.00	0.00	0.00	0.00
Di	18.01	13.77	0.00	24.02	13.86	18.30	25.67	10.28	17.17	16.54
Hy	0.00	0.00	15.64	0.00	0.00	0.00	0.00	4.98	0.00	0.00
Ol	7.86	11.84	0.00	5.22	8.34	7.24	5.97	16.95	14.28	14.54
Cr	0.00	.05	0.00	.11	0.00	0.00	0.00	0.00	0.00	0.00
Mt	.02	0.00	.55	0.00	1.03	0.00	7.01	1.31	0.00	0.00
Hm	7.90	9.06	8.91	7.82	6.85	7.87	1.64	8.16	9.18	11.83
Il	11.36	10.07	11.77	9.72	11.74	10.13	9.56	11.01	11.42	10.01
Ru	0.00	.58	0.00	.74	0.00	.57	0.00	0.00	.50	.88
Ap	3.10	3.01	3.12	3.01	3.24	3.01	1.69	3.36	2.12	1.89
C	0.00	0.00	1.41	0.00	0.00	0.00	0.00	0.00	0.00	0.00
Total	97.88	97.98	97.11	96.94	97.50	96.50	98.50	97.65	97.09	97.58

Table 4-3

VOLATILE-FREE ANALYSES AND NORMS

Sample	BF4-4	BF5-4	BF8-12	BF9-9	BF11-7	BF12-12	BD4-4	BD5-4	BD9-2	BD10-4
SiO_2	40.62	40.39	41.33	40.16	41.06	39.41	40.17	38.96	35.35	35.42
TiO_2	5.81	5.72	5.75	5.75	6.04	5.63	4.62	5.66	5.81	5.58
Al_2O_3	12.37	12.19	12.52	12.31	12.91	12.23	11.12	10.64	10.05	10.15
Cr_2O_3	0.00	.03	0.00	.07	0.00	0.00	0.00	0.00	0.00	0.00
Fe_2O_3	7.70	8.82	8.62	7.66	7.38	7.51	5.93	8.85	8.19	10.74
FeO	6.19	5.52	6.68	5.96	6.90	6.23	6.63	6.56	6.10	5.30
MnO	.21	.19	.11	.21	.16	.21	.27	.16	.14	.21
NiO	0.00	0.00	0.00	0.00	0.00	0.00	0.00	0.00	0.00	0.00
MgO	7.65	9.08	5.83	7.33	7.18	7.20	7.52	13.30	10.15	10.36
CaO	12.01	10.68	10.31	13.91	10.74	13.39	18.28	10.56	18.79	18.61
Na_2O	2.44	2.64	2.22	2.00	4.43	3.23	2.23	1.97	1.60	1.58
K_2O	3.01	2.59	3.58	3.14	1.72	2.48	2.00	1.28	1.80	1.66
P_2O_5	1.30	1.26	1.25	1.28	1.37	1.24	.67	1.41	.81	.74
CO_2	0.00	0.00	0.00	0.00	0.00	0.00	0.00	0.00	0.00	0.00
H_2O	0.00	0.00	0.00	0.00	0.00	0.00	0.00	0.00	0.00	0.00
S	1.00	.95	1.30	1.46	1.19	1.62	.67	1.12	1.27	1.08
Total	100.31	100.06	99.50	101.24	101.08	100.38	100.11	100.47	100.06	101.43
Or	17.76	15.32	21.30	6.88	10.07	6.05	0.00	7.54	0.00	0.00
Ab	1.33	5.68	7.85	0.00	10.95	0.00	0.00	9.94	0.00	0.00
An	13.87	13.76	13.69	15.16	10.16	11.51	14.41	16.34	14.92	14.59
Ne	10.44	9.02	5.98	9.06	14.17	14.76	10.21	3.61	7.33	7.14
Lc	0.00	0.00	0.00	9.00	0.00	6.72	9.27	0.00	8.35	7.60
Wo	0.00	0.00	0.00	0.00	0.00	0.00	8.34	0.00	1.24	.12
Di	28.86	24.12	22.98	34.86	26.25	36.31	32.36	20.74	19.61	20.74
Ol	3.94	8.01	2.77	1.32	3.88	.73	2.60	16.38	11.35	11.10
La	0.00	0.00	0.00	0.00	0.00	0.00	3.18	0.00	13.89	13.59
Cr	0.00	.04	0.00	.10	0.00	0.00	0.00	0.00	0.00	0.00
Mt	.18	0.00	.53	0.00	.95	0.00	6.44	1.21	0.00	0.00
Hm	7.55	8.82	8.30	7.57	6.65	7.49	1.49	7.98	8.19	10.60
Il	11.01	9.79	10.98	9.40	11.35	9.75	8.77	10.71	10.18	8.96
Ru	0.00	.57	0.00	.73	0.00	.48	0.00	0.00	.45	.78
Ap	3.01	2.92	2.92	2.94	3.15	2.87	1.55	3.26	1.88	1.69
Total	97.95	98.05	97.31	97.03	97.58	96.68	98.62	97.71	97.39	97.81

Table 4-4

FE-ADJUSTED ANALYSES AND NORMS

Sample	BF4-4	BF5-4	BF8-12	BF9-9	BF12-12	BD9-2	BD10-4
SiO_2	37.72	37.44	36.75	38.05	35.69	39.66	30.98
TiO_2	5.40	5.30	5.11	5.45	5.10	5.68	4.88
Al_2O_3	11.49	11.30	11.13	11.66	11.07	12.08	8.88
Cr_2O_3	0.00	0.00	0.00	0.00	0.00	0.00	0.00
Fe_2O_3	6.84	7.04	7.21	6.84	6.60	7.52	7.43
FeO	6.06	6.25	6.39	6.07	5.85	6.05	6.59
MnO	.19	.18	.10	.20	.19	.16	.18
NiO	0.00	0.00	0.00	0.00	0.00	0.00	0.00
MgO	7.10	8.42	5.18	6.94	6.52	7.46	9.06
CaO	11.15	9.90	9.17	13.18	12.13	8.84	16.28
Na_2O	2.27	2.45	1.97	1.89	2.92	2.39	1.38
K_2O	2.79	2.40	3.18	2.97	2.25	2.93	1.45
P_2O_5	1.21	1.17	1.11	1.21	1.12	1.27	.65
CO_2	2.74	2.58	5.91	2.87	4.45	0.00	9.25
H_2O	4.70	4.79	4.67	3.62	5.37	4.94	4.72
S	.93	.88	1.16	1.38	1.47	.98	.94
Total	100.59	100.10	99.04	102.33	100.73	99.96	102.67
Q	0.00	0.00	5.32	0.00	0.00	0.00	0.00
Or	17.22	14.90	19.95	17.81	13.97	18.25	8.76
Ab	14.12	17.63	17.68	7.80	16.98	12.09	11.93
An	13.48	13.38	.92	14.76	10.97	14.29	14.05
Ne	3.21	2.24	0.00	4.56	4.85	4.99	0.00
Lc	0.00	0.00	0.00	0.00	0.00	0.00	0.00
Di	13.94	10.14	0.00	19.55	11.66	18.01	3.41
Hy	0.00	0.00	13.68	0.00	0.00	0.00	11.33
Ol	8.40	12.13	0.00	5.93	8.16	7.86	7.10
Mt	1.19	2.30	2.04	0.00	0.00	.02	4.38
Hm	6.32	5.80	6.24	6.94	6.93	7.90	4.57
Il	10.70	10.57	10.29	10.12	9.74	11.36	9.47
Ru	0.00	0.00	0.00	.20	.22	0.00	0.00
Ap	2.93	2.85	2.73	2.85	2.73	3.10	1.54
C	0.00	0.00	0.00	0.00	0.00	0.00	0.00
CC	6.50	6.16	14.25	6.62	10.62	0.00	21.49
Total	98.00	98.10	97.47	97.12	96.83	97.88	98.03

The average compositions of the Deep Drill-1972 lavas and sheets and a compilation of average kimberlite, nephelinite, and alkali basalt analyses are given in Table 4-5. Of all the analyses presented, the new samples are most akin to the average nephelinite.

A cursory inspection of the down-hole variation in the major element oxides (Figure 4-1) shows no significant correlation of composition with depth for any one element. The chemistry of the intrusives, however, is consistently different from that of the cooling units, but only by a few weight percent of any one oxide. Nonetheless, several conclusions about the extrusives and intrusives can be drawn from this figure and Figure 4-2. In Figure 4-1 it can be seen that the TiO_2, Al_2O_3, and P_2O_5 contents show little variation, well within the analytical error of the analyses. Also SiO_2, FeO, Fe_2O_3, and K_2O show moderate amounts of variation. MgO, CaO, Na_2O, H_2O, and CO_2 show the greatest amount of variation.

These variations may be due to alteration of the rocks by hydrothermal fluids (i.e. hot seawater). Alteration trends may delineated by plotting oxide percentages against total volatile content (Figure 4-2). In this plot TiO_2, SiO_2, and P_2O_5 show almost no change. K_2O, Na_2O, FeO, and MgO vary, but show no net change. Fe_2O_3 and Al_2O_3 vary and but show a slight net drop. CaO varies considerably and increases markedly in the most volatile rich samples. These variations are not consistent with general models of rock-seawater interaction which indicate a loss of CaO, MgO, SiO_2, and some Al_2O_3, and a gain in Na_2O, K_2O, H_2O, CO_2 and possibly, P_2O_5, TiO_2, and Fe^{total} with progressive alteration (Aumento et al., 1976). Instead, these trends may reflect the alteration of these rocks by their own volatiles with only a minor

Table 4-5

AVERAGE KIMBERLITE, NEPHELINITE AND ALKALI BASALT COMPOSITIONS, PLUS THE 1972 LAVA AND SHEET AVERAGES

	Kimberlite*	Nephelinite*	Alkali Basalt*	1972 Lavas	1972 Sheets
SiO_2	31.45	40.30	48.38	48.16	38.32
TiO_2	1.97	2.80	2.40	1.31	4.63
Al_2O_3	3.57	11.64	15.00	14.16	10.94
Cr_2O_3	.32	.05	.03	n.d.	n.d.
Fe_2O_3	0.00	0.00	0.00	8.61	12.78
FeO	9.21	11.71	11.67	0.0	0.0
MnO	.16	.19	.19	0.16	0.20
NiO	0.00	0.00	0.00	0.0	0.0
MgO	26.53	11.80	7.50	5.53	6.82
CaO	9.85	12.59	9.10	11.45	13.93
Na_2O	.27	3.41	3.10	3.81	2.23
K_2O	1.25	1.47	1.60	0.66	2.05
P_2O_5	.89	.87	.48	0.16	0.69
CO_2	5.94	.07	0.00	3.21	4.48
H_2O	0.00	0.00	0.00	2.72	2.67
S	.20	.06	0.00	0.07	0.25
Total	91.61	96.96	99.45	100.01	99.99
Q				0.46	0
Or	8.07	0.00	9.52	4.05	12.64
Ab	2.49	0.00	23.22	33.45	15.41
An	5.28	12.49	22.41	20.33	14.37
Ne	.00	16.12	1.71	0.0	2.31
Lc	0.00	7.03	0.00	0.0	0.0
Di	.57	28.15	16.38	13.31	18.71
Hy	.00	.00	.06	14.47	0.0
Ol	61.54	24.87	21.02	0.0	9.74
La	0.00	3.40	0.00	0.0	0.0
Mt	.00	.00	.00	3.23	4.84
Cr	.51	.08	.04	0.0	0.0
Il	4.08	5.48	4.58	2.58	9.17
Ap	2.25	2.08	1.12	0.38	1.67
Cc	14.75	.16	0.00	7.58	10.62
Total	99.55	99.87	100.00	99.85	99.46

*From Wedepohl and Muramatsu (1979).

Figure 4-1. Down-hole changes in the major element chemistry.

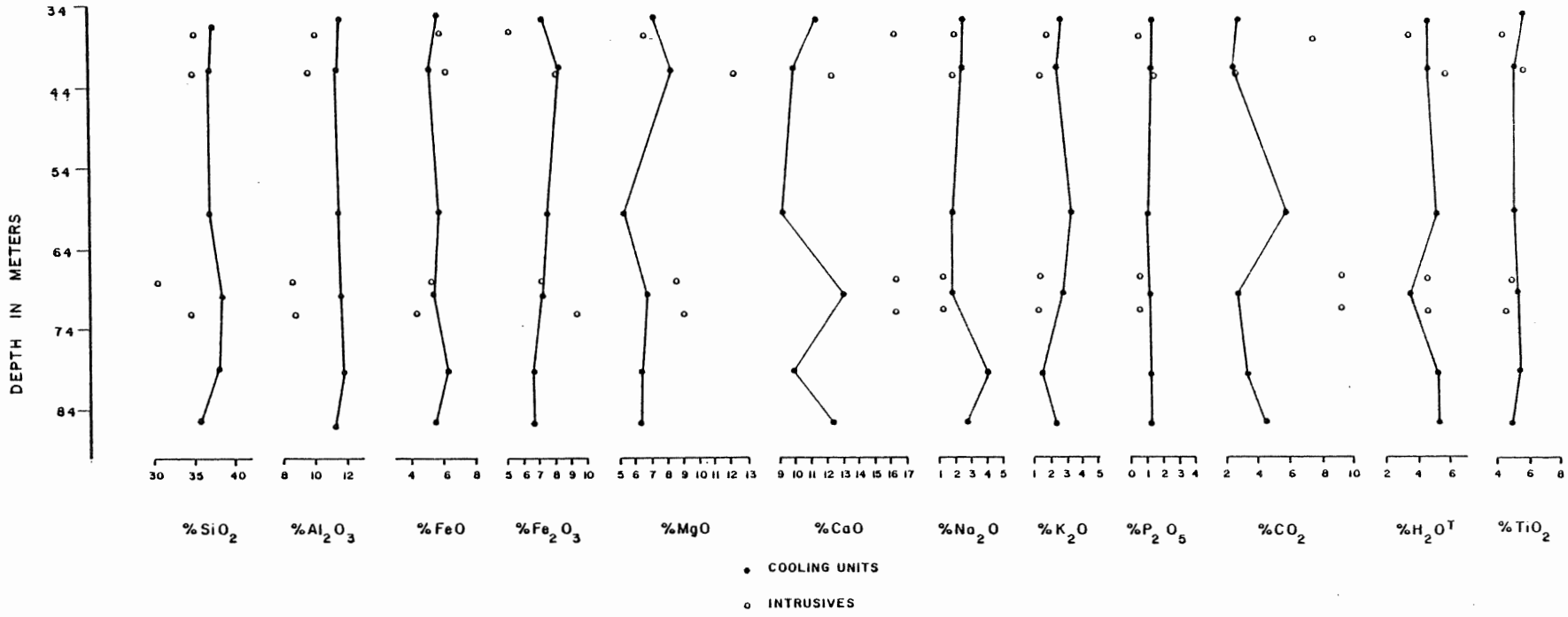
DEPTH IN METERS
34
44
54
64
74
84
30 35 40
%SiO2
8 10 12
%Al2O3
4 6 8
%FeO
5 6 7 8 9 10
%Fe2O3
5 6 7 8 9 10 11 12 13
%MgO
9 10 11 12 13 14 15 16 17
%CaO
1 2 3 4 5
%Na2O
1 2 3 4 5
%K2O
0 1 2 3 4
%P2O5
2 4 6 8 10
%CO2
2 4 6
%H2OT
4 6 8
%TiO2
COOLING UNITS
INTRUSIVES

Figure 4-2. Plot of (CO_2+H_2O) versus oxides showing some of the effects of increased volatile contents. Numbers refer to Table 4-1 for all figures.

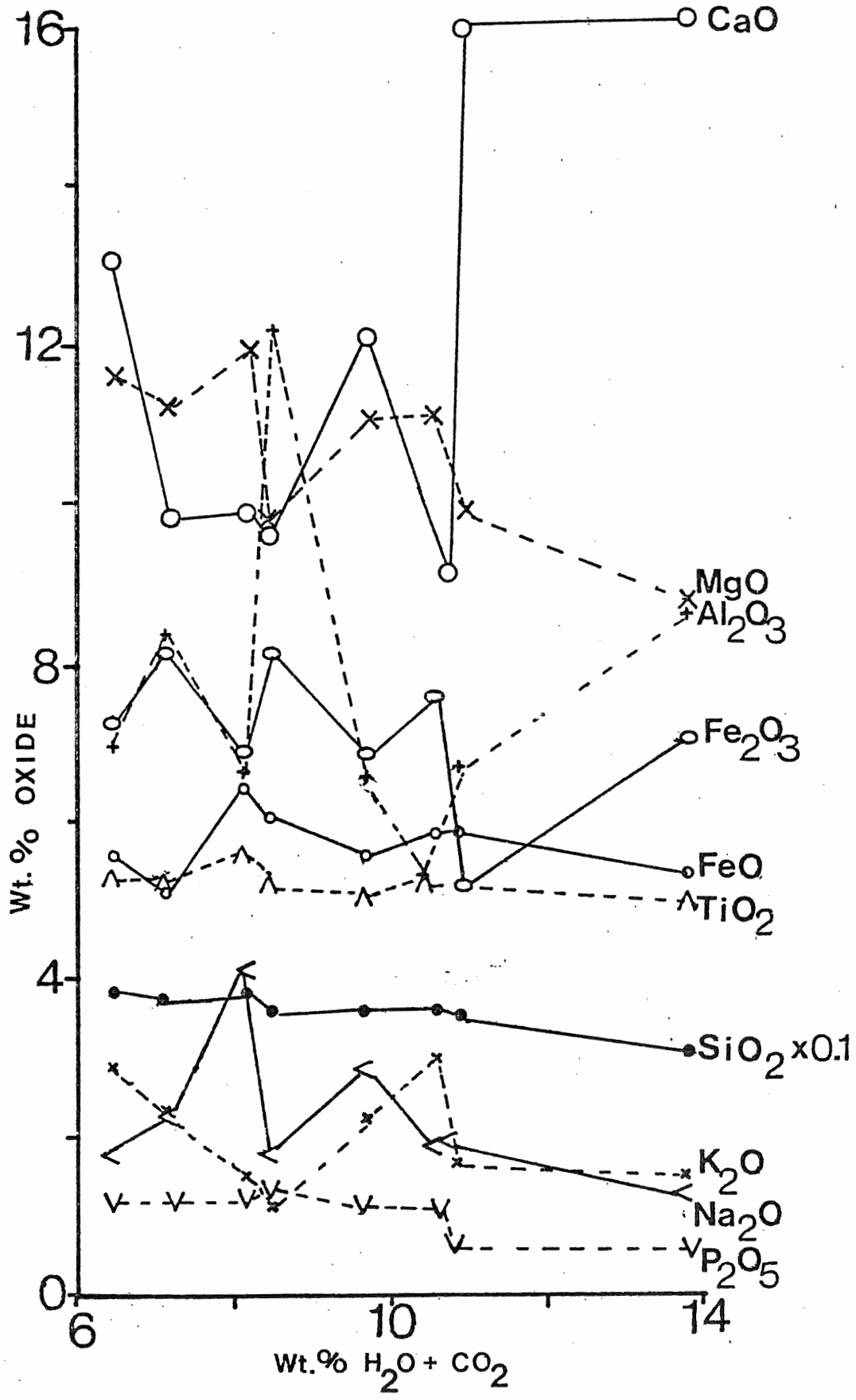
16
12
8
4
0
6
10
14
Wt. % OXIDE
Wt.% $H_2O + CO_2$
CaO
MgO
Al_2O_3
Fe_2O_3
FeO
TiO_2
SiO_2 x0.1
K_2O
Na_2O
P_2O_5

amount of rock-seawater interaction. This probably holds true for the intrusives which have higher volatile contents and also show more extreme variations in their compositions.

The oxidation state of these rocks may also be a function of the volatile content (Figure 4-3). The relationship expressed in Figure 4-3 suggests that the volatile content has little affect upon the Fe_2O_3/ $FeO+Fe_2O_3$ ratios. It appears that the measured ratios reflect the oxidation state of the rocks which seems to be independent of the volatile content. This relationship may be explained by assuming that either the volatiles had no affect on the oxidation state or that the oxidation state is controlled by both the CO_2-H_2O ratios and the rock mineralogies.

An examination of the oxide-oxide variations can be used to determine the chemical classification of these rocks, as well as to help filter out the variations due to alteration. These trends will then be used to interpret the normative mineralogies. If the rocks form a tight cluster on chemical classification diagrams then either they are unaltered, or they have suffered exactly the same degree and type of alteration. Also, if these rocks are altered, then there will be a discrepancy between the original mineralogical classification and the chemical classification.

It is apparent from the mineralogy that these rocks are of strong alkaline affinity, therefore the first classification to be applied is the alkali-silica diagram devised by Nockolds (1954) (Figure 4-4). All of the extrusives plot neatly in the nephelinite field with the intrusives extending into the melilite facies. The lavas

Figure 4-3. Plot of (CO_2+H_2O) versus Fe_2O_3/Fe_2O_3+FeO showing the apparent lack of correlation between these two quantities. The correlation coefficient for the regression line is 0.126.

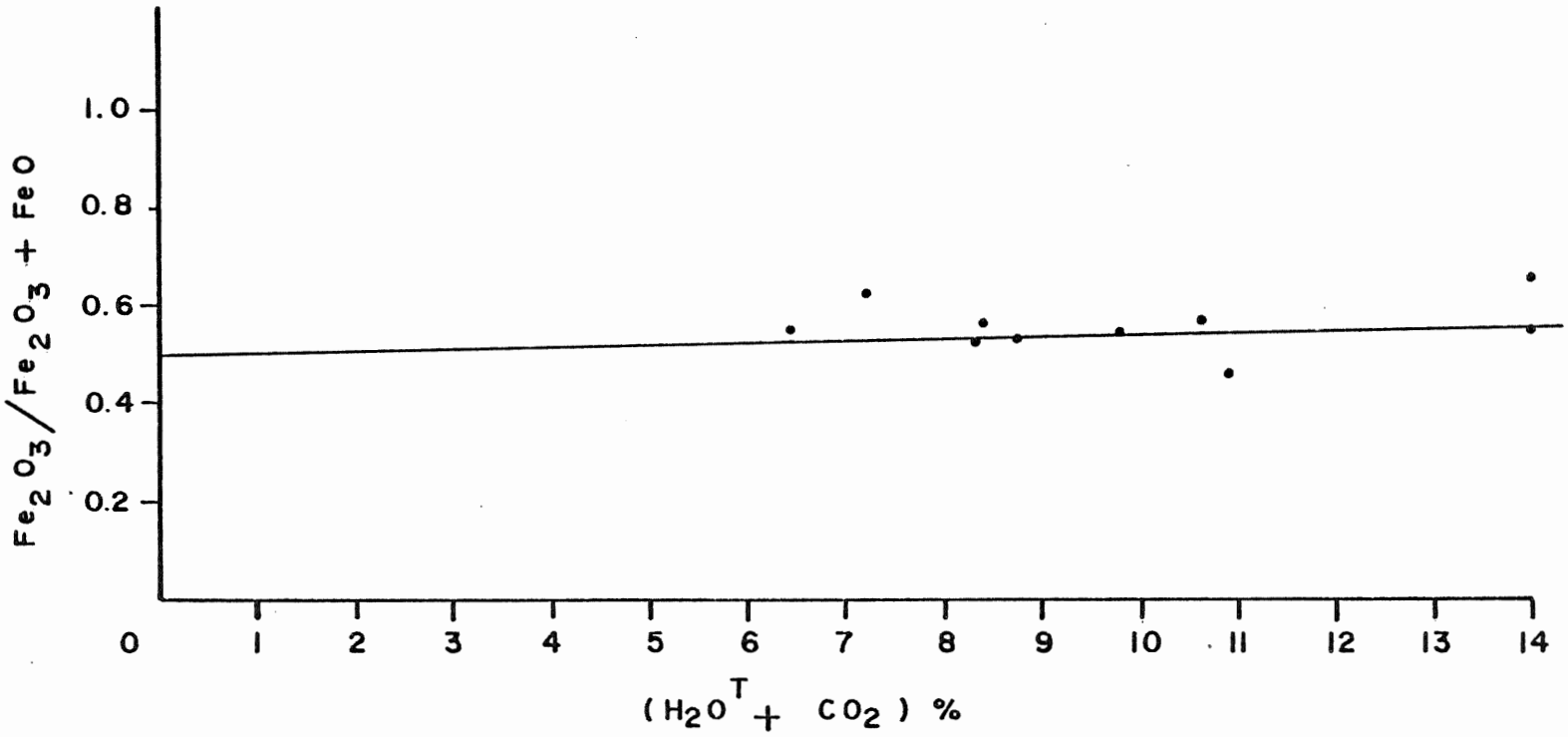
1.0
0.8
0.6
0.4
0.2
$Fe_2O_3/Fe_2O_3 + FeO$
0
1
2
3
4
5
6
7
8
9
10
11
12
13
14
$(H_2O^T + CO_2)$ %

Figure 4-4. Alkali versus silica plot, after Nockolds (1954).

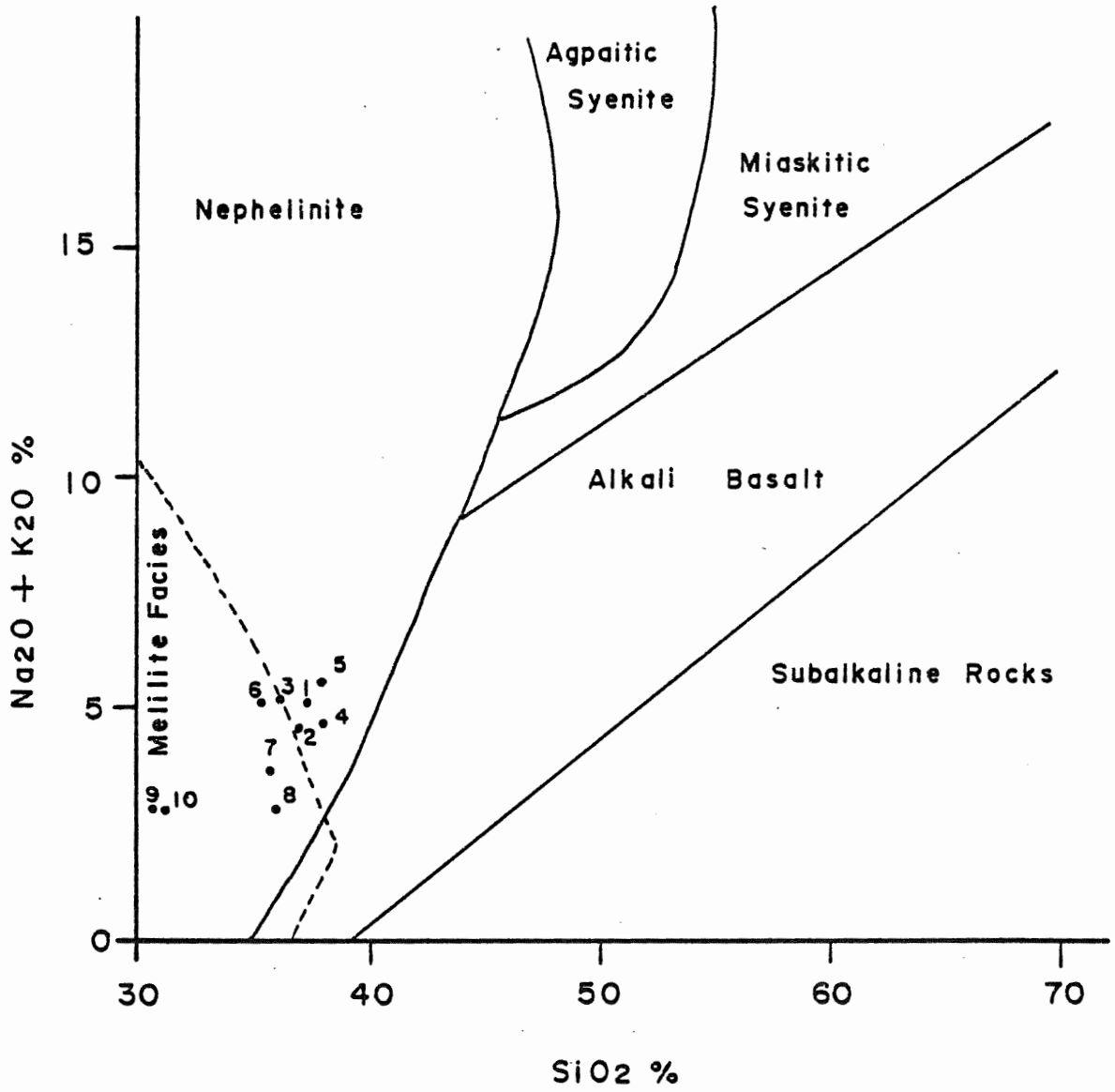
Agpaitic
Syenite
Miaskitic
Syenite
Nephelinite
Alkali Basalt
Subalkaline Rocks
Melilite Facies
Na2O + K2O %
SiO2 %
0
5
10
15
30
40
50
60
70
1
2
3
4
5
6
7
8
9
10

form a more coherent group than the intrusives. This classification is substantiated by an examination of these rocks on an AFM plot (Figure 4-5). With the exception of BF8-11(#3), the lavas form a grouping which is relatively concordant. This locus falls within the lesser evolved region of oceanic-island alkaline suites. All of the analyses, with the obvious exceptions, fall within the field of Hawaiian nephelinites. It should be stressed that many other rock types will also fall within this zone and this projection is non-diagnostic.

The nephelinite classification has been further subdivided using the systematics of LeBas (1978). He has divided the nephelinites into two subclasses: Group I - basaltic association and Group II - carbonate association. These two groups are distinguishable both mineralogically and chemically. Group I nephelinites have olivine phenocrysts, and are rich in accessory clinopyroxene (titan-augite) while Group II nephelinites are olivine poor with high Al/Ti clinopyroxene phenocrysts predominating. These two groups are distinguished chemically on the basis of MgO+FeO versus CaO+Fe_2O_3 and MgO versus CaO (Figure 4-6). Figure 4-6a indicates that the Bermudian igneous rocks are melanephelinites of Group II. In Figure 4-6b, the rocks are mainly Group II melanephelinites, with a few samples following the Group I trend along the melanephelinite-nephelinite boundary.

A few trends are evident on the oxide versus silica plot (Figure 4-7). The following oxides generally decrease with increasing silica content, CaO and CO_2, while Al_2O_3, Na_2O_3, K_2O (slight), and TiO_2 (slight) increase. FeO and MgO show no distinctive trends although Fe_2O_3 may increase slightly. These trends do not compare well with

Figure 4-5. AFM projection of the Bermudian samples. The field of oceanic-island (dashed line) and Hawaiian nephelinites (solid line) are given for comparison (Irvine and Baragar, 1971). The projections of the average kimberlite, nephelinite, and alkali basalt are also given (Wedepohl and Muramatsu, 1979).

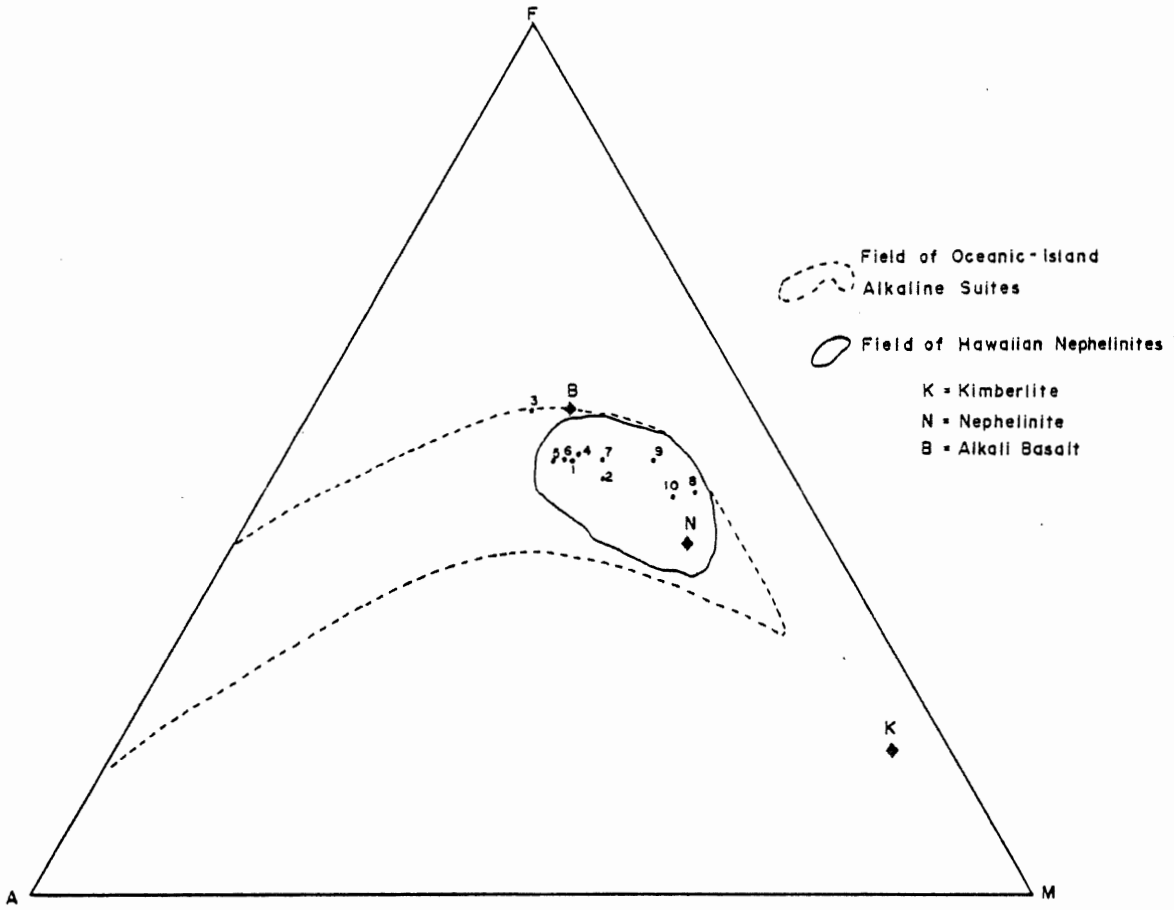
F
A
M
B
N
K
3
5
6
4
1
7
2
9
10
8
Field of Oceanic-Island Alkaline Suites
Field of Hawaiian Nephelinites
K = Kimberlite
N = Nephelinite
B = Alkali Basalt

Figure 4-6. Oxide variations of the Bermudian rocks with respect to the nephelinite trends of LeBas (1978). Group I and Group II nephelinites are differentiated on Figure 4-6a. On figure 4-6b, nephelinites and mela-nephelinites are distinguished.

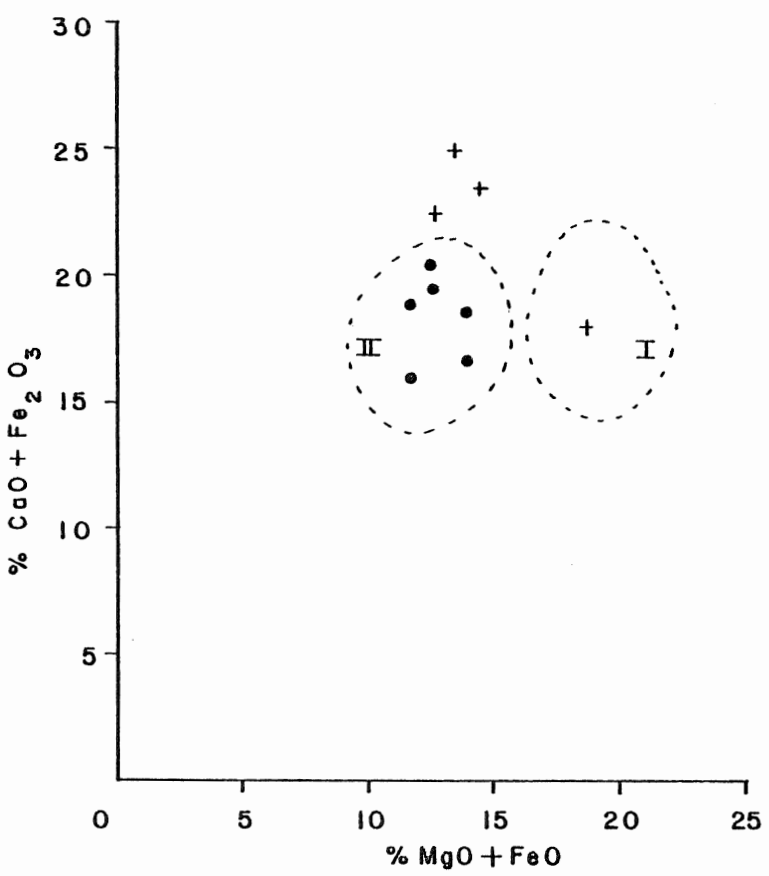
30
25
20
15
10
5
0
5
10
15
20
25
% CaO + Fe2 O3
% MgO + FeO
II
I

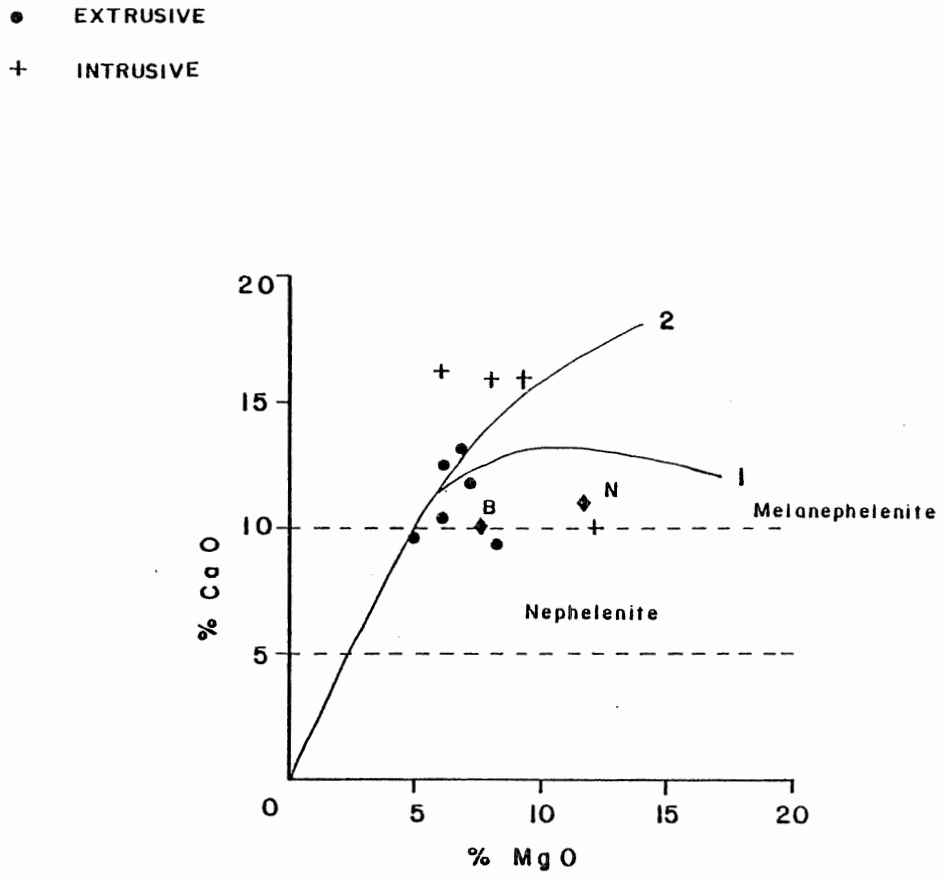
EXTRUSIVE
INTRUSIVE
20
15
10
5
0
5
10
15
20
% Ca O
% Mg O
2
1
N
B
Melanephelenite
Nephelenite

Figure 4-7. Plot of weight percent oxides versus weight percent SiO_2, note: many analyses have the same silica content.

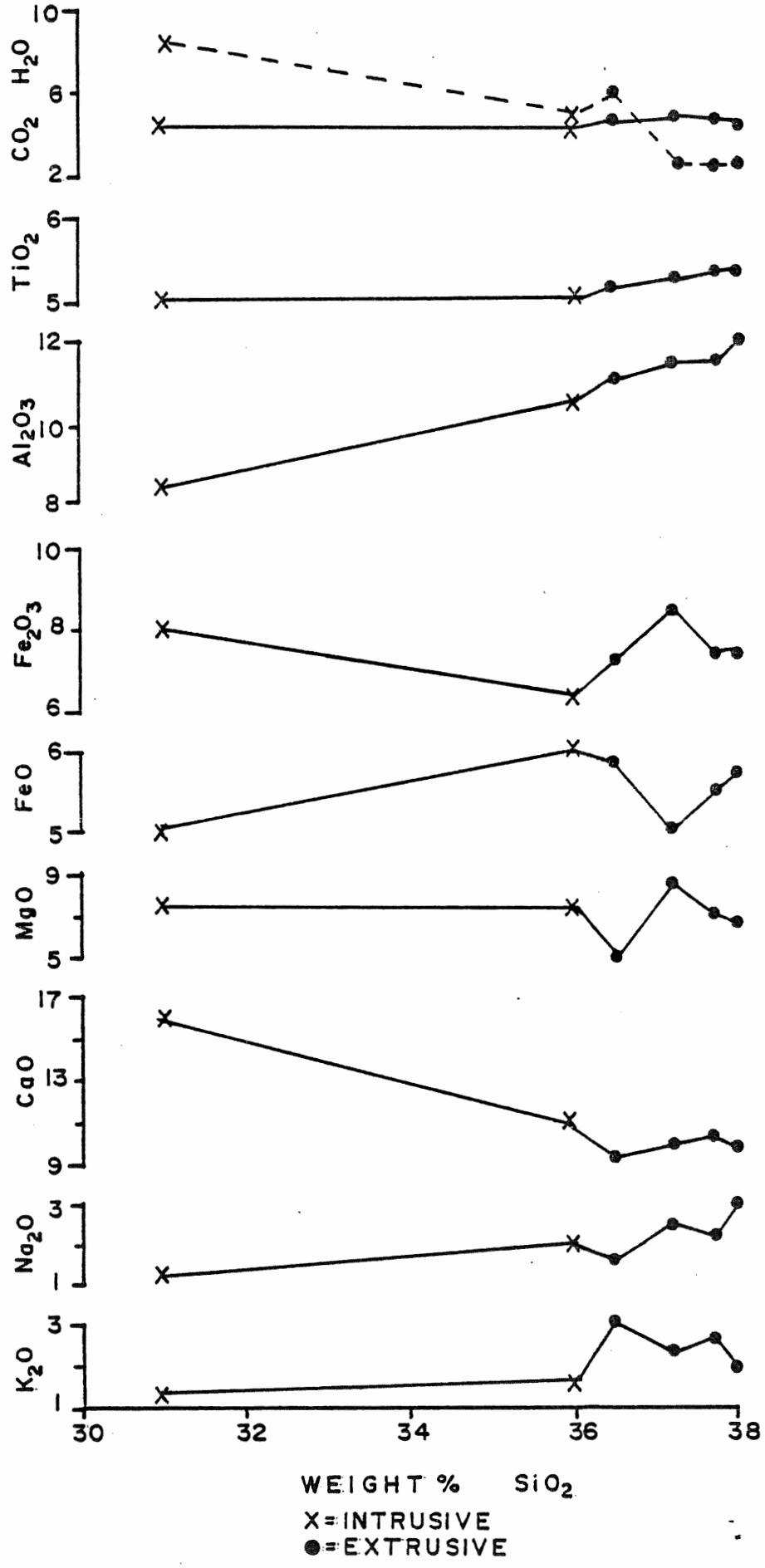
H_2O
CO_2
TiO_2
Al_2O_3
Fe_2O_3
FeO
MgO
CaO
Na_2O
K_2O
30
32
34
36
38
WEIGHT % SiO_2
X=INTRUSIVE
●=EXTRUSIVE

normal petrogenetic patterns seen as an increase in alkali elements and a decrease in MgO, CaO, and Al_2O_3 (Hyndman, 1975). The steep increase in CaO and CO_2 with decreasing SiO_2 content probably reflect the supression of SiO_2 by the addition of calcite.

On the basis of the major element geochemistry, the Bermudian rocks are compositionally similar, but they do show some minor variations. Another way to check the results is to compare their normative mineralogies. The modifications of the whole-rock chemistry (discussed previously) should be reflected in the resultant normative minerals. The norms can be compared to the average nephelinite computed by Wedepohl and Muramatsu (1979). The effects of alteration also can be discerned by determining which modification brought all the samples to a more homogeneous normative mineralogy.

The norms for the complete analyses are given in Table 4-1. The extrusives and intrusives can be readily distinguished on the basis of their normative minerals. The lavas are all nepheline normative, except for BF8-11, which is quartz, hypersthene, and corundum normative. The intrusives do not have nepheline, but instead are hypersthene normative. The other major distinction is that the intrusives have two to three times the amount of calcite in the norm than the lavas. The occurrence of normative corundums in sample BF8-11 is indicative of extensive alteration (Chayes, 1969).

The calcite-free norms are given in Table 4-2. These norms are more homogeneous. All but one intrusive and BF8-11 are nepheline normative. The normative mineralogies are much more uniform; suggesting that the major differences between the two lithologies is their calcite content. This agrees with the amount of modal calcite found in these rocks.

The volatile-free analyses, shown in Table 4-3, are very inconsistent. Leucite and larnite (Ca_2SiO_4) appear in the norms of many samples. It is doubtful that these rocks have a common volatile-free parent because even two samples which are similar in the complete analyses have very different volatile-free norms. The formation of larnite is a result of the high calcite contents, which, upon the removal of CO_2, leads to excess CaO and thus normative larnite.

Only seven samples were modified after the ferric-ferrous iron adjustment (Table 4-4). The only effect this had on the normative minerals is that the relative proportions of magnetite, hematite, and ilmenite are changed. The Fe-Mg silicates show only a very slight change.

Differences and similarities between the samples can also be seen in various projections and combinations of the normative minerals. One important test is the Thorton-Tuttle Differentiation Index, which for these rocks varies from 20 to 45. The rocks show low to moderate degrees of differentiation using this index. The oxides show few well-defined trends with increasing differentiation index (Figure 4-8). With increasing differentiation, CaO, Fe_2O_3, MgO, and CO_2 decrease, while Al_2O_3, Na_2O, and SiO_2 (weakly) increase. The alkali elements, K_2O and Na_2O, increase over the whole range of index values, but do so very erratically. This may reflect varying fluxes of alkalies during alteration and not magmatic differentiation.

The normative minerals can also be used to classify the rocks. Figure 4-9 shows the analyses (complete, calcite-free, and volatile-free) plotted in the system Ol'-Ne'-Q' where Q' = Q + 2/5 AB + ¼ OPX,

Figure 4-8. Plot of weight percent oxides versus the differentiation index (D.I.) determined from the normative minerals.

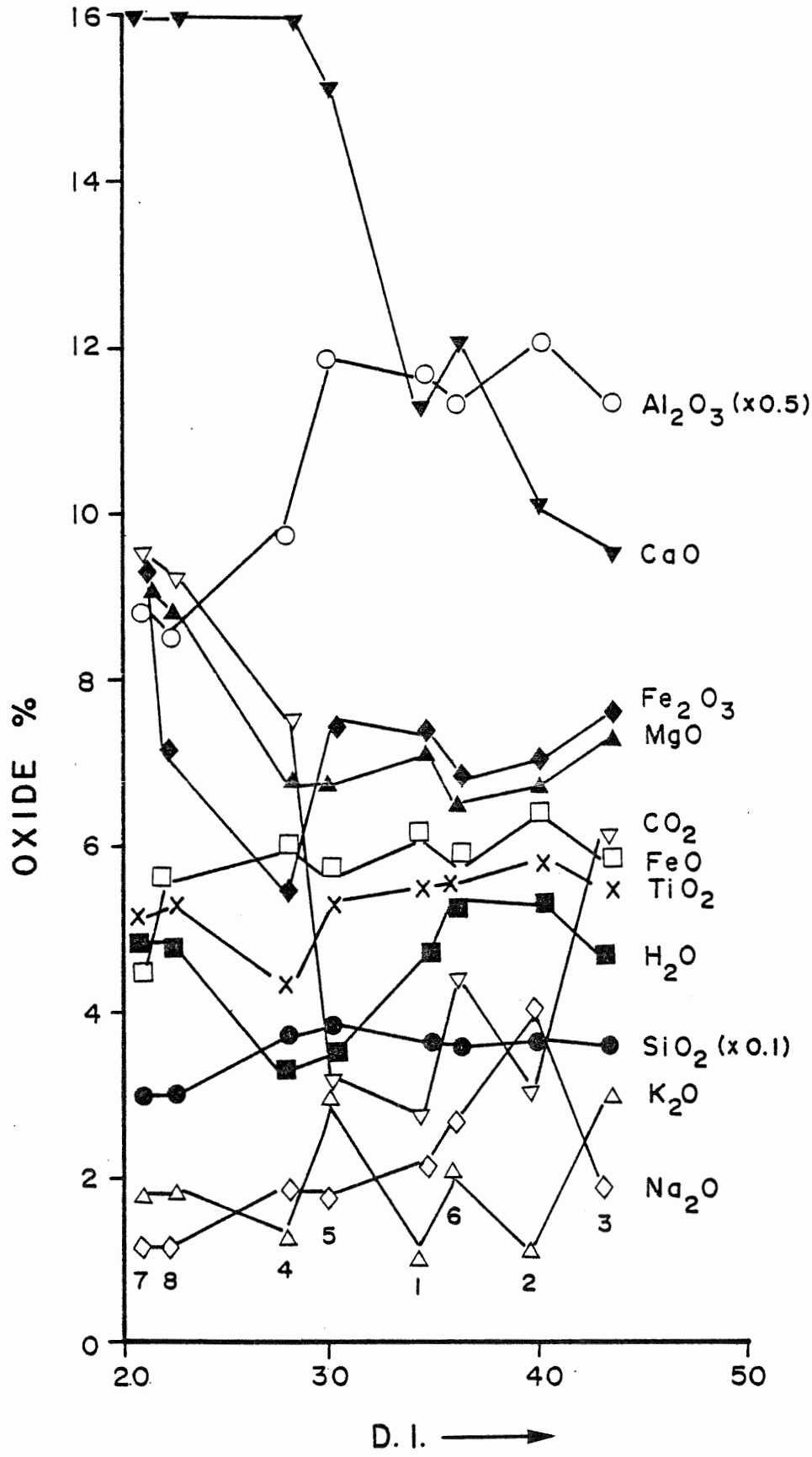
16
14
12
10
8
6
4
2
0
OXIDE %
20
30
40
50
D. I.
Al2O3 (x0.5)
CaO
Fe2O3
MgO
CO2
FeO
TiO2
H2O
SiO2 (x0.1)
K2O
Na2O
7 8
4
5
1
6
2
3

Figure 4-9. Projection of the Bermudian rocks into the normative system Ol'-Ne'-Q' (see text). The dashed line shows the Tilley-Yoder critical plane of silica-saturation. The solid divisor is the alkaline-subalkaline boundary of Irvine and Baragar (1971).

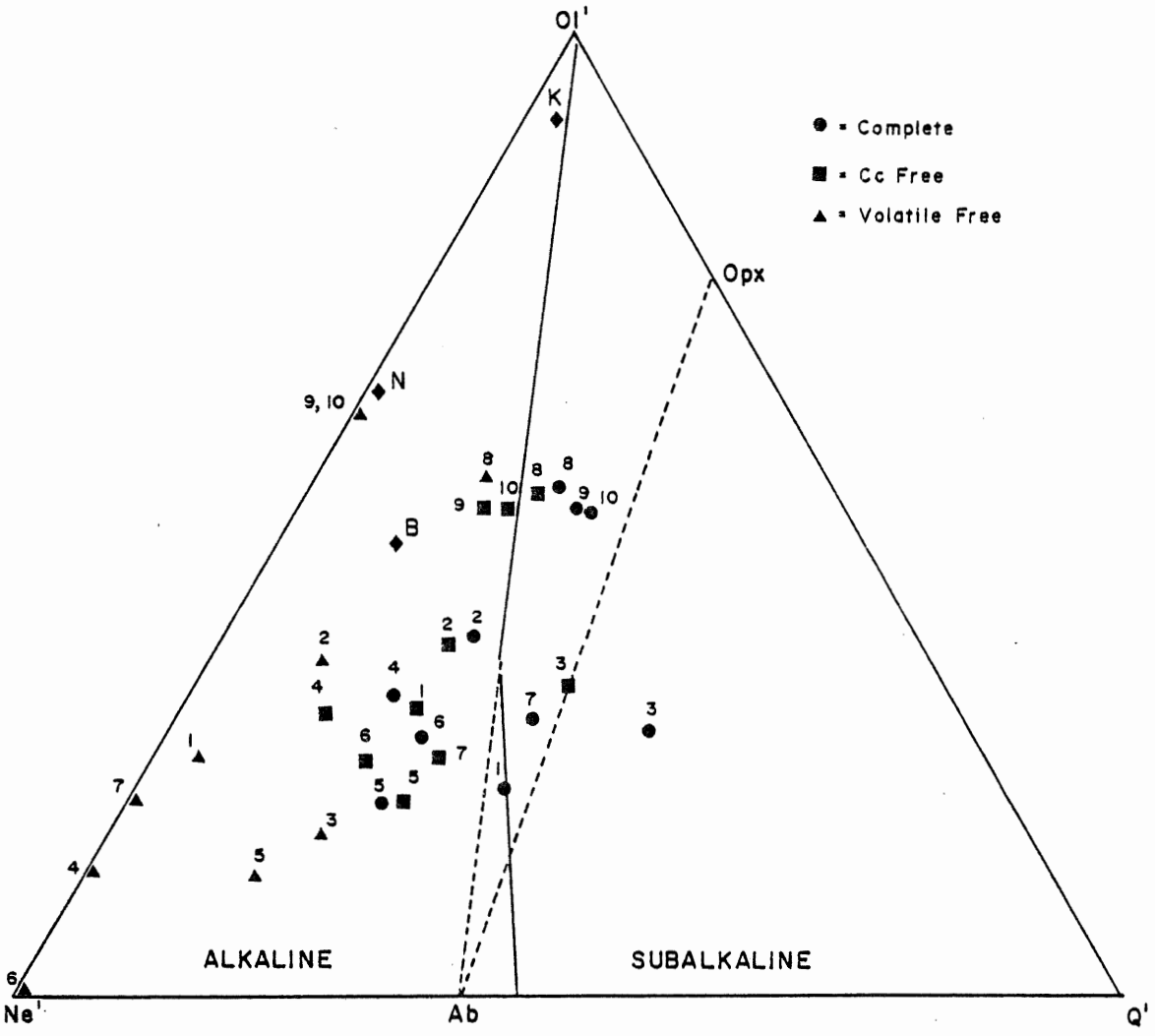
Ol'
Opx
Ne'
Ab
Q'
ALKALINE
SUBALKALINE
● = Complete
■ = Cc Free
▲ = Volatile Free
K
N
B

Ne' = NE + 3/5 AB, and Ol' = OL + 3/4 OPX. In this diagram many of the complete analyses fall along the alkaline-subalkaline boundary, while the calcite-free analyses are nearly all alkaline. In this plot none of the analyses seem similar to either the average nephelinite or alkali basalt.

In Figure 4-10 the rocks are classified by the combination of normative plagioclase composition and Color Index (C.I. = Ol+Cpx+Opx +Mt+Il+Hem+Ru). Not one sample plots as a nephelinite, rather they range from mugearite to ankaramite, even the average nephelinite plots out of the field of this diagram. It is obvious that this classification diagram does not adequately treat rocks of such extreme compositions.

Several conclusions may be deduced from the various interpretations and modifications of the chemical data. These rocks are altered and have high volatile contents. Much of this alteration may be due to the addition of calcite. The calcite may have been added from an external source, but there is no conclusive evidence for this source being seawater. The volatiles may be a primary component of these rocks. Chemically both the intrusives and extrusives are nephelinites, and they are similar in composition to an average nephelinite (Wedepohl and Muramatsu, 1979). The intrusives can be differentiated from the extrusives on the basis of normative mineralogies; the former are hypersthene bearing and the latter have nepheline in the norm. This difference is not seen in the calcite-free normative mineralogies. Normative rocks classifications indicate that the rocks are predominantly alkaline. The assignment of petrographical rock names on the basis of the normative mineralogies is not consistent with all the other classifications.

Figure 4-10. Classification plot of Color Index (C.I.) versus normative plagioclase composition from Irvine and Baragar (1971).

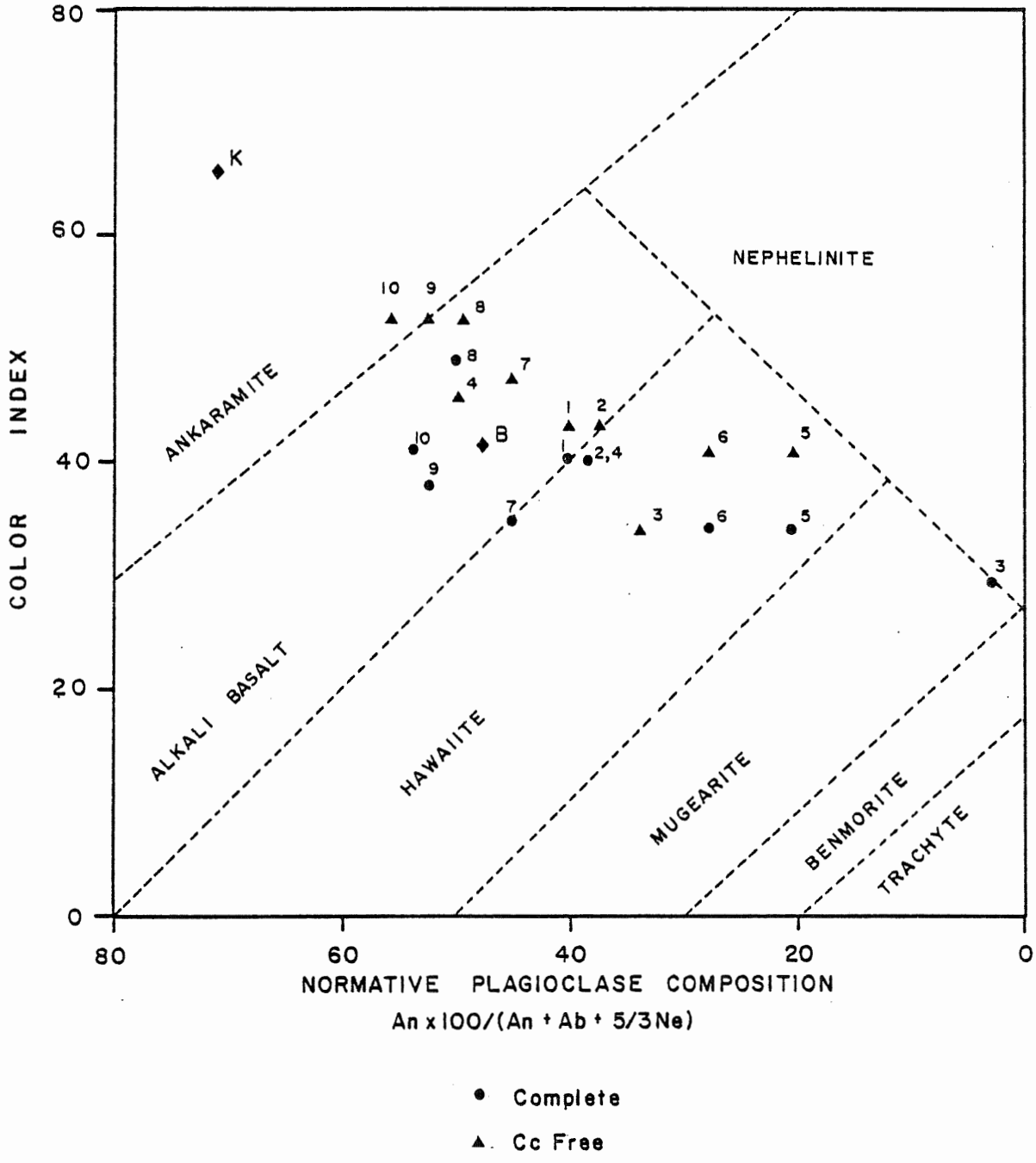
80
60
40
20
0
COLOR INDEX
K
B
NEPHELINITE
ANKARAMITE
ALKALI BASALT
HAWAIITE
MUGEARITE
BENMORITE
TRACHYTE
80
60
40
20
0
NORMATIVE PLAGIOCLASE COMPOSITION
An x 100/(An + Ab + 5/3Ne)
Complete
Cc Free

CHAPTER 5

PETROGENESIS

Introduction

The petrogenesis of alkaline rocks is very complex and poorly understood. The experimental evidence does not suggest one preferred mode of origin for these rocks. In this chapter two topics will be discussed, experimental studies and the geological setting of nephelinites and related rocks.

The experimental systems should model closely the paragenetic sequence seen in the Bermudian rocks (Figure 5-1). Biotite is the first phase to form, but it is metastable and is found only as relicts in the cores of some clinopyroxene phenocrysts. The next phase to appear, perhaps even contemporaneously with biotite, is olivine. This phase is pervasively altered and pseudomorphed by calcite, talc, and quartz. The timing of this alteration is unclear. Concentrically zoned clinopyroxenes start to form next. As the pyroxenes grew they incorporated some of the next phase to form, spinel. It is interesting to note that although clinopyroxene phenocrysts are of a consistently large size, the spinels show a spectrum of sizes from large to small. This suggests a continual nucleation of new spinels while the phenocrystic clinopyroxenes continued to grow on the same number of cores.

The groundmass minerals show a much more ordered nature which may reflect their rapid formation during extrusion and quenching of the lava. Clinopyroxene, melilite, spinel, and sphene all appear at approximately the same time, with clinopyroxene slightly in advance of the others. Melilite and sphene are the only two totally new phases

Figure 5-1. Generalized paragenetic sequence for all the 1980-core igneous rocks. Sphene may be a replacement of perovskite.

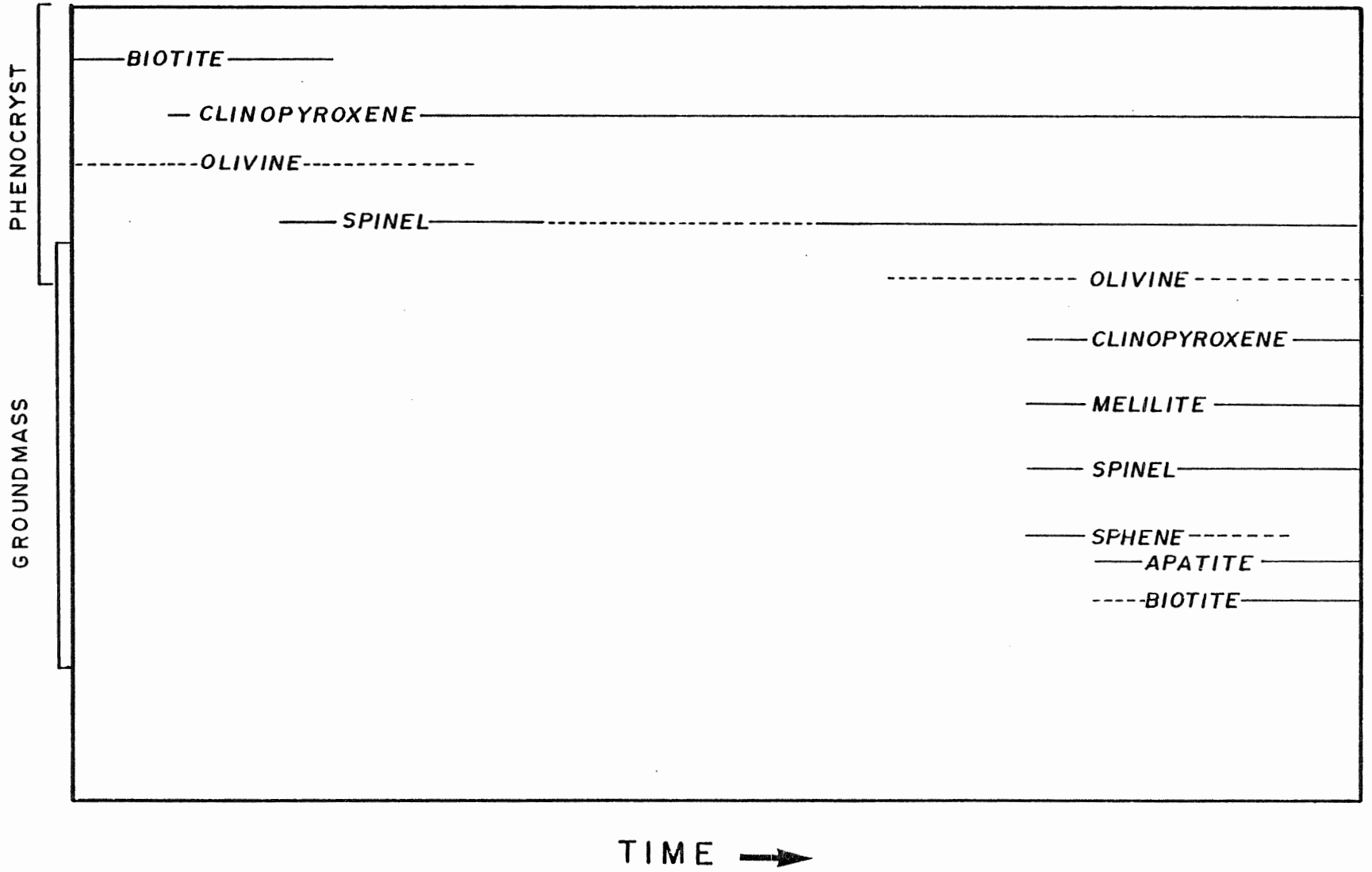
PHENOCRYST
GROUNDMASS
BIOTITE
CLINOPYROXENE
OLIVINE
SPINEL
OLIVINE
CLINOPYROXENE
MELILITE
SPINEL
SPHENE
APATITE
BIOTITE
TOTAL CRYSTALLIZATION
TIME

to appear and reflect enrichment in the melt in alkalis and titanium. Following these minerals comes biotite and rarer apatite, both forming from the volatile enriched residuum. Groundmass olivine forms intermittently.

Experimental Studies

The experimental studies derive the same types of rocks (melilitites to olivine-nephelinites) but from somewhat different parents and by many different processes. Most of the generalized flow sheets for alkaline rock systems are expanded from studies in the basalt system. In general the experimental models fall into three groups: (1) anhydrous crystal fractionation at high and low pressures, (2) crystal fractionation or partial melting at high PH_2O, and (3) partial melting of mantle peridotite at high pressure (Bailey, 1976).

Model 1

O'Hara and Yoder (1967) performed a series of anhydrous high-pressure melting experiments on garnet peridotite xenoliths from some South African kimberlites. They presume that garnet peridotite is the fertile mantle which melts to yield primary magmas. A dry garnet peridotite melts at 30 kilobars and about 1500^{o}C to yield a picritic liquid. High-pressure crystal fractionation of garnet and clinopyroxene (eclogite) from this picritic melt leaves a silica undersaturated liquid. Further fractionation of this liquid at intermediate pressures (10 to 20 kb) with the removal of spinel, olivine, clinopyroxene and orthopyroxene leave a nepheline normative liquid which can become melilite bearing at lower pressures.

The anhydrous, atmospheric pressure experiments and derivation of melilitites in the system CMAS ($CaO-MgO-Al_2O_3-SiO_2$) are best summarized by O'Hara and Biggar (1969). A generalized flow sheet for this system is shown in Figure 5-2. There is a thermal divide which separates silica-saturated invariant points, 1 through 5, from silica-undersaturated points, 6 through 8. The invariant point assemblage most similar to the mineralogy of the Bermudian rocks, 8 (Di, Fo, Sp, Mel) occurs at a temperature of about 1232°C. However, this system predicts several assemblages which do not exist in nature, notably those which contain coexisting anorthite and melilite. This problem is accommodated by adding sufficient Na_2O to the system to prevent the unnatural assemblages.

A projection of the sections Ne-La-Fo-Q and Ne-Di-An of Na_2O-CMAS for diopside-bearing equilibrium is shown in Figure 5-3. Five thermal divides are shown, the most important ones for this discussion being D and F. Divide D prevents any calcium enrichment of a liquid in equilibrium with Di+Sp+Mel. Divide F prevents liquids which are precipitating Di+Pl from entering into the melilite stability field. The invariant points of this diagram are not precisely understood or located. One important point derived from this figure is that a nephelinite can be derived from an alkali basalt by low-pressure fractionation. A possible differentiation mechanism is having the melt approach I (Di+Pl+Fo+Ne+Sp+l) from B, the liquid then migrates to J (Di+Mel+Sp+Fo+Ne+l) where plagioclase is reacted out, and the liquid may go further on to K (Di+Ne+Fo+Mel+l), where spinel is lost. The phase assemblages seen in the Bermudian rocks are most similar to point J (Temperature = 1200°C).

Figure 5-2. Generalized flow sheet for the system CMAS at 1 atmosphere (from O'Hara and Biggar, 1969).

Invariant Points

1 = An, Pr, Tr, Cord
2 = An, Pr, Di, Tr
3 = An, Fo, Sp, Cord
4 = An, Fo, Cord, Pr
5 = An, Di, Fo, Pr
6 = An, Di, Fo, Sp
7 = An, Di, Mel, Sp
8 = Di, Fo, Sp, Mel

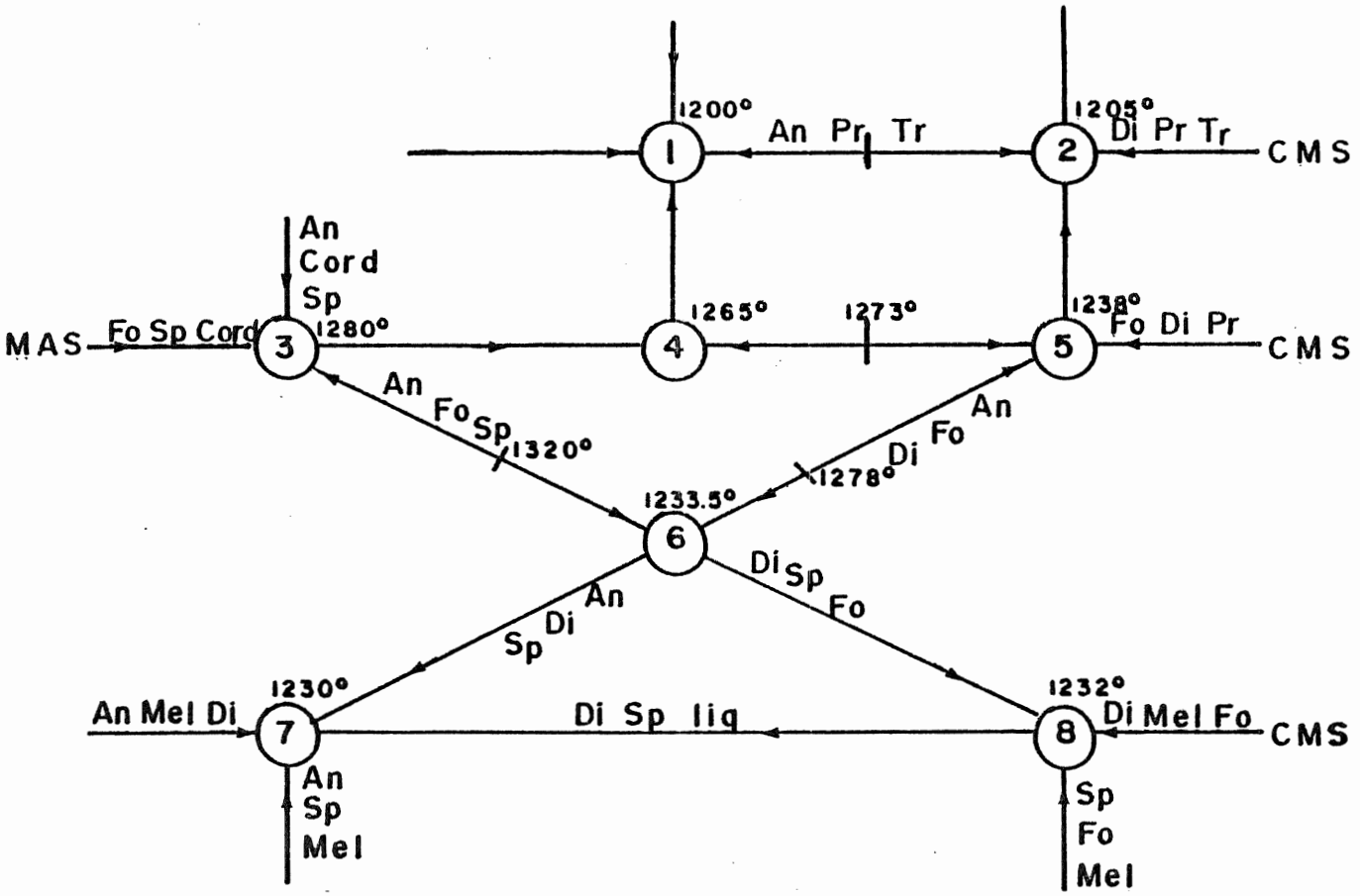
1200°
An Pr Tr
1205°
Di Pr Tr
CMS
1
2
An
Cord
Sp
MAS
Fo Sp Cord
3
1280°
4
1265°
1273°
5
1238°
Fo Di Pr
CMS
An Fo Sp
1320°
1278°
Di Fo An
1233.5°
6
Di Sp Fo
An Sp Di
1230°
An Mel Di
7
Di Sp liq
8
1232°
Di Mel Fo
CMS
An
Sp
Mel
Sp
Fo
Mel

Figure 5-3. Projection towards the Na-deficient region of Ne-La-Fo-Q and Ne-Di-An of the system Na_2O + CMAS (from O'Hara and Biggar, 1969).

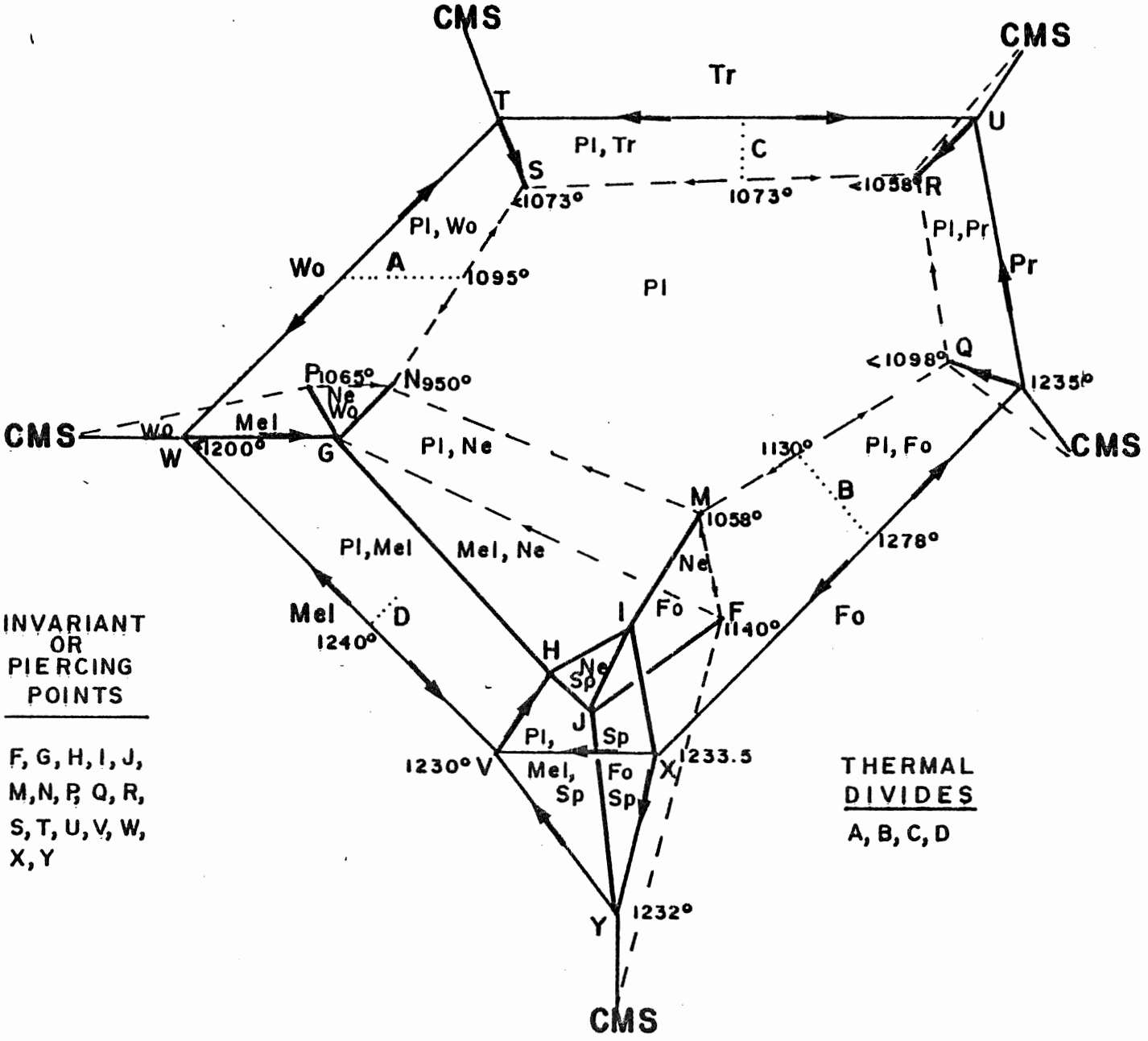
CMS
CMS
Tr
T
U
Pl, Tr
C
S
<1073°
1073°
<1058°
R
Pl, Wo
Pl, Pr
Pr
Wo
A
1095°
Pl
<1098°
Q
P1065°
N950°
1235°
Ne
Wo
CMS
Wo
Mel
1200°
W
G
Pl, Ne
1130°
Pl, Fo
CMS
M
B
1058°
1278°
Pl, Mel
Mel, Ne
Ne
Mel
1240°
D
I
Fo
F
1140°
Fo
H
Ne
Sp
J
Pl,
Sp
1230° V
Mel,
Sp
Fo
Sp
X
1233.5
Y
1232°
CMS
INVARIANT OR PIERCING POINTS
F, G, H, I, J, M, N, P, Q, R, S, T, U, V, W, X, Y
THERMAL DIVIDES
A, B, C, D

Model 2

Nephelinites can be formed by hydrous, high-pressure crystal fractionation of a partial melt of a peridotitic mantle. A hydrous or carbonated mantle is inferred to be the source because nephelinites are generally volatile rich and are associated with violent eruptions. Green (1969) presents two mechanisms for the formation of nephelinites. A 25 to 30 percent partial melt of pyrolite (75% harzburgite, 25% tholeiite) at 13 to 18 kilobars followed by isobaric fractionation of aluminous orthopyroxenes and clinopyroxene coupled with an increasing water content (2 to 5%) will eventually produce an olivine nephelinite. A 35 to 40 percent partial melting of pyrolite at 18 to 27 kilobars with isobaric fractionation of aluminous orthopyroxene, clinopyroxene, olivine, and garnet along with a progressively increasing water content (2 to 5%) will produce an olivine-melilite nephelinite. Olivine-melilite nephelinites also can be produced directly from a ten percent partial melting of wet pyrolite at 1200° to 1350°C and 15 to 30 kilobars.

Brey (1978) also investigated the effects of adding CO_2 to the mantle. He reports that an olivine-melilititic magma can be formed from a five percent partial melt of pyrolite at 27 kilobars from 1160° to 1180°C with 7 to 8 percent CO_2. The silica content of these melts decreases with both increasing depth of melting and CO_2 content of the source rocks. Thus this model predicts that nephelinites can be formed by low degrees of partial melting of a hydrated and carbonated mantle at great depths. Larger degrees of partial melting and total fractionation of orthopyroxene from such a melt can produce similar types of magmas.

Model 3

This model predicts that nephelinites can be formed by the partial melting of mantle peridotites at high pressures and is not too different from model 2. Melting studies of synthetic and natural peridotites by Kushiro (1968, 1972) show that with increasing pressure (30 to 40 kb) the olivine+orthopyroxene liquidus boundary is shifted in such a manner that initial melts (at 25% partial melting) forming at successively higher pressures become increasingly silica deficient. This shift towards silica-undersaturation may occur also with lower degrees of partial melting. If H_2O is added to the system the melts become more siliceous. In fact, nepheline normative magmas cannot be formed under hydrous conditions at pressures above 20 kilobars. Liquidus temperatures for the mantle rocks under these experimental conditions range from 1400° to 1500°C.

Low Pressure Studies

The occurrence of melilite in the Bermudian rocks is of petrologic importance. Akermanite (Ca-rich melilite) can form only under certain conditions and is generally considered to be the silica-undersaturated equivalent of anorthite. For temperatures below 1200°C, akermanite is stable up to about five kilobars (Yoder, 1975). As the level of CO_2 in the melt increases, the akermanite stability field decreases, and with excess CO_2, it completely breaks down to diopside and calcite. If there is an excess of H_2O, CO_2, and K_2O, akermanite can break down to phlogopite, calcite, and forsterite (Yoder, 1970). Thus, melilite is stable over a very tightly bounded region in pressure-

temperature-volatile composition space. The actual limits of this region in natural rocks is not known. It is interesting to note that the assemblage of phlogopite+calcite+forsterite, which is important in kimberlites, may be formed by the addition of excess volatiles and K_2O to a melilite-bearing rock.

Experimental studies in the system Na_2O-CaO-MgO-Al_2O_3-TiO_2-SiO_2 (Yagi and Onuma, 1969, 1978) at atmospheric pressure have identified several important crystallization trends pertinent to nephelinites (Figure 5-4). They find that perovskite occurs in their assemblages; but state that sphene is common in natural assemblages. They predict solidus temperatures in the range of 1100° to 1200°C. A typical paragenetic sequence for an olivine-melilite nephelinite is: olivine, pyroxene (titan-augite), melilite, nepheline, and perovskite or sphene. The actual mineralogy of a rock crystallizing in this system varies, depending upon when it is totally solidified, and compositions can range from olivine nephelinites to melilite and perovskite bearing nephelinites. They extrapolated their data to higher pressures and suggest that olivine-nephelinites form at higher pressures and melilite-nephelinites form at lower pressures.

Studies in the system Ab-Fo-La-Q at atmospheric pressure by Yoder (1979) indicate similar crystallization trends (Figure 5-5). Melilite will occur as phenocrysts only when (Na_2O+K_2O) > 7.25 percent. In the presence of excess CO_2 and at higher pressures melilite is converted to diopside and calcite. Thus melilite-bearing rocks are limited to volcanic or sub-volcanic facies ($\leqslant$10 kb).

Figure 5-4. Crystallization trends in the system Di-Ak-Ne-$CaTiAl_2O_6$ at 1 atmosphere (from Yagi and Onuma, 1969, 1978).

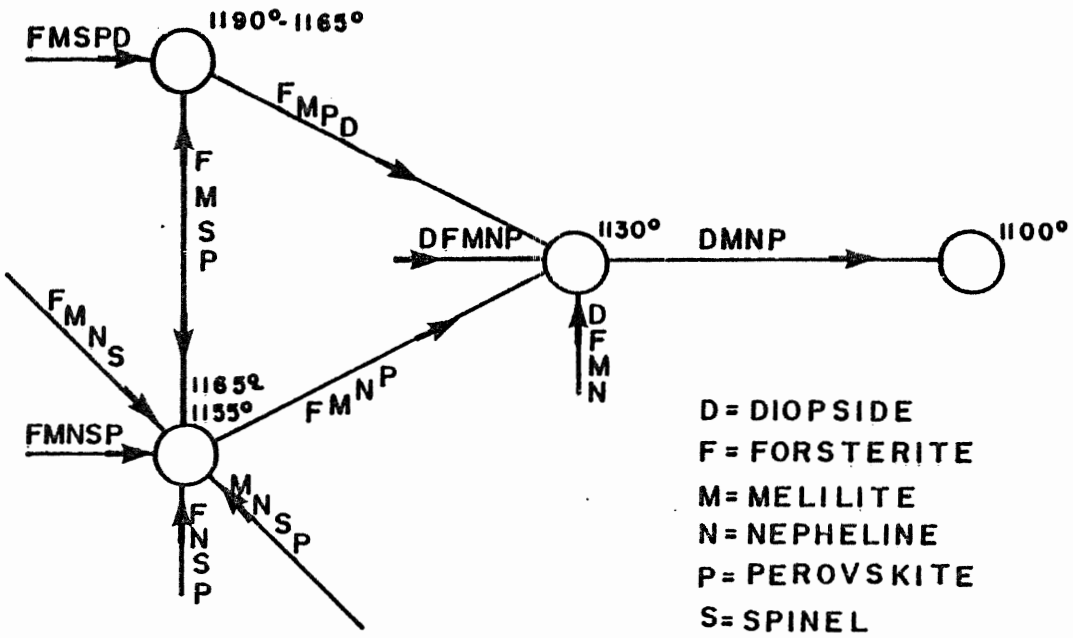
FMSPD
1190°-1165°
FMPD
FMSP
DFMNP
1130°
DMNP
1100°
FMNS
DFMN
1165°
1155°
FMNP
FMNSP
MNSP
FNSP
D = DIOPSIDE
F = FORSTERITE
M = MELILITE
N = NEPHELINE
P = PEROVSKITE
S = SPINEL

Figure 5-5. Flow sheet for a portion of the system Ab-Fo-La-Q (from Yoder, 1979).

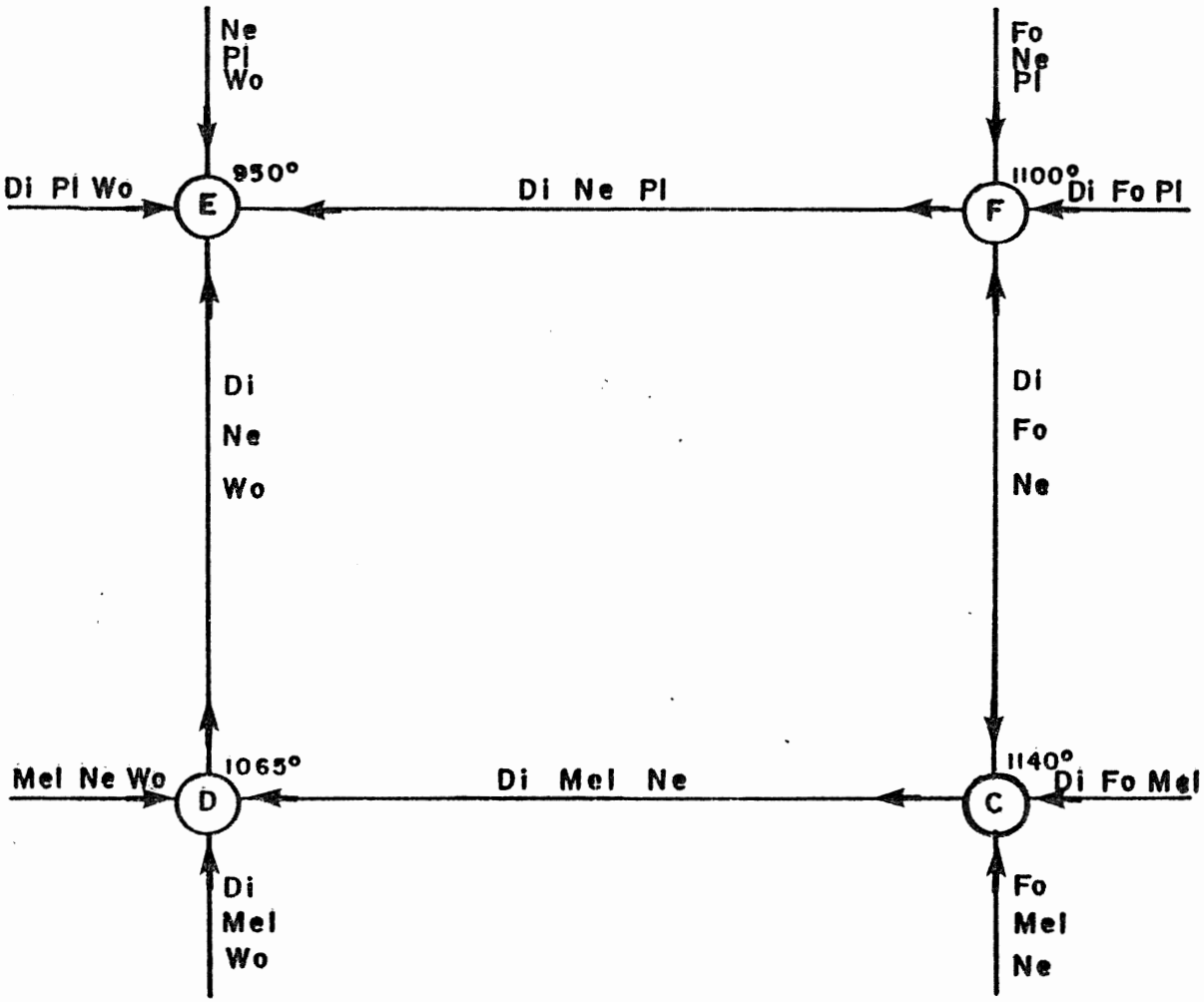

INVARIANT POINTS

C = Di, Fo, Mel, Ne

D= Di, Mel, Ne, Wo

E = Di, Ne, Pl, Wo

F= Di, Fo, Ne, Pl

Nature of the Parent Mantle

Most of the experimental studies indicate similar processes, a low degree of partial melting of the mantle at great depth (≥20 kb) with the mantle containing some CO_2 and H_2O. This partial melting is followed by intermediate to low-pressure crystal fractionation and the formation of melilite under near surface conditions. An important factor to be considered is what is composition of the parent mantle?

The composition of the mantle is generally thought to be similar to a peridotite with a typical mineralogy being: olivine, orthopyroxene, clinopyroxene, and with increasing pressure, either plagioclase, spinel, or garnet. The presence of volatiles is generally accepted (Wyllie, 1979). The presence of a sufficiently large volatile phase to convert the mantle to a phlogopite peridotite has been proposed by Edgar et al. (1976). Melts from this type of mantle yield hydrous, K-rich magmas. A partially carbonated (dolomite-bearing) peridotite will melt at pressures greater than 30 kilobars at approximately 1300°C to yield a carbonatitic magma. Kimberlites to olivine-melilitites can also be produced from greater degrees of partial melting of such a mantle (Wyllie, 1979).

It is possible that the volatile enrichment of the mantle may be a localized phenomenon. Petrographic and chemical studies of xenoliths from kimberlites, alkali basalts, and lamprophyres of deep-seated origin indicate that the parent mantle was metasomatised by K, Na, Ti, Fe, H_2O and CO_2 (Windom and Boettcher, 1980; Boettcher and O'Neill, 1980). Since a metasomatised mantle tends to have a lower liquidus temperature, there would be a greater chance of a melt forming where the liquidus

and geotherm intersect. On the basis of a compilation by Bailey (1980) this melting can occur only in a zone from 100 to 200 kilometers deep, at least for continental geotherms.

Synthesis

On the basis of these experimental studies an outline of the origin of the Bermudian volcanic rocks is possible. A volatile enriched mantle melts at depths near to 100 kilometers. This volatile-rich melt may have fractionated orthopyroxene and garnet at depth or it may have been only a very small partial melting, both processes yield a silica-poor melt. This melt migrated upwards and melilite formed in a low-pressure environment. Some of the carbonate in these rocks may have an origin in the mantle. Solidus temperatures for these rocks are approximately 1200^{o}C.

Nephelinite Associations

As suggested from the experimental studies, olivine-melilite nephelinites seem to be genetically related to kimberlites and carbonatites. Brey (1978) defined three associations: a) olivine melilite nephelinite and kimberlite, these rocks occur in the same region but the kimberlites are not diamond-bearing, b) olivine nephelinite and olivine melilite nephelinite, this is a common association, and c) olivine nephelinite and carbonatites, these rocks are related by differentiation processes but rarely occur together. All of these rocks occur in regions of tensional faulting or rifting.

McIver and Ferguson (1979) present a model which explains the relationships of these three associated undersaturated rocks. A kimberlitic magma, enriched in H_2O and CO_2 forms from a partial melt of a carbonated garnet lherzolite at depths of 100 to 200 kilometers. This magma rises slowly and fractionates out olivine and orthopyroxene. The magma stops its ascent at about 18 kilometers depth and olivine is either fractionated or reacted out to form an assemblage of melilite+monticellite+phlogopite+perovskite±zeolites. A carbonate phase is fractionated off to form a carbonatite magma while the residual liquid is an olivine melilitite magma.

Lamprophyres can be evolved from similar processes. Using a series of lamprophyric dikes with related kimberlitic and carbonatitic dikes, associated with the Mesozoic rifting of the Labrador Sea, Scott (1979) demonstrated that a lamprophyre can be formed from the fractionation of a kimberlitic magma, leaving a residuum of 78 percent olivine and 22 percent spinel. Carbonate unmixing and crystal fractionation of the same magma type forms the carbonatitic dikes (Hansen, 1980).

Nephelinitic volcanism is not uncommon on oceanic islands in the Atlantic Ocean (i.e. Trinidade and Fernando De Noronha). Generally these undersaturated rocks are part of the final phases of volcanism or plutonism. On these islands, augite-rich nephelinites predominate. Xenoliths of nepheline syenite to peridotites are found in many of the extrusive rocks (Mitchell-Thome, 1976).

Unlike the associations found in continental regions of nephelinite-carbonatite-kimberlite, carbonatitic volcanism is found only on the Cape Verde Islands. Unfortunately, very little information

about these rocks is available in English. The closest rocks related to kimberlites to be found in an oceanic environment are some alnoites from the Solomon Islands in the southwestern Pacific Ocean. These rocks are mineralogically and geochemically dissimilar from kimberlites, but they do contain mantle xenolith assemblages similar to kimberlites (Nixon et al., 1980). These alnoites are considered to result from a 4 percent partial melt of a carbonated mantle at 120 kilometers. Seismic studies of the Ontong-Java Plateau, which is an unusually thick (40 km) section of oceanic crust to the north of the Solomon Islands, reveals pipe-like bodies suggestive of volcanic plugs. Nixon (1980) suggests that this region may be suitable for kimberlite formation since the related alnoitic rocks have been found in the region and the geothermal gradient is comparable to the South African shield geotherms.

In conclusion, melilite bearing rocks, similar to those found on Bermuda, occur on other oceanic islands and in tensional regimes on continents. The associated rocks, kimberlite and carbonatite, which are commonly found on continental crust have not been well documented on oceanic crust, perhaps because no one has looked. It is obvious from nearly all studies that these rocks have a deep-seated origin in the mantle.

CHAPTER 6

MAGNETIC PROPERTIES

Introduction

The magnetic properties were first measured to work out a magnetic stratigraphy for the igneous rock samples from the 1980-core. The lack of any consistent stable inclinations instigated a more detailed study of the bulk magnetic properties. The relationship between the bulk-rock magnetism and opaque mineralogy also was studied.

Techniques

All samples are from oriented minicores taken perpendicular to the main core. Fiducial lines indicating the true vertical were transferred from the main core to each minicore. The oriented minicores were trimmed to approximately 2.5 centimeters in length. Sample densities were measured using a standard technique.

Magnetization was measured with a Schonstedt DSM-1 digital spinner magnetometer. An on-line PDP-12 microprocessor reduced the raw data to three orthogonal vectors (N,E.V.), moment (M), and tilt-corrected declination (D) and inclination (I).

Samples were demagnetized using three schemes. Most samples were demagnetized using alternating fields of the following peak intensities: 25, 50, 75, 100, 150, 200, 250, 300, 350, 400, and 500 Oersteds (Oe). After alternating field cleaning to 150 Oe thermal demagnetization was carried out on additional samples using a Schonstedt thermal specimen demagnetizer TSD-1 at: 100°, 200°, 250°, 300°, 350°,

400°, 450°, 500°, 550°, 575°, 600°, 625°, 650°, 675°, 700°, and 725°C. The viscous decay experiment was run as follows. End chips from minicores were placed in zero field in which the earth's field was opposed by the field of Helmholz coils. After six months, these samples were removed and the remaining remanence demagnetized using the alternating field method.

Results

The analysis of the remanent magnetism has yielded some interesting results. In general, the demagnetization spectra of all the samples are similar. There are a few, well-defined, stable inclinations. The results are difficult to interpret.

All of the igneous rocks have relatively intense remanences, in the order of 10^3 emu cm^{-3} (Table 6-1). There does not appear to be any significant difference between the average intensity of the intrusives and extrusives. The inclination of the natural remanent magnetism (NRM) varies from shallow to steep with a mean value near to +50°, the present day inclination for the main field.

A compilation of the AF demagnetization curves is shown in Figure 6-1. The samples can be characterized by a rapid decay in normalized moment with increasing destructive field. All of the median destructive fields (MDF) are less than 150 Oe, with the extrusives' MDF always less than 80 Oe and as low as 20 Oe.

Table 6-1

	Sample	NRM Intensity (10^{-3} emu cm^{-3})	I_{NRM}(°)	T_C(°C)	MDF(Oe)	I_{stable}
EXTRUSIVES	BF4-2.4	1.21	+35.3	597	75	+11.5
	BF6-6.8	3.60	+80.0	-	60	+71.6
	BF8-10.30	0.157	+51.9	597	45	+20.6
	BF9-7.4	1.44	+87.0	575	70	+ 1.86
	BF9-7.8	2.21	+14.2	-	75	+ 5.9
	BF10-11.25	0.0191	+48.9	597	50(?)	+10.1
	BF10-11.25(chip)	13.36	+89.0	-	45	?
	BF10-11.28	2.23	+53.7	-	55	+14.3
	BF10-19.138	3.55	+41.0	579	20	+48.6
	BF11-5.6	4.12	+62.7	539	50	+60.9
	BF12-12.50	2.44	+ 8.0	553	20	?
INTRUSIVES	BD4-4.9	2.71	+ 4.7	579	-	+ 7.6
	BD4-7.5	0.743	+38.4	-	45	+24.1
	BD5-6.12	3.92	+50.3	606	40	?
	BD5-8.6	1.61	+43.8	539	110	?
	BD5-6.18	1.40	+73.4	-	65	+57.0
	BD9-2.63	2.48	+33.9	-	150	?
	BD9-2.70	2.88	+39.0	539	140	?

Figure 6-1. Alternating field demagnetization curves for selected samples. BF = extrusive, BD = intrusive.

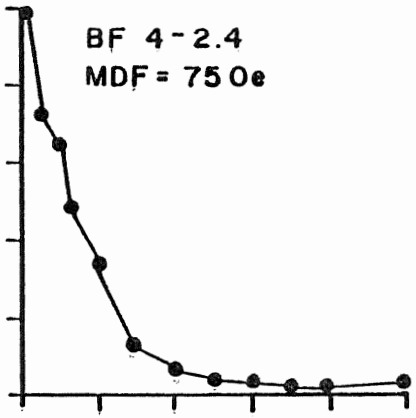
BF 4-2.4
MDF = 75 Oe

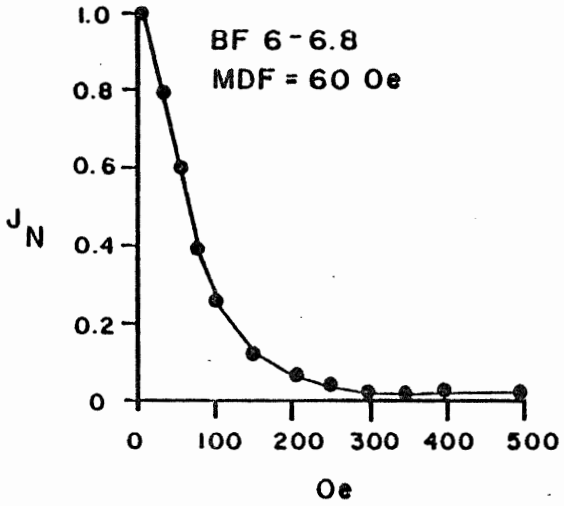
BF 6-6.8
MDF = 60 Oe
J_N
1.0
0.8
0.6
0.4
0.2
0
0
100
200
300
400
500
Oe

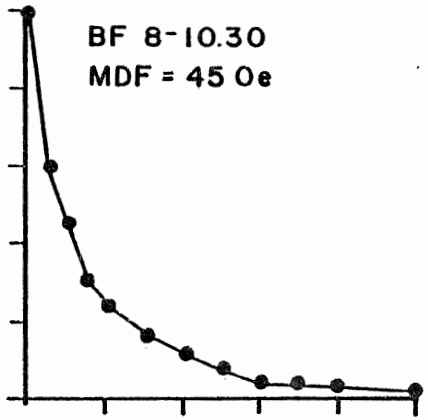
BF 8-10.30
MDF = 45 Oe

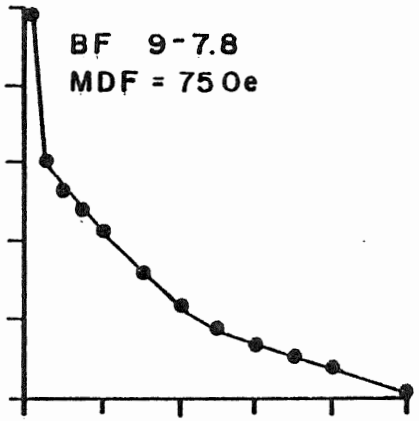
BF 9-7.8
MDF = 75 Oe

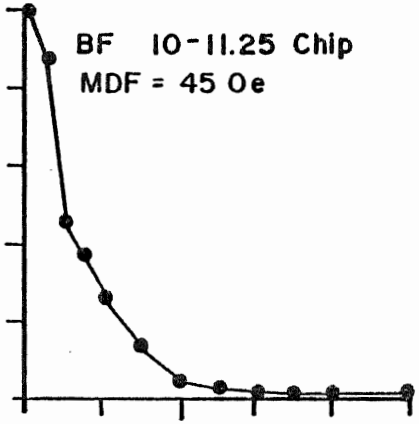
BF 10-11.25 Chip
MDF = 45 Oe

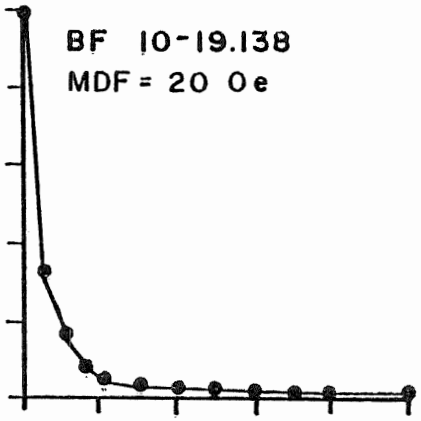
BF 10-19.138
MDF = 20 Oe

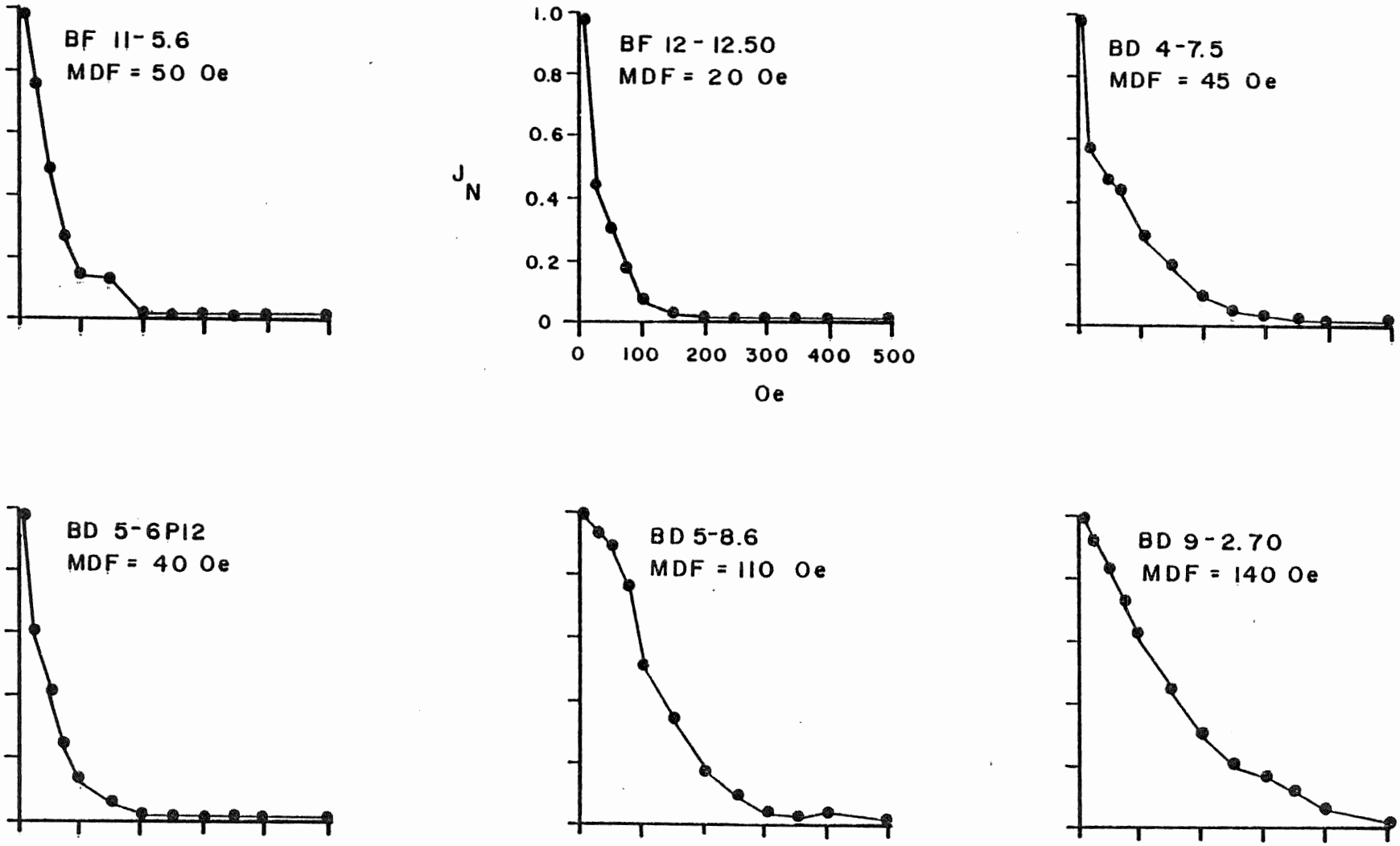
BF 11-5.6
MDF = 50 Oe
BF 12-12.50
MDF = 20 Oe
BD 4-7.5
MDF = 45 Oe
BD 5-6P12
MDF = 40 Oe
BD 5-8.6
MDF = 110 Oe
BD 9-2.70
MDF = 140 Oe
J N
1.0
0.8
0.6
0.4
0.2
0
0 100 200 300 400 500
Oe

Thermal demagnetization has yielded different magnetic vectors from af demagnetization. The demagnetization spectra are given in Figure 6-2. Notice that these rocks appear to have rather high total demagnetization temperatures, and narrow blocking temperature intervals.

Curie temperatures were measured by C. Walls; they are given in Table 6-1. The results are very consistent with average temperatures of $571^{o}C \pm 21^{o}C$ (±1. s.d). These values are very near the Curie point of pure magnetite ($570^{o}C$)(Figure 6-3).

The results of the viscous decay experiment (Table 6-2) are non-conclusive. The samples have very steep initial inclinations and no truly stable inclinations. This may be due to a DIRM.

Since no stable inclinations were readily evident, several techniques were used to determine stable inclinations: stereographic projections, Zijderfeld plots, and inclination versus af destructive field plots. A compilation of the stereo-plots is given in Figure 6-4 (note that the azimuth is arbitrary). There is one dominant trend observed in these plots. The NRM inclinations are all rather steep ($\sim 45^{o}$) and trend towards shallow dips ($\sim 15^{o}$) with demagnetization. There often is a clustering of points at a shallowly dipping direction in the vicinity of 200 Oe demagnetizing field. Both lithologies show this trend.

Representative Zijderfeld plots, for those units yielding stable inclinations are shown in Figure 6-5. The stable inclinations were taken from those points which yield a linear regression line through the origin (±10%, the error limits of the data). As would be expected, the values giving the best linear fit are the same that show clustering

Figure 6-2. Thermal demagnetization curves for selected samples after AF cleaning to 150 Oe.

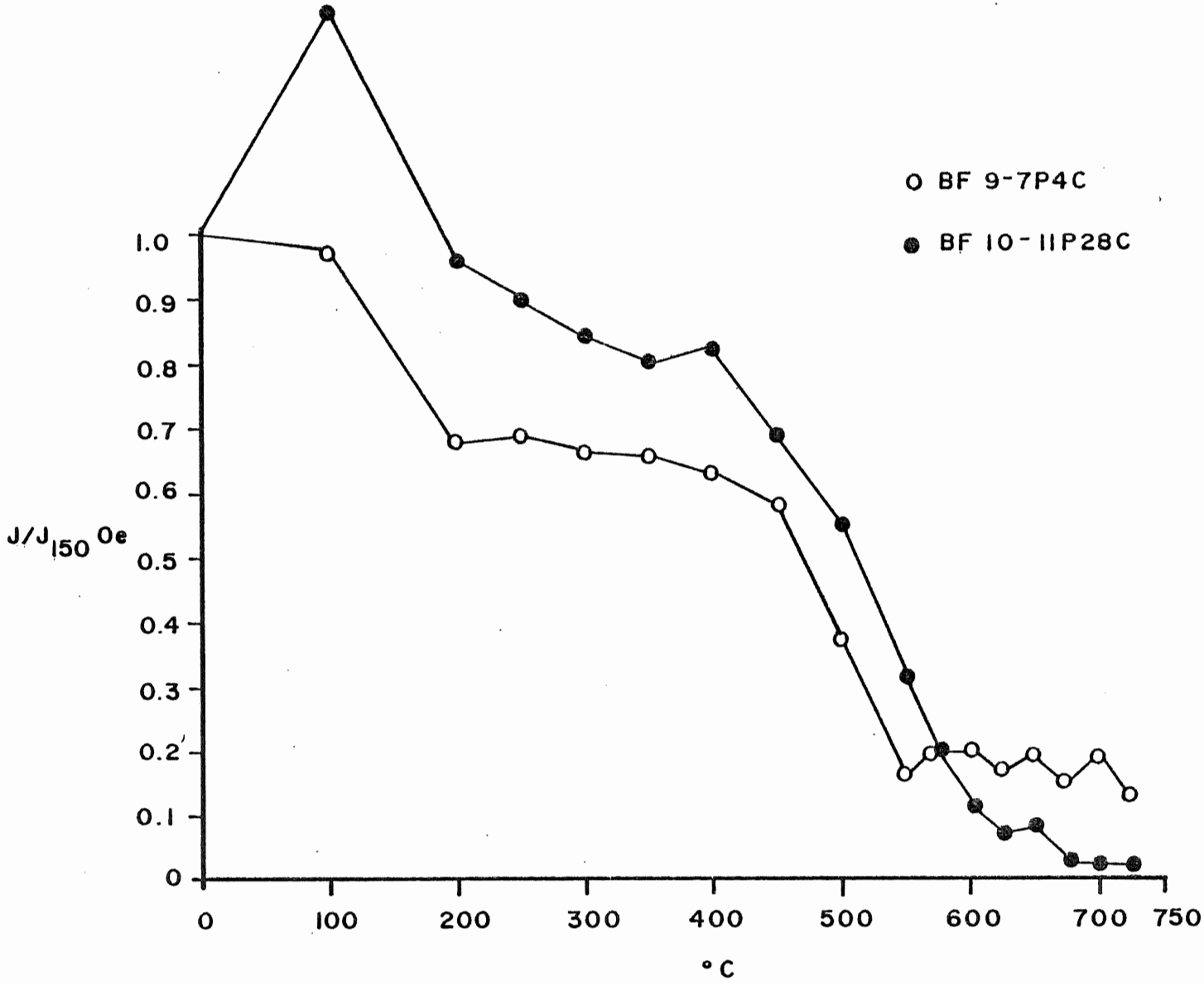
O BF 9-7P4C
BF 10-11P28C
1.0
0.9
0.8
0.7
0.6
0.5
0.4
0.3
0.2
0.1
0
J/J150 Oe
0
100
200
300
400
500
600
700
750
°C

Figure 6-3. Typical Curie temperature curve.

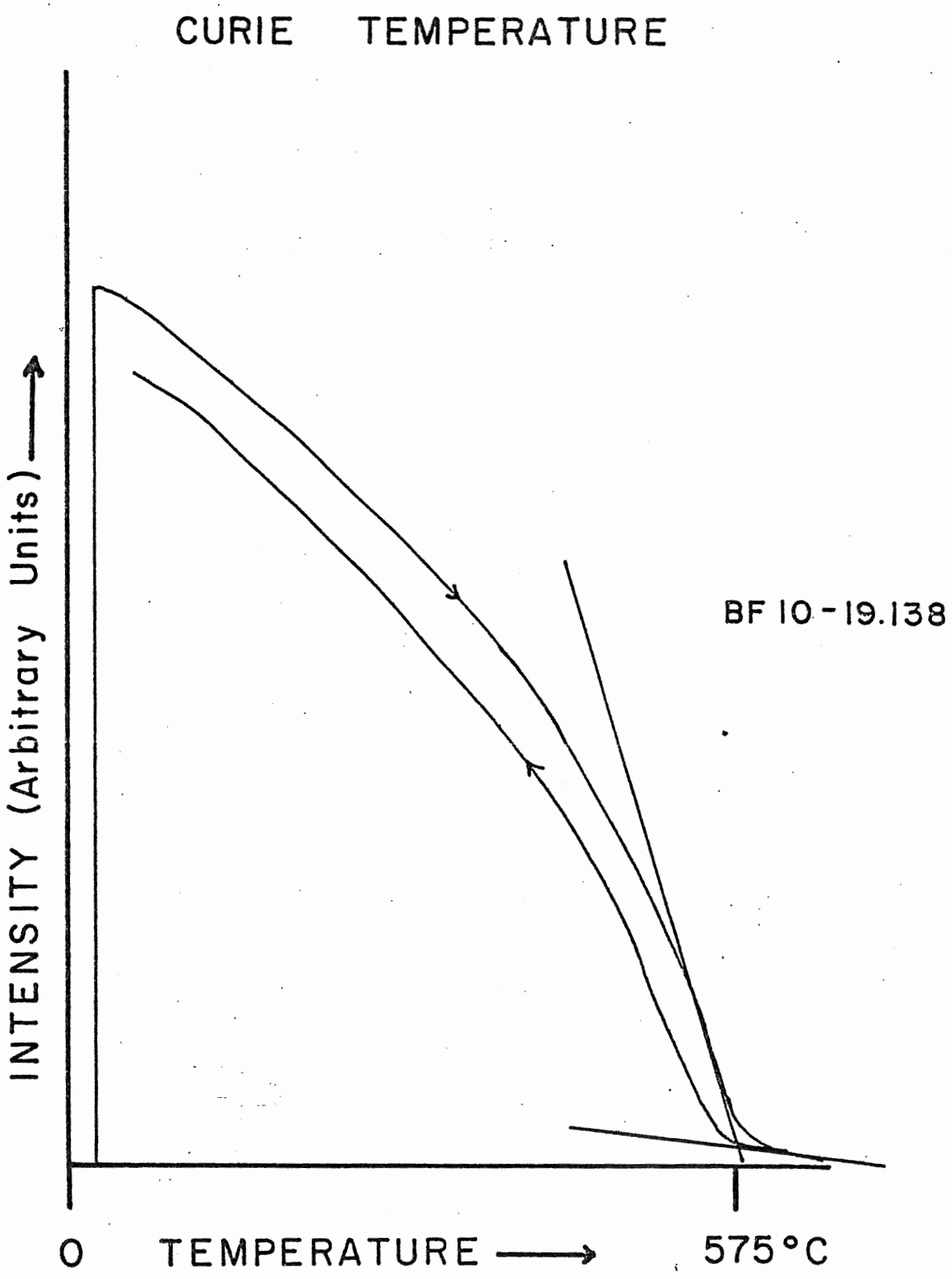
CURIE TEMPERATURE
INTENSITY (Arbitrary Units)
BF 10-19.138
0
TEMPERATURE
575°C

Table 6-2

VISCOUS DECAY EXPERIMENT - RESULTS
(after zero-field treatment)

Sample	NRM Intensity ($\times 10^{-3}$ emu g^{-1})	$I_{NRM}(^{o})$	$I_{STABLE}(^{o})$	MDF(^{o}C)
BF10-11.28	9.73	83.8	?	80
BD5-6.18	4.11	72.9	53(?)	80
BD9-2.63	144.2	88.0	?	110

Figure 6-4. Equal-area steronet plots of the demagnetization of selected samples.

COOLING UNITS

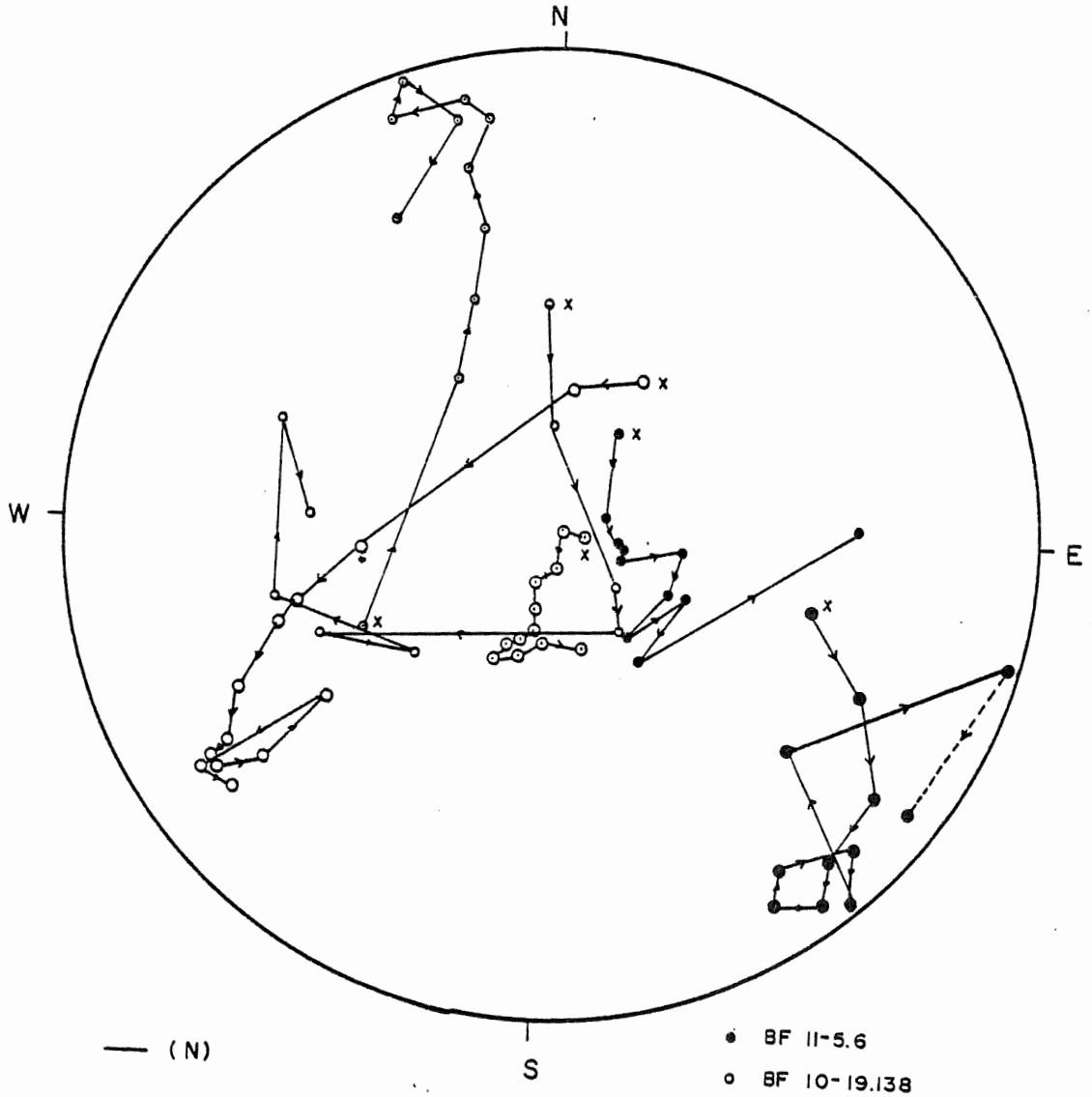

— (N)

— (R)

Arbitrary Declination

x = NRM

- BF 11-5.6
- BF 10-19.138
- BF 10-11.25
- BF 4 - 2.4
- BF 8 - 10.30
- BF 6 - 6.8

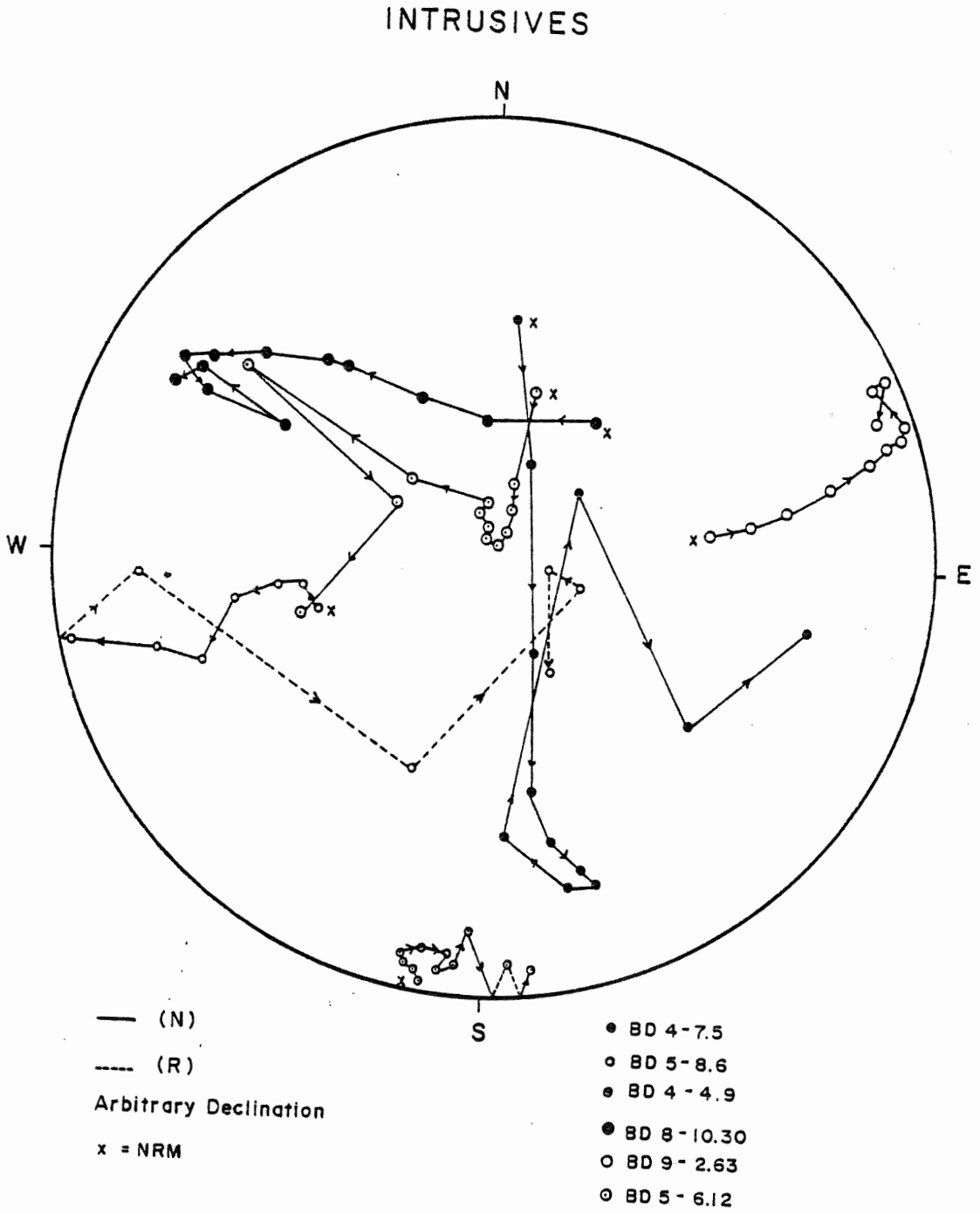
INTRUSIVES
N
W
E
S
(N)
(R)
Arbitrary Declination
x = NRM
BD 4-7.5
BD 5-8.6
BD 4-4.9
BD 8-10.30
BD 9-2.63
BD 5-6.12

Figure 6-5. Zijderfeld plots of some of the stabler units analyzed.

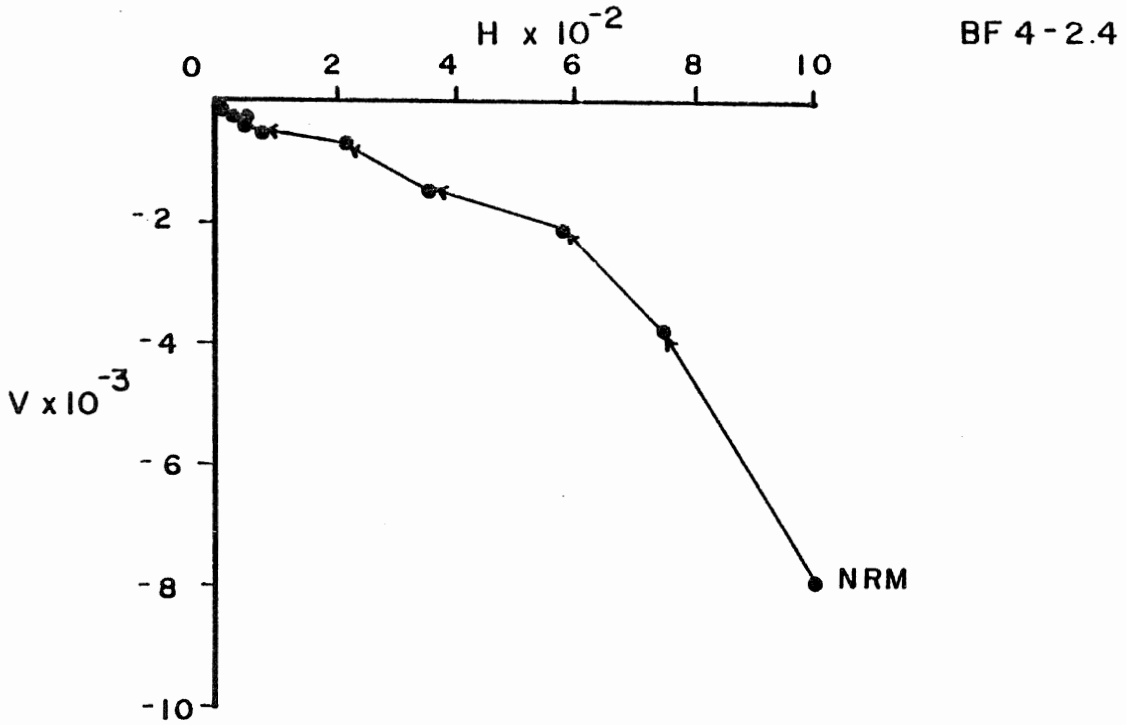
H x 10^-2
0
2
4
6
8
10
BF 4-2.4
-2
-4
V x 10^-3
-6
-8
-10
NRM

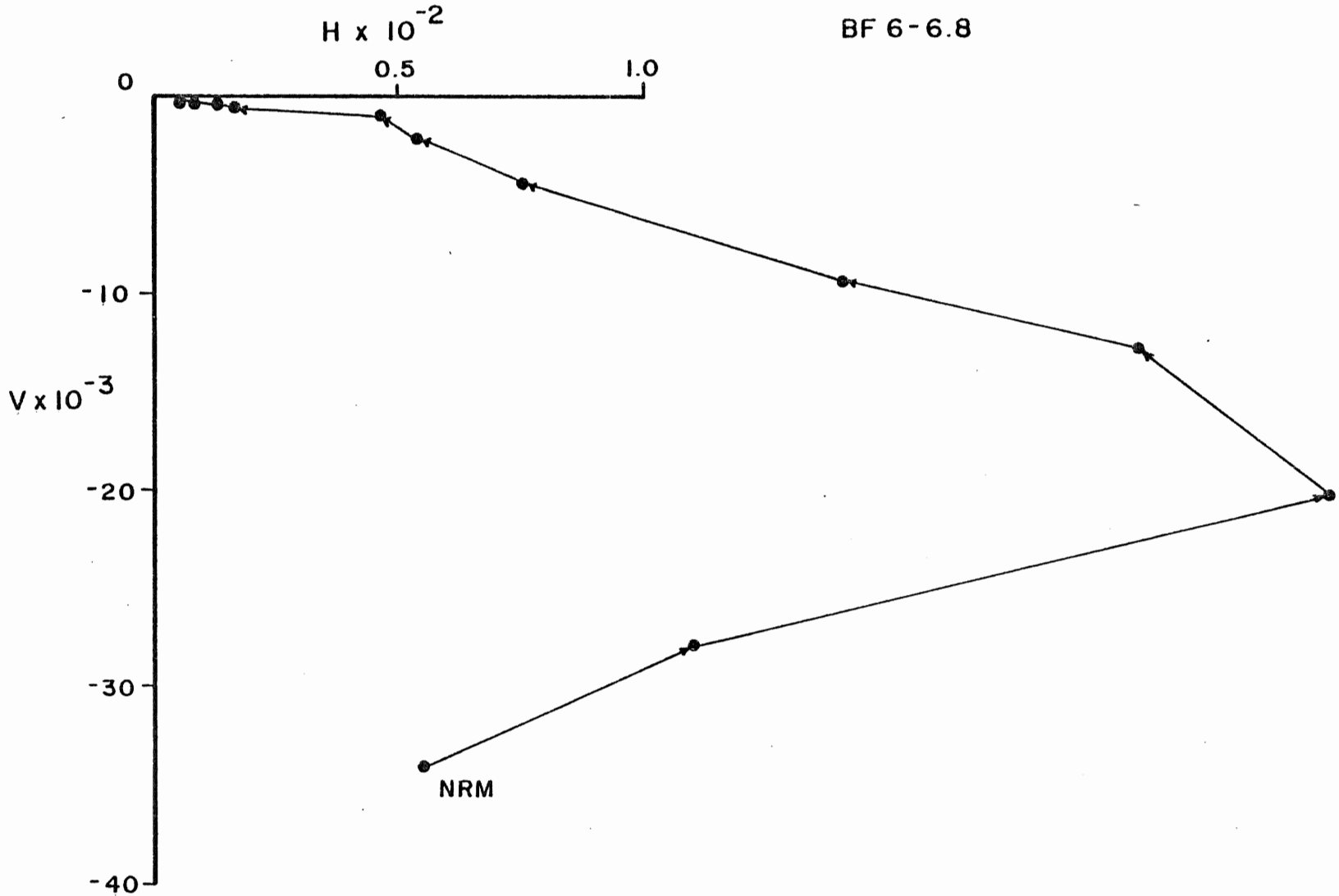
H x 10^-2
0.5
1.0
BF 6-6.8
0
-10
V x 10^-3
-20
-30
-40
NRM

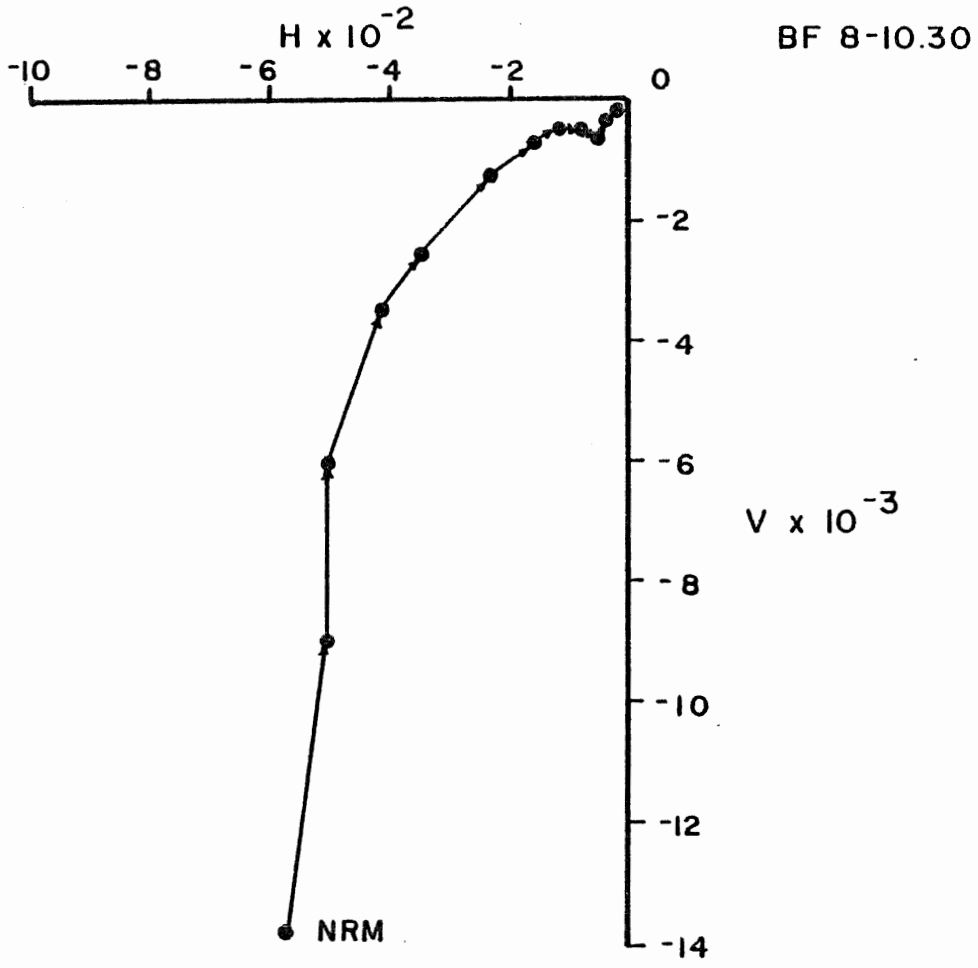
H x 10^-2
-10
-8
-6
-4
-2
0
BF 8-10.30
-2
-4
-6
-8
-10
-12
-14
V x 10^-3
NRM

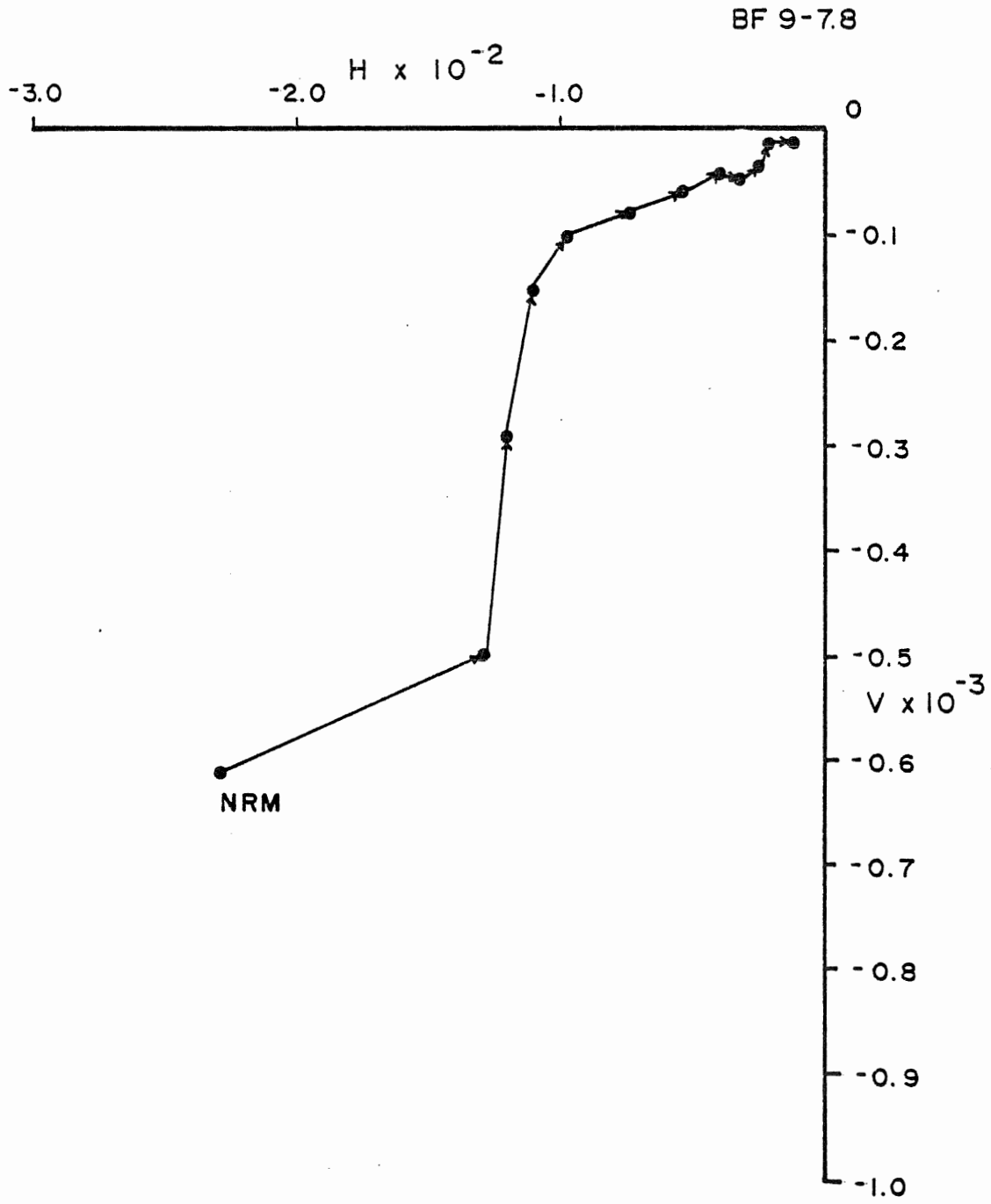
BF 9-7.8
H x 10^-2
-3.0
-2.0
-1.0
0
-0.1
-0.2
-0.3
-0.4
-0.5
V x 10^-3
-0.6
-0.7
-0.8
-0.9
-1.0
NRM

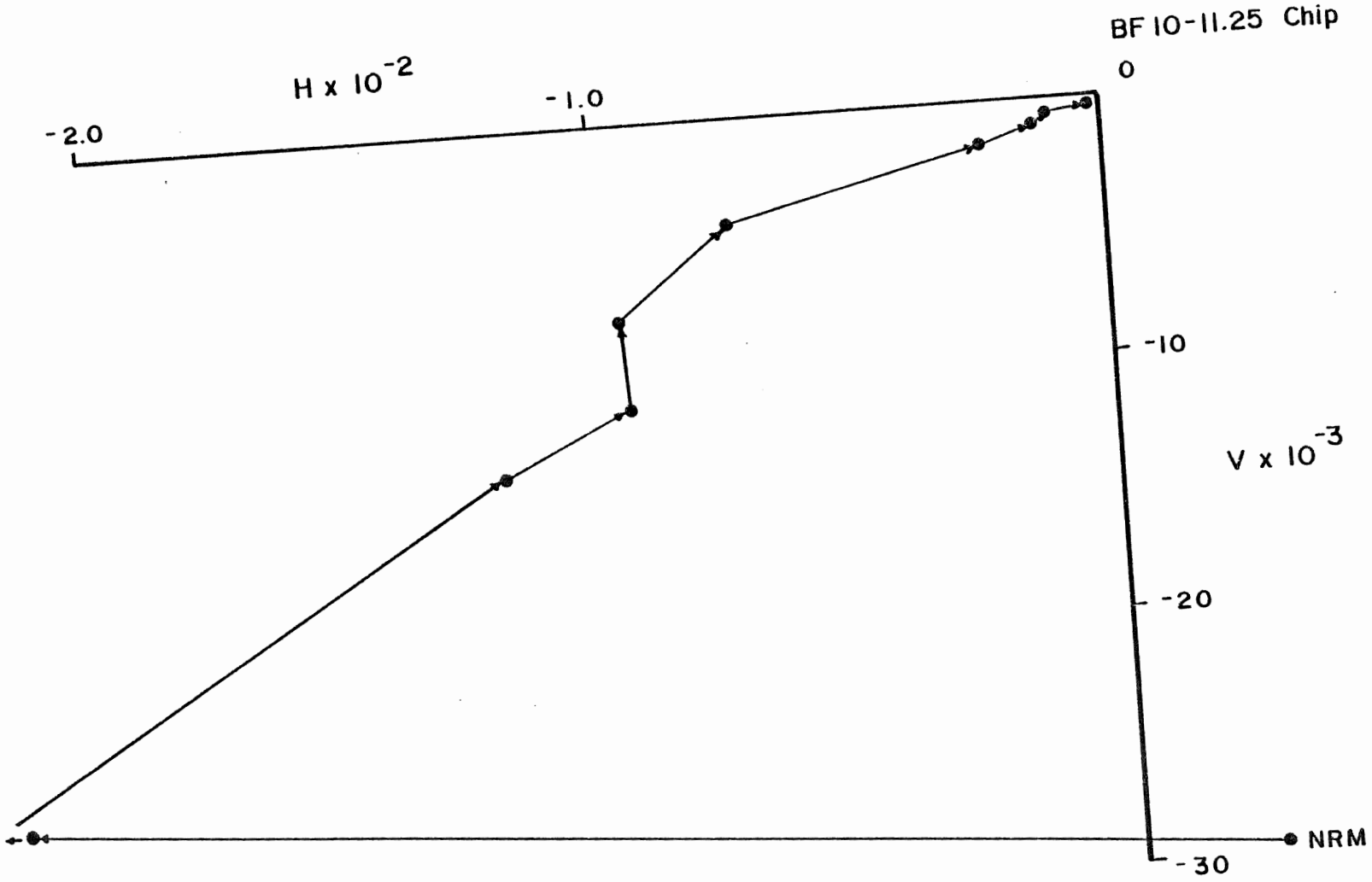
BF 10-11.25 Chip
H x 10^-2
0
-1.0
-2.0
-10
V x 10^-3
-20
NRM
-30

on the stereographic plots.

Another approach used was to look at the frequency distribution of the resultant inclination from each demagnetization step. These results are plotted (Figure 6-6). As the field intensity increases, inclinations for both the extrusives and intrusives attain a bimodal distribution. This distribution is most pronounced at the 200 Oe level with peaks at $+0^{o}$ to $+20^{o}$ and again at $+60^{o}$ to $+70^{o}$ for the flows with the higher peak for the dikes at $+80^{o}$ to $+90^{o}$. Further demagnetization beyond this level only causes a broad, nearly Gaussian distribution of inclinations with most values having a positive inclination and a mean close to the horizontal.

Discussion

Several problems are evident from an examination of the results. These rocks are intensely magnetized, but the magnetization is soft. It is very difficult to obtain a consistent inclination, especially for the intrusives. Why are these rocks so poor in holding a stable remanence? To what extent do VRM, DIRM, and SIRM contribute to the NRM?

Since stability of magnetization is a function of the grain size (Dunlop, 1977), the size of the magnetic oxides is important. In these rocks, spinel, the only suitable ferrimagnetic phase, makes up to 15% of the total volume. The grain size varies from large (1-2 mm) to very small (<50 microns) with greater than 80 percent of the grains being less than 100 microns. Comparisons with titanomagnetites studied by Soffel (1971), suggests that these magnetic spinels are all in the multi-domain grain size range. Rapid decrease in moment is typical of

Figure 6-6. Distribution of inclinations for each demagnetizing step. Notice the peaks at 200 Oe.

COOLING UNIT INCLINATIONS

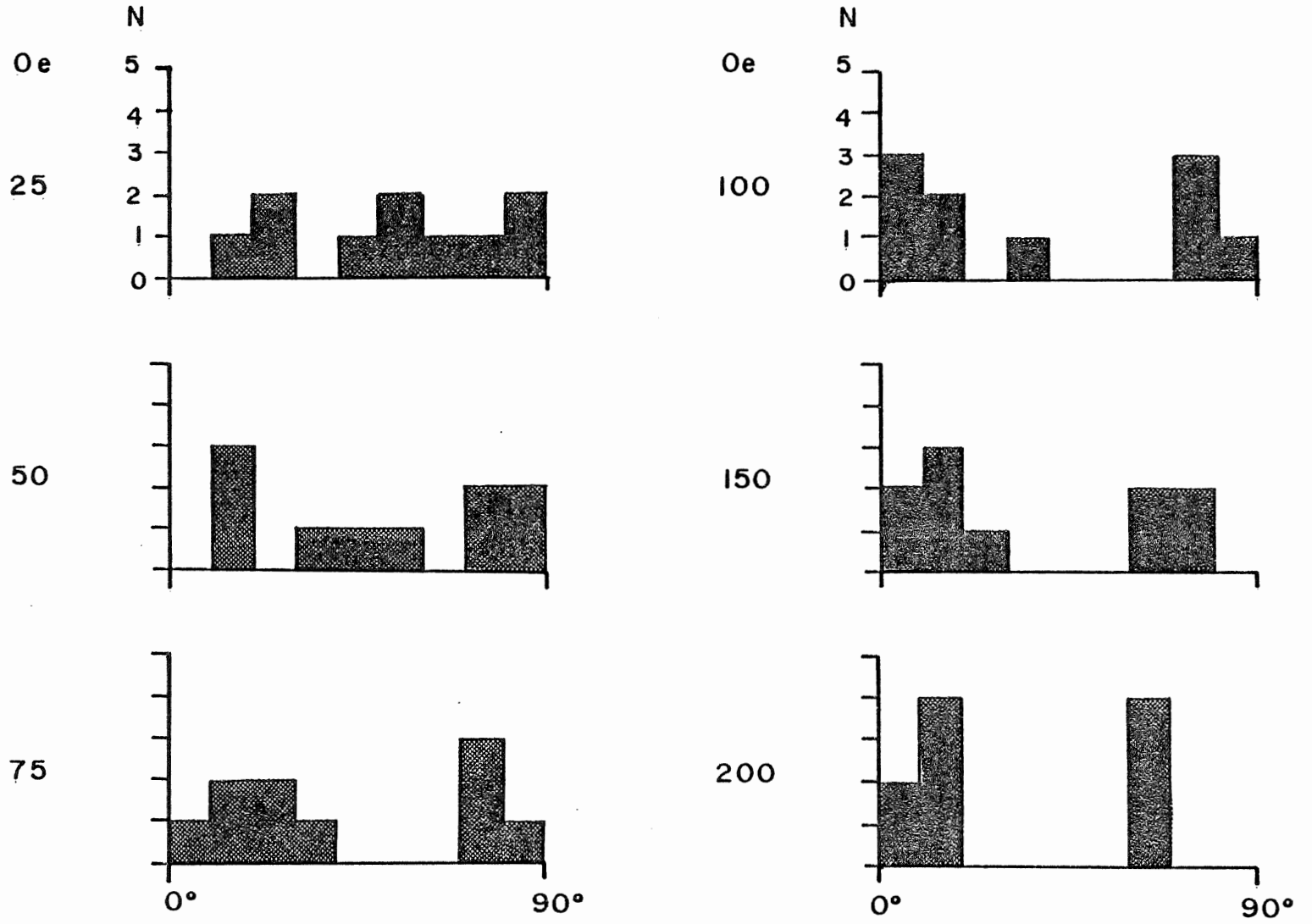

COOLING UNIT INCLINATIONS

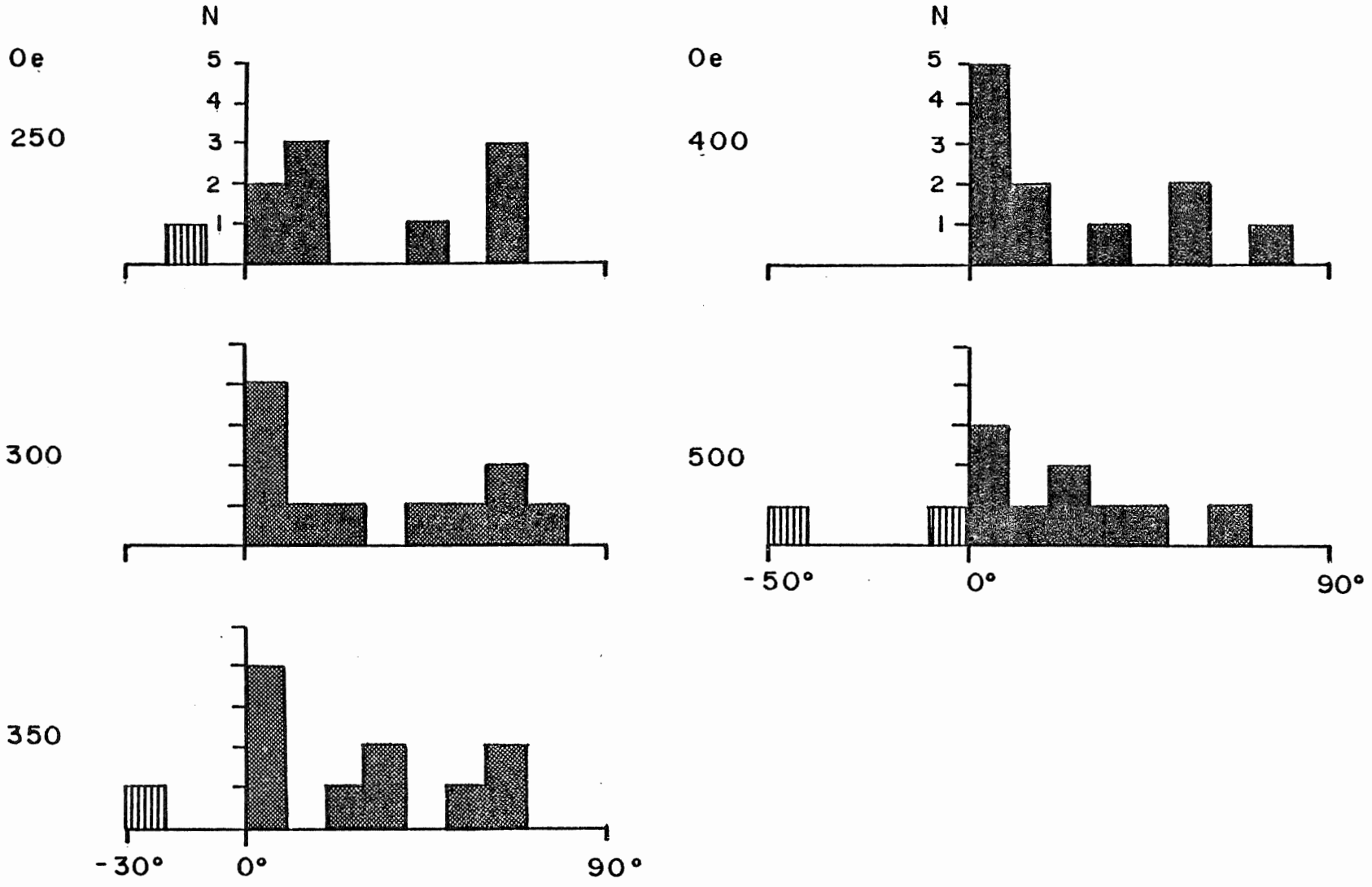

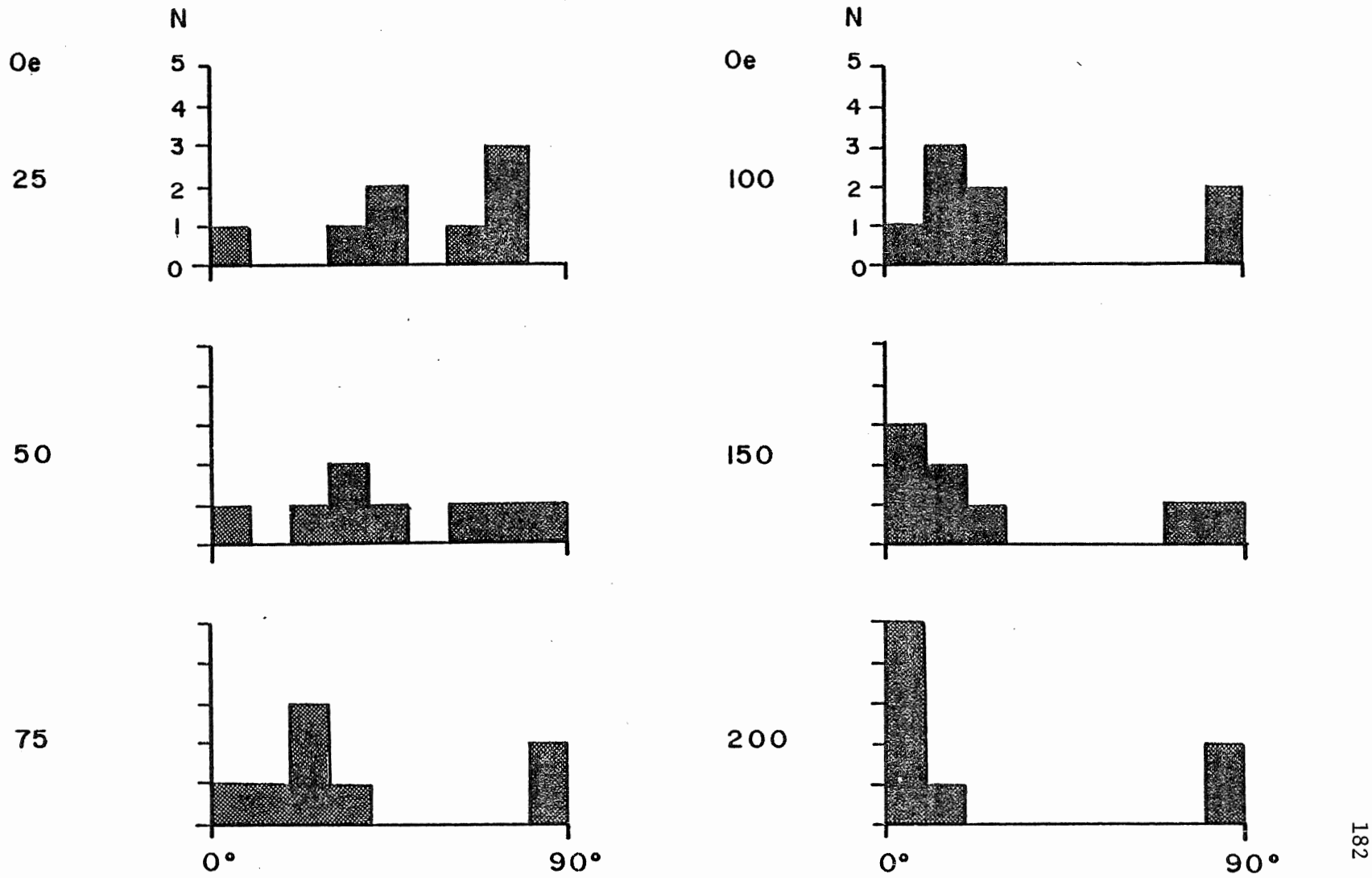
INTRUSIVE INCLINATIONS
N
0e
25
50
75
100
150
200
5
4
3
2
1
0
0°
90°

INTRUSIVE INCLINATIONS

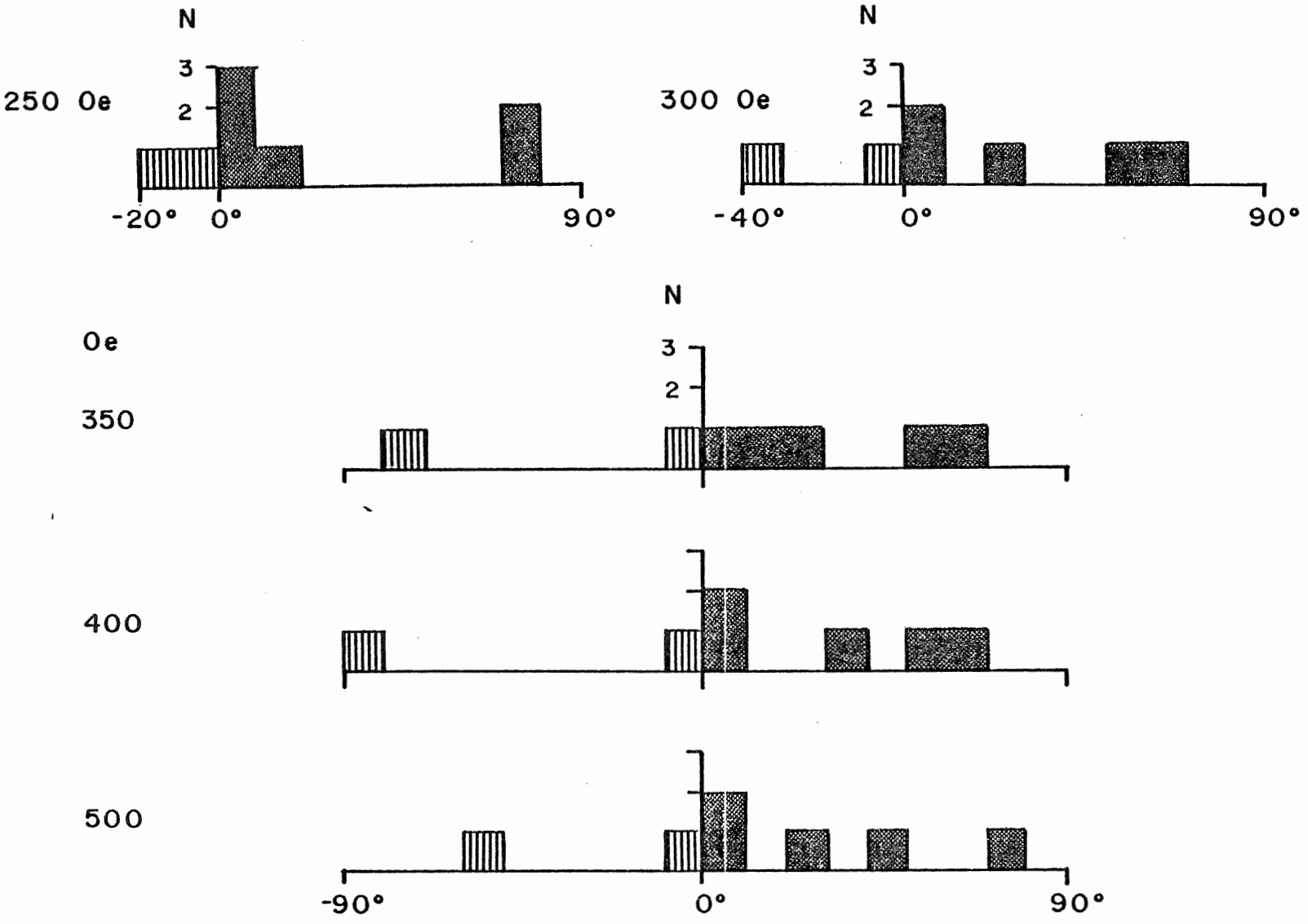

large multi-domain grains (Dunlop et al., 1973; Cisowski, 1980).

The magnetic behaviour can be interpreted in two ways: (1) the spinels carry the remanence and have high Curie temperatures, or (2) small, nearly pure magnetite, at the size of the single to multi-domain transition makes up about 10 percent (to generate the proper moment) of the opaque mineral volume and carries the remanence. Either of these mechanisms may be responsible for the magnetic properties observed. In order to delineate the differences, the pertinent properties of both minerals will be reviewed.

The magnetic properties of magnetite are well known. At room temperature ($300^{o}K$) the spontaneous magnetization is 90 emu g^{-1} (Stacey and Banerjee, 1974). The Curie temperature is 575^{o} (Readman and O'Reilly, 1971), but varies from 575^{o} to 581^{o} (Lindsley, 1976). The critical size for the single to multi-domain transition is 15 to 20 microns. The single to pseudosingle domain change occurs in magnetic grains at approximately 0.05 microns with the most profound domain structure changes occurring at sizes greater than 0.1 microns (Day, 1977). The average MDF for magnetite, with an average diameter of 2.7 microns, is 77 Oe (Day, 1977). Although Levi and Merril (1978) cautioned against the intuitive correlation of MDF and blocking temperature (T_B), there is a positive correlation of increase of MDF with T_B. For a magnetite with an MDF of 77 Oe, the corresponding value of T_B is $475^{o} \pm 15^{o}C$, which is not close to the estimated value of T_B of about $575^{o}C$ for the Bermudian rocks (Figure 6-2). These data make a powerful argument for magnetite being the carrier of remanence in the igneous rocks.

There are scant data available on the magnetic properties of the type of spinel encountered in the Bermuda samples. These spinels are unusual in that they are generally enriched in Mg and Al. Although some experiments have examined the substitution of Mg and Al in ulvöspinel (Fe_2TiO_4) the effect of a combination of Mg, Al, and Ti together has not been examined. Nonetheless, some experiments, using synthetic spinels, have outlined compositional trends which may be of use to this study.

Blasse (1964) synthesized a variety of spinels in the $MgFe_2O_4$ to Mg_2TiO_4 series. Although these samples are more magnesian than the Bermudian samples, the important point is that with increasing titanium content, the Curie point decreases. These results were substantiated by Stephenson (1972).

In a recent study, O'Donovan and O'Reilly (1977) examined the Curie temperatures of aluminous-titanomagnetites and magnesian-titanomaghemites. As expected from the previous studies, with increasing Al content the Curie point decreased. In fact this trend appears to apply for any diamagnetic ion. For example, an aluminous titanomagnetite with a composition of $Fe_{2.15}Al_{0.25}Ti_{o.60}O_4$, has a Curie temperature of nearly 0^oC and a remanence of 0.97 emu g^{-1}. A magnesian titanomaghemite of composition $Fe_{2.05}Ti_{0.60}Mg_{o.35}O_{4.625}$ has a Curie point of 440^oC (Ozdemir and O'Reilly, 1978).

Two problems hinder direct application of these results to the Bermudian rocks. One is that there have been experimental studies on complex spinels with variable amounts of Fe, Ti, Al, and Mg; and also these experiments are based on synthetic spinels which may not faithfully

mimic the magnetic structure of natural spinels. The other problem is that the size of the Bermudian spinels is certainly in the multi-domain range, which agrees with the af demagnetization spectra. Also, all of the analyzed spinels, down to the size limit of the probe (~5 microns) yield similar analyses. No magnetite has been identified optically in large enough concentrations to produce the desired magnetizations.

The remanence carrier is presently unknown. Although most of the evidence indicates magnetite, mineralogical considerations argue against this evidence. The magnetic nature of these Bermudian spinels is complex and requires more detailed study.

Regardless of the type of magnetic phase responsible for the remanence, the resultant stable (and unstable) inclinations are also difficult to interpret. A review of Table 6-1 shows a variation of stable inclination from about $+2^{o}$ to $+72^{o}$ with a mean of approximately $+28^{o}$. There is no systematic down-hole variation or major difference between the average inclinations of the extrusives and intrusives. Several problems are evident: are these inclinations meaningful, have the inclinations been modified tectonically, and have these rocks been overprinted magnetically by a secondary phase which has totally suppressed the original NRM (i.e. DIRM)?

The techniques used to determine the stable inclinations suggest that the inclinations are meaningful; although, nearly 40 percent of the samples did not yield stable inclinations. A re-examination of the Zijderfeld plots and stereoplots clearly indicates a stable inclination for many of the samples. Also, for the units with multiple samples, the inclinations are internally consistent ($\pm 5^{o}$). Therefore,

either the individual units have been tectonically rotated since initial magnetization or their NRM's, assumed to have been induced at the time of formation, have been lost.

There is reasonably good evidence supporting a tectonic alteration of the NRM. Assuming that the lavas cooled through their blocking temperature interval during extrusion, individual pillows may have rolled down slope after acquisition of NRM. Another, similar mechanism, is suggested by the breccia sections in the core. The same type of violent action that formed these breccias may have physically reoriented large blocks, or even caused a shock induced remagnetization (SIRM or piezoremanence-PRM). Thus not only could the NRM have been physically reoriented but a SIRM or PRM, which is similar to isothermal remanence in strength and stability, may have been induced (Stacey and Banerjee, 1974).

In their investigation of SIRM, Cisowski and Fuller (1978) found that this effect is most strongly developed in low-coercivity materials. Two modifications of the NRM can result from a shock of sufficient intensity ($\leq$10 kb). One is that the low-coercivity magnetic minerals will become magnetized parallel to the external field at the time of shock. Two is that the rock can be shock cleaned by demagnetizing the soft components of the NRM leaving the hard components intact.

A last possible source for the observed inconsistencies is an overprinting of the NRM by a drilling-induced remanence (DIRM). In this case, the measured NRM is actually the resultant of the true NRM and the DIRM. A possible model for this process is shown in Figure 6-7. In this model, a stable inclination of $\pm 51^{\circ}$, the Tertiary inclination

Figure 6-7. DIRM model for the Tertiary pole of ±51° for both normal and reversed NRM.

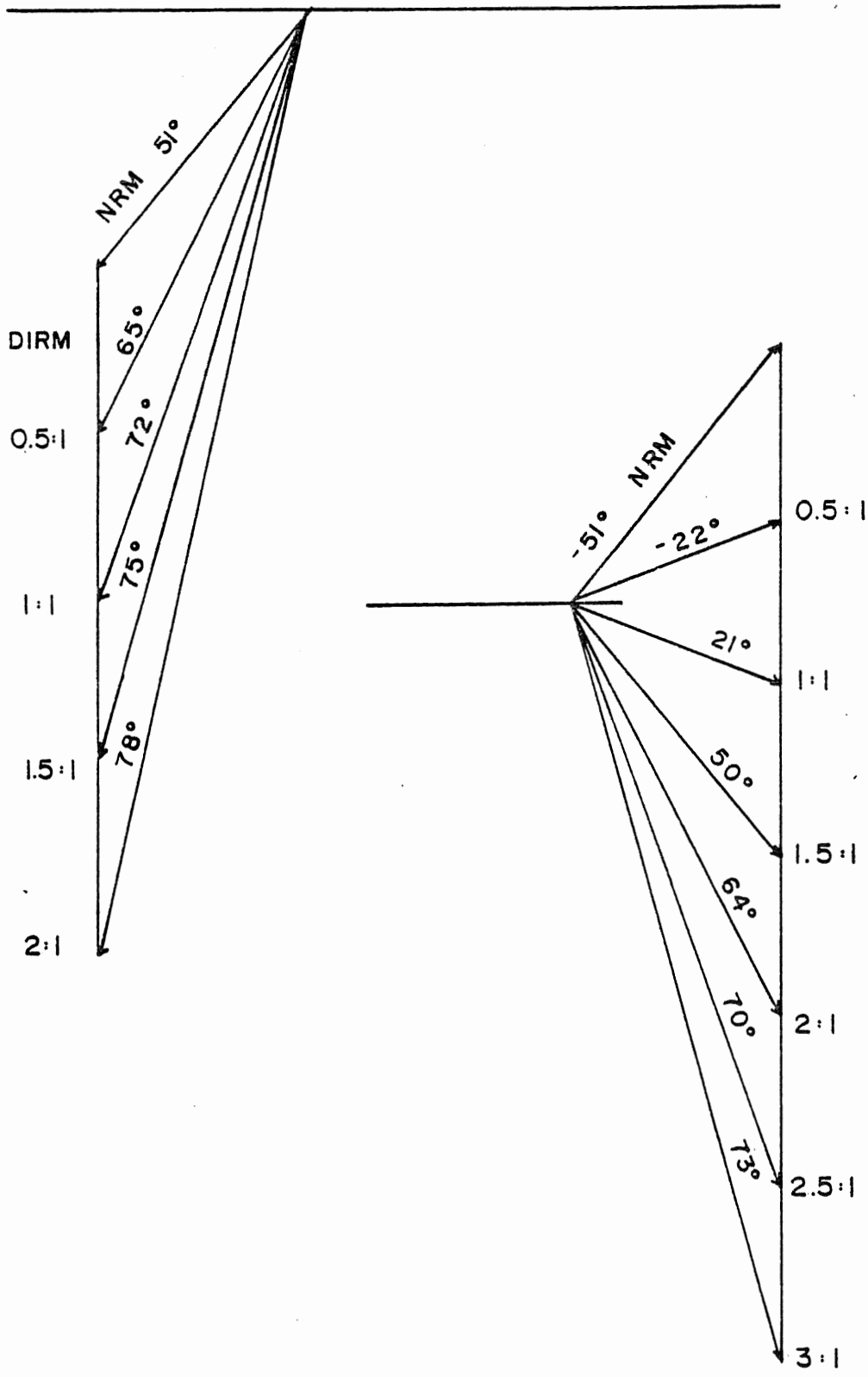
NRM 51°
DIRM
0.5:1
1:1
1.5:1
2:1
65°
72°
75°
78°
-51° NRM
-22°
21°
50°
64°
70°
73°
0.5:1
1:1
1.5:1
2:1
2.5:1
3:1

for Bermuda, is overprinted by a DIRM at $+90^{o}$, i.e. along the axis of the drill string. The resultant vector is very dependent upon the relative intensities of the NRM and DIRM. The DIRM is usually soft and the inclinations should migrate towards the true NRM during demagnetization.

The occurrence and strength of the DIRM was demonstrated with a special test using the end and center of one minicore and also by the lack of decay in the viscous decay experiment. Two pieces of sample BF10-11.25 were analyzed, the central portion of the minicore and an end piece. It is assumed that the end piece is more strongly affected by DIRM. Notice (Figure 6-8) that the NRM inclination for the chip is steep, $+89^{o}$, while the inner section is less steep, $+54^{o}$. Also, the end piece has a very intense moment (13.3×10^{-3} emu g^{-1}) compared to the interior (0.0191×10^{-3} emu g^{-1}) and has no stable inclination. All of the chips in viscous decay have steep NRM inclinations, especially when compared to the normal pieces from these same samples, which are magnetically strong components. These experiments provide very good evidence for a DIRM overprinting in these rocks.

In conclusion, these rocks are unreliable holders of a stable inclination. The average inclination of NRM is approximately equal to the calculated mid-Tertiary inclination for Bermuda of $\pm 51^{o}$ (Irving, 1975). The rocks yield a poorly defined stable inclination from af demagnetization which has a mean of about $+28^{o}$. Many samples do not yield stable inclinations. Nearly all the units sampled have a DIRM which ranges from soft to very hard. Thermal and AF techniques do not give the same results, with the thermally derived stable inclination being $+51^{o}$ ($\pm 19^{o}$) which is very similar to the Tertiary pole inclination

Figure 6-8. Equal-area steronet plots of the DIRM experiment. Notice how the end piece has a much steeper inclination which decreases but is not lost.

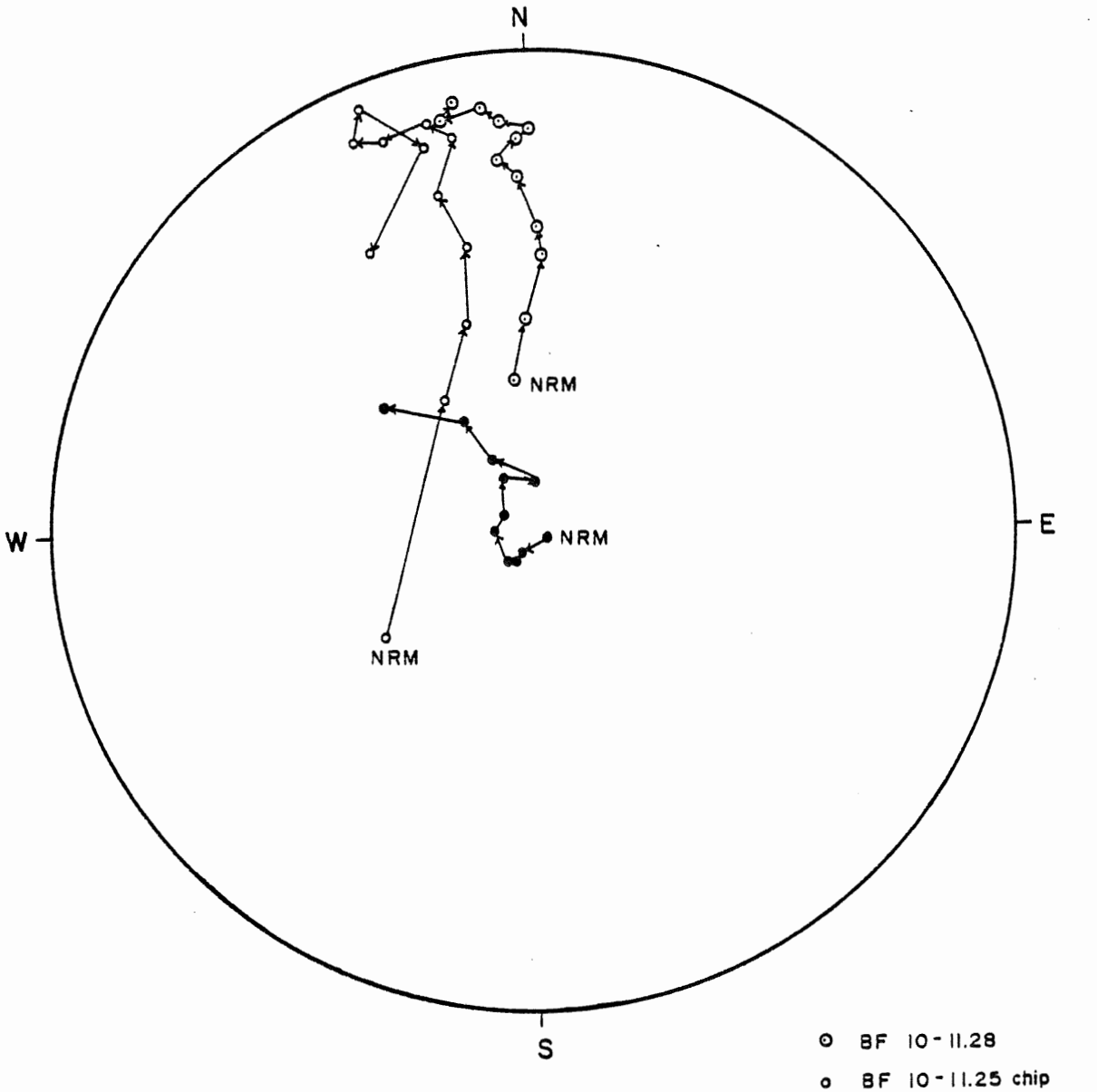

⊙ BF 10-11.28

o BF 10-11.25 chip

● BF 10-11.25

All Positive Inclinations

calculated for Bermuda. The discrepancy between the two techniques cannot be readily explained.

The rock magnetic properties resemble very closely the behaviour of magnetite. No significant volumes of magnetite have been identified from petrographic studies. It is unclear whether the spinels encountered in these rocks behave like pure magnetite or the magnetite is too finely dispersed to permit identification.

Within the limits of this study there does not appear to be a coherent magnetic stratigraphy within the volcanic section of the 1980-core. The bulk rock magnetic properties are not similar to those of the 1972-core (Rice et al., 1980).

CHAPTER 7

THE BERMUDA RISE

Introduction

The Bermuda Rise is an anomalous topographical region which is bordered by the Sohm Abyssal Plain to the north and east, Nares Abyssal Plain to the south, and Hatteras Abyssal Plain to the west (Johnson and Vogt, 1971). Definitions of the rise vary but generally, it is a topographic high or swell which is elongated from the northeast to southwest and measures approximately 800 by 400 kilometers. In this chapter the rise is redefined and an overview of the geological and geophysical nature of the rise are given.

The Bermuda Rise - Redefined

The Bermuda Rise is redefined on the basis of age-depth relationships which are corrected for subsidence due to sediment loading. The theoretical depths to oceanic basement (below mean sea-level) were determined for every 10 million year interval between 180 and 80 Ma using the systematics of Parsons and Sclater (1977). The age of the crust in the northwestern Atlantic was derived from the compilation of well-correlated linear magnetic anomalies given by Rona (1980). The predicted age-depth values were superimposed on the topography of the sea-floor for the region between 55^{o} to 70^{o}W and 25^{o} to 40^{o}N. Depths shallower than the predicted values were marked as anomalous crust. The anomalous crustal depths were corrected for sediment loading using isopach maps (Rona, 1980) and this correction for tectonic subsidence:

$$y = \frac{(\rho m - \rho s)}{(\rho m - \rho w)} S + H_w$$

where, y = tectonic subsidence, ρm = mantle density (3.5 g cm^{-3}), ρs = sediment density (2.3 g cm^{-3}), ρw = seawater density (1 g cm^{-3}), S = sediment thickness, and H_w = paleo-water depth (Keen, 1979).

The results of these calculations are presented in Figure 7-1. The eastern margin of the rise is poorly defined, mainly due to the lack of basement ages and the poor correlation of magnetic anomalies. The southern boundary may grade into the Caribbean Island arc, but there is no obvious correlation of the rise with the arc. The western margin of the rise is located tentatively due to thick sediment loads (up to 6 km thick), poor age control, and the uncertain location of the transition from continental to oceanic crust. The solid line shows the boundary as predicted from the model while the dashed line follows along the most westerly section of anomalous crust for which there is reasonably good age control. The northern boundary is just south of the New England Seamount chain. There is some anomalous crust to the north of the seamounts, but this chain cuts across the rise and is considered to represent a major discontinuity in the crust.

The redefined Bermuda Rise is larger than previous descriptions. The new dimensions are 1650 by 1210 kilometers with a very slight elongation from northeast to southwest. The Bermuda seamount and islands are situated slightly to the east of the major axis but in the central portion of the rise.

Figure 7-1. Redefined limits of the Bermuda Rise. The solid line shows the new limits, the dashed line shows the most westerly section of anomalous crust which is accurately located (see text). The limits to the east are poorly confined. The dotted line shows the Rise boundaries of Rona (1980).

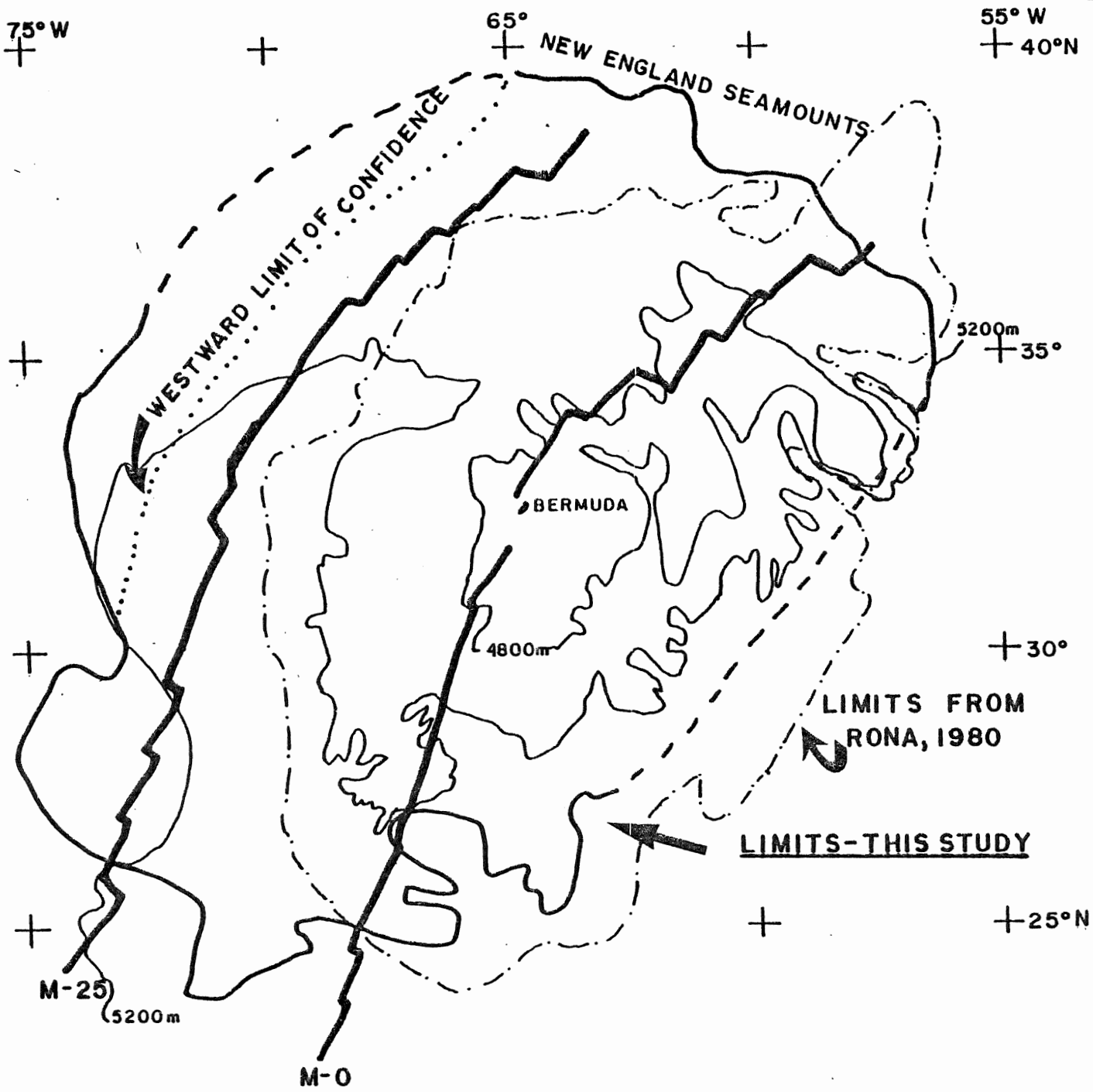
75° W
65°
55° W
40°N
NEW ENGLAND SEAMOUNTS
WESTWARD LIMIT OF CONFIDENCE
5200m
35°
BERMUDA
4800m
30°
LIMITS FROM
RONA, 1980
LIMITS-THIS STUDY
25°N
M-25
5200m
M-0

Geological Studies

On Leg 43 of the Deep Sea Drilling Project, basement rock was recovered at Sites 386 and 387 on the central and western Bermuda Rise, respectively. These are the only known basement rock samples from the rise and both are basaltic. The sample from Site 386 is a hypocrystalline, fine-grained, amygdaloidal phyric-basalt with plagioclase (An 65-70) and pyroxene (subcalcic-augite) phenocrysts. These are set in a groundmass of plagioclase laths and granular-interstitial pyroxene with lesser amounts of locally subophitic glass. This basalt is chloritized to varying degrees. The basalt from Site 387 is a black, holocrystalline, fine-grained, amygdaloidal phyric-basalt with xenoliths of calcareous claystone. This unit is underlain by a baked claystone and may be a sill. Phenocrysts are of plagioclase (An 70-80) and rarer pyroxene (subcalcic augite). The groundmass consists of felty plagioclase microlites with intergranular pyroxene and disseminated magnetite. There is a variable amount of alteration. The Site 386 sample is probably an altered oceanic ridge tholeiite, while the Site 387 sample is chemically similar to a mid-oceanic ridge tholeiite but petrographically appears to be a sill.

Houghton et al. (1979) also determined the radiometric ages of these basalts. The best estimate age for the Site 386 basalt is 125 ± 25 m.y. and for Site 387 is 126 ± 20 m.y. The certainty of these ages is relatively poor and the accuracy of the Site 387 data is fair to poor. Paleontological ages from fossils in the claystone inclusion at Site 387 indicates the basalt to be upper Berriasian to lower Valangian (128 - 133 m.y.).

The basalts from Sites 386 and 387 yielded stable magnetic inclinations of $57.1^{o} \pm 6.2^{o}$ (±1 s.d.) and $58.8^{o} \pm 7.1^{o}$ respectively. They have high Curie temperatures which range from 320^{o} to 490^{o}C. The major magnetic minerals are titanomagnetites. The stable inclinations are closer to the present day dipole field inclination of $\pm 51^{o}$ than the Cretaceous inclination of nearly $\pm 40^{o}$ which suggests that the rocks have undergone a chemical remagnetization due to low temperature oxidation (Petersen et al., 1979).

The cover over the Cretaceous basaltic basement at both sites is a thick (>800 m) sequence of upper Cretaceous to Recent sedimentary rocks. The sediments at Site 386 have recorded some of the volcanic activity associated with the formation of the Bermuda Seamount.

A schematic lithologic column for Site 386 is given in Figure 7-2. The sediments of possible volcanic origin are of greatest interest. In the middle part of unit five are some very thin (<1 cm), light-colored, unfossiliferous zones of zeolitic claystone with a distinctive mineralogy of quartz, feldspar and clay minerals with about 11 percent clinoptilite and 1 to 2 percent phillipsite. The sharp contact between the zeolitic claystone and surrounding lithologies suggests nearby volcanism during the Maestrichtian to upper Cenomanian. The zeolites and clays can readily be derived from volcanic ash, but the high quartz content calls for additional silica input, possibly from a biogenic source. On the basis of REE studies, Chamley (1979) has interpreted this horizon to be of non-volcanic nature.

Unit 3B is a 162 meter thick series of volcanoclastic turbidites ranging from late Eocene to late Oligocene. The more sandy layers are

Figure 7-2. Stratigraphy and schematic core log of the sedimentary sequence at DSDP Site 386.

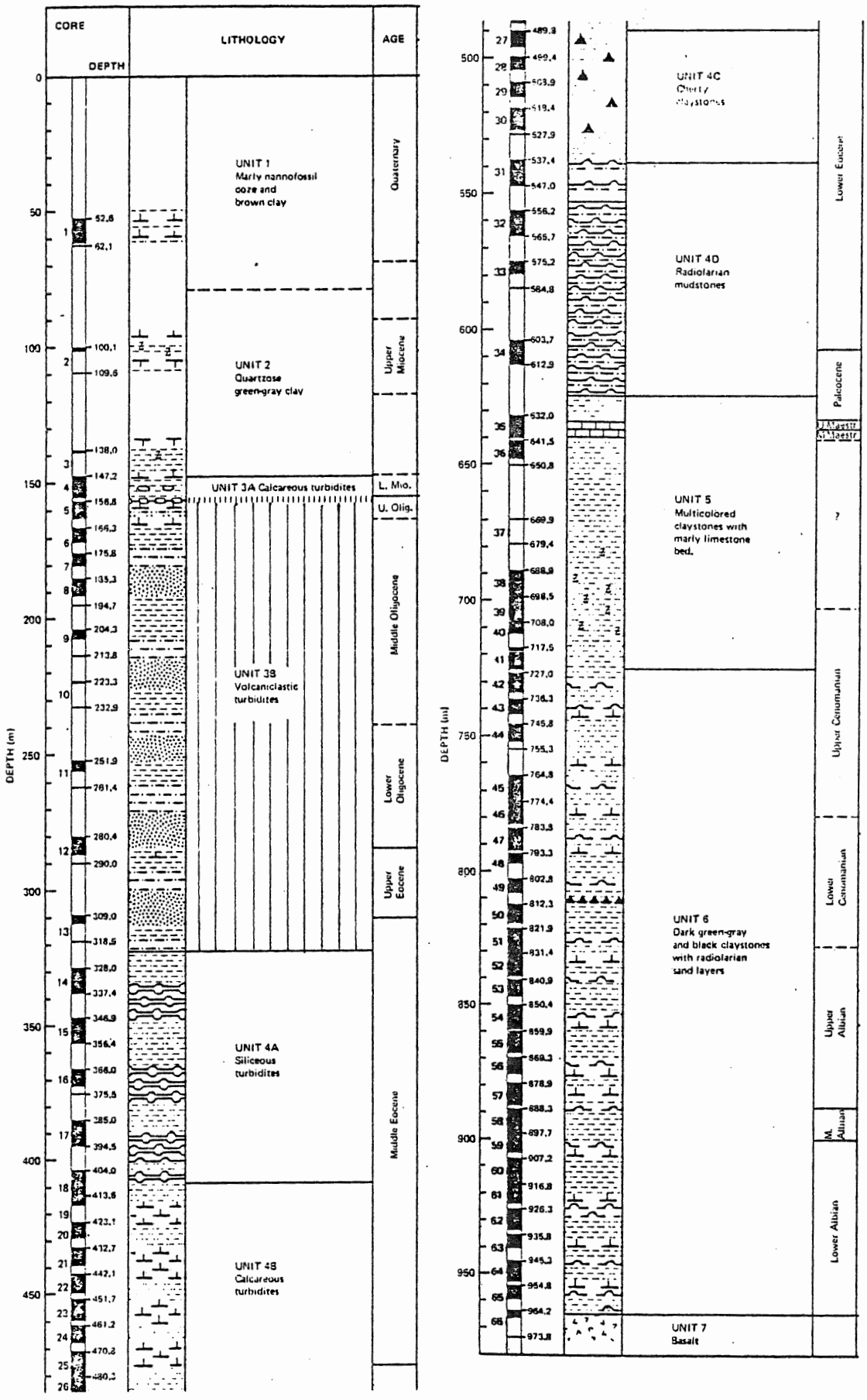
CORE
DEPTH
LITHOLOGY
AGE
DEPTH (m)
UNIT 1
Marly nannofossil ooze and brown clay
Quaternary
UNIT 2
Quartzose green-gray clay
Upper Miocene
UNIT 3A Calcareous turbidites
L. Mio.
U. Olig.
UNIT 3B
Volcaniclastic turbidites
Middle Oligocene
Lower Oligocene
Upper Eocene
UNIT 4A
Siliceous turbidites
Middle Eocene
UNIT 4B
Calcareous turbidites
UNIT 4C
Cherty claystones
Lower Eocene
UNIT 4D
Radiolarian mudstones
Paleocene
UNIT 5
Multicolored claystones with marly limestone bed.
?
UNIT 6
Dark green-gray and black claystones with radiolarian sand layers
Upper Cenomanian
Lower Cenomanian
Upper Albian
M. Albian
Lower Albian
UNIT 7
Basalt

dominated by angular mineral fragments of which clinopyroxene is most common. Accessory minerals are: hornblende, apatite, epidote, and rarely, garnet. Other components are: vesicular glass, palagonite, opaques (magnetite), phillipsite, and analcite as well as a variety of microfossils (Galehouse, 1979). The finer-grained sediments are made up of clinopyroxene, feldspar, phillipsite, and analcite. Quartz is very rare and occurs only when the volcanogenic sediments are scarce. Most likely, these volcanogenic sediments are derived from the Bermuda Seamount and were accumulated at about 9 mm yr^{-1}. Unit 3a is a calcareous turbidite (8.7 meters thick) of lower Miocene to upper Oligocene age. Mica and quartz+feldspar zones have been described within this unit as well as small apatite placers with up to 50 percent apatite. This unit (3a) too, may be related to the erosion of the Bermuda Seamount and Islands (Tulcholke et al., 1979).

The sediments recovered from Site 387 are shown in a schematic stratigraphic column (Figure 7-3). Unit 5 is only about 20 meters thick and is a red claystone of upper Cretaceous age. This claystone is Fe-rich and may be volcanogenic, but has been deposited at pelagic rates (2 mm/m.y.). A hiatus in unit 2 marks the abrupt end of turbidite accumulation in middle Eocene time. This cessation correlates well with the volcanism recorded post-facto at Site 386 and indicates a regional tumescene (formation of the Bermuda Rise).

The stratigraphic results from Leg 43 provide an excellent foundation for correlating the acoustic stratigraphy of the Bermuda Rise with the lithologic stratigraphy. The correlations are based on studies by Tulcholke and Mountain (1979) and Jansa et al. (1979). Of

Figure 7-3. Stratigraphy and schematic core log of the sedimentary sequence at DSDP Site 387.

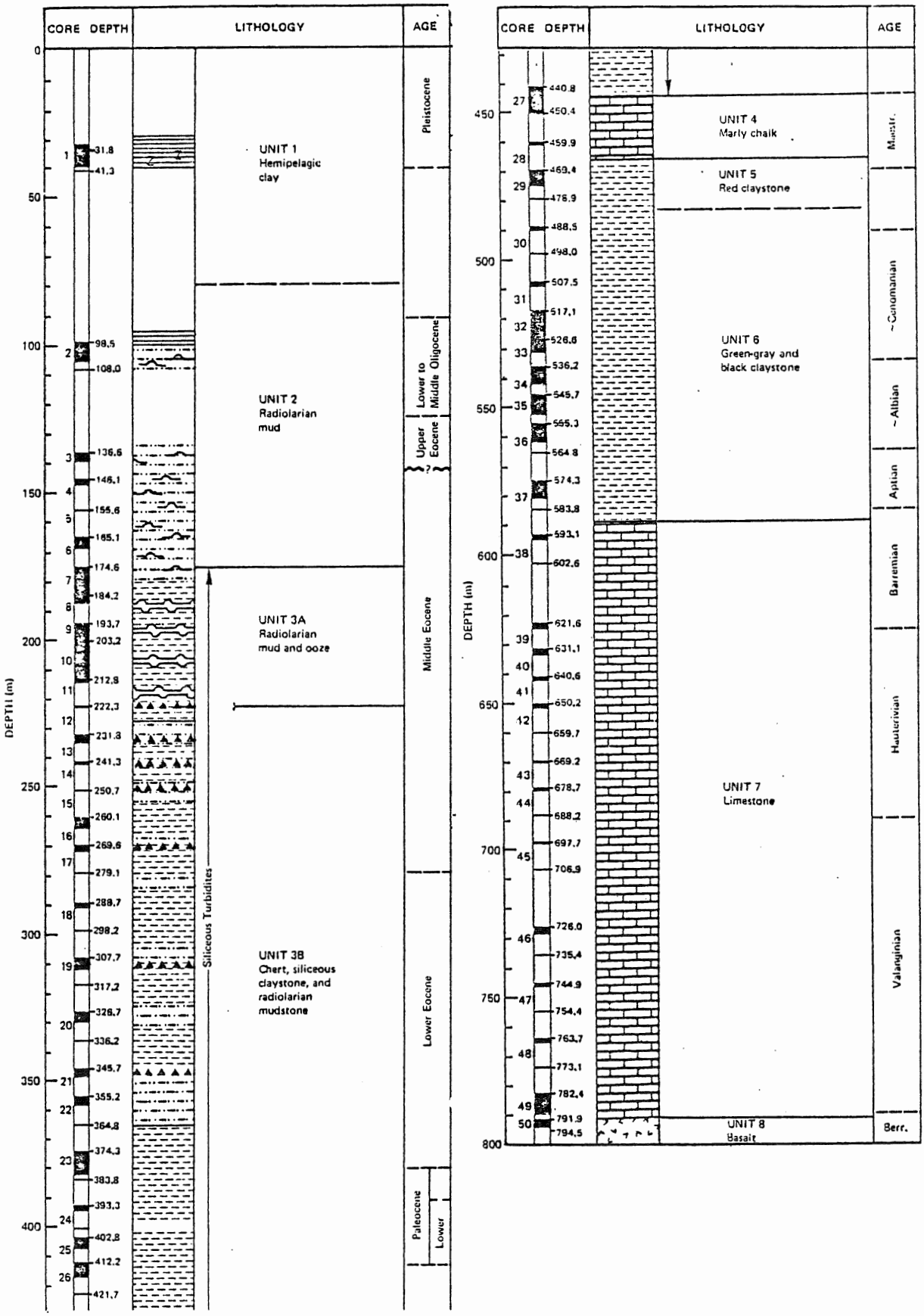
CORE DEPTH
LITHOLOGY
AGE
DEPTH (m)
UNIT 1
Hemipelagic clay
UNIT 2
Radiolarian mud
UNIT 3A
Radiolarian mud and ooze
UNIT 3B
Chert, siliceous claystone, and radiolarian mudstone
Siliceous Turbidites
Pleistocene
Lower to Middle Oligocene
Upper Eocene
Middle Eocene
Lower Eocene
Paleocene
Lower
UNIT 4
Marly chalk
UNIT 5
Red claystone
UNIT 6
Green-gray and black claystone
UNIT 7
Limestone
UNIT 8
Basalt
Maestr.
~Cenomanian
~Albian
Aptian
Barremian
Hauterivian
Valanginian
Berr.

greatest interest is the nature and extent of horizon A^V, the volcanoclastic turbidite.

Horizon A is actually four reflectors in one: A^V, A^T, A^C, and A^U. Horizon A^V is the uppermost reflector and is found within a 200 km radius of Bermuda (Figure 7-4). This unit correlates with the volcanoclastic turbidite of Site 386 and can be traced up to the base of the Bermuda Seamount where it blends into the pelagic apron. This is such a strong reflector that it masks many of the deeper reflections especially within 100 kilometers of Bermuda. Horizon A^T occurs about 0.15 to 0.20 seconds below A^V and about 0.05 to 0.20 seconds above Horizon A^C. Horizon A^T has not been found on the eastern Bermuda Rise, but is extensive to the west. Reflector A^T is a turbidite probably derived from the North American continent to the west and was prevented from traveling eastward by the uplift of the rise during the Eocene. Horizon A^C is the strongest reflector in the 'A' complex away from Bermuda and correlates with the lower to middle Eocene cherts recovered from many drill sites. This unit is widespread (Figure 7-4) and is attributed to very high productivity of siliceous microplankton during the early to middle Eocene. Perhaps more silica was being injected into the sea due to increased volcanism on Bermuda or in the Caribbean Arc. Horizon A^U is recorded only in the far western portions of the rise. This reflector records a regional unconformity possibly angular, at the Cretaceous-Tertiary boundary. Horizon A* is found along the east-central portion of the Bermuda Rise and continues further to the south. This reflector is locally discontinuous and regional correlation may not be meaningful. Nonetheless, this horizon has been correlated with the zeolitic claystones of DSDP Sites 386 and 9, making this

Figure 7-4. Areal distribution of the acoustic horizons in the northwestern Atlantic (from Tucholke et al., 1979).

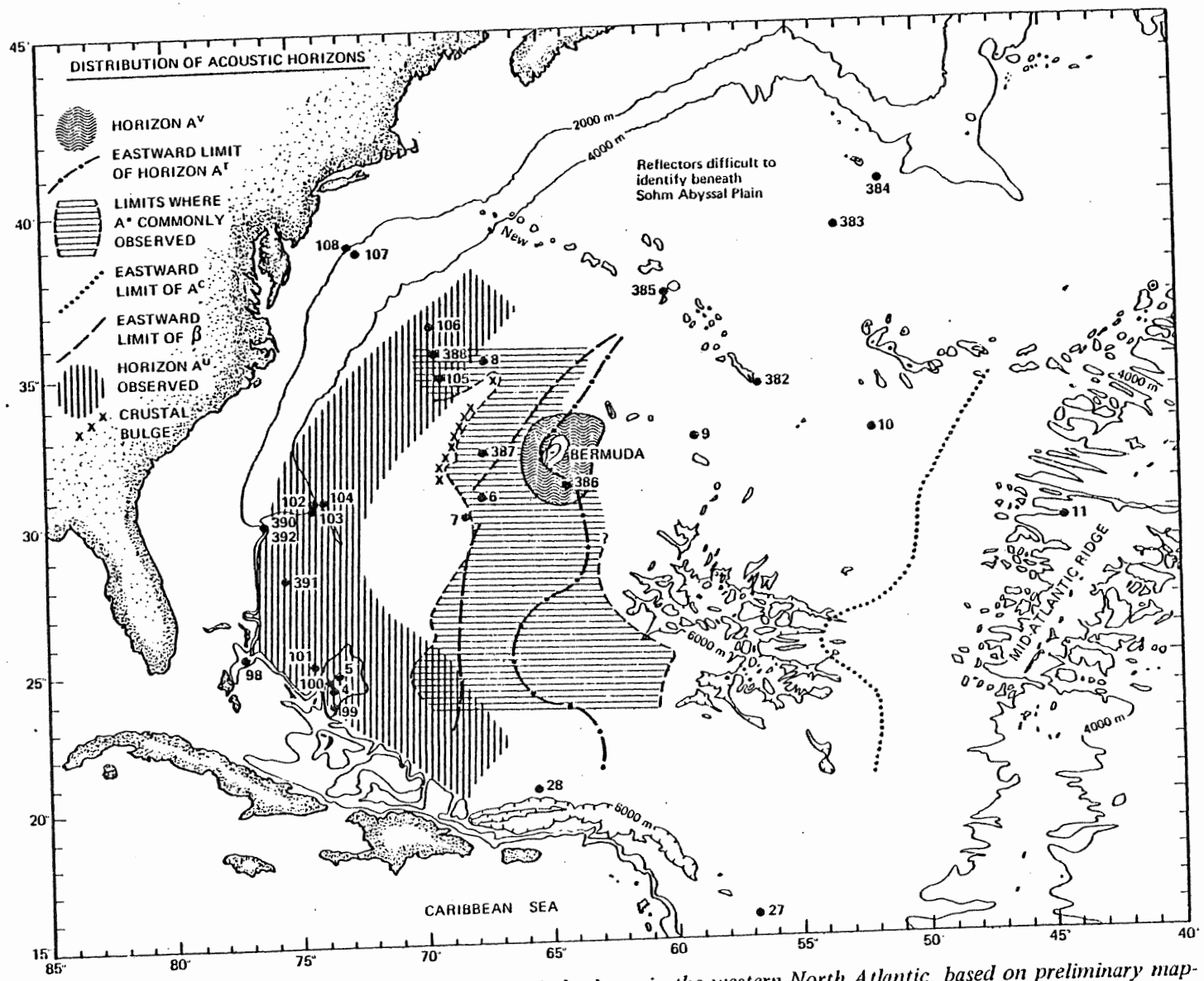

Approximate distribution of major acoustic horizons in the western North Atlantic, based on preliminary mapping from Lamont-Doherty seismic profiler records.

Figure 7-4a. Tracing of seismic reflection profile running west from Bermuda (Tucholke et al., 1979). Distance is marked in ship time. On this figure A* is shown as A^{o}.

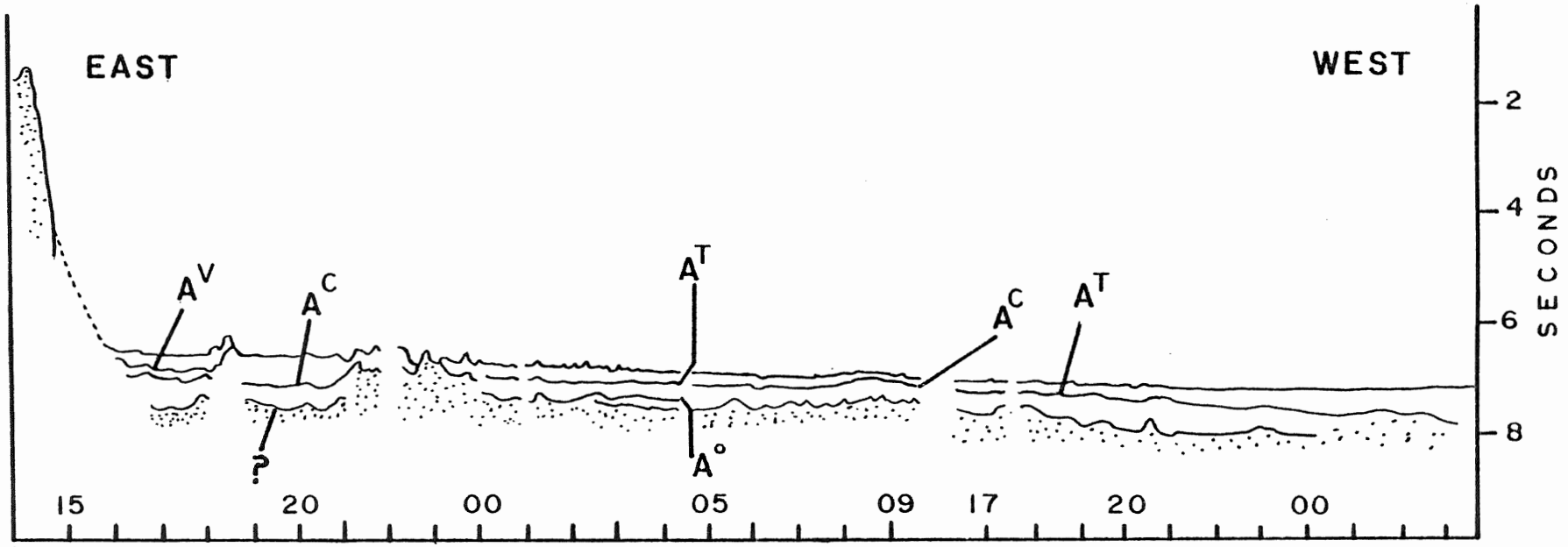
EAST
WEST
A^V
A^C
A^T
A^C
A^T
?
A^o
15
20
00
05
09
17
20
00
2
4
6
8
SECONDS

reflector a possible volcanogenic horizon of upper Cretaceous age. Alternately, the upper Maestrichian chalks could be the A* reflector. On a regional scale, this distinction cannot be made.

Horizon β marks the top of the sediments beneath Horizon A*. This horizon is limited to the northern and western parts of the rise. The reflector appears to be at the top of the Barremian to Hauterivian carbonates.

Horizon B is a very smooth reflector which often masks basaltic basement. It has a similar distribution to Horizon β. Its nature is unclear, but appears to be a limestone on the basaltic basement (Tucholke, 1979).

Bowles (1980) reported on a detailed study of the stratigraphy and sedimentation of a regional southeast of Bermuda. In this area, total sediment thickness varies considerably. Approximately 75 to 90 kilometers from Bermuda there is a 1 to 2 kilometer deep trough filled with sediments which are nearly six times thicker than sediments further out and closer in (Figure 7-5). He also saw that Horizon A^V is highly irregular and drapes over the basement with structures suggestive of either tectonic deformation or differential compaction. In this area, there is no evidence for a sediment source for the sub-A^V layers in the Bermuda Seamount region (these are not volcanogenic sediments). The thinness of these older sediments indicates that a slight topographic high was blocking sedimentation in the early Tertiary. In post-Oligocene time, the major acoustic horizon, A^V was deposited. The post-A^V sediments are derived predominantly from the surrounding seamounts and are products of Pleistocene sea-level changes, not renewed volcanism.

Figure 7-5. Schematic cross-section of the ocean crust to the southeast of Bermuda (Officer et al., 1952). Note the three basement troughs filled with sediments.

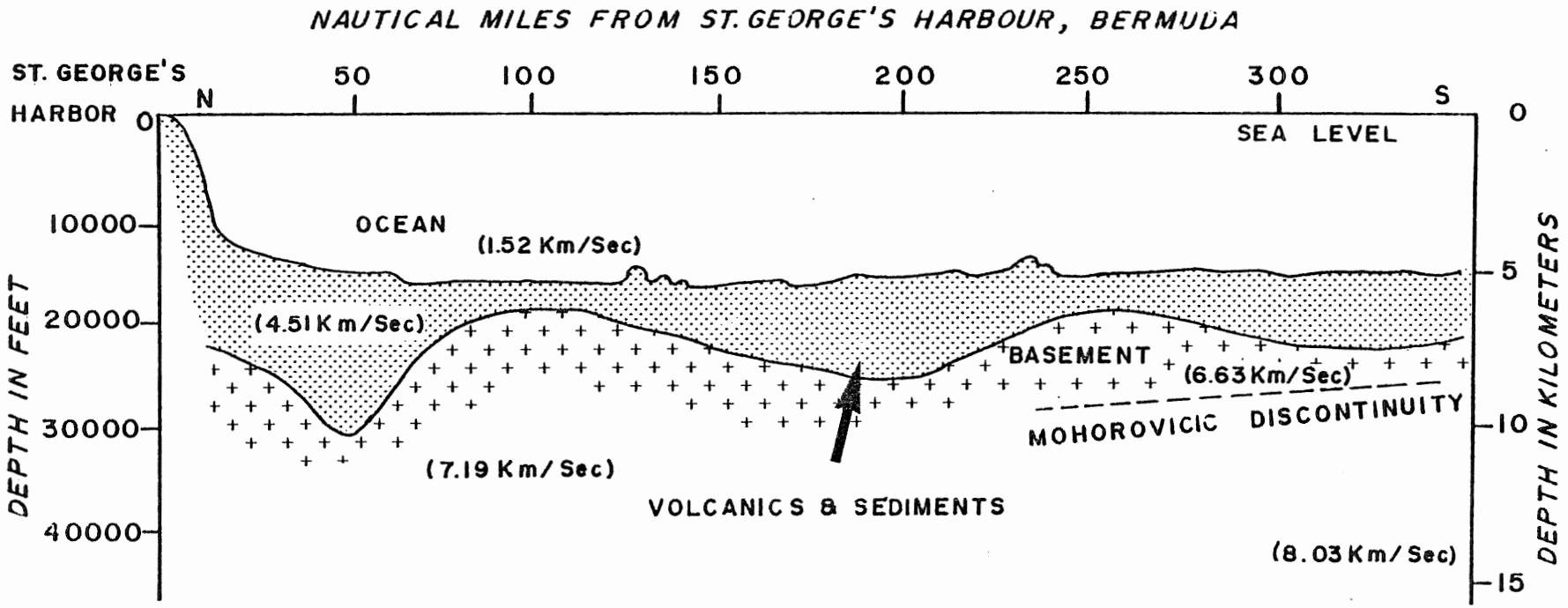
NAUTICAL MILES FROM ST. GEORGE'S HARBOUR, BERMUDA
ST. GEORGE'S HARBOR
N
50
100
150
200
250
300
S
0
SEA LEVEL
OCEAN
(1.52 Km/Sec)
(4.51 Km/Sec)
BASEMENT
(6.63 Km/Sec)
MOHOROVICIC DISCONTINUITY
(7.19 Km/Sec)
VOLCANICS & SEDIMENTS
(8.03 Km/Sec)
10000
20000
30000
40000
DEPTH IN FEET
5
10
15
DEPTH IN KILOMETERS

In summary, the sedimentation history begins with pelagic limestones being deposited on basaltic basement of early to middle Cretaceous age. Deposition during the middle to late Cretaceous is of continentally derived, eastward travelling turbidites. There is possibly some volcanogenic sediment input from the southwest or north during the earliest Tertiary. Formation (uplift) of the rise in the Eocene, makes a turbidite shadow zone to the east. Emplacement of Oligocene volcanoclastic turbidites is followed by continuous deposition into the Recent of pelagic sediments (Tucholke, 1979; Blair and Lane, 1980).

Geophysical Studies

Additional knowledge on the nature of the Bermuda Rise is derived from geophysical investigations. Seismic reflection profiles and magnetic surveys have yielded much valuable information on the shallower structures of the rise. Since the relation between the lithologic and acoustic stratigraphy was described earlier, the seismic reflection data will not be described here. The deep structures have been examined using several techniques; the most important tool being seismic refraction. Long wavelength gravity studies and geoid anomalies, as well as magnetotellurics have made valuable contributions to our knowledge of the rise.

The Bermuda Rise cuts across several marine magnetic anomaly trends. The central axis of the rise, along which the volcanic island is situated, acts as a division between the Keathley Sequence to the west and the Mercanton "smooth" zone to the east (Vogt and Einwich, 1979)

(Figure 7-6). The rise itself borders up against the magnetic smooth zone along anomaly M-25 to the west and merges into the Cretaceous quiet zone to the east. The Bermuda Seamount is situated along anomaly M-0.

Anomaly M-0 is unusual in its magnitude (500γ) and broad regional continuity; it represents a long geomagnetic epoch with reversed polarity in Cretaceous time (110-120 m.y.)(Vogt and Johnson, 1971). This anomaly coincides with the spatial boundary of a spreading rate change. The older crust was forming at 1.3 cm yr^{-1}, while after M-0 time the spreading rate became 2.4 cm yr^{-1}, nearly twice as fast (Vogt and Einwich, 1979). After this change, the magnetic anomalies become difficult to interpret. This change may relate to a major plate reorganization associated with the opening of the South Atlantic and a change in the relative velocities between Africa and North America (Vogt et al., 1971).

There are several important conclusions about the rise that can be derived from these studies. The linear magnetic anomalies older than M-0 can be traced across the Bermuda Rise without encountering any major discontinuities. To the east of the Bermuda Seamount, no trends are continuous. The rise cannot be made up of effusives related to the seamount since the linear magnetic anomalies are readily traceable across the rise and into other adjacent regions; unless these eruptives do not mask the deeper and older anomalies. There is no evidence of massive flows from DSDP Sites 386 and 387. Additionally, since Bermuda sits along the axis of spatial change (M-0), this zone may be a line of weakness along which the magmas which formed the

Figure 7-6. Magnetic anomalies in the northwestern Atlantic (Vogt and Einwich, 1979).

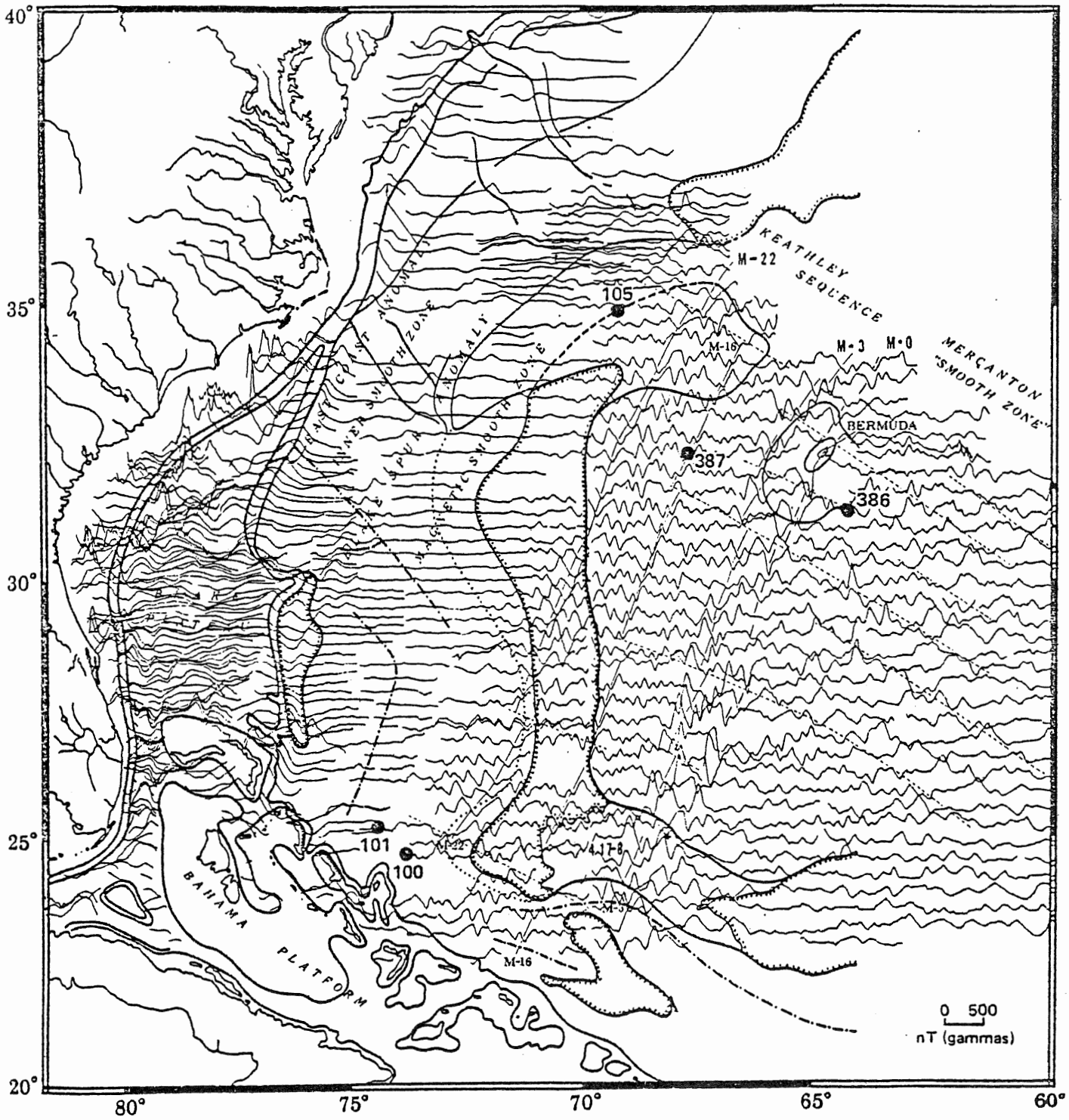

Magnetic anomalies in the southwestern North Atlantic

seamount rose. The local high intensity of magnetization along M-0 and the profound discontinuities across this zone indicate unusual spreading processes, about which, little is known. Very few high quality seismic refraction studies of the rise have been reported in the literature in recent years. Much of the data is old and collected with less sophisticated instruments (Officer et al., 1952; Officer, 1955; Katz and Ewing, 1956). Nonetheless, the data still are relevant to this study and can be used in compiling a regional crustal structure for the rise (Houtz, 1980; Rona, 1980). In this section a discussion of the regional deep structure will follow an overview of the seismic stratigraphy of the crust.

An average worldwide structure of the ocean crust consists of four layers: 2A, 2B, 2C, and 3 with respective velocities of 3.6, 5.1, 6.1, and 6.7 km sec^{-1} (Ewing and Houtz, 1979). The seismic structure for the Bermuda Rise is not clearly resolved, but three layers can be identified above the Moho (8.0 km sec^{-1}). These units are: unconsolidated sediments (layer 1) V = 1.83 km s^{-1} (30-85 meters thick), consolidated volcanics and sediments V = 4.5 km s^{-1} (0-4.9 kilometers) and basement V = 7.0 km s^{-1} (2 kilometers and up) (Officer et al., 1952). A very striking result from these studies is that the Moho discontinuity dips towards Bermuda and disappears from the records about 200 km from the seamount at depths below 15 kilometers.

Houtz (1980) has re-defined the sediments + volcanics layer (4.5 km s^{-1}) to be the upper interface of the acoustic basement. Rona (1980) however, has defined basement as having velocities greater than 5.6 km s^{-1}. These higher velocities are found only along the northern

flank of the rise, at the intersection with the New England Seamounts, and along the southern terminus of the rise. Nonetheless, the depth to basement averages seven kilometers over most of the rise (below sea-level), except at the seamount where volcanics are nearly above sea-level.

Houtz (1980) depicts the depth to the mantle as varying linearly across the rise with a depth of 10 kilometers to the east and nearly 12 kilometers to the west. This is, again, different from Rona's (1980) interpretation of an axial depression running parallel to the rise with depths of 10 kilometers along the extreme flanks dipping towards the center (i.e. dips into the seamount) to depths greater than 13 kilometers. It should be stressed that these determinations are based upon only a few data points. This limited data base does suggest crustal thickening beneath the rise.

Crustal thickening can be tested by an examination of the gravity field and topography of the rise. Early attempts to investigate the regional gravity field of the Bermuda Rise indicated a surface free-air anomaly of -20 mgal, which closely follows topography (Talwani and LePichon, 1969). Using empirical corrections for topography, much of the rise shows an absence of residuals, but the southeastern edge has a negative residual.

In the region of Bermuda, $1^{o} \times 1^{o}$ average free-air anomalies indicate that the seamount has a large positive anomaly (+80 mgal), while all but the eastern part of the rise follows close to the -20 mgal contour (Cochrane and Talwani, 1977, 1978). Haxby and Turcotte (1978) intrigued by this anomaly, examined the nature of the anomalous geoid

swell over the Bermuda Rise. They found that the rise has a larger anomaly than can be attributed only to crustal thickening with age. Their calculations suggest that the rise can be compensated by having anomalously low-density crust to the base of the lithosphere at nearly 100 kilometers.

Finally, the nature of the oceanic lithosphere on the rise has been examined using magnetotellurics. Poehls and Von Herzen (1976) interpret the data for the southern margin of the rise as indicating a rather conductive layer (10 Ω-m) down to about 100 kilometers with a more resistive layer below (90 Ω-m). Unfortunately, their data do not allow a finer division of conducting layers. In a more recent study, Cox (1980) and Cox et al. (1977) describe a conductivity profile with greater resolution (Figure 7-6). From a depth of about 10 to 70 kilometers, the resistivity is about 10 Ω-m, for the next 10 to 20 kilometers there is a marked decrease in resistivity to less than one Ω-m and this is followed by a profound rise to nearly 100 Ω-m which continues on to a great depth. These studies document a very conductive zone beneath the rise at a depth of about 100 kilometers which may represent a partially molten region.

It is interesting to compare this 100 kilometer deep anomaly with the shear velocity structure of the crust beneath the rise. In normal oceanic crust, shear wave velocities at 100 kilometers average about 4.3 km s^{-1} (Hart and Press, 1973). Weidner (1974) found that in the rise crust, there is an anomalously low shear velocity of 4.2 km s^{-1} from 100 to 140 kilometers depth. The shear velocities for magma chambers beneath the Mid-Atlantic Ridge are around 4.0 km s^{-1} from

100 to 300 kilometers depth. This shear velocity anomaly may not indicate a magma at depth but does reflect a zone of anomalous mantle.

Finally, some recent studies on the intraplate earthquakes occurring near the edge of the rise have indicated the presence of active movement. Kafka and Nishenko (1981) analyzed two events; one in 1976, the other in 1978. The 1976 event had an epicenter about 300 kilometers northeast of Bermuda and a focus at 10 kilometers. Fault-plane solutions suggest thrusting with a strike-slip component oriented at 320^{o}. This is subparallel to seamount trends in the area. The 1978 event had an epicenter 380 kilometers southwest of Bermuda and a focus at 6 kilometers. The fault-plane solutions indicate thrusting in a plane oriented at 340^{o} which is subparallel to the trend of a local steep magnetic gradient. Kafka and Nishenko (1981) interpret these data as indicative of stress release due to the continued uplift of the rise.

In summary, a variety of geophysical investigations indicate anomalous but consistent trends associated with the Bermuda Rise. The upper portions of the crust are magnetized in concordance with the northwestern Atlantic Ocean crust. The upper crust is of normal thickness, but has a trough surrounding the seamount. The Moho dips down towards the center of the rise to depths greater than 12 kilometers. This deep crust to lower lithospheric thickening is verified by long-wavelength gravity and geoid anomalies which indicate anomalous masses down to about 100 kilometers. Teleseismic and magnetotelluric studies show a zone with lower than normal shear velocities and high conductivity near 100 kilometers. All of these deep sounding studies suggest an anomalous zone at the base of the lithosphere beneath the rise, but

scant heat flow information does not indicate unusual thermal activity associated with the rise or the Bermuda Seamount (Hyndman et al., 1974; Sclater et al., 1976; Parsons and Sclater, 1977; Rona, 1980).

Assuming that Horizon A^V represents the eroded mass of the original Bermuda Volcano, the size of this volcano is estimated from the sediment volume. For this calculation, it is assumed that there is no net volume change between the original volcanic pile and the volcanoelastic sediments. The volume of the volcanoelastic sediments is calculated on the basis of the seismic data from Tucholke et al. (1979), and the shape of the sedimentary lens is approximated by a zone and segment of two bases of a sphere. The lower base has a radius of 100 km (re: figure 7-4)(average radius of horizon A^V around Bermuda) and the upper base has a radius of about 25 km (radius of the region of the Bermuda Islands above 100 meters below sea level, but excluding the southern seamounts). The thickness of the sediments at the base of the igneous platform is difficult to determine but does not appear to exceed 500 meters. The total volume of sediments is 8344 cubic kilometers.

The missing part of the volcano is reconstructed on the basis of a right circular cone with a radius of 25 kilometers. The necessary height to balance the volumes is 4.25 kilometers. This value is quite acceptable as a first order approximation since many oceanic islands have peaks at greater than 4 kilometers above sea-level.

CHAPTER 8

SUMMARY AND CONCLUSIONS

Summary

There are two types of igneous rocks collected from the igneous basement of Bermuda in 1980, submarine extrusives and related intrusives. The extrusives are thin non-vesiculated, pillowed, submarine lavas with intercalated breccias, probably flow or pillow breccias. The intrusives may form dikes or sills up to several meters thick, but more commonly form fine anastomosing sheets which intrude around pillowed margins or form complex, net-like bodies in the breccias. The larger dikes may be amygdaloidal.

Mineralogically, the extrusives and intrusives are very similar. A typical mineral assemblage for either lithology is: phenocrysts - clinopyroxene (titan-augite), spinel (Mg-Al titanomagnetite), and calcite plus chlorite pseudomorphs of olivine; groundmass - clinopyroxene (titan-augite), spinel (Mg-Al titanomagnetite), altered sphene (or perovskite), biotite (phlogopite-rich), altered melilite, altered olivine, apatite, and much altered glassy material. These rocks are very rich in calcite which occurs in the groundmass or in the numerous fine veins which cut across all of the samples. The intrusions have amygdules which are filled with calcite, and sometimes may include chlorite and dolomite. Petrographically, the lavas are altered glass-bearing melilite-nephelinites while the intrusives could be called melilite-bearing lamprophyres or nephelinites.

Chemically, the two rock types are similar with typical analyses being silica-poor and titanium-rich with high volatile contents. The

intrusives are slightly more silica-undersaturated than the extrusives so that on a silica versus total alkali plot, the extrusives plot as nephelinites while the intrusives fall within the melilite facies of the nephelinite field. The lavas are nepheline normative while the intrusives are hypersthene normative. Calcite-free normative mineralogies show few differences between the two rock types, thus the differences between the two lithologies may be due to variations in carbonate content.

Petrogenetic considerations suggest a related mode of origin for both rock types. A small degree of partial melting of carbonated and hydrated mantle at great depths (~100 km) yields a volatile rich, silica-undersaturated magma. This magma rises upwards and under near surface conditions crystallizes melilite. If the magma rises too quickly or the levels of CO_2 in the melt are too high, melilite will either not form in the former case, or break down to diopside and calcite in the latter. If the melt is held in a magma chamber prior to eruption, the intrusives may be derived from the volatile enriched residual magma.

Magnetically, both lithologies have similar properties. These rocks are not reliable carriers of a stable remanence. Many of the rocks have stable inclinations near to the present dipolar field inclination for Bermuda of $\pm 51^{o}$. Many of the rock samples may have been remagnetized by a drilling induced remanence.

The relationship of the rocks described in this thesis to the other known igneous rock samples from Bermuda is not clear. The 1980-hole rocks are most similar mineralogically and chemically to the 1912-hole rocks: melilite basalt and monchiquite. The lavas from Deep

Drill-1972 are distinctly different since they are richer in silica and are classified as altered tholeiites. Also, the 1972 lamprophyric sheets are different since many are plagioclase bearing, though the chemistry of these sheets is very similar to the chemistry of the 1980 rocks. The undersaturated rocks from these two drill-sites may be genetically related because plagioclase and melilite bearing rocks are closely related by slight changes in the concentrations of silica, alkalis, and volatiles.

The age of the 1980-hole extrusive rocks, based upon paleontological studies, is middle Tertiary. This age is roughly equivalent to the radiometric age for the 1972-hole sheets of about 30 Ma. The radiometric age of the 1972-hole lavas is approximately 100 Ma, very close to the age of the surrounding ocean crust.

The composition of the 1972-hole lavas is similar to the basalts collected at two recent DSDP sites on the Bermuda Rise. The sedimentary rocks from these same sites have recorded only one phase of Tertiary volcanism of possible Bermudian origin. There is some disputable evidence for a minor late Cretaceous volcanic event, but this event may be related to the formation of the crust at a mid-ocean ridge and not a separate volcanic episode associated with the formation of the Bermuda Islands.

The Bermuda Rise is a large section of anomalously uplifted oceanic crust and has a deep lithospheric root. Sedimentological patterns indicate that the rise did not exist until the Paleocene. Several problems relating to the rise remain, especially those relating to the origins of the rise and the Bermuda Islands. The following discussion centers on these topics: mid-plate volcanism and hot-spots,

similarities with other oceanic islands, and the synthesis of an evolutionary model for Bermuda.

Hot-Spots

There has been much recent interest in modelling the origin of oceanic islands and associated hot-spot swells on the basis of thermal perturbations of the lithosphere. Most of these studies are based on the hot-spot concept of Morgan (1972a, 1972b). The basic theory states that hot-spots (mid-plate volcanoes or volcanic chains) are situated over zones of 150 kilometers diameter of deep mantle convection with upwelling rates of about two meters per year. The movement of a lithospheric plate over these relatively immobile hot-spots gives rise to linear volcanic island or seamount chains. Often the volcanic chain is situated along the axis of a topographic swell which is also a product of the thermal upwelling.

Detrick and Crough (1978) found that the subsidence rate of hot-spot volcanoes in the Hawaiian chain are greater than predicted from simple cooling and thickening of the lithosphere after passing over a hot-spot. The subsidence can be modelled by having lithospheric thinning and uplift over the hot-spot and then rethickening with cooling; but only to the normal, pre-hot-spot thickness. Thus the sequence appears to be: heating and thinning over the thermal plume, cooling while moving off the plume, and a return to normal lithospheric thickness accompanied by isostatic sinking.

Crough (1978) further elaborated on the thermal nature of the hot-spot swells. He found that most swells, regardless of crustal age,

have a uniform depth of 4250 meters below sea-level. This corresponds to the depth for 25 million year old crust, and indicates that all swells should have similar thermal mechanisms or similar ages (Parsons and Sclater, 1977). Crough (1978) inverted the regional gravity gradient and width of the Bermuda Rise to calculate depth of compensation of about 100 kilometers. Unfortunately, his predicted subsidence for the assumed age of Bermuda of nearly one kilometer is unseen and does not match the observed subsidence for Pacific atolls. Either the Bermuda volcano is unlike those in the Pacific Ocean, or there has been recent volcanism on Bermuda.

Obviously, there is a difficulty in applying the hot-spot theory to the Bermuda region. There is no seamount chain, only the four peaks on the main seamount. Also the elongation of this seamount (NE-SW) is quite different from the New England Seamount trend (NW-SE) further to the north. It is unlikely that this hot-spot has recorded a 90^{o} shift in plate motion during the middle Tertiary; especially since the direction of change for Bermuda is 180^{o} opposite the change observed in the Corner Seamounts. It is doubtful that the Bermuda Seamount is related to the New England Seamounts since it is separated from them by a large distance (about 1200 km). However, the youngest seamount in the New England chain is about 80 million years old (Vogt and Tucholke, 1979; Crough, 1981) and the hot-spot may have trekked southeastwards, but with less frequent activity, thus leaving a gap.

Alkaline magmatism and volcanism have been associated with intraplate seismicity along weak crustal zones (Sykes, 1978). The location of the New England Seamounts may be controlled by a transform fault but

no transform faults have been identified near to Bermuda (Barrett and Keen, 1976). Perhaps Bermuda sits along a small section of an abandoned ridge-crest. Topographic features to the south and east of Bermuda, suggestive of mid-ocean rift valleys, have been described by Bowles (1980).

The occurrence of mid-plate volcanism may be a consequence of both lithospheric thickness and plate velocity. Gass et al. (1978) attempted to quantify the controlling parameters and derived a relationship which predicts that older or thicker crust, moving at high speeds will be the least likely to suffer from hot-spots. Vogt (1981) in opposing this theory, postulates that hot-spots form regardless of plate velocity or thickness. Hot-spots seem instead to group along the transition between geoid highs and lows (e.g. along zero-anomaly contours). Perhaps the geoid highs reflect mantle upwellings, while the lows reflect down-flow. Pollack et al. (1981) reiterated the theory of Gass et al. (1978) and expanded the model to a world-wide scale. Their mid-plate volcanism vulnerability parameter does not seem to yield a consistent relationship with hot-spot locations. Not one of these models indicates the Bermuda Rise as being susceptible to hot-spot magmatism.

Using the general conceptions of a hot-spot as a working model, Bermuda does not fit well. There are no zones of previous weakness clearly defined on the rise. The rise has had only one phase of volcanism in the Tertiary and possibly another in the late Cretaceous. In fact, the seamount and rise are probably derived from some single-stage process which until recently has not been identified in the ocean

basins. Before abandoning the hot-spot theory, a comparison with other oceanic islands more akin to hot-spots, and similar to Bermuda in their exposed lithologies is in order.

Oceanic Islands

The first association is to connect the evolution of the Bermuda Seamount with the Madeira, Canary, or Cape Verde Islands in the north-eastern Atlantic. These island groups are geometrically opposite from Bermuda to the east of the Mid-Atlantic Ridge and lie on oceanic crust of nearly the same age as the Bermuda Rise. The Madeira Archipelago is made up of three larger islands and about eight smaller islands situated about 700 kilometers from the coast of Africa. The Canary Islands lie about 100 kilometers northwest of Cape Juby, Morocco and are made up of seven islands. Some of these islands may lie on continental crust. Fifteen islands comprise the Cape Verde group, which lies 460 kilometers west of Cape Verde, Senegal. For the most part, the geological evolutions of the various islands were derived from the summary of Mitchell-Thomé (1976).

The evolution of the Madeira Islands follows very closely the general concept of oceanic island formation. The islands are situated to the east of anomaly M-0 in a region of thick Cretaceous sediments. Submarine volcanism began in the late Cretaceous. Volcanism has been more or less continuous from that time and the islands were emergent by the early Miocene (Mitchell-Thomé, 1976). Schmincke (1973) indicates that subaerial volcanism only started in the Miocene and continued until very recently. Typical eruptive lithologies range from basalt to

hawaiite, mugearite, and basanite as well as more siliceous trachytes and rhyolites.

The Canary Islands show a long period of tectonism and volcanism. The oldest units found are deformed Mesozoic (Cretaceous) sedimentary rocks on an altered tholeiitic basement (at least for the western islands). This 'basement' is overlain by a complex volcanic-plutonic series consisting of four basaltic series. A typical basaltic series ranges from olivine basalts to trachybasalts, with differentiates becoming more strongly alkaline in each successive series such that alkali-basalts and tephrites become common in the latter series (Mitchell-Thomé, 1976). Volcanism continues into the present.

K/Ar ages for Gran Canaria, Canary Islands, indicate several hiati during its evolution (McDougall and Schmincke, 1977). The subaerial development of the basaltic shield occurred between 13.7 and 13.5 million years ago with related alkalic and siliceous volcanism persisting until 9 million years ago. After a hiatus, basanitic units were erupted from 4.4 to 3.4 million years ago, followed after another shorter hiatus, by olivine nephelinites (2.0 m.yr. ago). Very silica-undersaturated magmas were formed about 10 million years after the initiation of the subaerial phase and make up a very small volume of the island (Schmincke, 1976).

A long hiatus between the basal lavas (series I) and the younger lavas (series II) is proposed by Storetvedt et al. (1979). They suggest, from paleomagnetic evidence, that the series I lavas formed near the Cretaceous-Tertiary boundary and that there is an unconformity of 50 million years between series I and II. This conclusion implies

that many of the earlier, whole-rock K/Ar ages are wrong.

The Cape Verde Islands are probably the most geologically unusual islands in the Atlantic Ocean. These islands lie on the relatively shallow (4000 m) Cape Verde Rise along anomaly M-0. The oldest igneous rocks are altered oceanic tholeiites (Klerxx and DePaepe, 1971) of Cretaceous age. A later, much more alkaline, volcanic phase started in the late Cretaceous (Mitchell-Thomé, 1976). This volcanism has continued into recent times and has been divided into four stages. Stage I consists of late Cretaceous to early Tertiary basalts to lamprophyric dikes and sills. Stage II is an early to middle Tertiary basaltic volcanism phase. Stage III began with late Tertiary alkali basalts but trends towards silica-undersaturated units with time (phonolites to tahitites, melilitites and ankaratrites). Stage IV started in the Quaternary and is now in the basaltic phase. Carbonatites are found on some of the islands.

The evolution of the Cape Verde Islands and Rise show many similarities to the Bermuda Seamount and Rise. A good picture of the regional development has been derived from Leg 41 of the Deep Sea Drilling Project. Volcanogenic sediments, which correspond with onland volcanism, have been documented (Figure 8-1). The area was a normal ocean basin from the late Jurassic to the early middle Cretaceous. Large volumes of turbidites were carried in from the east from the late Cretaceous to middle Miocene. The rise was formed in the Miocene and volcanism was more or less contemporaneous with uplift. A basaltic sill drilled on the rise has an age of about 19 million years corresponding to the time of uplift. Also at this time, turbidity currents were deflected away by the rise and sedimentation rates dropped.

Figure 8-1. Correlation of volcanism in the eastern North Atlantic with the islands off Africa (Lancelot and Seibold, 1978).

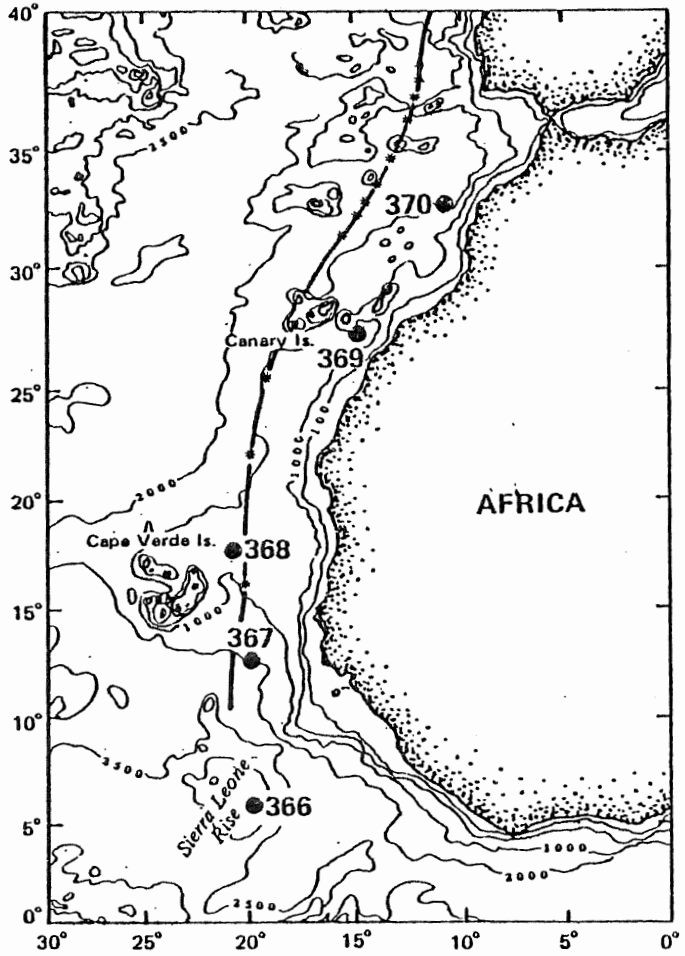

Location of Leg 41 drill sites.

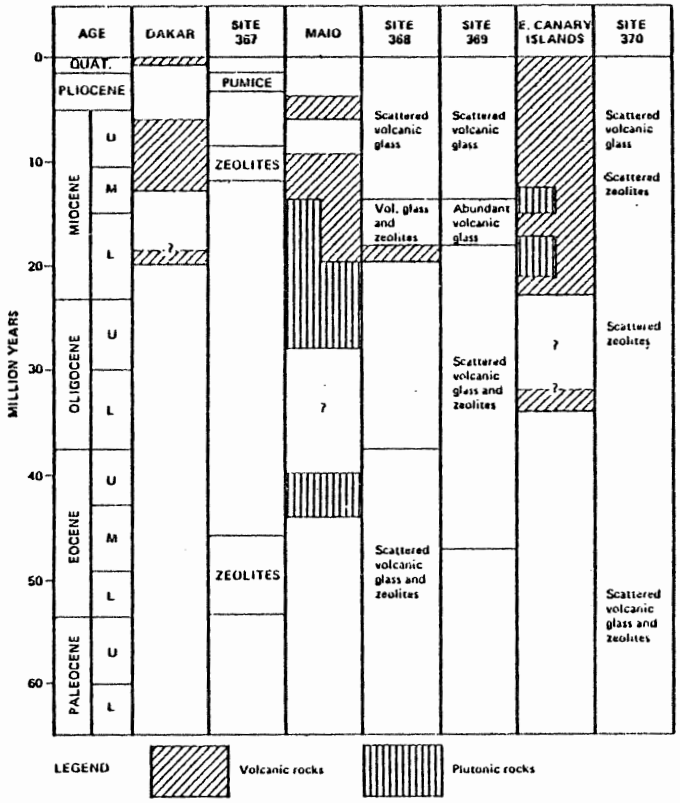

Summary of occurences of volcanic rocks and volcanogenic elements at and around Leg 41 drill sites.

Displaced and deformed blocks of deep-sea sediments are found on the islands (Lancelot and Seibold, 1978). The older (Cretaceous) tholeiites described by Paepe et al. (1971) may also be an uplifted block of old sea-floor. In fact, these islands may be the site of an abandoned Mesozoic ridge (Rona et al., 1970).

Conclusion

The rocks from the 1980-core are significantly different from the Deep Drill-1972 rocks in several respects. The newer samples consist of pillowed, melilite-bearing lavas and related instrusives, while the 1972-core mainly consists of submarine basaltic lavas.

Chemically the 1980-samples are deficient in SiO_2 and rich in TiO_2, alkali and volatiles. Their mineralogy is dominated by titanium-rich clinopyroxene and some magnesium-rich titanomagnetite phenocrysts. The groundmass consists of varying proportions of: clinopyroxene, titanomagnetite, melilite, biotite, some olivine, altered mesostasis or glass, and a variety of lesser minerals.

The magnetic properties of these rocks are difficult to interpret. There is no consistent stable inclination. The rocks have low MDFs (<100 Oe) and high Curie temperatures (~575^{o}C). The experimental results suggest that the magnesian-titanomagnetites do not carry the remanence but that magnetite is the primary holder of the natural magnetism. The occurrence of magnetite is not substantiated by petrographic and microchemical studies.

The occurrence of submarine, melilite-bearing lavas is very unusual, with these Bermudian rocks being the only known examples.

This study has not clarified the petrogenetic relationship of the Deep Drill-1972 basalts with the evolution of the Bermuda seamount and island. It is unlikely, but not impossible, that these two distinct lithologies are part of the same volcanic cycle.

The volcanic geology of Bermuda is complex. On the basis of this study it appears that silica-undersaturated rocks played an important role in the evolution of the Bermuda Islands. A more rigorous sampling of the volcanic basement is required to determine a more accurate volcanic stratigraphy for Bermuda.

The Model

On the basis of linear magnetic anomalies, the age of the oceanic crust surrounding the present-day Bermuda is about 100 to 110 Ma (anomaly M-0). This portion of the crust probably formed at the cretaceous mid-ocean ridge and had no anomalous characteristic. Immediately following this time the magnetic record becomes unclear. Either the geomagnetic was unsteady or the crust is highly tectonised.

Pelagic and continentally derived, eastward travelling turbidites were spread over what is now the Bermuda Rise in a continuous manner. In the earliest Tertiary, Paleocene to Eocene the Bermuda Rise began to form. As this section of oceanic crust was lifted up the turbidites flows were deflected and stopped from depositing material to the east of anomaly M-0. This uplift is of a thermal origin, but of an uncertain nature. By the Eocene the Bermuda Island was formed and volcanism may have continued to the Oligocene.

There are two possible origins for the volcanic island which take into account the known lithologies and the scant paleontological and radiometric age controls. Assuming that the basalts are about 100 Ma, the age of the surrounding oceanic crust, then it is possible that the basalts from the Deep Drill-1972 core are stoped blocks of oceanic crust. This mechanism, however, calls for an uplift of at least four kilometers for the basalts. This may be possible but seems to be geologically extravagant. The island was formed in the early to middle Tertiary and it is the lamprophyres and melilitites that are representative of the island building volcanics.

An alternate possibility is that the basalts are part of the early phase of seamount formation. This model works best by assuming that the basalts are closer to 50 than 100 Ma. The basalts were part of the shield building phase, as seen on many other oceanic islands. This phase of volcanism is not recorded in the surrounding sediments because it was subaqueous. As the seamount approached wave base the volcanism became more silica-undersaturated. This is commonly seen in the various volcanic cycles on other islands where each cycle becomes more alkaline and silica-poor (or silica-rich in some cases). The lavas near wave-base or subaerially extruded eroded to form the volcanoclastic turbidite (horizon A^V). Regardless of the model the volcanism appears to have ceased by the Oligocene.

REFERENCES

Akasaka, M. and I. Onuma. 1980. The join $CaMgSi_2O_6$-$CaFeAlSiO_6$-$CaTiAl_2O_6$ and its bearing on the Ti-rich fassaitic pyroxenes. Contrib. Mineral. Petrol., 13, 301-312.

Aumento, F., J.M. Ade-Hall and M.J. Keen. 1975. 1974 - The year of the Mid-Atlantic ridge. Rev. Geophy. Space Phys., 13, 53-65.

Aumento, F., W.S. Mitchell and M. Fratta. 1976. Interactions between sea water and oceanic Layer Two as a function of time and depth - I. Field evidence. Can. Mineral., 14, 269-290.

Aumento, F. and B. Gunn (un-published). Deep Drill-1972 Petrology and Geochemistry, 23 pp.

Bailey, D.K. 1976. Applications of experiments to alkaline rocks. In, Bailey, D.K. and R. MacDonald, eds., The Evolution of the Crystalline Rocks, Academic Press, N.Y., pp. 419-469.

Bailey, D.K. 1980. Volatile flux, geotherms, and the generation of the kimberlite-carbonatite-alkaline magma spectrum. Mineral. Mag., 43, 695-699.

Barrett, D.L., F. Aumento, J.M. Hall and R.D. Hyndman. 1973. Deep Drill 1972: Elastic properties of the rocks and the inferred oceanic crustal model, (abs.). Trans. Amer. Geophys. Un., 54, 486.

Barrett, D.L. and C.E. Keen. 1976. Mesozoic magnetic lineations, the magnetic quiet zone, and sea-floor spreading in the northwest Atlantic. Jour. Geophys. Res., 81, 4875-4884.

Blasse, G. 1964. Crystal chemistry and some magnetic properties of mixed metal oxides with spinel structures. Philips Res. Notes, 3, 139 pp.

Boettcher, A.L. and J.R. O'Neill. 1980. Stable isotope chemical, and petrographic studies of high-pressure amphiboles and micas: Evidence for metasomatism in the mantle source regions of alkali basalts and kimberlites. Amer. Jour. Sci., 280-A, 594-621.

Bowles, F.A. 1980. Stratigraphy and sedimentation of the archipelagic apron and adjoining area southeast of Bermuda. Mar. Geol., 37, 267-294.

Brey, G. 1978. Origin of olivine melilitites-chemical and experimental constraints. Jour. Volc. Geotherm. Res., 3, 61-88.

Cameron, M. and J.J. Papike. 1981. Structural and chemical variations in pyroxenes. Amer. Mineral., 66, 1-50.

Carlisle, D. 1963. Pillow breccias and their aquagene tuffs, Quadra Island, British Columbia. Jour. Geol., 71, 48-71.

Carmichael, I.S.E., F.J. Turner and J. Verhoogen. 1975. Igneous Petrology. McGraw-Hill, N.Y. 739 pp.

Chamley, H. 1979. North Atlantic clay sedimentation since the Late Jurassic. In, Talwani, M., W. Hay and W.B.F. Ryan, eds. Deep Drilling in the Atlantic Ocean: Continental Margins and Paleo-environment, Amer. Geophys. Un., 342-361.

Chayes, F. 1969. On the occurrence of corundum in the norms of the common volcanic rocks. Carn. Inst. Yr. Book, 68, pp. 179-182.

Cisowski, S.M. 1980. The relationship between the magnetic properties of terrestrial igneous rocks and their composition and internal structure of their component Fe-oxide grains. Geophys. Jour. Roy. Astr. Soc., 60, 107-122.

Cisowski, S.M. and M. Fuller. 1978. The effect of shock on the magnetism of terrestrial rocks. Jour. Geophys. Res., 83, 3441-3458.

Cochran, J.R. and M. Talwani. 1977. Free air gravity anomalies in the world's oceans and their relationship to residual elevation. Geophys. Jour. Roy. Astr. Soc., 50, 495-552.

Cochran, J.R. and M. Talwani. 1978. Gravity anomalies, regional elevation and the deep structures of the North Atlantic. Jour. Geophys. Res., 83, 4907-4924.

Cole, J.F. 1908. Magnetic declination and latitude observations in the Bermudas. Terr. Mag. Atm. Elec., 13, 49-56.

Cox, C. 1980. Electromagnetic Induction in the oceans and inferences on the constitution of the Earth. Geophys. Sur., 4, 137-156.

Cox, C.S., J.H. Filloux, D.I. Gough, J.C. Larsen, K.A. Poehls, R.P. Von Herzen and R. Winter. 1977. Atlantic lithospheric soundings. (abs.) Trans. Amer. Geophys. Un., 58, 734.

Crough, S.T. 1978. Thermal origin of mid-plate hot-spot swells. Geophys. Jour. Roy. Astr. Soc., 55, 451-470.

Crough, S.T. 1981. Mesozoic hotspot epeirogeny in eastern North America. Geology, 9, 2-6.

Day, R. 1977. TRM and its variation with grain size. Adv. Earth Planet. Sci., 1, 1-33.

Deer, W.A., R.A. Howie and J. Zussman. 1976. An Introduction to the Rock-Forming Minerals. Longman, London, 528 pp.

DePaepe, P., J. Klerxx, J. Hertogen and P. Plinke. 1974. Oceanic tholeiites on the Cape Verde Islands: Petrochemical and geochemical evidence. Earth Planet. Sci. Lett., 22, 347-354.

Detrick, R.S. and S.T. Crough. 1978. Island subsidence, hot spots, and lithospheric thinning. Jour. Geophys. Res., 83, 1236-1244.

Dewit, M.J. and C. Stern. 1978. Pillow Talk. Jour. Volc. Geotherm. Res., 4, 55-80.

Duda, A. and H.U. Schmincke. 1978. Quaternary basanites melilite nephelinites and tephrites from the Laacher Sea area (Germany). Neu. Jahr. Mineral. Abh., 132, 1-33.

Dunlop, D.J., J.A. Hanes and K.L. Buchan. 1973. Indices of multi-domain magnetic behaviour in basic igneous rocks: Alternating field demagnetization, hysteresis, and oxide petrology. Jour. Geophys. Res., 78, 1387-1393.

Edgar, A.D., D.H. Green and W.O. Hibberson. 1976. Experimental petrology of a highly potassic magma. Jour. Petrol., 17, 339-356.

Ewing, J. and R. Houtz. 1979. Acoustic stratigraphy and structure of the oceanic crust. In, Talwani, M., C.G. Harrison and D.E. Hayes, eds. Deep Drilling in the Atlantic Ocean: Ocean Crust, Amer. Geophys. Un., 1-14.

Furnes, H. and Fridleifsson. 1978. Relationship between the chemistry and axial dimensions of some shallow water pillow lavas of alkaline olivine basalt- and olivine tholeiitic composition. Bull. Volc., 41, 136-146.

Galehouse, J.S. 1979. Heavy mineralogy and provenance of volcanoclastic turbidites of site 386. In, Tucholke, B.E., P.R. Vogt et al. Initial Reports of the Deep Sea Drilling Project, v. 43, Washington, pp. 407-410.

Gass, I.G., D.S. Chapman, H.N. Pollack and R.S. Thorpe. 1978. Geological and geophysical parameters of mid-plate volcanism. Philos. Trans. Roy. Soc. Lon., Ser. A, 288, 581-597.

Gees, R.A. 1969. The age of the Bermuda seamount. Mar. Sed., 5, 56-57.

Gees, R.A. and F. Medioli. 1970. Continuous seismic survey of Bermuda, Part II, Harrington Sound. Mar. Sed. 6(3), 118-120.

Green, D.H. 1969. The origin of basaltic and nephelinitic magmas in the earth's mantle. Tectonophys. 7, 409-422.

Hall, J.M., W. Lowrie, N.D. Opdyke and F. Aumento. 1973. Deep Drill 1972: The paleomagnetism of a long succession of submarine lavas from Bermuda. Trans. Amer. Geophys. Un., 54, 486.

Hall, J.M., C. Walls and S.L. Hall. 1981. On inclined features in the Iceland Research Project drill-hole. Jour. Geophys. Res., in press.

Haggerty, S.E. 1976. Opaque mineral oxides in terrestrial igneous rocks. In, Rumble, D. III, ed., Oxide Minerals. Mineral. Soc. Amer. Short Course Notes, 3, Hg101-Hg300.

Hansen, K. 1980. Lamprophyres and carbonatitic lamprophyres related to rifting in the Labrador Sea. Lithos, 13, 145-152.

Haxby, W.F. and D.L. Turcotte. 1978. On isostatic geoid anomalies. Jour. Geophys. Res., 83, 5473-5478.

Hart, R.S. and F. Press. 1973. S_n velocities and the composition of the lithosphere in the regionalized Atlantic. Jour. Geophys. Res., 78, 407-411.

Houghton, R.L. 1979. Petrology and geochemistry of basaltic rocks recovered on Leg 43 of the Deep Sea Drilling Project. In, Tucholke, B.E., P.R. Vogt et al., Initial Reports of the Deep Sea Drilling Project, Volume XLIII, pp. 721-738.

Houghton, R.L., J.E. Thomas, jr., R.J. Diecchio and A. Tagliacozzo. 1979. Radiometric ages of basalts from DSDP Leg 43: Sites 382 and 385 (New England Seamounts), 384 (J-Anomaly), 386 and 387 (Central and western Bermuda Rise). In, Tucholke, B.E., P.R. Vogt et al., Initial Reports of the Deep Sea Drilling Project, v. 43, Washington, 739-754.

Houtz, R.E. 1980. Crustal structure of the North Atlantic on the basis of large-airgun-sonobuoy data. Geol. Soc. Amer. Bull., 91, 406-413.

Hyndman, D.W. 1972. Petrology of Igneous and Metamorphic Rocks. McGraw-Hill, N.Y., 533 pp.

Hyndman, R.D. and F. Aumento. 1973. Deep Drill 1972: Heat flow in Bermuda. Trans. Amer. Geophys. Un., 54, 486.

Hyndman, R.D., G.K. Muecke and F. Aumento. 1974. Heat flow and heat production in Bermuda. Can. Jour. Earth Sci., 11, 809-818.

Hyndman, R.D., N.I. Christensen and M.J. Drury. 1979. Seismic velocities, densities, electrical resistivities, porosities and thermal conductivities of core samples from boreholes into the islands of Bermuda and the Azores. In, Talwani, Harrison and Hayes, eds., Deep Drilling Results in the Atlantic Ocean: Ocean Crust. Amer. Geophys. Un. Ewing Series, 3, 94-112.

Irvine, T.N. and W.R.A. Baragar. 1971. A guide to the chemical classification of the common volcanic rocks. Can. Jour. Earth Sci., 8, 523-548.

Irving, E. 1964. Paleomagnetism and Its Application to Geological and Geophysical Problems. J. Wiley and Sons, N.Y., 399 pp.

Ivanov, I.P. and L.P. Gurevich. 1975. Experimental s study of T-X_{CO_2} boundaries of metamorphic zeolite facies. Contr. Mineral. Petrol., 53, 55-60.

Jansa, L.F., P. Enos, B.E. Tucholke, F.M. Gradstein and R.E. Sheridan. 1979. Mesozoic-Cenozoic sedimentary formations of the North American Basin: western North Atlantic. In, Talwani, M., W. Hay and W.B.F. Ryan, eds., Deep Drilling Results in the Atlantic Ocean: Continental Margins and Paleo-environment. Amer. Geophys. Un., 1-57.

Johnson, G.L. and P.R. Vogt. 1971. Morphology of the Bermuda Rise. Deep-Sea Res., 18, 605-617.

Jones, J.G. 1969. Pillow lavas as depth indicators. Amer. Jour. Sci., 267, 181-195.

Kafka, A.L. and S.P. Nishenko. 1981. Earthquake focal mechanisms and the intraplate setting of the Bermuda Rise. Trans. Amer. Geophys. Un. (EOS), 62, 324.

Katz, S. and M. Ewing. 1956. Seismic refraction measurements in the Atlantic Ocean, Part VII: Atlantic Ocean basin west of Bermuda. Geol. Soc. Amer. Bull., 67, 475-510.

Keen, C.E. 1979. Thermal history and subsidence of rifted continental margins - evidence from wells on the Nova Scotian and Labrador shelves. Can. Jour. Earth Sci., 16, 505-522.

Keller, F., jr., J. Meuschke and L. Alldredge. 1954. Aeromagnetic surveys in the Aleutian, Marshall, and Bermuda Islands. Trans. Am. Geoph. Un., 35, 558-572.

Klerxx, J. and P. Paepe. 1971. Cape Verde Islands: Evidence for a Mesozoic oceanic ridge. Nature Phys. Sci., 233, 117-118.

Kushiro, I. 1968. Compositions of magmas formed by partial zone melting in the earth's upper mantle. Jour. Geophys. Res., 73, 619-634.

Kushiro, I. 1972. Effect of water on the composition of magmas formed at high pressures. Jour. Petrol., 13, 311-334.

Lancelot, Y. and E. Seibold. 1978. The evolution of the central northeastern Atlantic - Summary of results of DSDP Leg 41. In, Lancelot, Y., E. Seibold et al., eds., Initial Reports of the Deep Sea Drilling Project, v. 41, Washington, pp. 1215-1245.

Land, L.S., F.T. Mackenzie and J.J. Gould. 1967. The Pleistocene history of Bermuda. Geol. Soc. Amer. Bull., 78, 993-1006.

LeBas, M.J. 1978. Nephelinite volcanism at plate interiors. Bull. Volc., 41, 459-462.

LeBas, M.J. 1978. Are olivine-poor nephelinites a primary melt product from the mantle? Bull. Volc., 41, 463-465.

Levi, S. and R.T. Merrill. 1978. Properties of single-domain, pseudo-single-domain and multidomain magnetite. Jour. Geophys. Res., 83, 309-324.

Lindsley, D.H. 1976. The crystal chemistry and structure of oxide minerals as exemplified by the Fe-Ti oxides. In, Rumble, D. III, ed., Oxide Minerals. Mineral. Soc. Amer. Short Course Notes, 3, L1-L52.

MacKay, R.M. 1981. Whole rock analysis using the electron microprobe. B.Sc. Thesis, Dalhousie University, Halifax, N.S.

Mapstone, N.B., A.P. Rood and N.C. Jackson. 1975. Underwater studies of recent lava flows around Sao Miguel (Azores). Geol. Mag., 112, 309-314.

McBirney, A.R. 1963. Factors governing the nature of submarine volcanism. Bull. Volc., 26, 455-469.

McDougall, I. and H.U. Schmincke. 1977. Geochronology of Gran Canaria, Canary Islands: Age of shield building volcanism and other magmatic phases. Bull. Volc., 40, 1-21.

McIver, J.R. and J. Ferguson. 1979. Kimberlitic, melilititic, trachytic, and carbonatite eruptives at Saltpetre Kop, Sutherland, South Africa. In, Boyd, F.R. and H.O.A. Meyer, eds., Kimberlites, Diatremes and Diamonds: Their Geology, Petrology, and Geochemistry. Proc. Sec. Int. Kimb. Conf., Amer. Geophys. Un., v. 1, pp. 111-128.

Mitchell-Thomé, R.C. 1976. Geology of the Middle Atlantic Islands. Beit. zur Region. Geol. der Erde, b. 12, Gerruder Borntaeger, Berlin, 382 pp.

Moore, J.G., R.L. Phillips, R.W. Griggs, D.W. Peterson and D.A. Swanson. 1973. Flow of lava into the sea, 1969-1971, Kilauea Volcano, Hawaii. Geol. Soc. Amer. Bull., 84, 537-546.

Morgan, W.J. 1972a. Plate motions and deep mantle convection. In, Shagam, R. et al., eds., Studies in Earth and Space Sciences. Geol. Soc. Amer. Mem., 132, pp. 7-22.

Morgan, J. 1972b. Deep mantle convection plumes and plate motion. Amer. Assoc. Pet. Geol. Bull., 56, 203-213.

Muan, A., J. Hauck and T. Lofall. 1972. Equilibrium studies with a bearing on lunar rocks. Proc. Third Lunar Sci. Conf., 1, 185-196.

Nixon, P.H. 1980. Kimberlites in the south-west Pacific. Nature, 287, 718-720.

Nixon, P.H., R.H. Mitchell and N.W. Rogers. 1980. Petrogenesis of alnöitic rocks from Malaita, Solomon Islands, Melanesia. Min. Mag., 43, 587-596.

Nockolds, S.R. 1954. Average composition of some igneous rocks. Geol. Soc. Amer. Bull., 66, 1007-1032.

O'Donovan, J.B. and W. O'Reilly. 1977. The preparation characterization and magnetic properties of synthetic analogues of some carriers of the paleomagnetic record. Adv. Earth. Planet. Sci., 1, 99-112.

Officer, C.B. 1955. Geologic interpretation of a series of seismic reflection profiles from Bermuda to the continental margins. Deep Sea Res., 2, 253-260.

Officer, C.B., M. Ewing and P.C. Wuenschel. 1952. Seismic refraction measurements in the Atlantic Ocean. Part IV: Bermuda, Bermuda Rise, and Nares Basin. Bull. Geol. Soc. Amer.

O'Hara, M. and G.M. Biggar. 1969. Diopside - spinel equilibria, anorthite and fosterite relationships in silica-poor liquids in the system $CaO-MgO-Al_2O_3-SiO_2$ at atmospheric pressure and their bearing on the genesis of melilitites and nephelinites. Amer. Jour. Sci., 267-A, 364-390.

O'Hara, M.J. and H.S. Yoder, jr. 1967. Formation and fractionation of basic magmas at high pressures. Scot. Jour. Geol., 3, 67-117.

Ozdimir, O. and W. O'Reilly. 1978. Magnetic properties of monodomain aluminum-substituted titanomagnetite. Phys. Earth Planet. Int., 16, 190-195.

Parsons, B. and J.G. Sclater. 1977. An analysis of the variation of ocean floor bathymetry and heat flow with age. Jour. Geophys. Res., 82, 805-827.

Petersen, N., U. Bleil and P. Eisenach. 1979. Rock- and paleo-magnetism of Leg 43 basalts. In, Tucholke, B.E., P.R. Vogt et al., Initial Reports of the Deep Sea Drilling Project, v. 43, Washington, pp. 773-780.

Pirsson, L.V. 1914. Geology of Bermuda Island: The igneous platform. Amer. Jour. Sci., 38, 189-206 and 331-334.

Poehls, K.A. and R.P. Von Herzen. 1976. Electrical resistivity structure beneath the Northwest Atlantic Ocean. Geophys. Jour. Roy. Astr. Soc., 47, 331-346.

Pollack, H.N., I.G. Gass, R.S. Thorpe and D.S. Chapman. 1981. On the vulnerability of lithospheric plates to mid-plate volcanism: Reply to comments by P.R. Vogt. Jour. Geophys. Res., 86, 961-966.

Press, F. and M. Ewing. 1952. Magnetic anomalies over oceanic structures. Trans. Amer. Geophys. Un., 33, 349-355.

Readman, P.W. and W. O'Reilly. 1971. The synthesis and inversion of non-stoichiometric titanomagnetites. Phys. Earth Planet. Int., 4, 121-128.

Reynolds, P.H. and F. Aumento. 1974. Deep Drill 1972. Potassium-argon dating of the Bermuda drill core. Can. J. Earth Sci., 11, 1269-1273.

Rice, P.D. 1977. The Bermuda Seamount: An investigation into the magnetic properties and the $^{40}Ar/^{39}Ar$ radiometric age of hydrothermally altered submarine flows. M.Sc. Thesis, Dalhousie University, 219 pp.

Rice, P.D., J.M. Hall and N.D. Opdyke. 1980. Deep Drill 1972: a paleomagnetic study of the Bermuda Seamount. Can. J. Earth Sci., 17, 232-243.

Robinson, P.T., M.F.J. Flower, D.A. Swanson and H. Staudigel. 1980. Lithology and eruptive stratigraphy of Cretaceous oceanic crust, western North Atlantic. In, Donnelly, T., J. Francheteau, W. Bryan, P. Robinson, M. Flower, M. Salisbury et al., Initial Reports of the Deep Sea Drilling Project, v. 51, 52, 53 part 2. Washington, pp. 1535-1556.

Rona, P.A. 1980. The Central North Atlantic Ocean - basin and continental margins. NOAA Atlas #3, 100 pp.

Rona, P.R., J. Brakl and J.R. Heirtzler. 1971. Magnetic anomalies in the Northeast Atlantic between the Canary and Cape Verde Islands. Jour. Geophys. Res., 75, 7412-7420.

Sahama, Th.G. 1976. Composition of clinopyroxene and melilite in the Nyiragongo rocks. Carn. Inst. Yr. Book 75, pp. 585-591.

Scientific Staff. 1979. Initial Reports of the Deep Sea Drilling Project, Leg. 43, Washington.

Schenk, P.E. 1973. Deep Drill 1972: Pleistocene stratigraphy. Trans. Amer. Un., 54, 486.

Schmincke, H-U. 1973. Magmatic evolution in the Canary, Madeira, and Azores Island groups. Geol. Soc. Amer. Bull., 84, 633-648.

Schmincke, H-U. and H. Staudigel. 1976. Pillow lavas on central and eastern Atlantic Islands (La Palma, Gran Canaria, Porto Santo, Santa Maria). Bull. Soc. Geol. Fr., 18, 871-883.

Sclater, J.G., L.A. Lawver and B. Parsons. 1975. Comparisons of long wavelength residual elevation and free air gravity anomalies in the North Atlantic and possible implications for the thickness of the lithospheric plate. Jour. Geophys. Res., 80, 1031-1052.

Sclater, J.G., J. Crowe and R.N. Anderson. 1976. On the reliability of oceanic heat flow averages. Jour. Geophys. Res., 81, 2993-3006.

Scott, B.H. 1979. Petrogenesis of kimberlites and associated lamprophyres from central west Greenland. In, Boyd, F.R. and H.O.A. Meyer, eds., Kimberlites, Diatremes and Diamonds: Their Geology, Petrology, and Chemistry. Proc. Sec. Int. Kimb. Conf., v. 1, Amer. Geophys. Un., pp. 190-205.

Stacey, F.D. and S.K. Banerjee. 1974. The Physical Principles of Rock Magnetism. Elsevier, Amsterdam, 195 pp.

Staudigel, H. and H. Schmincke. 1981. Effects of contrasting tectonic environments on the structure of the oceanic crust: The uplifted seamount of La Palma and DSDP/IPOD sites 417 and 418. (abs.) Amer. Geophys. Un. Chapman Conf. on The Generation of Oceanic Lithosphere, April, 1981.

Stephenson, A. 1972. Spontaneous magnetization curves and Curie points of spinels containing two types of magnetic ions. Phil. Mag., 25, 1213-1232.

Stoffel, H. 1971. The single-domain/multi-domain transition in intermediate titanomagnetites. Z. Geophys., 37, 451.

Streckeisen, A. 1979. Classification and nomenclature of volcanic rocks, carbonatites, and melilitic rocks: Recommendations and suggestions of the IUGS Subcommission on the Systematics of Igneous Rocks. Geology, 7, 331-335.

Storetvedt, K.M., H.M. Vage, S. Aase and R. Lovlie. 1979. Paleomagnetism and the early magmatic history of Fuerteventura (Canary Islands). Jour. Geophys., 46, 319-334.

Stuart, W.D. 1969. Interpretation of Bermuda Gravity Measurements in Terms of Pedestal Structure and Carbonate Stratigraphy. M.Sc. Thesis, Northwestern University, 65 pp.

Sykes, L.R. 1978. Intraplate seismicity, reactivation of preexisting zones of weakness, alkaline magnetism, and other tectonism postdating continental fragmentation. Rev. Geophys. and Space Phys., 16, 621-687.

Talwani, M. and X. LePichon. 1969. Gravity field over the Atlantic Ocean. In, P. Hart, ed., The Earth's Crust and Upper Mantle. Amer. Geophys. Un. Mon. 13, 341-351.

Thompson, A.B. 1971. PCO_2 in low-grade metamorphism: Zeolite, carbonate, clay mineral, prehnite relations in the system $CaO-Al_2O_3-SiO_2-CO_2-H_2O$. Contrib. Mineral. Petrol., 33, 145-161.

Tracy, R.J. and P. Robinson. 1977. Zoned titanian augite in alkali olivine basalt from Tahiti and the nature of titanium substitutions in augite. Amer. Mineral., 62, 634-645.

Tucholke, B.E. 1979. Relationships between acoustic stratigraphy and lithostratigraphy in the western North Atlantic basin. In, Tucholke, B.E., P.R. Vogt et al., eds., Initial Reports of the Deep Sea Drilling Project, 43, Washington, pp. 827-846.

Tucholke, B.E. and G.S. Mountain. 1979. Seismic stratigraphy, lithostratigraphy, and paleosedimentation patterns in the North American Basin. In, Talwani, M., W. Hay and W.B.F. Ryan, eds., Deep Drilling in the Atlantic Ocean: Continental Margins and Paleoenvironment. Amer. Geophys. Un., 58-86.

Tucholke, B.E. and P.R. Vogt. 1979. Western North Atlantic: Sedimentary evolution and aspects of tectonic history. In, Tucholke, B.E., P.R. Vogt et al., eds., Initial Reports of the Deep Sea Drilling Project, 43, Washington, pp. 791-826.

Vogt, P.R. 1981. On the applicability of thermal conduction models to mid-plate volcanism: Comments on a paper by Gass et al. Jour. Geophys. Res., 86, 950-960.

Vogt, P.R. and G.L. Johnson. 1971. Cretaceous sea-floor spreading in the western North Atlantic. Nature, 234, 22-25.

Vogt, P.R., C.M. Anderson and D.R. Bracey. 1971. Mesozoic magnetic anomalies, sea-floor spreading, and geomagnetic reversals in the southwestern North Atlantic. Jour. Geophys. Res., 76, 4796-4823.

Vogt, P.R. and Einwich, A.M. 1979. Magnetic anomalies and sea-floor spreading in the western North Atlantic, and a revised calibration of the Keathley (M) geomagnetic reversal chronology. In, Tucholke, B.E., P.R. Vogt et al., eds., Initial Reports of the Deep Sea Drilling Project, 43, Washington, pp. 857-876.

Vogt, P.R. and Tucholke, B.E. 1979. The New England Seamounts: Testing Origins. In, Tucholke, B.E., P.R. Vogt et al., eds., Initial Reports of the Deep Sea Drilling Project, Leg 43, pp. 847-856.

Wedepohl, K.H. 1981. Tholeiitic basalts from spreading ocean ridges: The growth of the oceanic crust. Nature, 68, 110-119.

Wedepohl, K.H. and Y. Muramatsu. 1979. The chemical composition of kimberlites compared with the average composition of three basaltic magma types. In, Boyd, F.R. and H.O.A. Meyer, eds., Kimberlites, Diatremes, and Diamonds: Their Geology, Petrology, and Chemistry. Proc. Sec. Int. Kimb. Conf., v. 1, Amer. Geophys. Un., pp. 300-312.

Weidner, D.J. 1974. Rayleigh wave phase velocities in the Atlantic Ocean. Geophys. Jour. Roy. Astr. Soc., 36, 105-140.

Williams, H. and A.R. McBirney. 1979. Volcanology. Freeman, Cooper and Co., San Francisco, 397 pp.

Windom, K.E. and A.L. Boettcher. 1980. Mantle metasomatism and the kimberlite-lamprophyre association: Evidence from an eclogite nodule from Roberts Victor Mine, South Africa. Jour. Geol., 88, 705-712.

Woollard, G.P. 1954. Crustal structure beneath oceanic islands. Proc. Roy. Soc. Lond., Ser. A, 222, 361-387.

Wones, D.R. and H.P. Eugster. 1965. Stability of biotite: Experimental, theory, application. Amer. Mineral., 50, 1228-1272.

Wyllie, P.J. 1979. Petrogenesis and physics of the earth. In, Yoder, H.S., jr., ed., The Evolution of the Igneous Rocks. Princeton Univ. Press, pp. 483-520.

Yagi, K. and K. Onuma. 1969. An experimental study on the role of titanium in alkalic basalts in the light of the system Diopside-Akermanite-Nepheline-$CaTiAl_2O_6$. Amer. Jour. Sci., 267, 509-549.

Yagi, K. and Onuma, K. 1978. Genesis and differentiation of nephelinitic magma. Bull. Volc., 41, 466-472.

Yoder, H.S., jr. 1970. Phlogopite-H_2O-CO_2: an example of the multi-component gas problem. Carn. Inst. Wash. Yr. Book 68, pp. 236-240.

Yoder, H.S., jr. 1973. Melilite stability and paragenesis. Fortschr. Mineral., 50, 140-173.

Yoder, H.S., jr. 1975. Relationship of melilite-bearing rocks to kimberlite: A preliminary report on the system Akermanite-CO_2. In, L.H. Ahrens et al., eds., Phys. Chem. Earth, 9, 883-893.

Yoder, H.S., jr. 1979. Melilite-bearing rocks and related lemprophyres. In, Yoder, H.S., ed., The Evolution of the Igneous Rocks. Princeton Univ. Press, pp. 391-412.

Young, G.A. and A.L. Kontis. 1964. A study of aeromagnetic component data: Plantagenet Bank. U.S. Nav. Ocean. Office Tech. Rept. TR-144, 18 pp.

APPENDIX I

Pictoral core logs of

the 1980 Drilling Project.

Visual Core Description

Depth Interval
(cm) ☐☐☐☐☐☐ to ☐☐☐☐☐☐

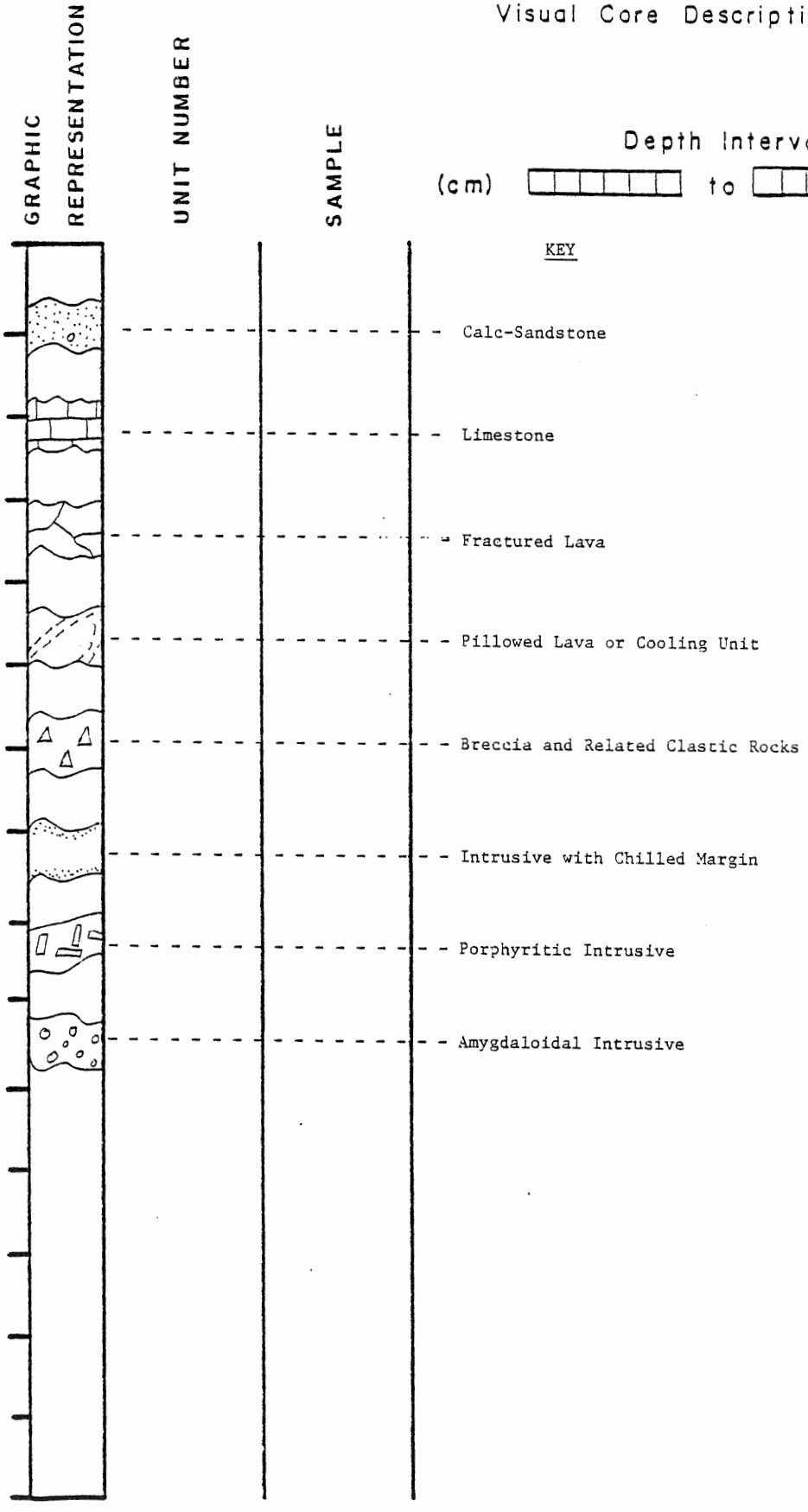

Visual Core Description

Hole #1
Box # 1

Depth Interval
(cm) 0 to 150

GRAPHIC REPRESENTATION | UNIT NUMBER | SAMPLE

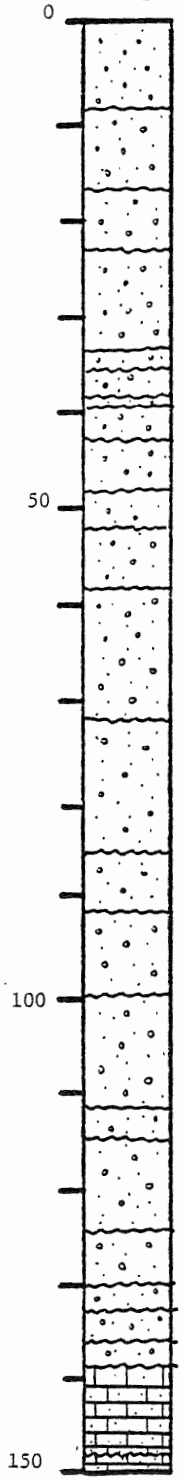

PETROGRAPHY

Sandy-porous pale-yellow to white carbonate rock with shell fragments. Poorly cemented. This unit is darker gray near the surface. There is a large variation in porosity down the hole.

Notes
130-139 cm dull orange color (Fe-stain)
139-150 cm chalky-white, well-cemented limestone

BERMUDA DRILLING PROJECT
1980

Visual Core Description

Hole #1
Box #1

Depth Interval
(cm) 150 to 300

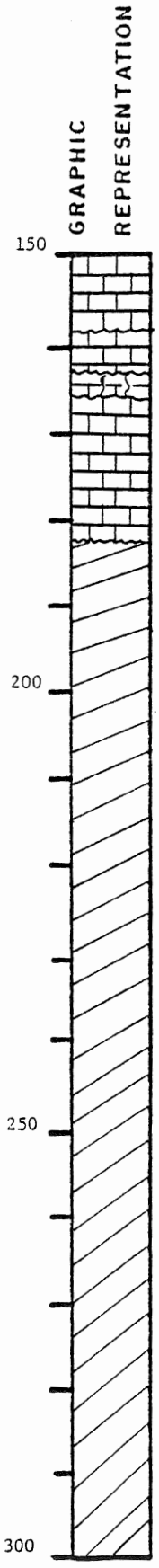

PETROGRAPHY
150-182 cm Chalky-white limestone.

NOTES
182-300 cm missing (small cave)

Visual Core Description

Hole #1
Box #1

Depth Interval
(cm) 300 to 450

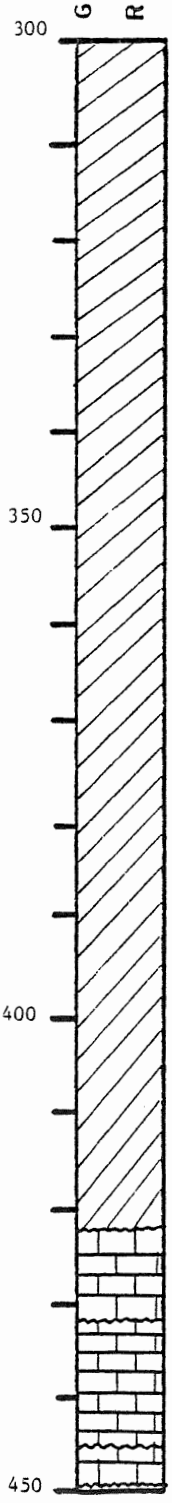

PETROGRAPHY
422-450 cm Well cemented, white limestone with rusty discoloration

NOTES
300-422 cm missing (cave)

BERMUDA DRILLING PROJECT
1980

Visual Core Description

Hole #1
Box #1

Depth Interval
(cm) 450 to 600

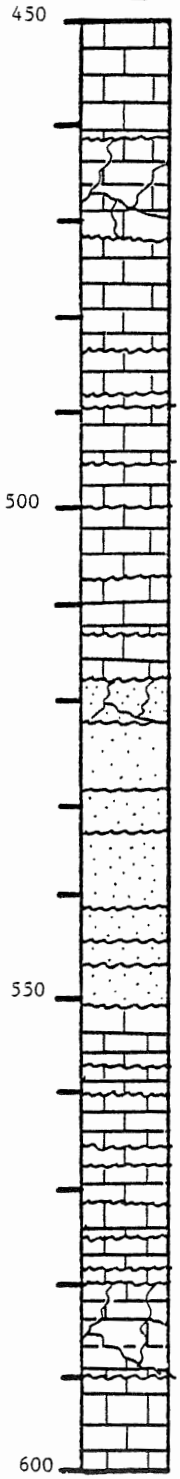

PETROGRAPHY

450-471 cm White limestone.
471-500 cm Limestone becomes grainier with rusty discoloration.
500-518 cm Degree of consolidation increases.
518-550 cm Rock becomes loosely consolidated, grainy and very rusty in color.
550-600 cm Rock becomes well consolidated, rust color continues with occasional large pores.

BERMUDA DRILLING PROJECT
1980

Visual Core Description

Hole #1
Box #1-#2

Depth Interval
(cm) 600 to 750

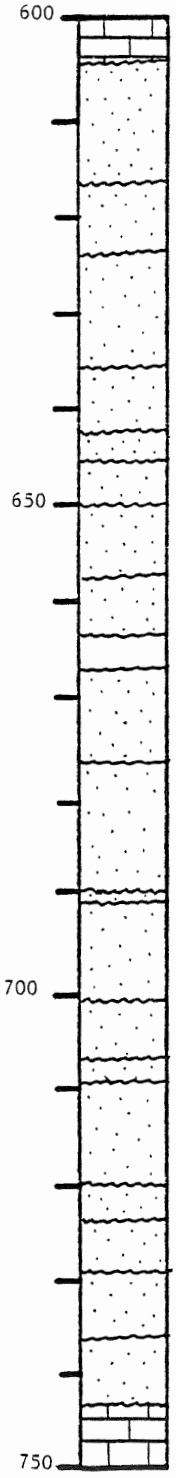

PETROGRAPHY
600-604 cm Limestone
604-750 cm White carbonate (grainstone) with patches of well consolidated and poorly consolidated material. More porous zones are more buff colored. Below 667cm the rock becomes more porous and poorly consolidated with rusty discolorations.

NOTES
664-667 cm missing
667-750 cm oil staining on core

Visual Core Description

Hole #1
Box #2

Depth Interval (cm) 750 to 900

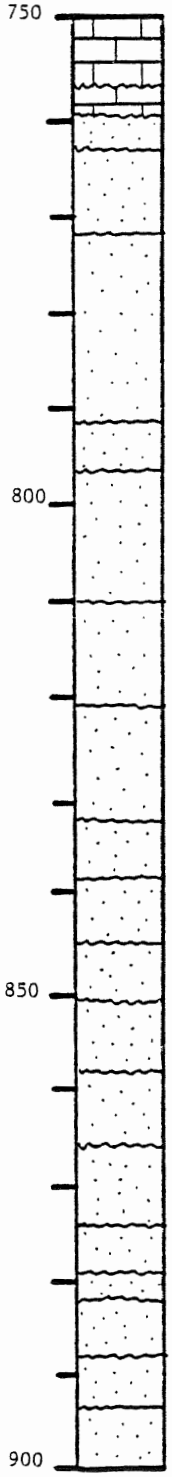

PETROGRAPHY

744-759cm Buff-coloroed limestone.

759-894cm Carbonate grainstone with low porosity, small grains, and poorly cemented. This unit is lightly banded with white and buff-colored zones.

894-900cm Carbonate becomes more porous and yellower, with open spaces (cm^3) filled with orange-brown material.

BERMUDA DRILLING PROJECT
1980

Visual Core Description

Hole #1
Box #2

GRAPHIC REPRESENTATION | UNIT NUMBER | SAMPLE

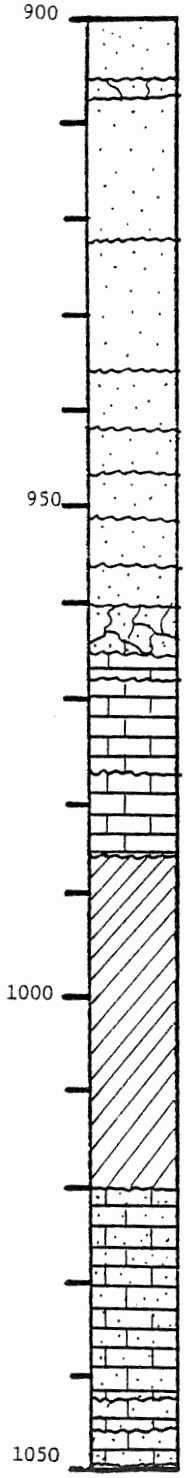

Depth Interval

(cm) 9100 to 10500

PETROGRAPHY

900-966cm Continuation of same unit from 894cm.
966-1050cm White well-cemented limestone becoming grainier down-hole.

NOTES

985-1020cm No core recovered.

BERMUDA DRILLING PROJECT
1980

Visual Core Description

Hole #1
Box #2

GRAPHIC REPRESENTATION | UNIT NUMBER | SAMPLE

Depth Interval (cm) 1050 to 1200

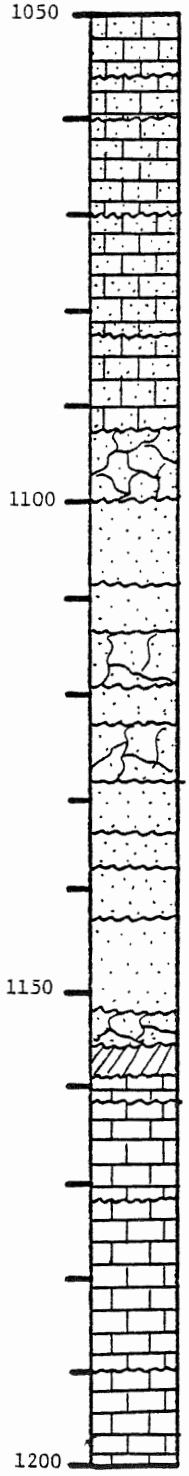

PETROGRAPHY

966-1155cm Continuation of same unit with a gradual increase in porosity and Fe-staining down the hole.

1159-1200cm White, well-consolidated and less porous limestone with marginal Fe-staining.

NOTES

1155cm Mistake in original drill-site log. After this point many sections are missing (not recovered), misoriented, etc.. Occasional gaps occur, probably not in actual place of occurrence, but at point where depth is determined directly from drill string. Thirty cm missing in final tally, proper measuring readjusted by 1680cm.

BERMUDA DRILLING PROJECT
1980

Visual Core Description

Hole #1
Box #2-#3

Depth Interval
(cm) 1200 to 1350

GRAPHIC REPRESENTATION | UNIT NUMBER | SAMPLE

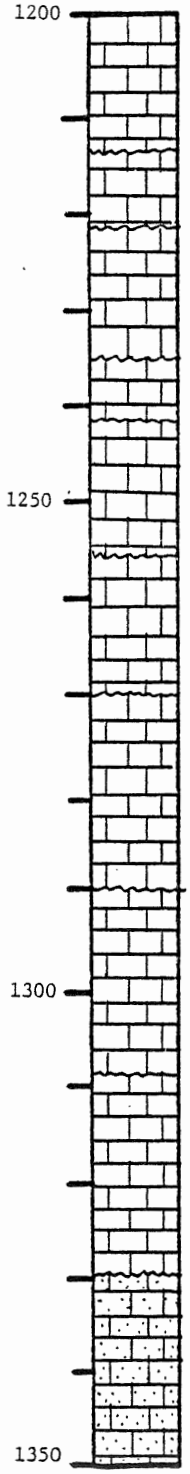

PETROGRAPHY

1159-1329cm Continuation of the same white, well-cemented, grainy limestone with occasional zones of a buff color.

1329-1350cm Limestone becomes more porous and darker (gray to pale-buff) with scattered buff patches.

NOTES

1214cm Box #2 ends, Box #3 begins.
1309cm Break in fiducal line, rotated 10°.

Visual Core Description

Hole #1
Box #3

Depth Interval
(cm) 113501 to 115001

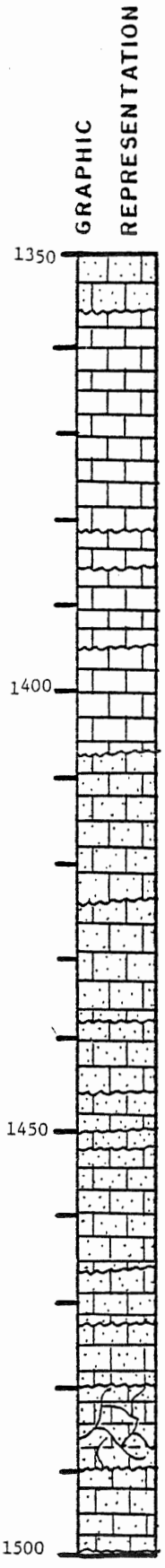

PETROGRAPHY

1329-1381cm Continuation of same unit.
1381-1407cm Light yellow limestone, well-cemented with occasional rusty zones and large cavities (2-3cm) filled with blue clay and secondary carbonate minerals.
1407-1500cm Limestone becomes more porous and poorly cemented, as well as grainier.

NOTES

1452cm Open spaces with much rusty weathering.

BERMUDA DRILLING PROJECT
1980

Visual Core Description

Hole #1
Box #3

Depth Interval
(cm) 1500 to 1650

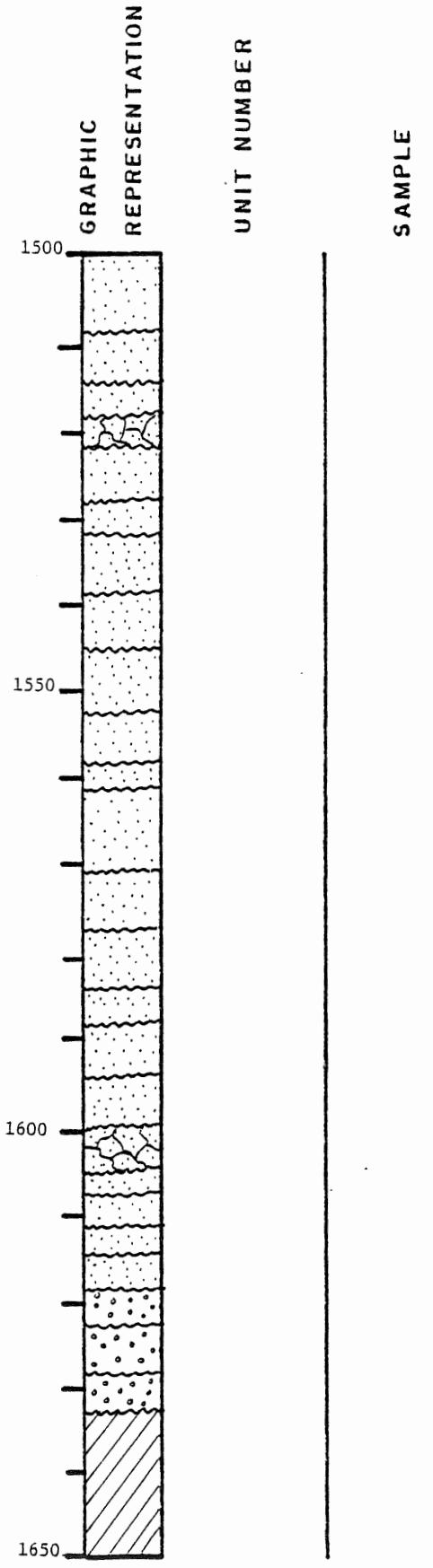

PETROGRAPHY

1500-1618cm White calcareous *lime*stone

1618-1634cm Grain size increases (0.0-2.0mm) with addition of shell fragments. This unit is very porous.

NOTES

1545cm Break in orientation of 10°.
1634cm Discrepencies in numbering now accounted for.
1634-1650cm No core recovered.

BERMUDA DRILLING PROJECT
1980

Visual Core Description

Hole #1
Box #3

Depth Interval
(cm) 11650 to 11800

GRAPHIC REPRESENTATION | UNIT NUMBER | SAMPLE

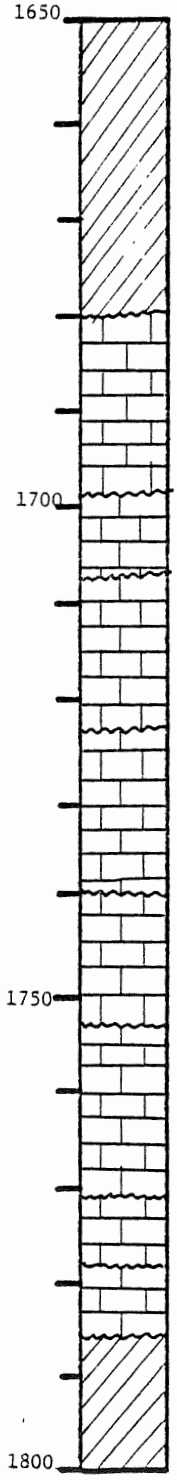

PETROGRAPHY
1680-1785cm Well cemented, pale yellow-limestone with occasional cavities (1-2cm^2).

NOTES
1755cm Rock acquires a chalky hue which intensifies with depth.
1780cm Blue clay (marine?) on core here.
1785-3000cm No core, large cave encountered.

1800-3300cm No core descriptions because there is no core for this interval.

BERMUDA DRILLING PROJECT
1980

Visual Core Description

Hole #1
Box #3-#4

Depth Interval
(cm) 3310 to 3450

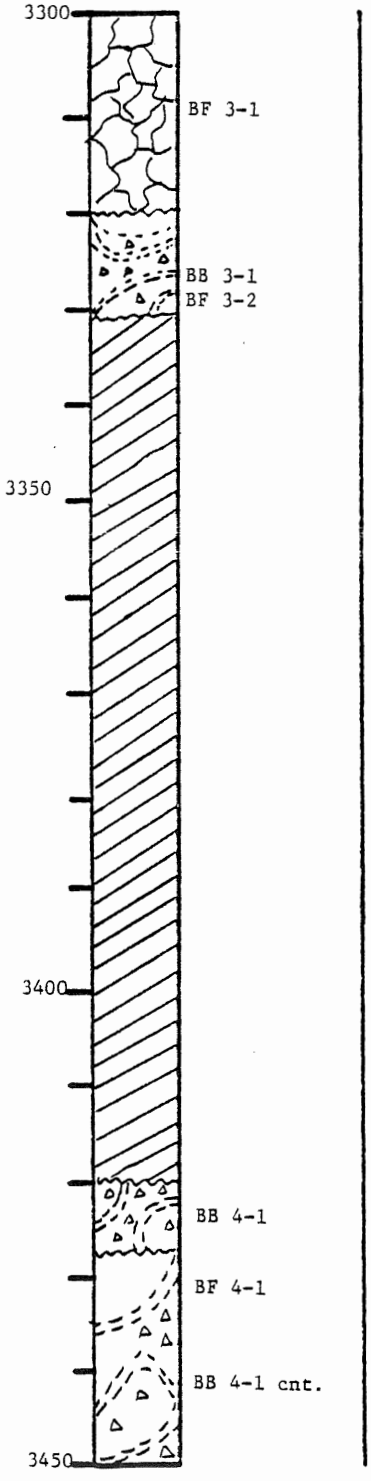

PETROGRAPHY

3300-3320cm Well-weathered light-gray to reddish-brown volcanic rock-pebbles(?) with brown mud.

3320-3333cm Dark-gray pillowed volcanic flow with some glassy sections with inter-pillow light blue limey mud. Flow is fractured with calcite filling the open spaces. Some pieces of glass are totally supported in the mudstone.

3420-3450cm Brecciated flow with lightblue to white fracture filling material (carbonate + quartz). The breccia is made up of glassy to chloritized angular fragments in a carbonate matrix with variable amounts of cementation.

NOTES

3333cm Box #3 ends.
3333-3420cm No core recovered.
3420 cm Box #4 begins.

BERMUDA DRILLING PROJECT
1980

Visual Core Description

Hole #1
Box #4

Depth Interval
(cm) 13450 to 13600

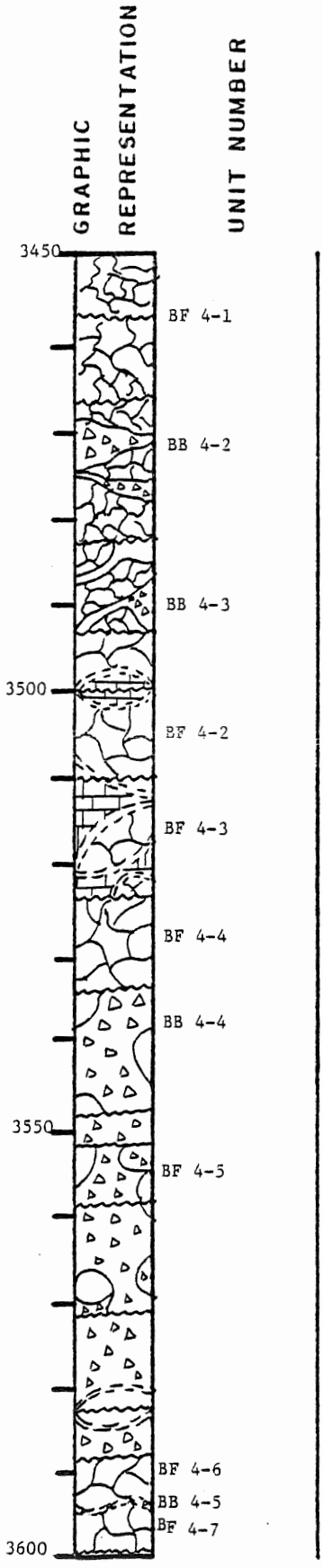

PETROGRAPHY

Flow material is dark gray (looks like basaslt) with microamygdules (0.1mm) and calcite filled veins.

Breccia is made up of angular to sub-rounded clasts of the flow material. Clast size ranges from mm^2 to cm^2.

NOTES

3485-3492cm Hematite-filled veins common.
3500cm Pillows with sediments and breccia along pillow rim.
3583cm Hematite and limonite staining.
3586cm Extremely fine-grained breccia with light gray matrix, one small area is grainy to sandy.

General- Pillows are zoned with cores of gray flow unit, shell of hematite enrichment, and an outer shell of chlorite which is pervasively fractured. The inter-pillow sediment appears to be a calcareous-mudstone to biomicrite.

Visual Core Description

Hole #1
Box #4

Depth Interval
(cm) 3600 to 3750

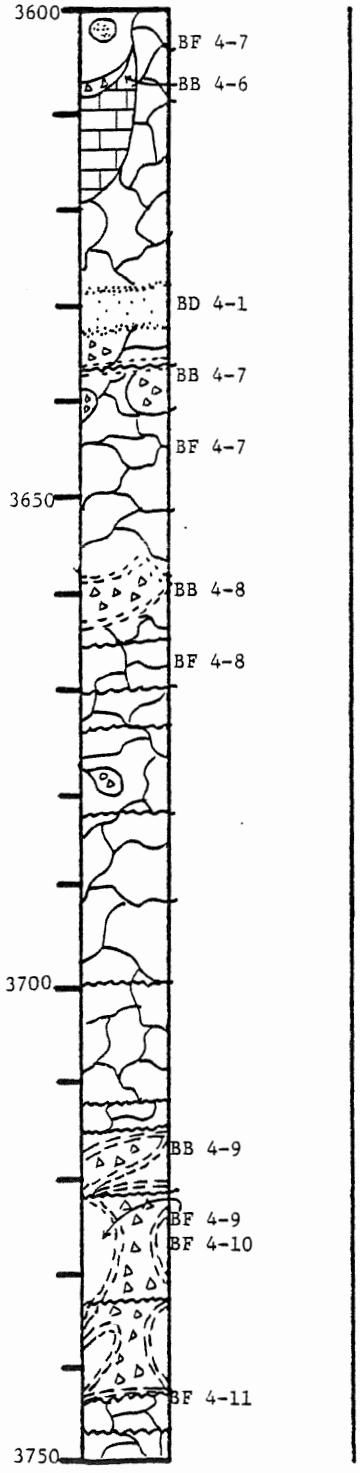

PETROGRAPHY

Blue gray flow material, very fractured with calcite filled veins (up to 5mm thick).

Breccia of flow material.

Dike- dark gray to black with distinct chill margins. This unit is amygdaloidal with some porphyritic zones (pyroxene phenocrysts) in the core. Calcite veins (0.05mm wide) parallel the contact, with some dikes cutting the dike also.

NOTES

3602cm- Reddish brown granular material, possibly volcanogenic sand.
3610cm Interpillow blueish-limestone.
3630cm First dike in section.

Visual Core Description

Hole #1
Box #4

Depth Interval
(cm) 3750 to 3900

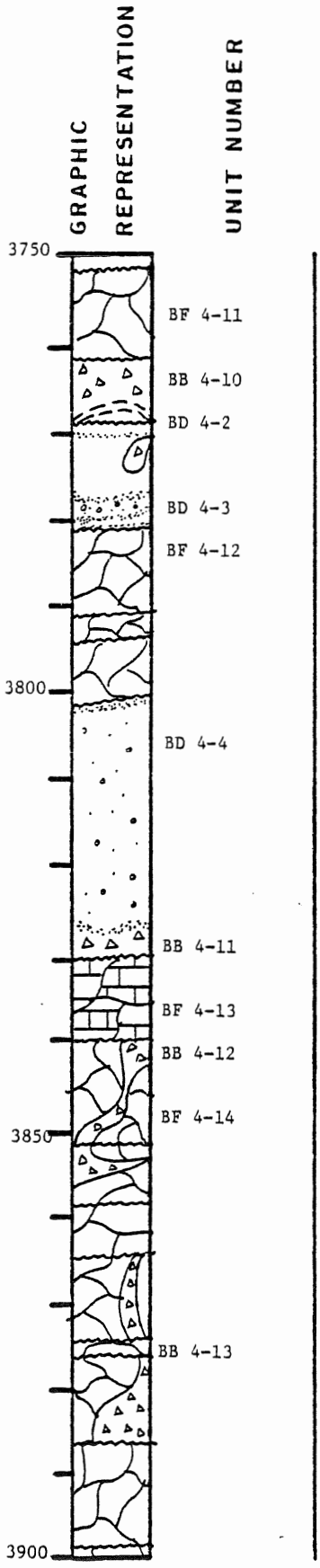

PETROGRAPHY
Flow- dark blue-gray, well fractured with calcite filled veins.

Dike-dark gray to black, microphenoctystic.

NOTES
3762cm Calcite+limonite vein.
3780cm Three chill margins on dike.
3900cm Rotate orientation line 45°.
The breccia rests in a blue, carbonate cement.

BERMUDA DRILLING PROJECT
1980

Visual Core Description
Hole #1
Box #4-#5

Depth Interval
(cm) 3900 to 4050

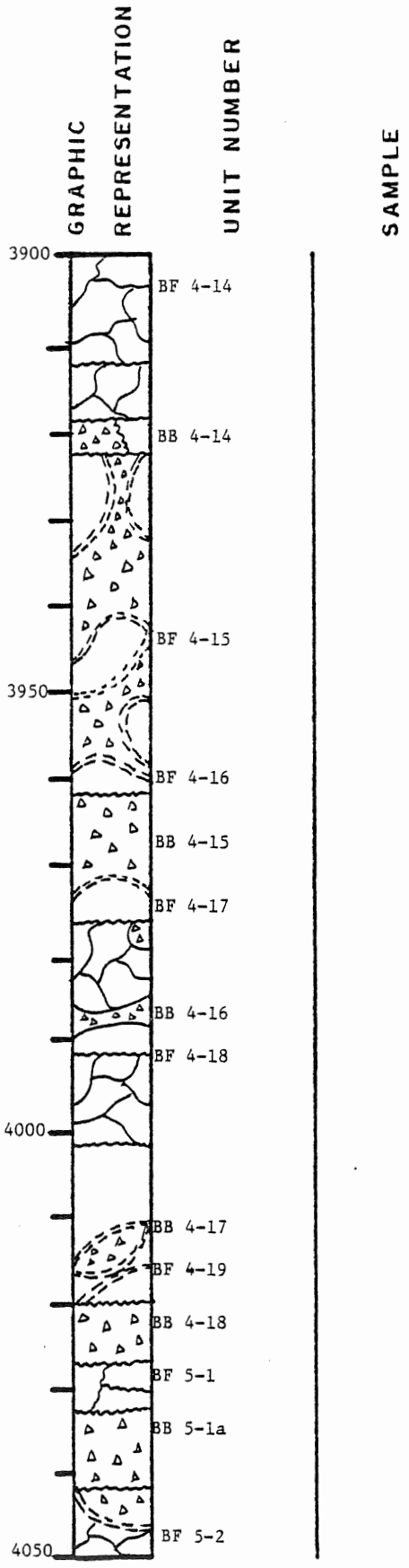

PETROGRAPHY
Flow-blue-gray flow with numerous small pillows. Breccia- fractured flow material and pillows, altered to a dark-green color with a white carbonate matrix.

NOTES
4026cm Box #4 ends, #5 begins.
4045cm Hematite enriched zone along pillow margin.

BERMUDA DRILLING PROJECT
1980

Visual Core Description

Hole #1
Box #5

Depth Interval
(cm) 4050 to 4200

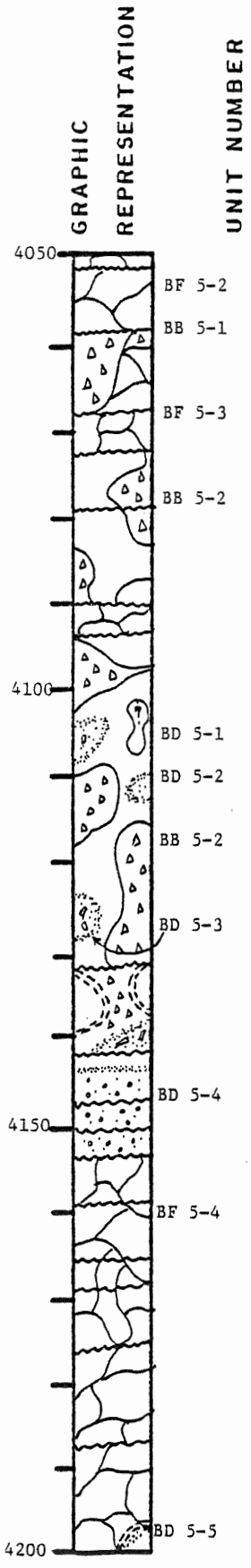

PETROGRAPHY
Flow-blue-gray, very fractured with pillows in top of section, more massive towards the base.

Dike- Black, very fine-inticate intrusions in the breccia. Dike BD5-4 is brownish-green and seems to be very altered.

NOTES
4088cm Siliceous secondary mineral pocket
4105cm Zoned, white colored, siliceous minerals (mainly quartz + calcite) with limonite along margin.
4120cm Occasional small dikes.
4198cm Hematite along pillow margin.

BERMUDA DRILLING PROJECT
1980

Visual Core Description

Hole #1
Box #5

Depth Interval
(cm) 4200 to 4350

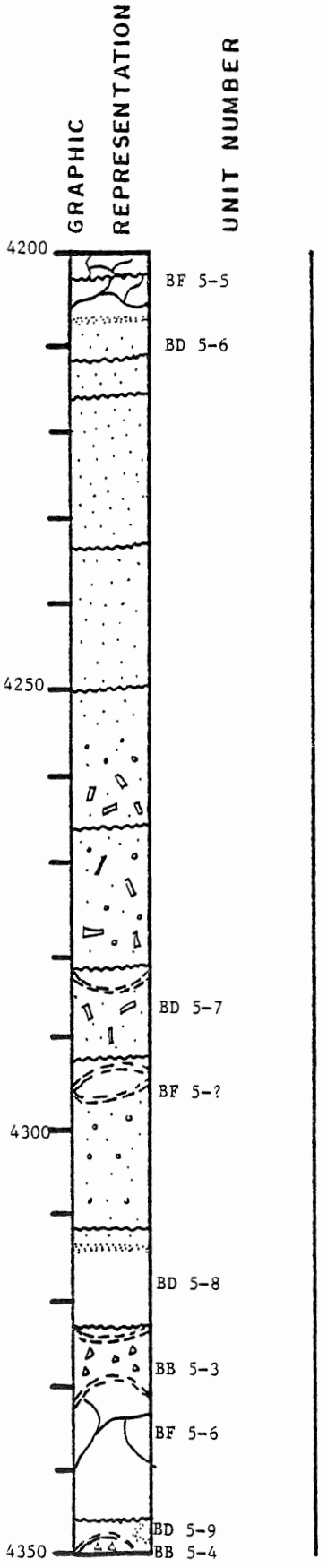

PETROGRAPHY
Dike-dark-gray to black, porphyritic in the core becoming aphanitic near the chilled margins. Phenocrysts are of pyroxene and biotite (rare).

Flow-blue-gray and slightly fractured.

NOTES
4208cm Dike contact not pronounced, very aphanitic.
4275cm Fractured dike with biotite phenocrysts.
4292cm Possile pillowed flow.

BERMUDA DRILLING PROJECT
1980

Visual Core Description

Hole #1
Box #5

Depth Interval
(cm) 43|50 to 45|00

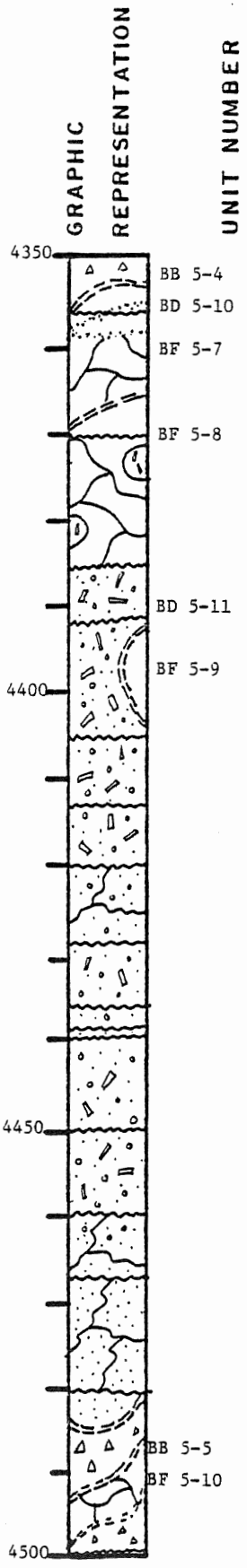

PETROGRAPHY

Flow- small blue-gray flows, very fractured with many pillows and related breccias.

Dike-dark gray to black with phenocrysts of pyroxene and rarely biotite.

NOTES

4386cm Possible glass inclusions.
4395cm Fractured dike rock (pyroxene cumulate ?)
4460-4480cm Very friable dike rock.

BERMUDA DRILLING PROJECT
1980

Visual Core Description

Hole #1
Box #5

Depth Interval
(cm) 4500 to 4650

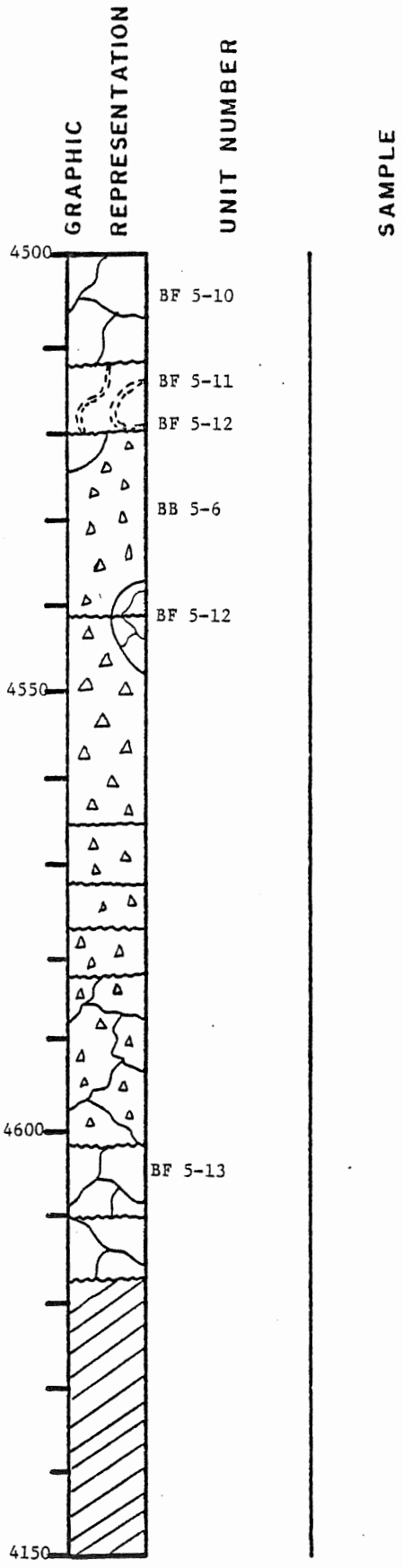

PETROGRAPHY
Flow-blue gray with pillows.

Breccia- extensive breccia of flow material with carbonate cement. Clasts have varying degrees of alteration.

NOTES
4518cm Corroded pillow.
4565cm Very punky breccia.
4580-4600cm Possibly some dike rock here.
4617cm Box #5 ends.
4617-4150cm No core recovery.

BERMUDA DRILLING PROJECT
1980

Visual Core Description

Hole #1
Box #6

Depth Interval
(cm) 4650 to 4800

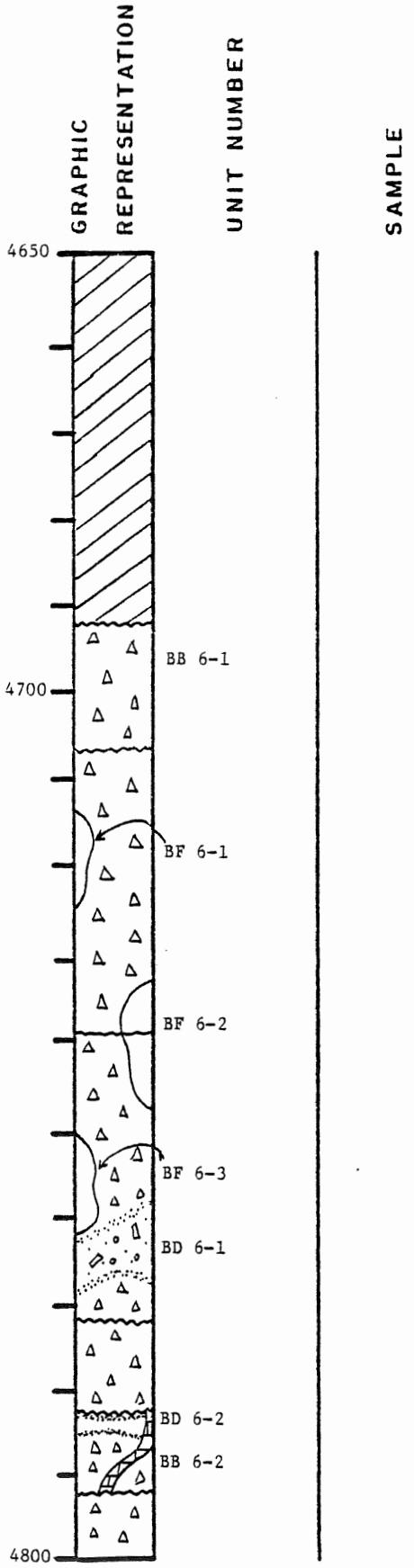

PETROGRAPHY
Breccia- extensive dark-gray breccia of flow material in carbonate cement with some larger clasts-small flows.

NOTES
BF 6-1 and 6-2 may be dikes.
4755cm Possible fractured/brecciated dike.

BERMUDA DRILLING PROJECT
1980

Visual Core Description

Hole #1
Box #6

Depth Interval
(cm) 4800 to 4950

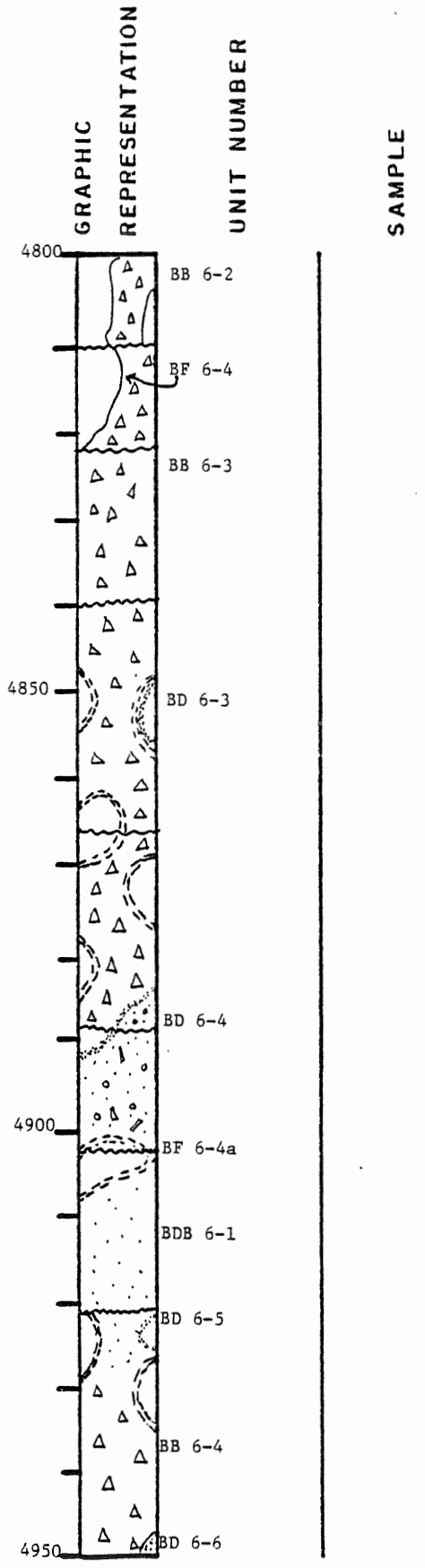

PETROGRAPHY

Flow- fews flows of blue-gray lava in this section.

Breccia-made up of flow material, appears light or dark depending on amount of cement.

Dike-dark gray to black making very inticate and highly irregular intrusions into the breccia. In some cases the intrusives themselves appear to be brecciated and cut by calcite rich veins (fragments-1 to 1.5cm).

NOTES

4850cm Hard to distinguish whether this is a dike or a flow (hematite rich).
4895cm Amygdaloidal dike.
4906-4921cm Finely fractured or brecciated dike which seems to be composed of numerous smaller dikes.
4921cm BB 6-4 may be the continuation of BB 6-3.
4800-4950cm Pillows shown in breccia may either be small flows or large clasts.

Visual Core Description

Hole #1
Box #6

Depth Interval
(cm) 4960 to 5100

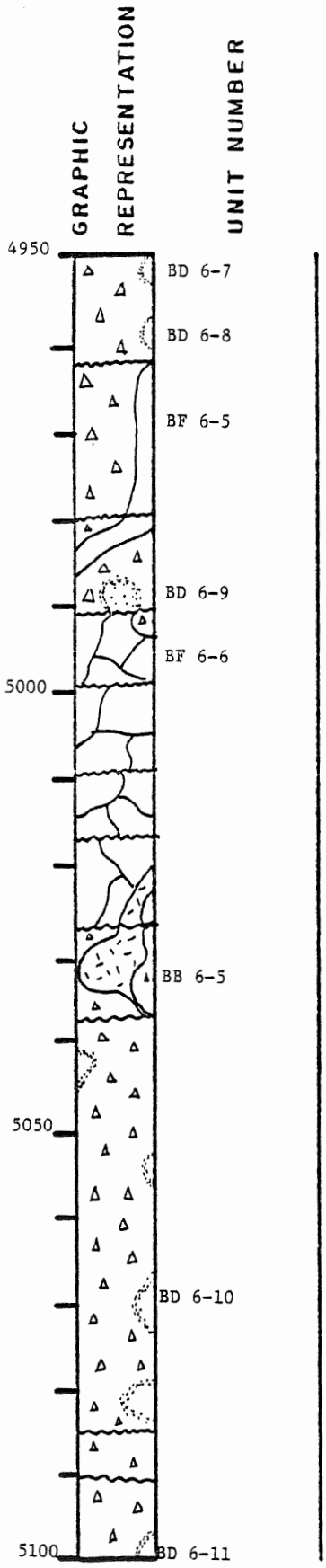

PETROGRAPHY
Flow- blue-gray material
Breccia- mainly dark colored with clasts of flow material with minor carbonate cement.

Dike-black, aphanitic and sinuous.

NOTES
4994cm BF 6-6 may be a dike.
5041-5086cm Numerous small sections of dike, considered as one unit, but may be several small dikes.
5020-5037cm Large (several cm) carbonate filled vein with embayed rock chips cutting flow and breccia.

BERMUDA DRILLING PROJECT
1980

Visual Core Description

Hole #1
Box #6

Depth Interval
(cm) 5100 to 5250

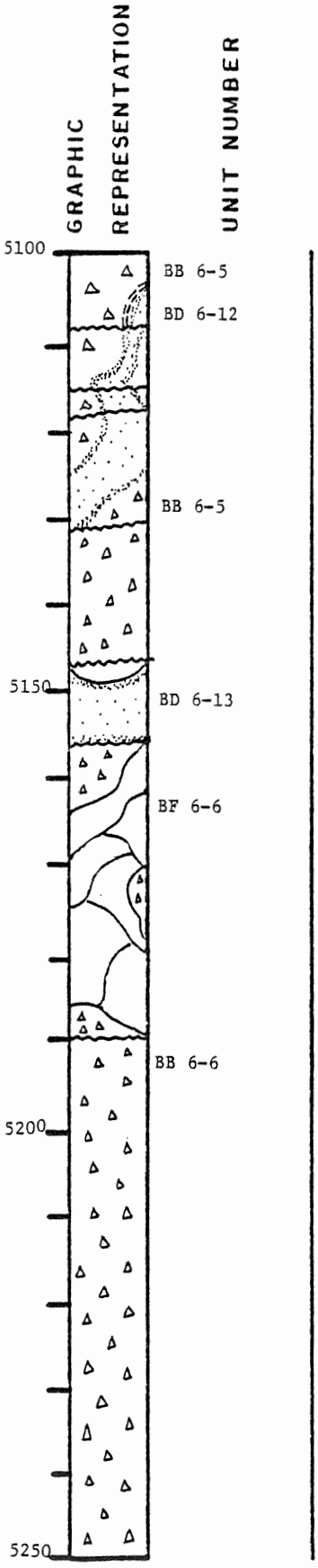

PETROGRAPHY

Breccia- very fine (0.25-1cm) to very coarse (1-4cm) breccia of flow material.

Dike- dark with chilled margins.

NOTES

5120 and 5150cm BD 6-12 and 6-13 may be flows.
5155-5189cm Large clasts or flow ?

Visual Core Description

Hole #1
Box #6-#7

Depth Interval
(cm) 5250 to 5400

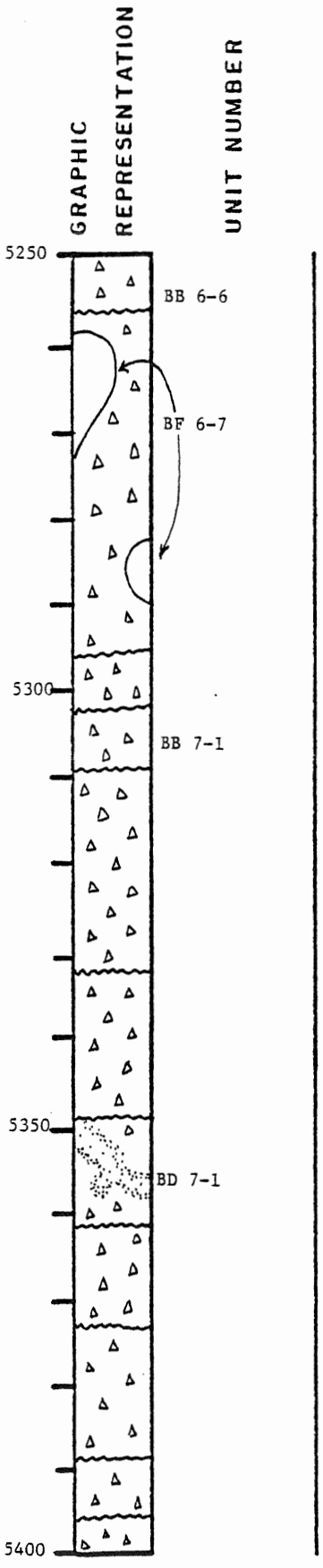

PETROGRAPHY
Flow-small sections of blue-gray flow in breccia, very aphanitic.

Breccia- light colored becoming darker down the section. Some clasts show chilled margins or zonation.

Dike-small and thin, very dark.

NOTES
5250-5255cm Several small dikes (?) in BB 6-6 but not differentiated.
5295cm Box #6 ends, #7 begins.
5296cm Calcite vein 2mm wide with open spaces.
5362-5373cm Possibly some dikes in this breccia.
5388-5395cm White siliceous carbonate blobs in breccia.

Visual Core Description

Hole #1
Box #7

Depth Interval
(cm) 5400 to 5550

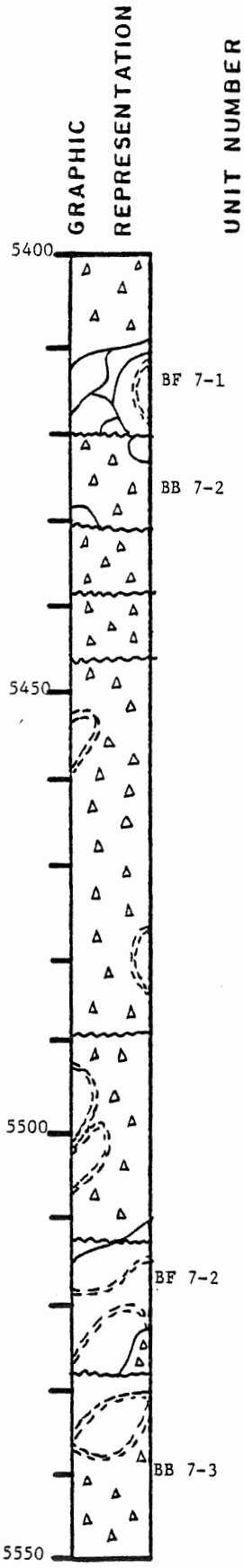

PETROGRAPHY

Flow- blue-gray, aphanitic to fine-grained.

Breccia- made up of flow material clasts with variable clasts size and percentage carbonate cement.

NOTES

5450-5500cm Small flow pillows in breccia not differentiated.

BERMUDA DRILLING PROJECT
1980

Visual Core Description

Hole #1
Box #7

Depth Interval
(cm) 5550 to 5700

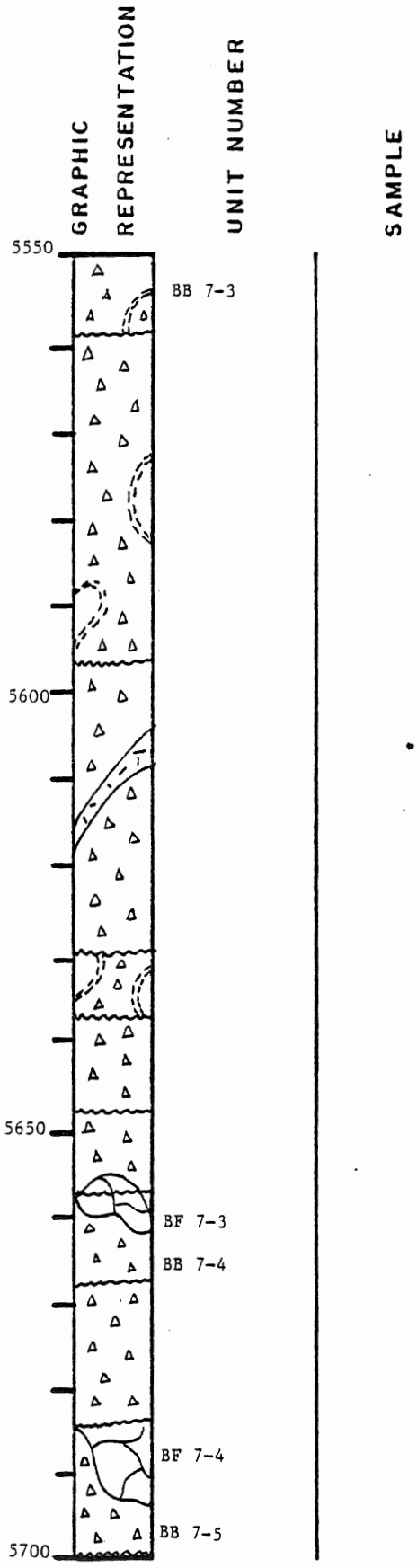

PETROGRAPHY
Flow-small pillows of blue-gray lava.

Breccia-medium sized clasts of lava in a light gray matrix. Some clasts are chlorite and clay rich.

NOTES
5605-5615cm Calcite vein (1-4cm) cuts breccia.

BERMUDA DRILLING PROJECT
1980

Visual Core Description

Hole #1
Box #7

Depth Interval
(cm) 57|00 to 58|50

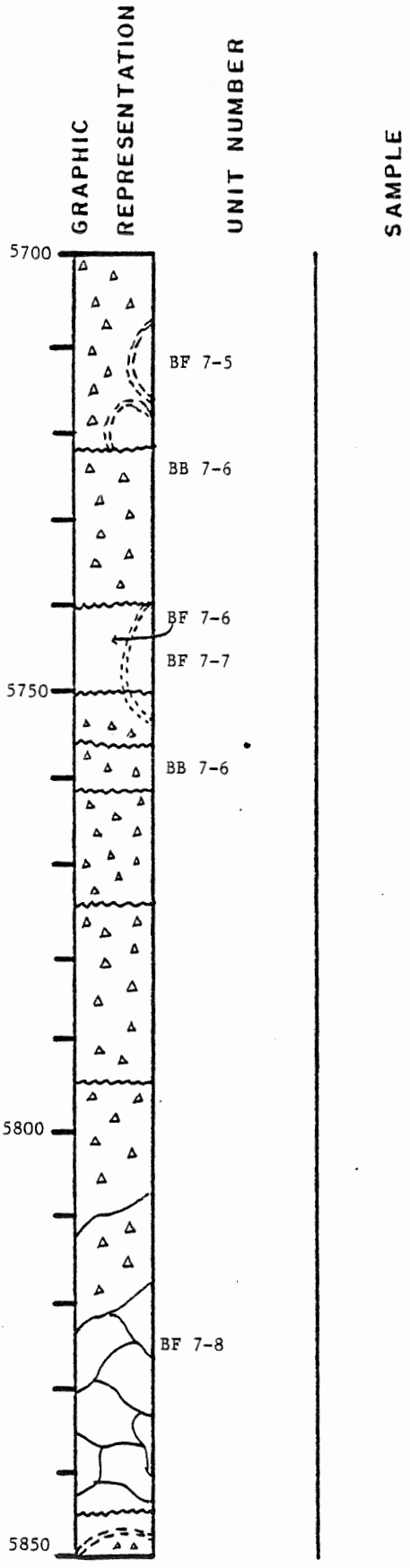

PETROGRAPHY
Flow-blue-gray fractured lava, identical to all previous lavas.

Breccia- comparatively larger clasts (1-4cm) of flow material in a darker gray matrix.

NOTES
5750cm Coreline rotated 2°.
5810-5822cm This breccia has many carbonate filled veins.

BERMUDA DRILLING PROJECT
1980

Visual Core Description

Hole #1
Box #7-#8

Depth Interval
(cm) 5850 to 6000

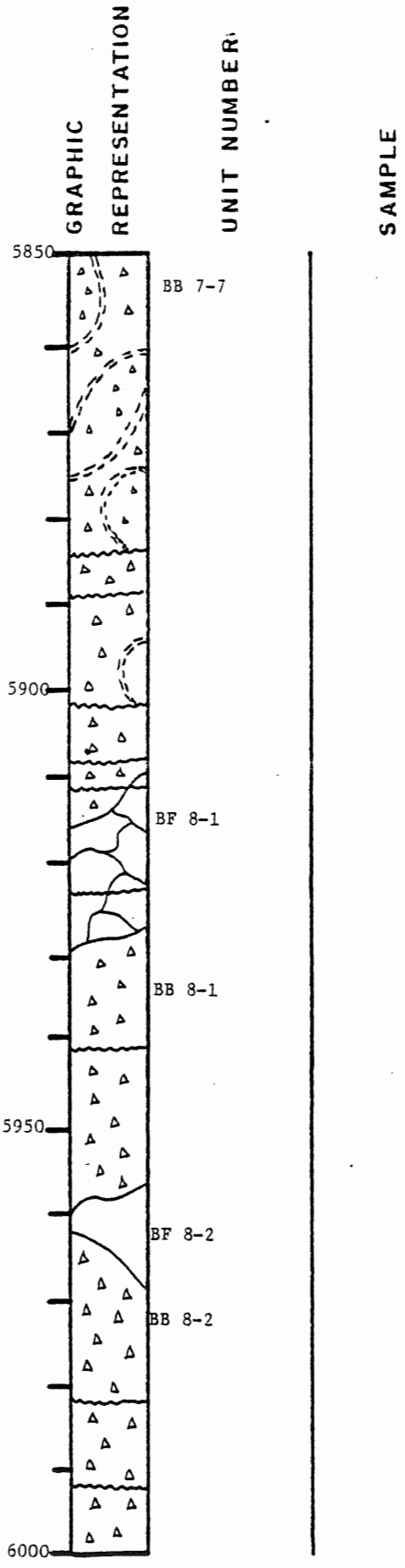

PETROGRAPHY
Flow- the blue-gray lava continues.

Breccia-of the same, often clasts show chilled margins and are altered to chlorite and possibly celadonite.

NOTES
5908cm Box #7 ends, #8 begins.

BERMUDA DRILLING PROJECT
1980

Visual Core Description

Hole #1
Box #8

Depth Interval
(cm) 60100 to 61510

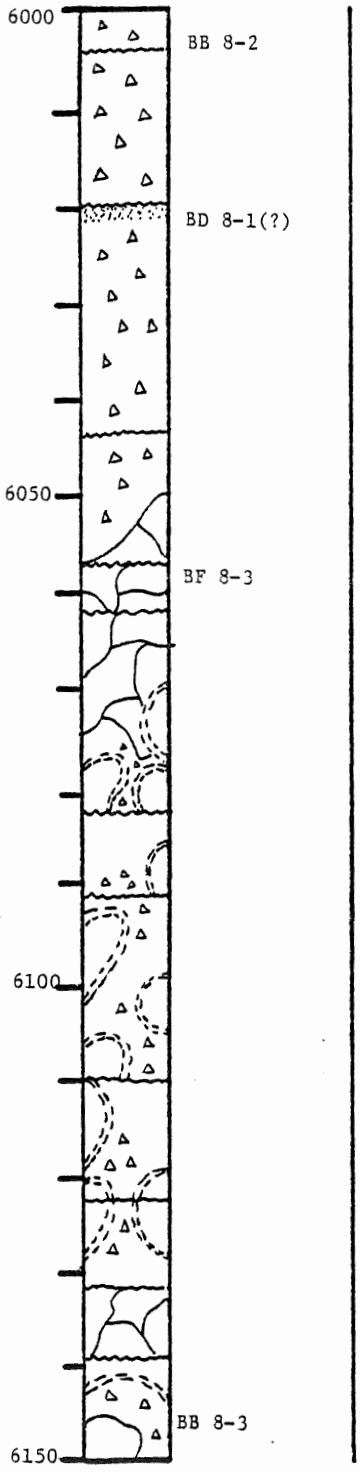

PETROGRAPHY
Flow- two types of altered lava, plus small pillows in breccia: 1) greenish color, now mainly clay minerals-very soft, and 2) gray less-altered material, extreme alteration may be related to the fracture/veining event.

Breccia-made up of flow material with either a quartz + calcite or gray-carbonate cement.

NOTES
6046cm Veins of calcite + quartz.
6080cm Pillow breccia.
6148cm White siliceous cavity filling.

BERMUDA DRILLING PROJECT
1980

Visual Core Description

Hole #1
Box #8

Depth Interval
(cm) 61150 to 63100

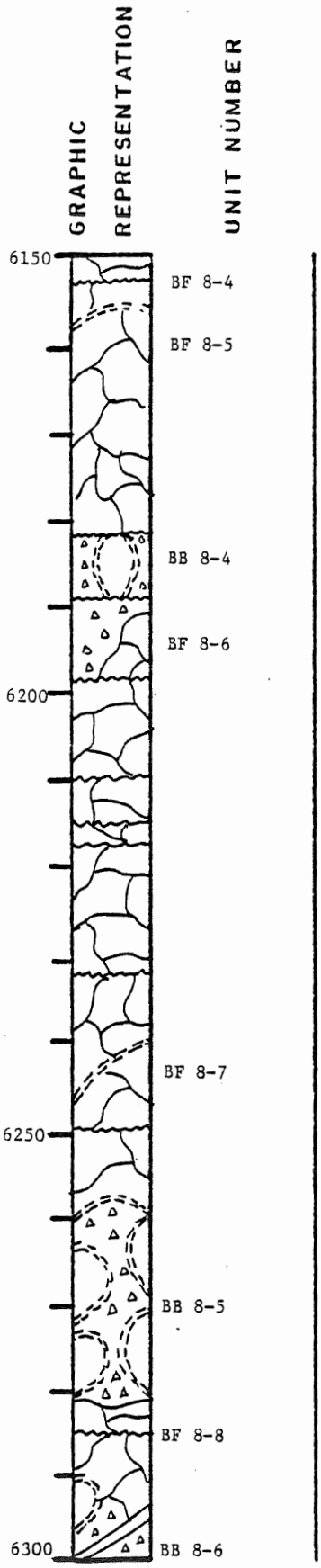

PETROGRAPHY
Flow-fractured blue-gray lava.

Breccia-clasts of above.

NOTES
6295cm Fracture with large vein minerals probably carbonates.

BERMUDA DRILLING PROJECT
1980

Visual Core Description

Hole #1
Box #8

Depth Interval
(cm) 6300 to 6450

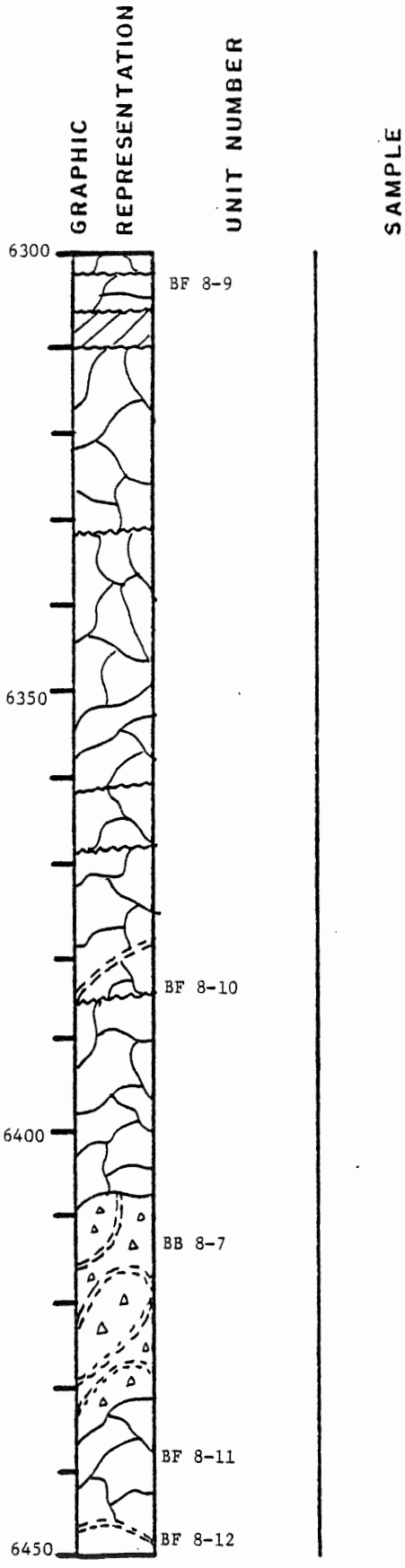

PETROGRAPHY
Flow-blue-gray lava, somewhat fractured with calcite filled veins.

Breccia-clasts of above.

NOTES
6355cm Large open space filled with calcite and siliceous minerals.
6305-6309cm No core recovery.

BERMUDA DRILLING PROJECT
1980

Visual Core Description

Hole #1
Box #8-#9

Depth Interval
(cm) 6450 to 6600

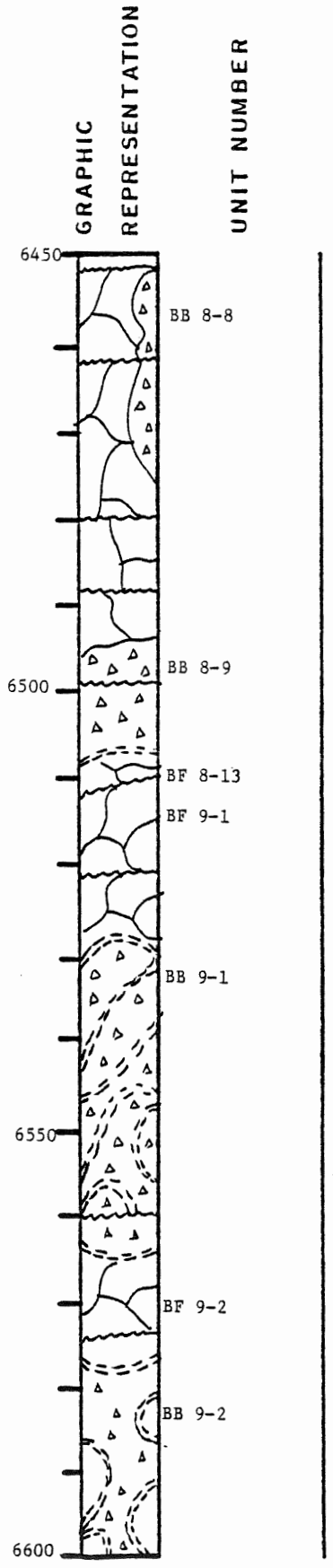

PETROGRAPHY
Flow- blue gray to black flow, with some rare pyroxene phenocrysts (1-4mm).

Breccia- clasts of lava.

NOTES
6460cm Possible dike here, not differentiated.
6512cm Box #8 ends, #9 begins.
6540-6550cm Large (several cm) clasts in breccia.

BERMUDA DRILLING PROJECT
1980

Visual Core Description

Hole #1
Box #9

Depth Interval
(cm) 66600 to 67500

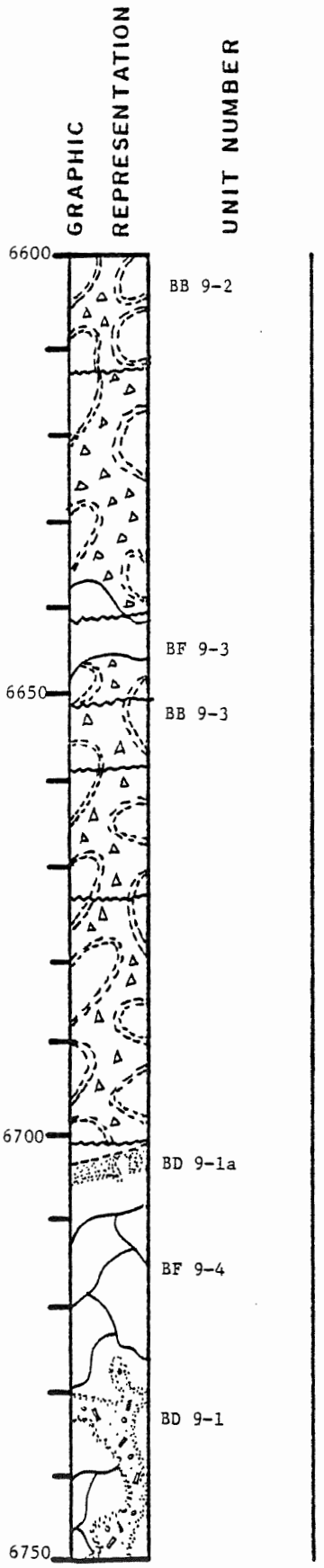

PETROGRAPHY
Flow-blue-gray fractured basalt

Breccia-clasts of above, very fine grained (less than 2-4mm) at top of section.

Dike- dark, fine grained to porphyritic to aphanitic.

NOTES

6612cm Very fine-grained breccia.
6780cm Large biotite phenocrysts in dike.

BERMUDA DRILLING PROJECT
1980

Visual Core Description

Hole #1
Box #9

Depth Interval
(cm) 67510 to 69100

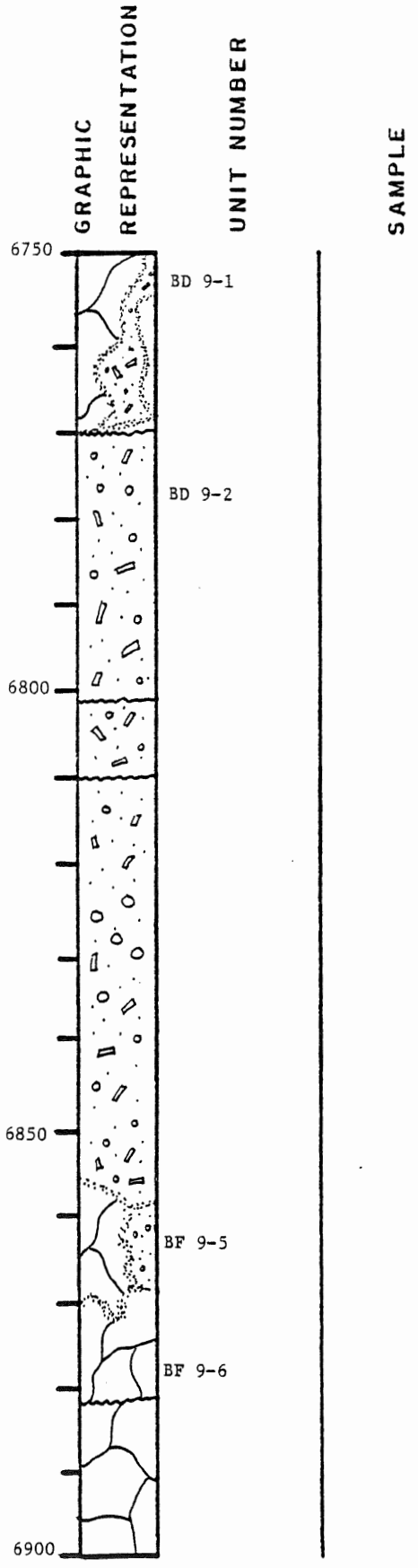

PETROGRAPHY
Flow-fractured blue-gray flow.

Dike-thick porphyritic to amygdaloidal dike with pyroxene phenocrysts..

NOTES
6770cm Chill margin between dikes.
6830cm Very amygdaloidal zone of dike.
6860cm Dike becomes finer grained and is discontinuous.
6870cm Possible pillow margin.
6870cm + BF9-6 may be a continuation of 9-5.

Visual Core Description

Hole #1
Box #9-#10

Depth Interval
(cm) 7050 to 7200

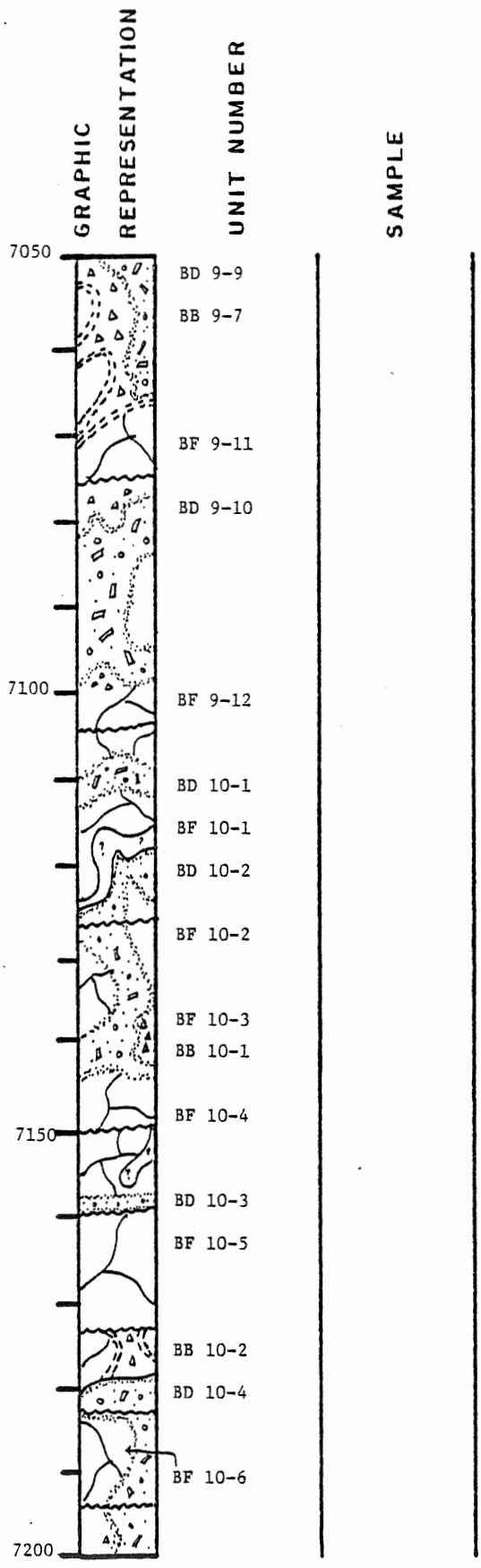

PETROGRAPHY
Flow-fractured blue-gray lava with carbonate veins, fracturing very intense in places.

Breccia-of above at pillow margins.

Dike-dark porphyritic, and sinuous.

NOTES
7070cm Very fractured flow.
7106cm Box #9 ends, #10 begins.
7120cm White siliceous veins along dike contact.
7152cm White siliceous mineral in cavity.

Visual Core Description

Hole #1
Box #10

Depth Interval
(cm) 7200 to 7350

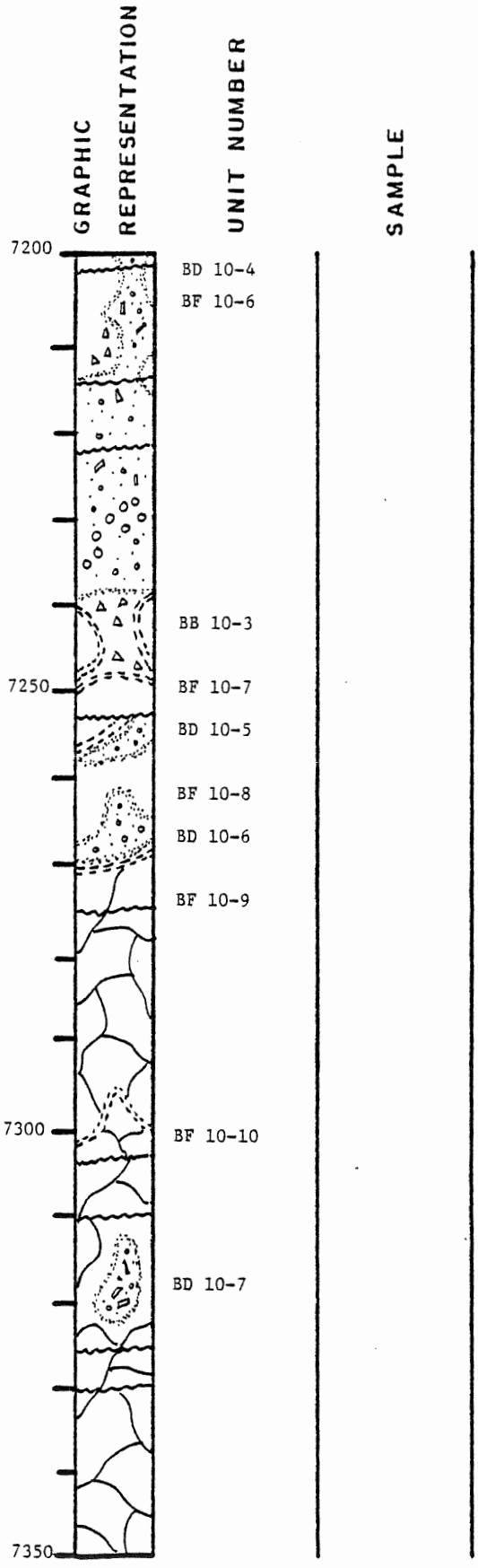

PETROGRAPHY
Flow- blue-gray lava, rather massive at base of section.

Breccia-of above with pillows

Dike- thin, porphyritic to amygdaloidal, especially common at pillow margin-breccia zone.

NOTES
7230cm Very large (1-4cm) amygdukes in dike.

Visual Core Description

Hole #1
Box #10

Depth Interval
(cm) 7350 to 7500

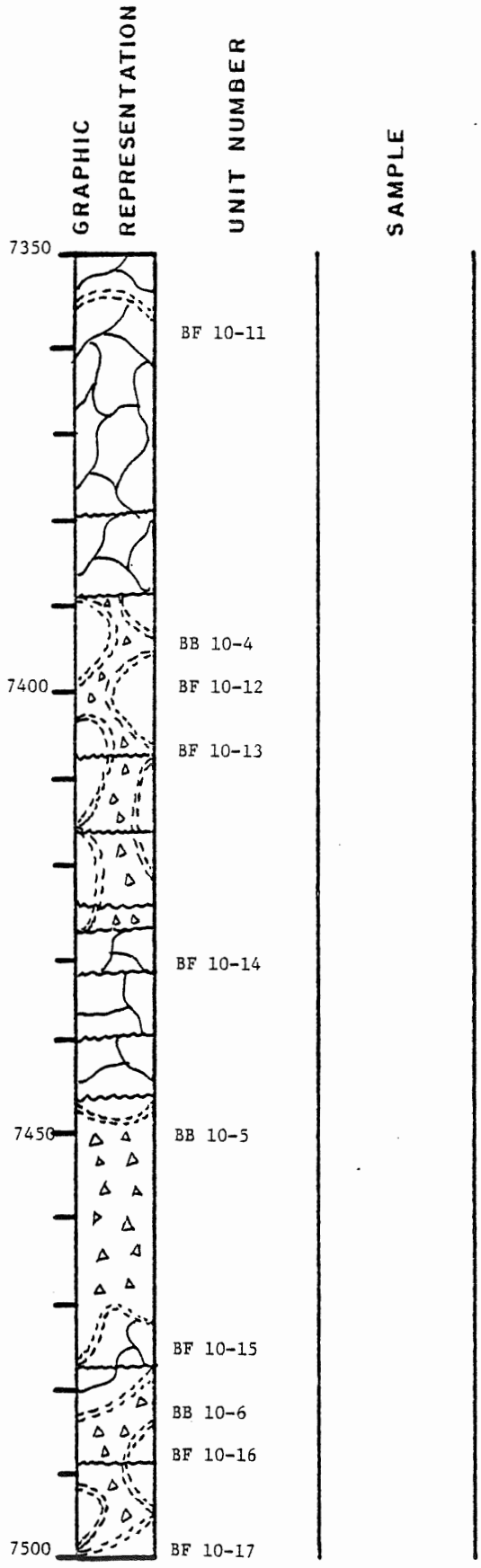

PETROGRAPHY
Flow-fractured blue-gray lava with calcite veins in fractures.

Breccia-of above at pillowed margins.

NOTES
7350-7360cm Large fractures with calcite veins up to 4mm wide.
7450-7470cm Large clasts in breccia.

BERMUDA DRILLING PROJECT
1980

Visual Core Description
Hole #1
Box #10

Depth Interval
(cm) 7500 to 7650

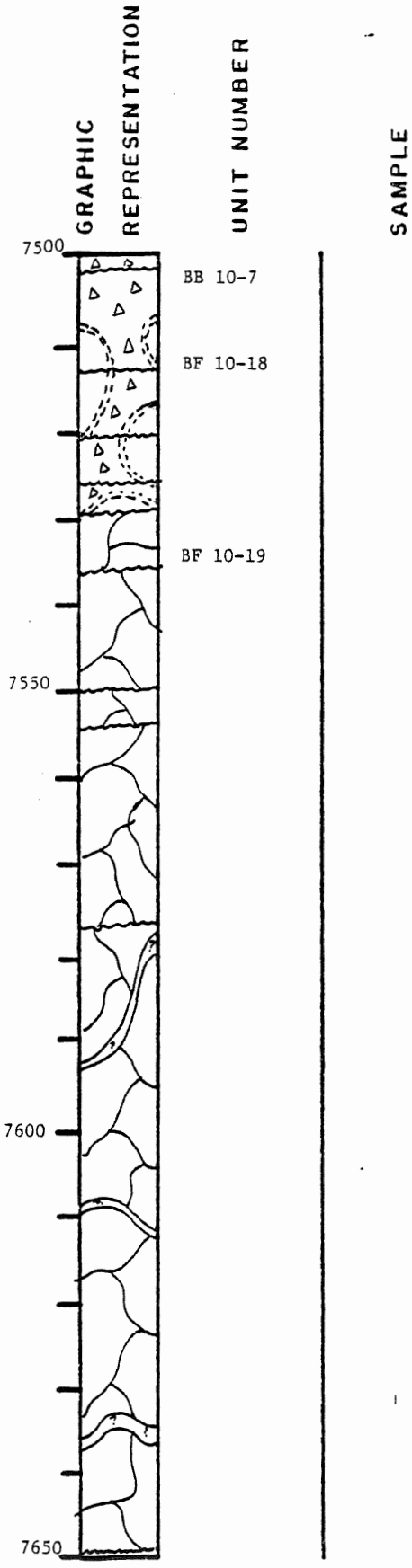

PETROGRAPHY
Flow-fractured blue-gray flow with most of this section being one relatively massive flow.

Breccia-of above at top of large flow in pillow margin.

NOTES
7530-7650cm Large white siliceous pockets and scattered throughout the flow.
7537cm Core line rotated 2°.

BERMUDA DRILLING PROJECT
1980

Visual Core Description

Hole #1
Box #10-#11

Depth Interval
(cm) 7650 to 7800

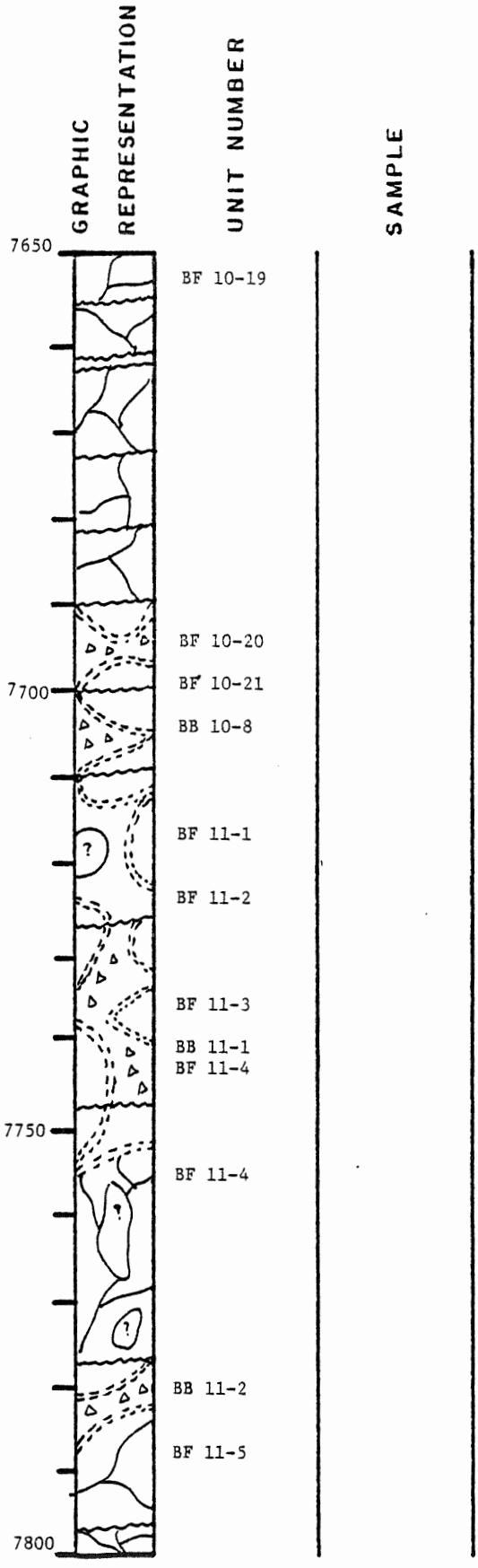

PETROGRAPHY
Flow-continuation of massive flow from other section.

Breccia-of above lithology.

NOTES
7710cm Box #10 ends, #11 begins.
7720 and 7760-7775cm Occasional white siliceous minerals in veins or blobs.

Visual Core Description

Hole #1
Box #11

Depth Interval
(cm) 7800 to 7950

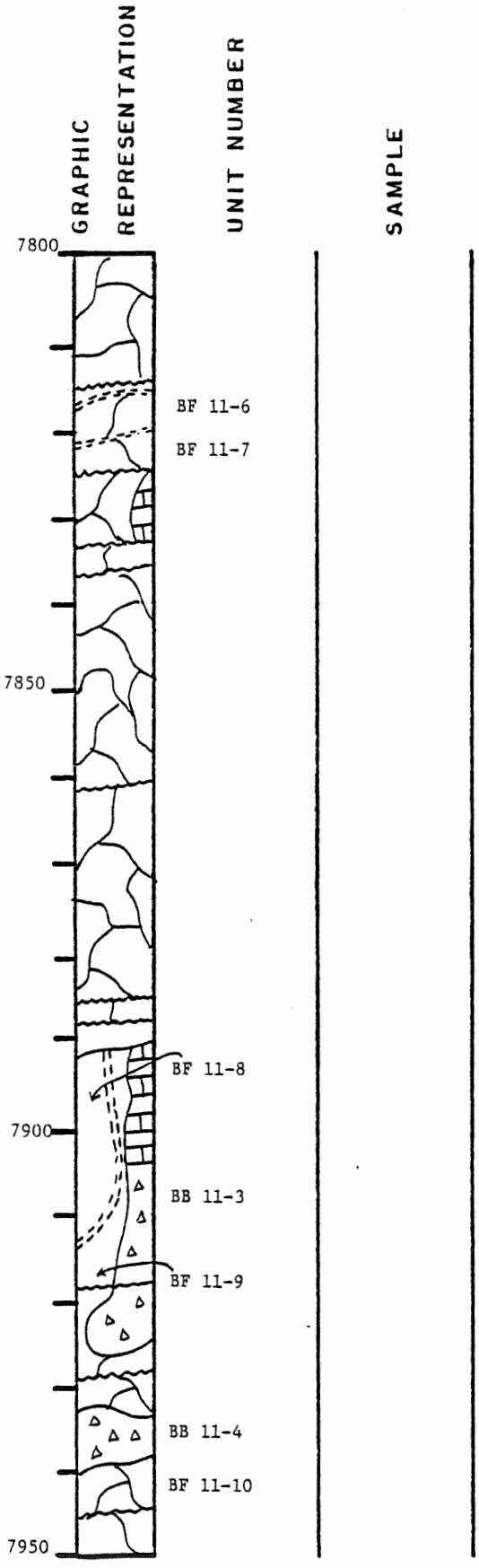

PETROGRAPHY
Flow-relatively large, albeit fractured, flow of blue-gray lava.

Breccia-of above, especially pronounced at pillow margins.

NOTES
7820cm Hematite staining along pillow margin.
7890-7918cm Micritic interpillow sediments.

BERMUDA DRILLING PROJECT
1980

Visual Core Description

Hole #1
Box #11

Depth Interval
(cm) 7950 to 8100

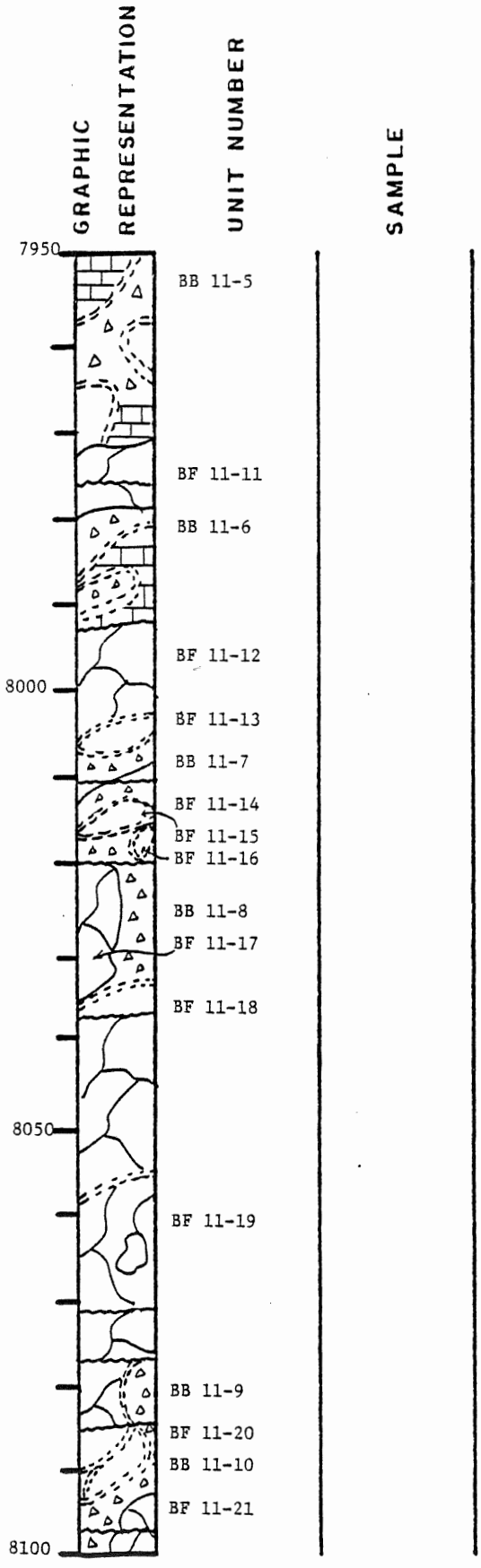

PETROGRAPHY
Flow- fractured blue-gray lava with many pillowed margins.

Breccia- clasts of flow material in carbonate cement.

NOTES
7950-8100cm Limey interpillow sediments common.

BERMUDA DRILLING PROJECT
1980

Visual Core Description

Hole #1
Box #11

Depth Interval
(cm) 8100 to 8250

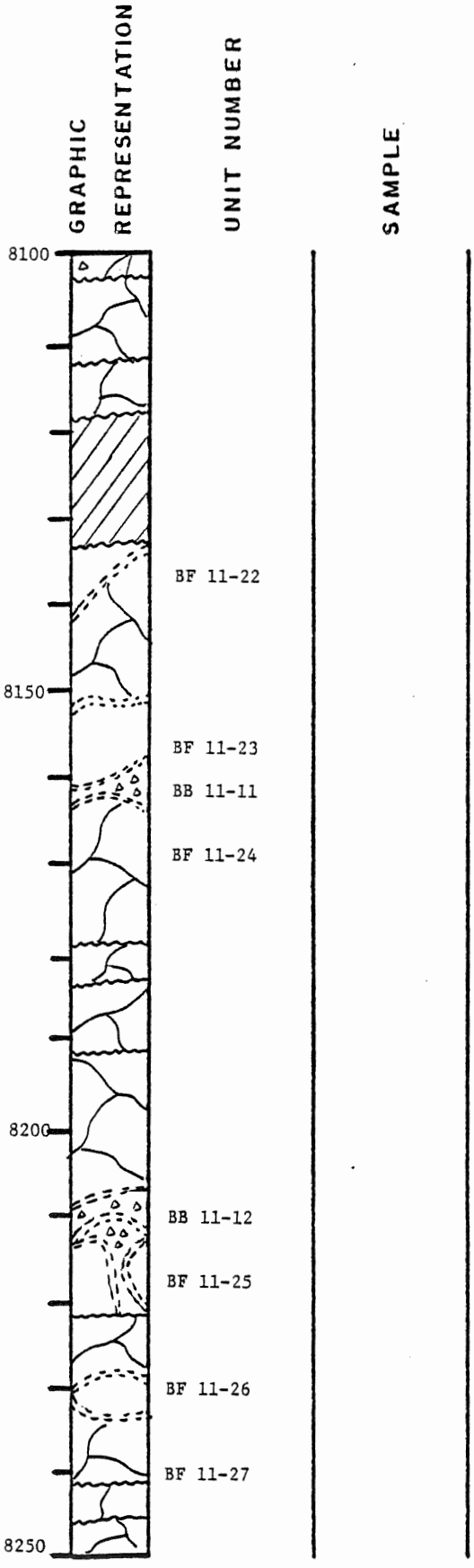

PETROGRAPHY
Flow-continuous series of flows of blue-gray lava, somewhat fractured with calcite veins.

Breccia-of above in pillowed areas.

NOTES
8118-8137cm No core recovery.

BERMUDA DRILLING PROJECT
1980

Visual Core Description

Hole #1
Box #11-#12

Depth Interval
(cm) 8250 to 8400

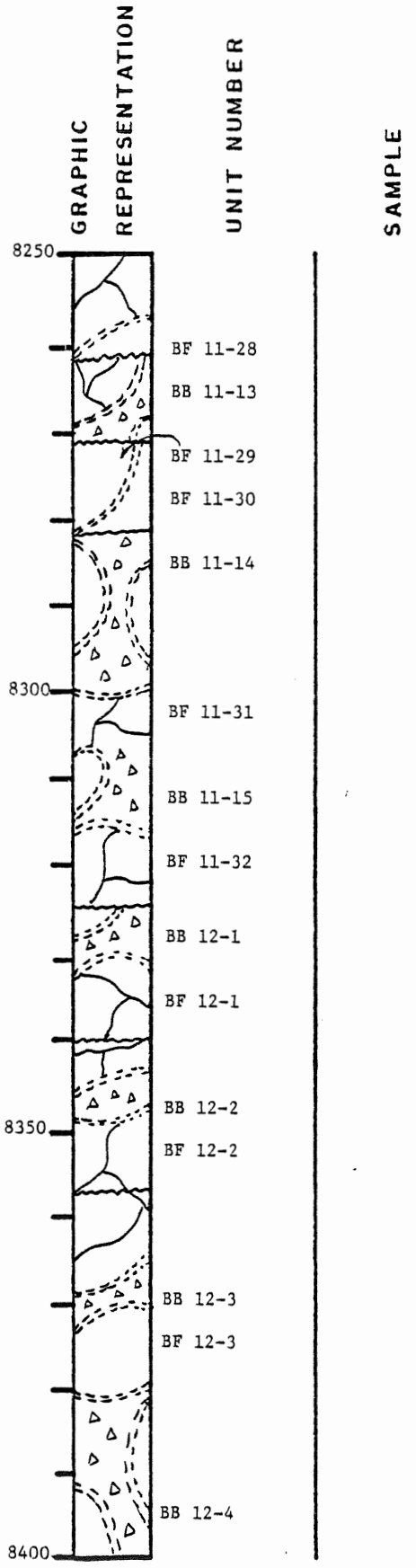

PETROGRAPHY
Flow-several small flows of blue-gray lava.

Breccia-interpillow breccias of above lava.

NOTES
8325cm Box #11 ends, #12 begins.

BERMUDA DRILLING PROJECT
1980

Visual Core Description

Hole #1
Box #12

Depth Interval
(cm) 84|00 to 85|50

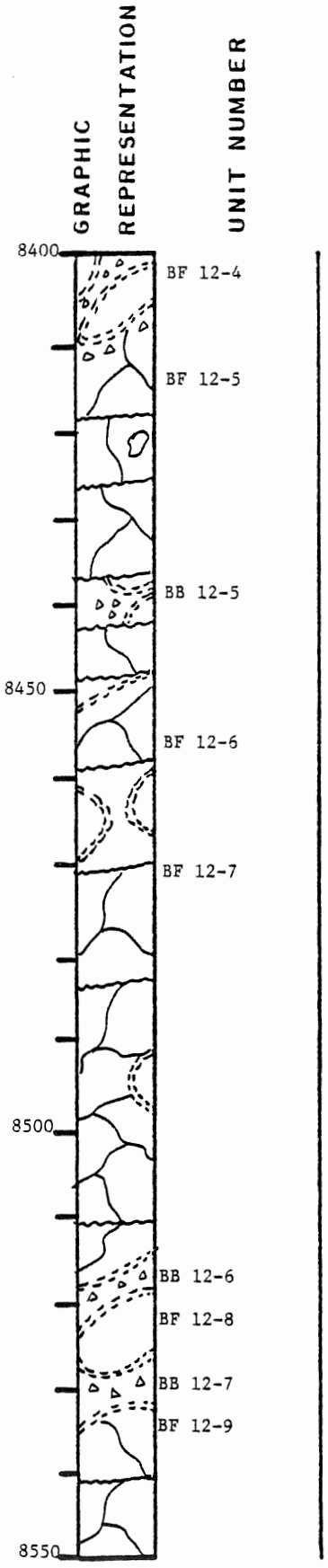

PETROGRAPHY

Flow-several relatively thin to thick flows of blue-gray lava.

Breccia-of above in interpillow regions.

BERMUDA DRILLING PROJECT
1980

Visual Core Description

Hole #1
Box #12

Depth Interval
(cm) 8550 to 8700

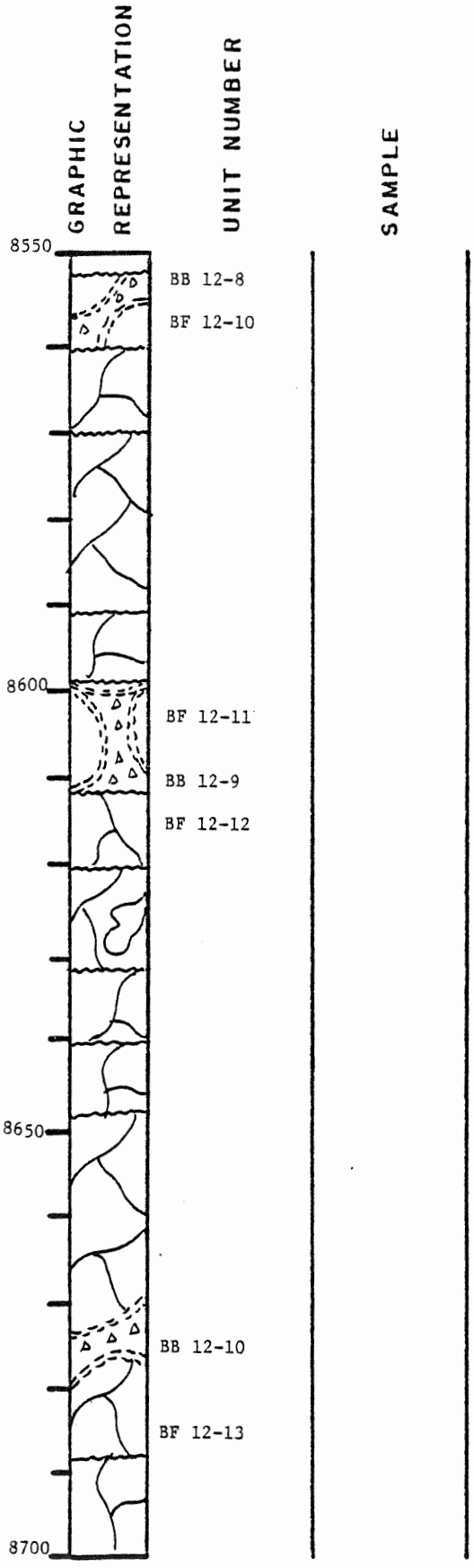

PETROGRAPHY
Flow-fractured blue-gray flow.

Breccia-interpillow breccia of above.

NOTES
8672cm Large clasts in breccia.

BERMUDA DRILLING PROJECT
1980

Visual Core Description

Hole #1
Box #12

Depth Interval
(cm) 87|00 to 88|50

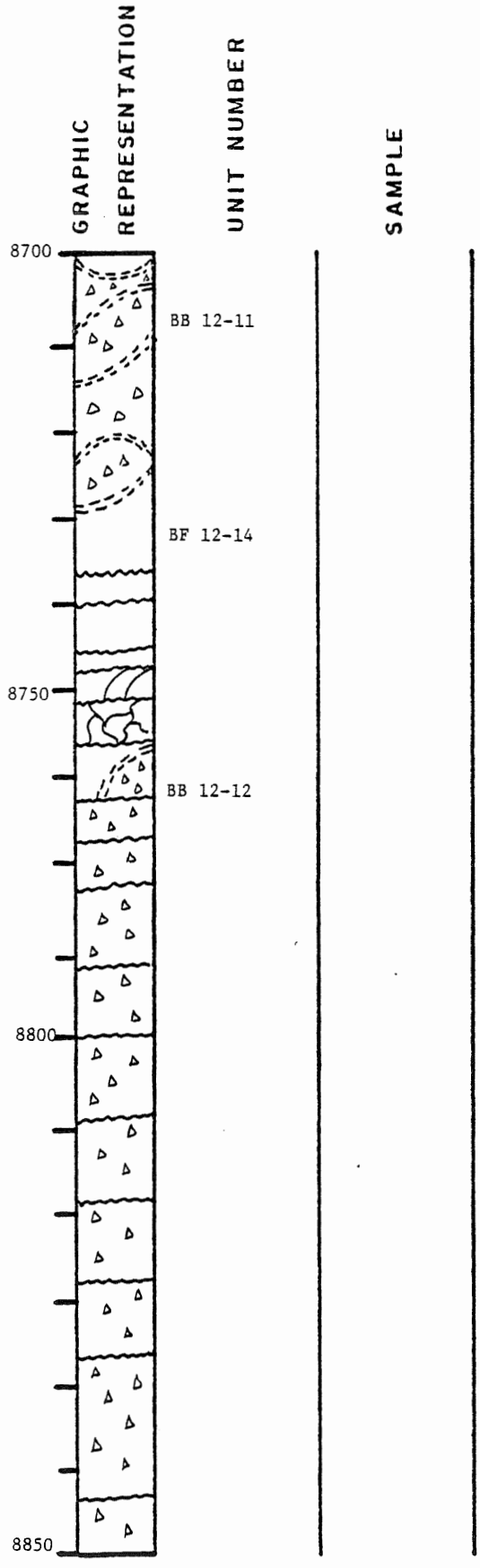

PETROGRAPHY
Flow-small sections of blue-gray lava.

Breccia-extensive in this section and with two types of clasts. In the upper portion the clasts are of relatively unalterd lava. In the lower portion the clasts are extremely altered with mineralogical-color zonations. The rims of the clasts are chlorite-rich, followed by a hematite-rich zone, with cores of blueish-green clay minerals and altered lava.

NOTES
8763cm Extremely altered breccia begins.

Visual Core Description

Hole #1
Box #12

Depth Interval
(cm) 8850 to END

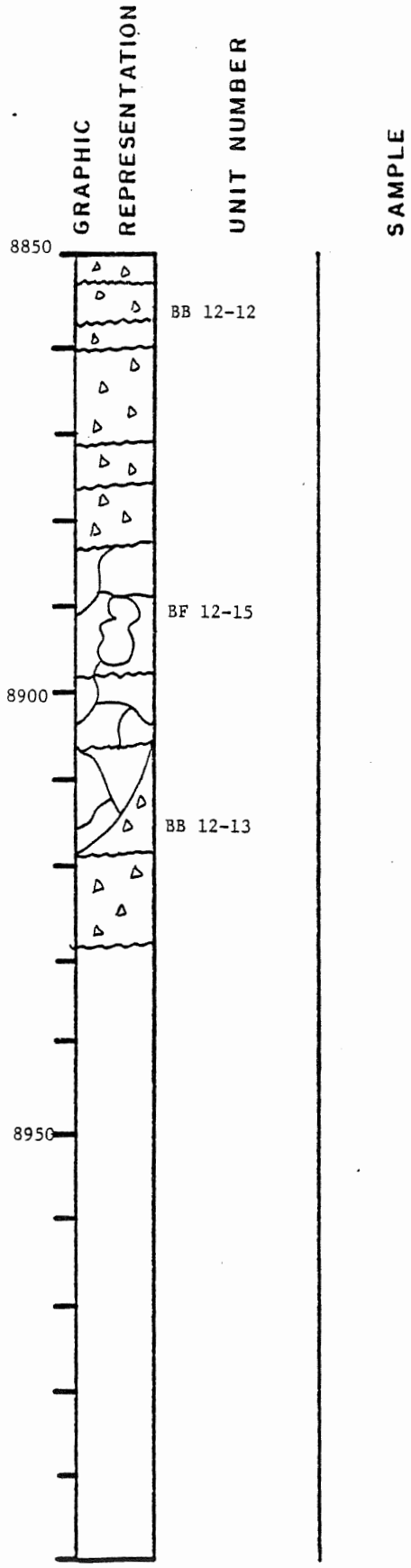

PETROGRAPHY
Flow-small blue-gray lava.

Breccia-continuation of extremely altered clasts.

NOTES
8918cm Box #12 ends.
8918-8925cm Last piece in J. Peckenham's possession.
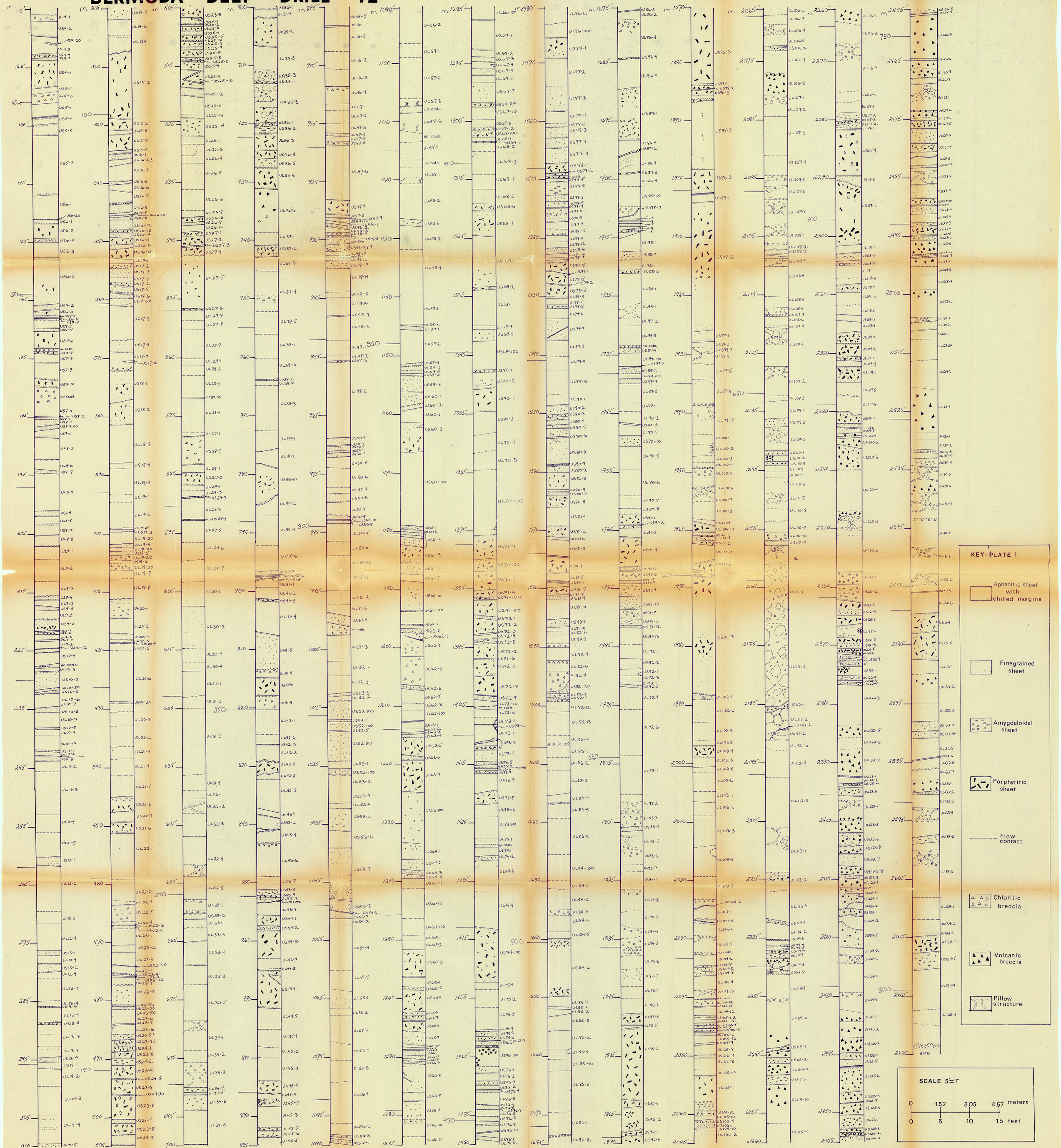
BERMUDA DEEP DRILL '72